Predictive Modelling of Gold Mineral System in Northern New Brunswick: Insights from the Analysis of Multiple Geoscience Data

by

Farzaneh Mami Khalifani

B.Sc. in Mining Engineering (Mineral Exploration), Urmia University of Technology

M.Sc. in Mining Engineering (Mineral Exploration), Urmia University of Technology

A Dissertation Submitted in Partial Fulfillment

of the Requirements for the Degree of

Doctor of Philosophy

In the Graduate Academic Unit of Earth Sciences

Supervisor: David R. Lentz, Ph.D., Department of Earth Sciences

Examining Board: Jim Walker, Ph.D., New Brunswick Department of Natural Resources and Energy Development

Kynan Hughson, Ph.D., Department of Earth Sciences

Ian Church, Ph.D., Department of Geodesy and Geomatics Engineering

External Examiner: Martiya Sadeghi, Ph.D., Geological Survey of Sweden

This dissertation is accepted by the Dean of Graduate Studies

THE UNIVERSITY OF NEW BRUNSWICK,

December 2025

© Farzaneh Mami Khalifani, 2025

ABSTRACT

The study area lies within the Tobique–Chaleur Zone of northern New Brunswick, specifically in the Chaleur Bay Synclinorium. The synclinorium contains Upper Silurian to Early Devonian volcanic and sedimentary rocks that host several epithermal gold occurrences spatially linked to the trans-crustal Rocky Brook–Millstream Fault system. This research advances the understanding and prediction of epithermal gold mineralization through a multidisciplinary and multi-scale approach that integrates geoscientific modeling, machine learning, and geochemical analysis. First, the study addresses the need for geochemical validation by employing portable X-ray fluorescence (pXRF) and micro-XRF (μXRF) spectrometry to characterize pathfinder elements, indicator minerals, and alteration assemblages across four key gold occurrences. Multivariate compositional data analysis (CoDA), including biplots and clustering, reveals geochemical signatures associated with gold-bearing quartz veins. These veins are dominantly hosted in felsic to intermediate volcanic and intrusive rocks and are characterized by sericitic (illitic), potassic, and silica alteration, with gold commonly associated with sulfide phases, such as pyrite, arsenopyrite, and chalcopyrite. The second study applies a mineral systems framework to translate ore-forming processes into mappable criteria using both knowledge-driven methods (fuzzy logic and geometric average) and a data-driven approach (logistic regression). The integration of these models, reclassified through a concentration–area fractal method, allows segmentation of the region into distinct favourability zones, with the fuzzy logic model yielding the highest predictive success.

The consistent alignment of high-potential zones with known gold occurrences validates the hybrid modeling approach.

Complementing this, the third study develops mineral prospectivity maps (MPM) using supervised machine learning algorithms Random Forest (RF), Support Vector Machine (SVM), and XGBoost, based on 24 evidence layers derived from geological, geophysical, and geochemical datasets. These models, evaluated through Receiver Operating Characteristic (ROC) and prediction–area (P–A) analyses, demonstrate high predictive accuracy, with ensemble modeling and confidence indexing further enhancing robustness and interpretability. Together, these integrated studies establish a scientifically rigorous and spatially coherent framework for predictive targeting and mineral exploration in covered and structurally complex terrains. The combination of machine learning, geological knowledge, and geochemical validation provides a replicable model for gold exploration in analogous regions worldwide.

DEDICATION

To my wonderful parents, and to the kind hearts who embraced my persistence with patience and care. This achievement belongs to you.

ACKNOWLEDGEMENTS

I would like to express my gratitude to my supervisor, Dr. David Lentz, for his unwavering support, guidance, and encouragement throughout my PhD. His mentorship extended far beyond academic supervision, consistently challenging me to think critically, fostering independence while providing steady support, and demonstrating confidence in my ideas even during times of uncertainty. Dr. Lentz's enthusiasm for geoscience and his patient, thoughtful guidance was central to the development of this research and to my growth as a scientist.

I am also sincerely thankful to my supervisory committee members, Dr. Jim Walker from New Brunswick Department of Natural Resources and Energy Development and Dr. Stefan Kruse (Terrane Geoscience Inc), for their valuable insights, constructive feedback, and kind encouragement during the most critical stages of this project. Dr. Walker's extensive knowledge and field expertise, along with his practical and grounded advice, were instrumental in refining both technical and conceptual components of this work. Dr. Kruse's thoughtful critiques and geological perspective significantly strengthened the overall quality of this dissertation.

Together, your collective mentorship and support have been instrumental to my academic journey. I feel incredibly fortunate to have had such a dedicated and knowledgeable team guiding me through this process.

I would like to thank Dr. Karl Butler for his guidance and support in the geophysical analysis and interpretation, which contributed meaningfully to this research.

I would like to acknowledge my friend, Saleh Ghadernejad, for his guidance and thoughtful discussions, which contributed meaningfully to this research. His clear explanations, patience, and willingness to share his expertise greatly strengthened my work.

This research was financially supported by the New Brunswick Department of Natural Resources and Energy Development, particularly through the Geological Surveys Branch, as well as the New Brunswick Innovation Foundation (NBIF). I am also grateful to the University of New Brunswick (UNB) for providing institutional support through multiple funding sources, including the Graduate Student Teaching Assistantship (GSTA), Graduate Research Award (GRA), and Graduate Academic Award (GAA). Their collective support has been essential in enabling the successful completion of this research.

I am sincerely grateful to have received the Dr. W.J. Wright Graduate Fellowship, the Dean W. McDonald Bursary, and the UNB Graduate Bursary, which provided valuable support throughout my graduate studies.

Many thanks to Tammy O'Donnell and Heidi Stewart for their constant support and guidance through the administrative and financial challenges I faced. Your help made the journey smoother.

Lastly, I am deeply thankful to my parents for their unwavering love, endless patience, and constant encouragement. Their belief in me, emotional support, and quiet sacrifices sustained me throughout the challenges and milestones of this long academic journey.

Table of Contents

ABSTRACT ii

DEDICATION iv

ACKNOWLEDGEMENTS v

Table of Contents vii

List of Tables xiii

List of Figures xiv

1.Introduction and Background and Regional Geology 1

1.1. Northern Appalachians 1

1.2. Gold mineralization types in the northern Appalachians 2

1.3. New Brunswick 4

1.4. Northern New Brunswick 6

1.5. Tectonic setting 7

1.6. Major Stratigraphic Divisions 7

1.7. Significant folds, faults, and cleavage in the Matapédia Cover Sequence 9

1.8. Gold deposits and occurrences in Northern New Brunswick 13

1.8.1. Williams Brook 16

1.8.2. McIntyre Brook 17

1.8.3. Mulligan Gulch 18

1.8.4. Simpsons Field 19

1.9. Epithermal gold mineralization 20

1.10. pXRF Analysis 25

1.11. μXRF Analysis 30
1.12. Mineral Prospectivity Mapping 33
1.13. Purpose and framework of the study.....36
1.14. Co-author contributions 38
References.....42
2. Advancing Gold Mineralization Detection in Northern New Brunswick Through Portable X-ray and Micro-X-ray Fluorescence Spectrometry with Multivariate Compositional Data Analysis (CoDA) and Clustering for Pathfinder Elements and Alteration Analysis 54
Abstract..... 54
2.1. Introduction.....55
2.2. Geological setting and gold mineralization 58
2.3. Epithermal Gold System in Northern New Brunswick 63
2.4. Alteration, veins, host rock, structures, and mineralization.....66
2.5. Materials and Methods.....70
2.5.1. Sampling 71
2.5.2. p-XRF Data Analysis.....72
2.5.3. QA/QC 73
2.5.4. Log-ratio approach to compositional data 75
2.5.5.CoDA-Compositional Data Analysis.....75
2.5.6. Cluster analysis 76
2.5.7. μ-XRF mapping 77
2.6. Results.....78

2.6.1. Mineralogy Studies 78
2.6.2. Portable X-Ray Fluorescence (pXRF) Spectrometry data analysis 85
2.6.3. Principle Component Analysis (PCA) of pXRF data 92
2.6.4. Micro (μXRF) X-ray Fluorescence (μXRF) Spectrometry 95
2.7. Discussion 98
2.8. Summary and conclusions 101
2.9. Future Work and Recommendations 103
References 106
3. Applying Mineral System Criteria to Develop a Predictive Modelling for Epithermal Gold Mineralization in Northern New Brunswick: Using Knowledge-Driven and Data-Driven Methods 120
Abstract… 120
3.1. Introduction 122
3.2. Geology of the study area 124
3.3. Epithermal Gold System 128
3.4. Epithermal Gold Mineralization in New Brunswick 129
3.5. Materials and Methods 133
3.5.1. Framework of Model 133
3.5.2.Dataset 135
3.5.2.1. Geological data 135
3.5.2.2. Surficial geochemical till data 135
3.5.2.3. Geophysical data 136
3.5.3. Methods 137

3.5.3.1. Log-ratio Approach and Principal Component Analysis 137
3.5.3.2. Logistic transformation 138
3.5.3.3. Fuzzy logic 138
3.5.3.4. Geometric average 139
3.5.3.5. Logistic regression 140
3.5.3.6. Fractal-based discretization of MPM maps 141
3.5.3.7. Receiver Operating Characteristic 142
3.6. Mineral system approach 143
3.6.1. Mapping components to targeting criteria 144
3.6.1.1. Source 144
3.6.1.2. Pathway 144
3.6.1.3. Trap 145
3.7. Results and discussion 146
3.8. Conclusions and recommendations 162
References 165
4. Machine Learning-Based Mineral Prospectivity Mapping of Epithermal Gold Mineralization in Northern New Brunswick: A Comparative Study of Random Forest, Support Vector Machine, and XGboost Classifiers 186
Abstract… 186
4.1. Introduction 187
4.2. Geology of the study area 192
4.2.1. Regional geology 192
4.2.2. Tectonic Setting 193

4.3. Epithermal Gold in Northern New Brunswick 195
4.4. Methodologies 201
4.4.1. Modelling workflow 201
4.4.2. Methods.....203
4.4.2.1. Random Forest 203
4.4.2.2. Support Vector Machine 205
4.4.2.3. Extreme Gradient Boosting XGBoost 206
4.4.2.4. Majority voting 207
4.4.2.5. Confidence index (CI) to measure uncertainty 207
4.5. Experiment and analysis 208
4.5.1. Targeting criteria.....208
4.5.1.1. Geological criteria.....209
4.5.1.2. Geophysical criteria 214
4.5.1.3. Geomagnetic data.....215
4.5.1.4. Radiometric data 217
4.5.1.5. Geochemical criteria 220
4.5.2. Selection of Training and Testing Samples 224
4.5.2.1. Sampling positive data.....226
4.5.2.2. Sampling of Negative Data.....226
4.6. Results and discussion 228
4.6.1. Mineral Prospectivity Mapping (MPM) 228
4.6.2. Evaluation of Predictor Variables.....229
4.6.3. Machine Learning Models and Hyperparameter Optimization 230

4.6.4. Mineral Prospectivity Mapping outputs....233
4.7. Discussion....236
4.7.1. Receiver Operating Characteristic (ROC) curve....236
4.7.2. Prediction-Area (P-A) Plot....237
4.7.3. Ensemble and Confidence Mapping....241
4.7.4. Comparative Analysis of RF, SVM, and XGBoost....242
4.7.5. Interpretation of Epithermal Gold Mineralization Controls....244
4.7.6. Implications and Future Directions....247
4.8. Conclusion....248
4.9. Recommendations....250
References....252
5. Conclusion and recommendations for future....263
5.1. Conclusion....263
5.2. Recommendation....267
5.2.1. Field Validation and Ground-Truthing....267
5.2.2. Geochronology and Paragenesis....267
5.2.3. Data Integration and Methodological Enhancements....268
5.2.4. Broader Applications and Scalability....269
5.2.5. Sustainability, Environmental, Social....269
Curriculum Vitae

List of Tables

Table 2-1. Overview of property names and commodities in the Tobique-Chaleur belt (New Brunswick computerized mineral occurrence database)..... 63

Table 2-2. Element accuracy and precision for Williams Brook (left) and McIntyre Brook (right) according to Hall et al. (2011) criteria..... 86

Table 2-3. Element accuracy and precision for Mulligan Gulch (left) and Simpsons Field (right) according to Hall et al. (2011) criteria..... 87

Table 2-4. Statistical summary of corrected pXRF Data for Williams Brook and McIntyre Brook samples..... 89

Table 2-5. Statistical summary of corrected pXRF Data for Mulligan Gulch and Simpsons Field samples. 90

Table 3-1. Evidence layers employed in this study. 149

Table 4-1. Predictor variables used to characterize the geological processes responsible for the deposition and concentration of epithermal gold mineralization. (RTP=Reduction to the pole), (AS=Analytic Signal), (TDR=Tilt Derivative), (FVD=First Vertical Derivative), (K%= Potassium concentration), (eU= equivalent Uranium), (eTh=equivalent Thorium). 209

Table 4-2. Hyperparameters for the Random Forest algorithm utilized in the randomized search strategy..... 231

List of Figures

Figure 1-1. Map of the northern Appalachians. 3

Figure 1-2. Regional geological map displaying the distribution of various gold 5

Figure 1-3. Simplified geology and principal structural elements 9

Figure 1-4. Significant folds, faults a), and cleavage b) 13

Figure 1-5. Regional geological map of northern New Brunswick 15

Figure 1-6. Simplified model for porphyry, LS and HS systems 24

Figure 1-7. Simplified model for fluid types and alteration zoning 24

Figure 1-8. Portable X-ray fluorescence (pXRF) analyzer 26

Figure 1-9. Reference standards in sample cups and bags for pXRF 27

Figure 1-10. μXRF workstation used in this study 31

Figure 2-1. Regional geological map of western and northern New Brunswick..... 62

Figure 2-2. Regional geological map of the Chaleur Bay Synclinorium 66

Figure 2-3. A flowchart illustrates the steps for identifying indicator minerals 71

Figure 2-4. a) Photo of quartz-carbonate veins in the altered rhyolite host rock 72

Figure 2-5. Photomicrograph images (crossed polarized light, CPL) of minerals 81

Figure 2-6. Variation plots of core samples from gold mineralization 83

Figure 2-7. Photomicrographs reflect light plane polarized light of various sulphides ... 84

Figure 2-8. Scatter plots of pXRF data for gold occurrences. 92

Figure 2-9. Biplots of principal component analysis (PCA)..... 94

Figure 2-10. Cluster analysis (dendrogram) diagrams 95

Figure 2-11. Multielement μXRF- Energy Dispersive Spectrometry (EDS)..... 97

Figure 3-1. Location and geology of the study area 127

Figure 3-2. Drill core samples from epithermal gold occurrences 132

Figure 3-3. The workflow utilized in this study 134

Figure 3-4. Biplots of principal component analysis (PCA) 146

Figure 3-5. Fuzzified input evidence layers for MPM..... 154

Figure 3-6. Fuzzified input evidence layers for MPM..... 155

Figure 3-7. Fuzzified input evidence layers for MPM..... 156

Figure 3-8. MPM assessment of the study area. 160

Figure 3-9. Geology of the study area showing areas of high mineral prospectivity ... 162

Figure 4-1 Location of study area and National Topographic System. 193

Figure 4-2. Photographs of selected rock and drill core samples 198

Figure 4-3. Rock and drill core samples from epithermal gold occurrences. 200

Figure 4-4. The workflow used in this study outlines the process 202

Figure 4-5. Flowchart of classification using RF algorithm. 204

Figure 4-6. Schematic diagram of the SVM model. 206

Figure 4-7. Targeting Criteria used in this study 213

Figure 4-8. Targeting Criteria used in this study 214

Figure 4-9. Targeting Criteria of intrusive and extrusive bodies 216

Figure 4-10. Radiometric targeting Criteria used in this study..... 219

Figure 4-11. Radiometric targeting Criteria used in this study..... 220

Figure 4-12. Targeting Criteria based on the till geochemical data..... 223

Figure 4-13. Targeting Criteria based on till geochemical data 224

Figure 4-14. Loss vs. epoch (trees for XGBoost; bootstrap steps for SVM) 227

Figure 4-15 ROC curves for training (blue) and testing (orange) performance 227

Figure 4-16. ROC curves illustrating the performance of predictor variables. 230

Figure 4-17. Mineral prospectivity maps for the study area 235

Figure 4-18. ROC validation curves of mineral prospectivity models 237

Figure 4-19. Prediction–area (P–A) plot analysis of the three models 240

Figure 4-20. Assessment of results of this study (a) Majority voting model..... 242

1. Introduction and Background and Regional Geology

1.1. Northern Appalachians

The northern Appalachian belt is a complex collage of supra-subduction zone terranes and microcontinents assembled during the closure of the Iapetus and Rheic oceans from the late Cambrian to the Permian (van Staal, 2007; Romer and Kroner, 2018; Figure 1-1). The suprasubduction zone terranes contain various types of arc rocks that formed during subduction of oceanic crust, whereas the microcontinents comprise crustal blocks of peri-Laurentian (Dashwoods terrane) and peri-Gondwanan (Ganderia, Avalonia, and Meguma) provenance (van Staal, 2007; Hatcher, 2010; Romer and Kroner, 2018). It should be noted that the northern part of the Appalachian belt displays systematically younger ages of deformation from the west to the east, reflecting the relative timing of accretion of the various arcs and the microcontinents (e.g., Hatcher, 2010). As mentioned by Williams (1995), the Appalachians include rocks affected by several orogenies, during which they were subjected to combination of folding, faulting, metamorphism, and plutonism. Accordingly, Paleozoic folds and faults are generally northeast trending as are the major tectonic zones of the Canadian Appalachians that, from northwest to southeast are Humber, Dunnage, Gander, Avalon, and Meguma. The sequence of oceanic and continental accretion and closure of the Iapetus and Rheic oceans led to several collisional events, namely the Taconic, Penobscot, Salinic, Acadian, and Neoacadian orogenies (Fyffe et al., 1981; Fyffe and Fricker, 1987; Romer and Kroner, 2018; Waldron et al., 2025). Each of which was accompanied by a variety of mineralization types.

1.2. Gold mineralization types in the northern Appalachians

Northern Appalachians and Maritime Canada area underlain by a collage of major tectonic stratigraphicunits terranes related to the closure of the Iapetus and Rheic oceans during, the Acadian, Neoacadian, Variscan, Hercynian, and Alleghanian orogenies (Hibbard et al., 2007; van Staal and Barr, 2012). Based on Sangster and Smith (2007) and van Staal (2007), Figure 1-1 shows the distribution of Au mineralization in northern Appalachian. It should be noted that only Silurian-Devonian intrusions, which are related to crustal thickening processes and post-Acadian uplift, are mineralized with granophile elements, such as Sn, W, Mo, Cu, Au, and Sb (Fyffe et al., 1981; Zhang et al., 2016; Azadbakht, 2019).

The structural setting of polymetallic Cu-Pb-Zn-Au occurrences and the Au-bearing veins in the southern Gaspé peninsula suggest that Acadian strike-slip tectonics along the Grand Pabos-Restigouche Fault played a significant role in focusing hydrothermal fluid flow and in preparing the host rocks for mineralization (Moritz and Malo 1996). Various authors (e.g., Williams-Jones, 1982) have suggested the existence of a NE-trending northern Appalachian porphyry-skarn province that stretches from northern Maine to Gaspé. However, some mineralization in the southern part of the Gaspé Peninsula, including skarns and gold-bearing quartz veins, is spatially associated with the composite Grand Pabos-Restigouche Fault, a major break in the Canadian Appalachian. In northern New Brunswick the trans-crustal Rocky Brook–Millstream Fault system, which has spatially related to gold mineralization, is a comparable and similar in scale to the Grand Pabos-(Restigouche) Fault.

It should be noted that major sources for Au in the Appalachians are probably related to earlier Cambrian to Ordovician sedimentary rocks and Cambrian to Ordovician magmatic

arcs and back arcs. Gold mineralization is primarily associated with volcanogenic massive sulfide deposits that occur in supra-subduction zone volcano-sedimentary sequences that were thrust into their present configuration analogous to ophiolites, i.e. an accretionary complex. Sedimentary rocks previously deposited at the continent margin, which has a significant contribution to the Au deposits of supra-subduction zone accretionary complex (Figure 1-1).

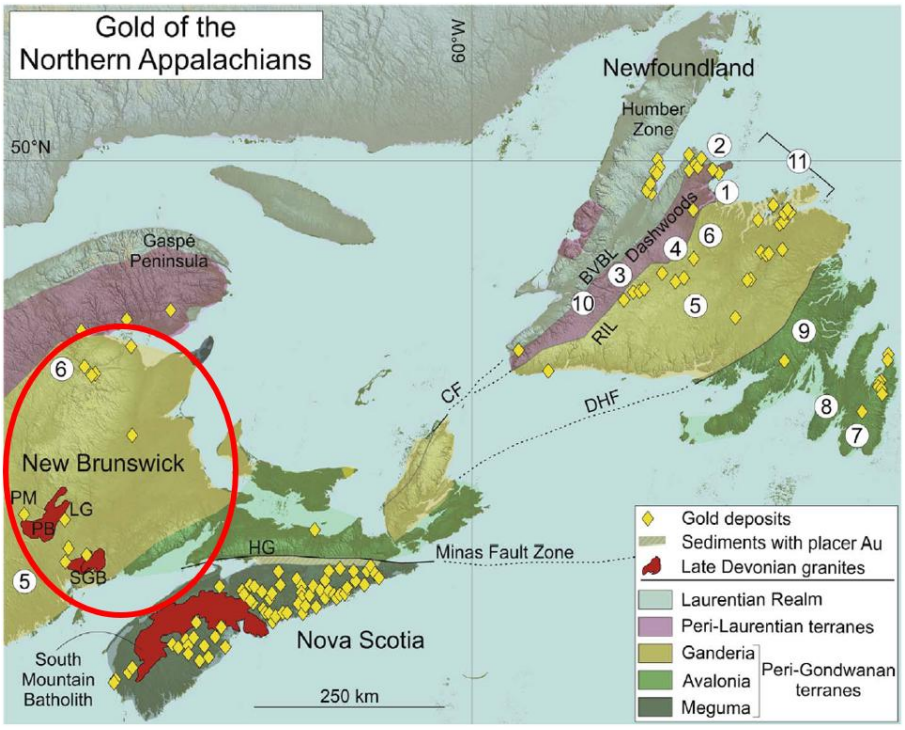

Figure 1-1. Map of the northern Appalachians (including Maritime Canada) showing major tectonic terranes associated with the various episiodes of closure of the Iapetus and Rheic oceans, and distribution of Au mineralization in northern Appalachian (modified from Romer and Kroner, 2018).

During the early Paleozoic, the accretion and obduction of magmatic arcs onto Laurentia and Laurussia led to a redistribution of gold, partly concentrated near older deposits that are linked to structural features (Fig. 1-1). With the beginning of the Armorican Spur

(Gondwana) collision with Laurussia at c. 400–380 Ma, the style of Au mineralization and redistribution becomes highly varied at or near the boundary between Gondwana and Laurussia with magmatic Au mineralization (New Brunswick), shear zone associated with mineralization (e.g., Southern Alleghanian, Newfoundland, Ireland, Scotland), and Au-bearing quartz veins in greenschist to amphibolite facies metasedimentary rocks (Nova Scotia) (Romer and Kroner, 2018). It should be mentioned that in Maritime Canada, Au mineralization is associated with subduction, whereas in other areas gold mineralization is related to reactivation of strike-slip shear zones and to redistribution within older deposits (Romer and Kroner, 2018). In continental collision settings with subduction, gold occurs primarily in shear zone vein-type deposits and structurally associated magmatic rocks. Shear zone hosted quartz-vein gold deposits in low-grade metamorphic zones containing older Au mineralization areas, and granite-hosted Au mineralization, occured along the belt in distinctive pulses that are controlled by earlier structures in diverse stress systems (Romer and Kroner, 2018). In the study area, two important styles of Au mineralization formed during orogenic events in the (Silurian through Devonian), namely metamorphic orogenic and intrusion-related magmatic hydrothermal to hydrothermal (Williams, 1995; Yang and Lentz, 2005).

1.3. New Brunswick

The New Brunswick portion of the Canadian Appalachians hosts several types of gold deposits and occurrences formed during the Appalachian orogeny and subsequent episodes of exhumation and erosion (Wilson et al., 2017; Romer and Kroner, 2018). In New Brunswick, gold occurrences include Middle Ordovician volcanogenic massive sulfide deposits of the Bathurst Mining Camp (e.g., Murray Brook, Caribou, and Brunswick), as

well as younger skarn, porphyry, epithermal, orogenic, intrusion-related, and placer deposits formed during and after the Appalachian orogeny (Thorne et al., 2008; Thorne, 2011; Fig.1-2) .

Among these, the structurally controlled, orogenic- and intrusion-related to epithermal gold systems are the most important. The project focuses on gold deposits/occurrences in the Tobique-Chaleur belt of northern New Brunswick and includes the Williams Brook, McIntyre Brook, Mulligan Gulch, and Simpsons Field gold occurrences within NTS map areas in 21O.

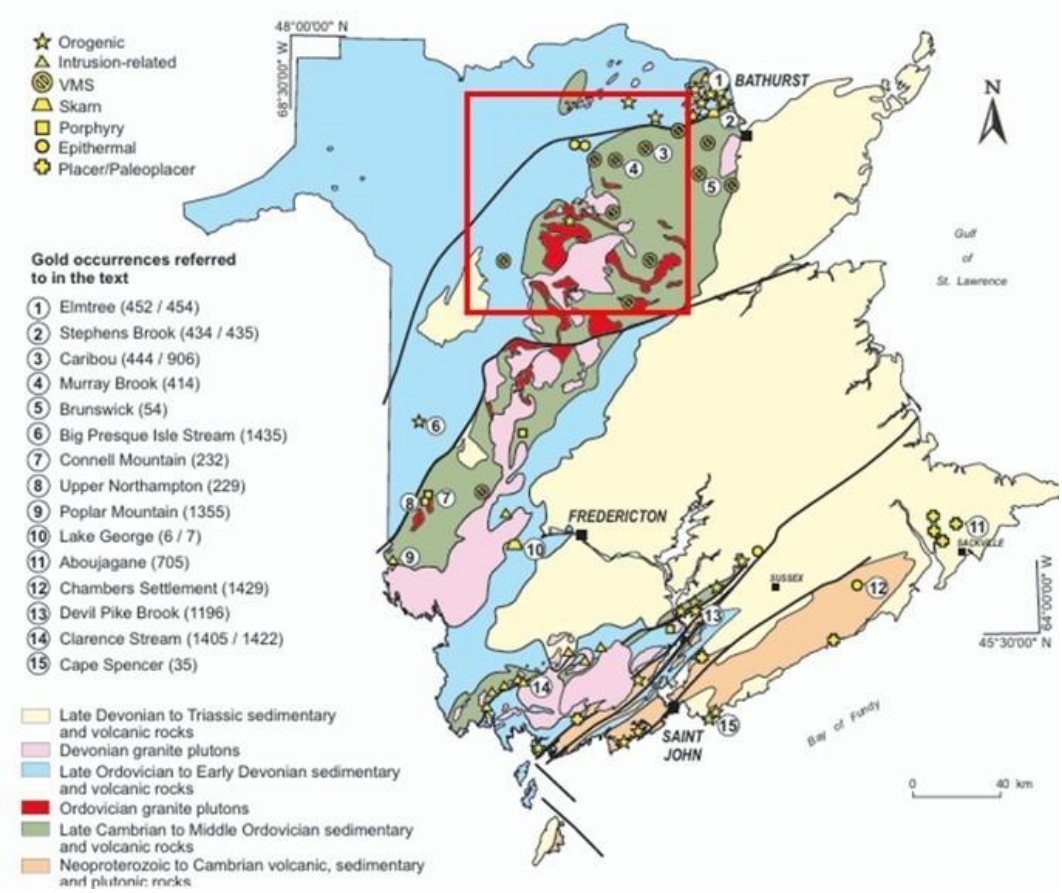

Figure 1-2. Regional geological map displaying the distribution of various gold deposit types in New Brunswick, the red box highlights the study area in the western Chaleur Bay Synclinorium (from Thorne, 2011).

1.4. Northern New Brunswick

Northern New Brunswick is underlain by the post-Taconic, Middle Paleozoic Matapédia Cover Sequence (MCS) and underlying deformed Early Paleozoic Popelogan, Miramichi, and Elmtree inliers (Wilson, 2017). The Brunswick Subduction Complex (Miramichi Inlier) was established during the Late Ordovician to Early Silurian, thrust faulting associated with the destruction of oceanic crust and microcontinental blocks of the Tetagouche backarc basin. Clastic and carbonate sedimentary rocks of the Grog Brook and Matapedia groups of the MCS were deposited in the Matapédia forearc basin between the Laurentian margin and the accretionary wedge. It should be noted that upper Silurian to Early Devonian, turbiditic sedimentary and related volcanic rocks are assigned to the Dalhousie and Tobique groups in the eastern MCS, and the Fortin Group in the western MCS. Upper Silurian to Lower Devonian volcanic rocks in the MCS were constructed in a complex tectonic setting, which occurred on the upper (Laurentian) plate associated with the subducted Tetagouche back arc slab and Ganderia's trailing passive margin. In addition, all volcanic rocks investigated display geochemical signatures indicative of formation by partial melting of the same subcontinental lithospheric mantle source. According to estimation, Acadian deformation of the MCS in northern New Brunswick occurred in the Early Devonian between 415 and 395 Ma and was accompanied in its later stages by dextral strike-slip faulting on the Rocky Brook – Millstream, Restigouche–Grand Pabos, and Catamaran Brook faults, and numerous related satellite faults (van Staal et al., 2009; Wilson, 2017).

1.5. Tectonic setting

According to Fyffe and Fricker (1987), the Middle Paleozoic Matapédia Cover Sequence (MCS) is a Late Ordovician to Middle Devonian basin fill sequence (Fyffe and Fricker, 1987). The Matapédia Cover Sequence is divided into three structures that from northwest to southeast, are: 1) the Connecticut Valley–Gaspé Synclinorium, 2) Aroostook–Percé Anticlinorium, and 3) Chaleur Bay Synclinorium (Rodgers, 1970; Bernier and Webber, 1989). The gold occurrences investigated within the Chaleur Bay Synclinorium are mainly underlain by Upper Silurian to Early Devonian rocks. The Chaleurs Bay Synclinorium has a more diverse geology and a more complex tectonic history relative to the adjacent Aroostook–Percé Anticlinorium. The rocks of the Chaleur Bay Synclinorium are divided into the Chaleurs, Petit Rocher, Quinn Point, Dickie Cove, and Dalhousie groups north of the Rocky Brook–Millstream Fault and to the Tobique Group south of the fault (Wilson, 2017) (Fig. 1-3).

1.6. Major Stratigraphic Divisions

In order to convey the spatial variation in the stratigraphic record, and demonstrate regional relationship within the study area (Fig 1-3), stratigraphic columns for five structural domains are presented: 1) the Kedgwick Domain contains the Connecticut Valley–Gaspé Synclinorium and Aroostook – Percé Anticlinorium, west the McKenzie Gulch and Sellarsville faults (Carroll, 2000, 2003a, 2003b), 2) the Upsalquitch domain includes the eastern part of the Aroostook–Percé Anticlinorium and Lower Silurian to Lower Devonian strata of the western Chaleur Bay Synclinorium, 3) the Benjamin domain includes Upper Silurian to Lower Devonian strata of the Chaleur Bay Synclinorium lying west of the Black Point – Arleau Brook Fault to the east and north of the Rocky Brook–Millstream Fault, 4)

the Nigadoo River syncline is confined to the south by Ordovician rocks of the Miramichi Inlier to the south and, by the Melanson Brook Fault (Elmtree Inlier) to the north, and 5) the Tobique domain is confined to the east by an unconformity with Lower Paleozoic rocks of the Miramichi Inlier, and to the north and west by the Rocky Brook – Millstream Fault (Wilson, 2017).

Silurian rocks in the Chaleur Bay Synclinorium are divided into the Quinn Point, Petit Rocher, Dickie Cove and Chaleurs groups. The Quinn Point Group, extends from the Upsalquitch Forks area northeast to Chaleur Bay. The Petit Rocher Group contains Upper Silurian sedimentary rocks along the northern margin of the Miramichi Inlier, from the Nigadoo River on Chaleur Bay west to the Simpsons Field area, the Dickie Cove Group contains the Upper Silurian mainly volcanic succession in the Charlo – Benjamin River area, whereas the Chaleurs Group comprises upper Silurian to lower Devonian sedimentary rocks (Figure 1-3). The Dalhousie Group contains all lower Devonian volcanic and sedimentary rocks in the Chaleur Bay Synclinorium lying north of the Rocky Brook – Millstream Fault. South of the RBMF, Upper Silurian rocks are included in the Petit Rocher Group, whereas Early Devonian volcanic and sedimentary rocks are included in the Tobique Group. Lower Devonian terrestrial sedimentary rocks in the Chaleur Bay Synclinorium are included in the Gaspé Group, e.g. the Campbellton Formation in the core of the Restigouche Syncline (Figure 1-3).

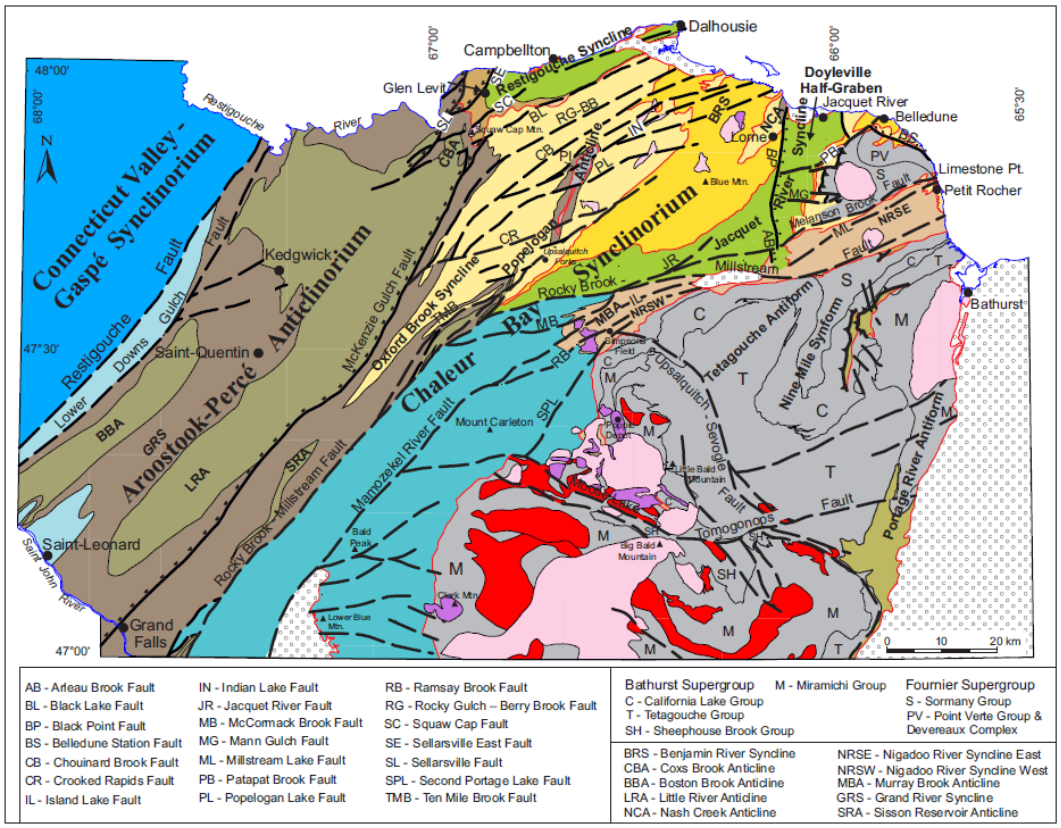

Figure 1-3. Simplified geology and principal structural elements of western and northern New Brunswick (from Wilson et al., 2017).

1.7. Significant folds, faults, and cleavage in the Matapédia Cover Sequence

Acadian deformation produced folds, cleavage, and most faults, i.e. the dominant structural elements affecting all rock units in the MCS. The significant folds and faults in the MCS (Fig. 1-4a, b) and a compilation of average Acadian cleavage and fold axial trends in various parts of the Matapédia Cover Sequence is presented in (Wilson et al., 2017).

In this study, D1–D3 refer sequentially to early Salinic thrust-related deformation (ca. 450–430 Ma), subsequent Silurian folding/fabric development, and latest Silurian–earliest Devonian extensional collapse (van Staal, 1994; Wilson et al., 2017).

D1 is the earliest deformation phase and is expressed by penetrative foliation (S1), stretching lineation (L1), and asymmetric F1 folds. It formed under high-strain conditions associated with thrusting, resulting in sheath folds, younging reversals, boudinage, mylonitization, vein networks, and stratigraphic repetitions where older rocks overlie younger successions. In the Aroostook–Percé Anticlinorium, D1 features are attributed to the Late Silurian Salinic event that is manifested by broad, upright, northwest-trending F1 macrofolds, which are open to tight, shallowly plunging, and typically lack cleavage development (Wilson et al., 2005).

D2 is characterized by steeply dipping to upright F2 folds, commonly associated with a crenulation cleavage (S2). In the northern Miramichi Terrane, peak D2 deformation has been linked to sinistral transpression during the Late Silurian (van Staal, 1994; van Staal and de Roo, 1995). The timing of this Salinic deformation is constrained by structural and stratigraphic relationships, with D2 sinistral transpression occurring between 430 and 418 Ma. Uplift and erosion of the Miramichi Terrane around 426–421 Ma (late Wenlockian–early Ludlovian) supplied detritus to the Simpsons Field Formation (van Staal et al., 2003; Wilson et al., 2005).

Although the majority of faults are Acadian, a few in the vicinity of the Miramichi and Elmtree inliers may have originated during latest Silurian to earliest Devonian Salinic (D2-D3) uplift and extensional collapse of Ordovician rocks, and reactivated during Acadian deformation (Wilson et al., 2017). Based on Figure 4a, the major Acadian dextral transcurrent faults in northern New Brunswick are, from north to south: Restigouche (Grand Pabos), Rocky Brook–Millstream, Moose Lake, and Catamaran Brook faults (Malo et al., 2000). In the western Chaleur Bay Synclinorium, Acadian structures are overprinted

by kink bands and crenulation cleavage, probably linked to D3 deformation of the Aroostook–Percé Anticlinorium (Wilson et al., 2005).

The Restigouche – Grand Pabos Fault shows evidence of brittle deformation superimposed on an earlier ductile deformation, which is consistent with early northwest directed reverse movement, followed by dextral strike-slip that continued into the Early Carboniferous (Malo et al., 2000).

It should be noted that the damage zone related to the Grand Pabos Fault in the Gaspé Peninsula is reportedly 9 km wide (Malo et al., 2000). Some compressive shortening occurred proximal to the Restigouche Fault in New Brunswick, based on the tight folding of rocks on the east side of the fault. A subsidiary fault, the Lower Downs Gulch Fault, is located 2 to 5 km east of the Restigouche Fault (Figure 1-4a).

Rocks between the Restigouche and the Lower Downs Gulch faults are brecciated and intruded by granodiorite dykes associated with the Patapédia copper skarn deposit (St Peter, 1978; Malo et al., 2000). In this study area, the Rocky Brook – Millstream Fault and its numerous splays are the major structural break in northeastern New Brunswick. Acadian cleavage is rotated clockwise in the vicinity of late-stage dextral faults of the Rocky Brook – Millstream Fault, and fold axes are similarly rotated and offset dextrally (Fig. 1-4b).

Faults in the MCS record multiple deformation phases. Salinic deformation (ca. 430–420 Ma, Late Silurian) produced early folding, thrusting, and regional unconformities, whereas Acadian deformation (ca. 415–395 Ma, Early Devonian) is characterized by an initial compressive phase of reverse faulting, followed by folding and cleavage development, and later dextral strike-slip faulting on major fault systems (e.g., Rocky Brook–Millstream, Restigouche–Grand Pabos) (Wilson et al., 2017).

It appears that the compressive stage is more complex, as some Acadian fold axes are truncated by reverse faults. The McKenzie Gulch Fault extends approximately 120 km from near the Maine border in the southwest to just east of Squaw Cap Mountain, where it is truncated by the Black Lake Fault (Figs. 1-3, 1-4). St. Peter (1978) proposed that several hundreds of metres of vertical offset occurred between the Boland Brook Formation (Grog Brook Group) to the west and the White Head Formation (Matapédia Group) to the east and noted that rocks adjacent to the fault are brecciated and carbonate veined (St Peter, 1978).

The McKenzie Gulch Fault may have been reactivated as a late Acadian normal fault, as a swarm of mainly felsic dykes (e.g., the late Early to Middle Devonian McKenzie Gulch Porphyry) are spatially associated with the fault.

Fault-associated folds overprint Acadian folds and strike northwest, highly inclined to the fault. They have an association with minor thrusts, shallow strike-slip surfaces having horizontal axes (Dimitrov et al., 2003; Wilson et al, 2017). Ductile strain is locally noted in rocks proximal to the Rocky Brook–Millstream Fault and some of the many splays related to it. The Campbellton area is transected by a network of ENE-trending dextral transcurrent faults and NNE-trending reverse faults. Detailed investigation of major faults in northern New Brunswick (i.e. Black Lake, Squaw Cap, Sugar Loaf, Mckenzie Gulch, Rocky Brook-Berry Brook, Rocky Brook- Millstream, and Sellarsville faults and their association with damage zones) indicate that during the Middle Paleozoic the region was part of a larger dextral transpressive system that extended north into the Gaspé Peninsula. The damage-zone assessment proposes that the these faults acted as a partial barrier to fluid flow during deformation. The structural control on gold mineralization and vein

emplacement is primarily related to dextral movement along the Rocky–Brook–Millstream fault system and its splays, e.g., the McCormack-Ramsay Brook faults, during Early Devonian Acadian orogenesis (Wilson , 2017).

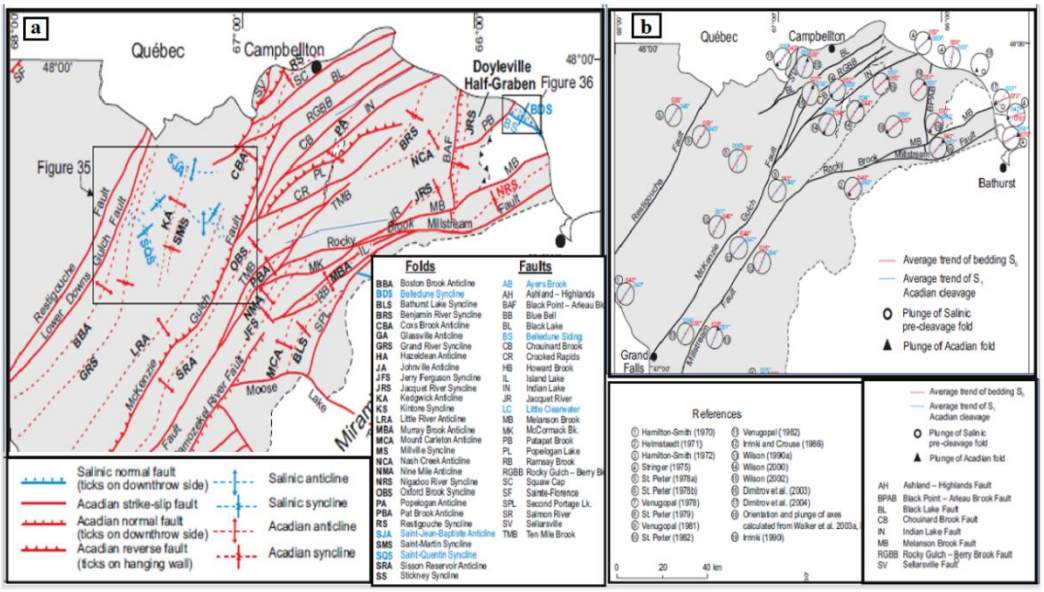

Figure 1-4. Significant folds, faults a), and cleavage b) in the Matapédia Cover Sequence (from Wilson, 2017).

1.8. Gold deposits and occurrences in Northern New Brunswick

Numerous gold occurrences/deposits occur in and around the Tobique-Chaleur Zone in northern New Brunswick and the adjacent Gaspé Peninsula (Table 1-1 and Fig. 1-5). Although these are dominantly orogenic style Au occurrences, a few epithermal style occurrences spatially related to the Rocky Brook-Millstream and the Restigouche Grand Pabos faults are recognized. For example, gold mineralization in the Williams Brook area exhibits characteristics of low-sulfidation epithermal style systems (Wilson, 2017; Mami Khalifani et al., 2025a, b). In northern New Brunswick, epithermal breccia and vein deposits carrying base metals ± Au and Ag occur in the northeastern part of the Chaleur

Bay Synclinorium and are commonly related to felsic intrusive rocks. Several Au occurrences in northern New Brunswick are spatially associated with major intrusions including the Nicholas Denys Granodiorite (Bradley Brook and Stephens Brook), the Nigadoo Porphyry (Nigadoo deposit), and a possible blind felsic intrusion near the Antinouri Lake Granite (Patapat Brook). The McKenzie Gulch Cu-Ag deposit is hosted by garnet-diopside skarn and hornfels and calc-silicate-altered rocks peripheral to a series of north-northeast-striking, porphyritic felsic-intermediate dykes of the McKenzie Gulch Porphyry. Dykes occur in two types, with mineralization associated with plagioclase-hornblende porphyry type (Massawe and Lentz, 2020a, b; and 2021). Several occurrences of low-grade Au mineralization hosted by pyritiferous iron carbonate-altered sedimentary rocks of the Free Grant Formation have been investigated in the Upsalquitch Forks – Ramsay Brook area. These occurrences are spatially related to major splays of the Rocky Brook – Millstream Fault, specifically the McCormack Brook and Ramsay Brook faults, and with fine-to-medium grained mafic intrusions (Tremblay et al., 1993; Wilson, 2017).

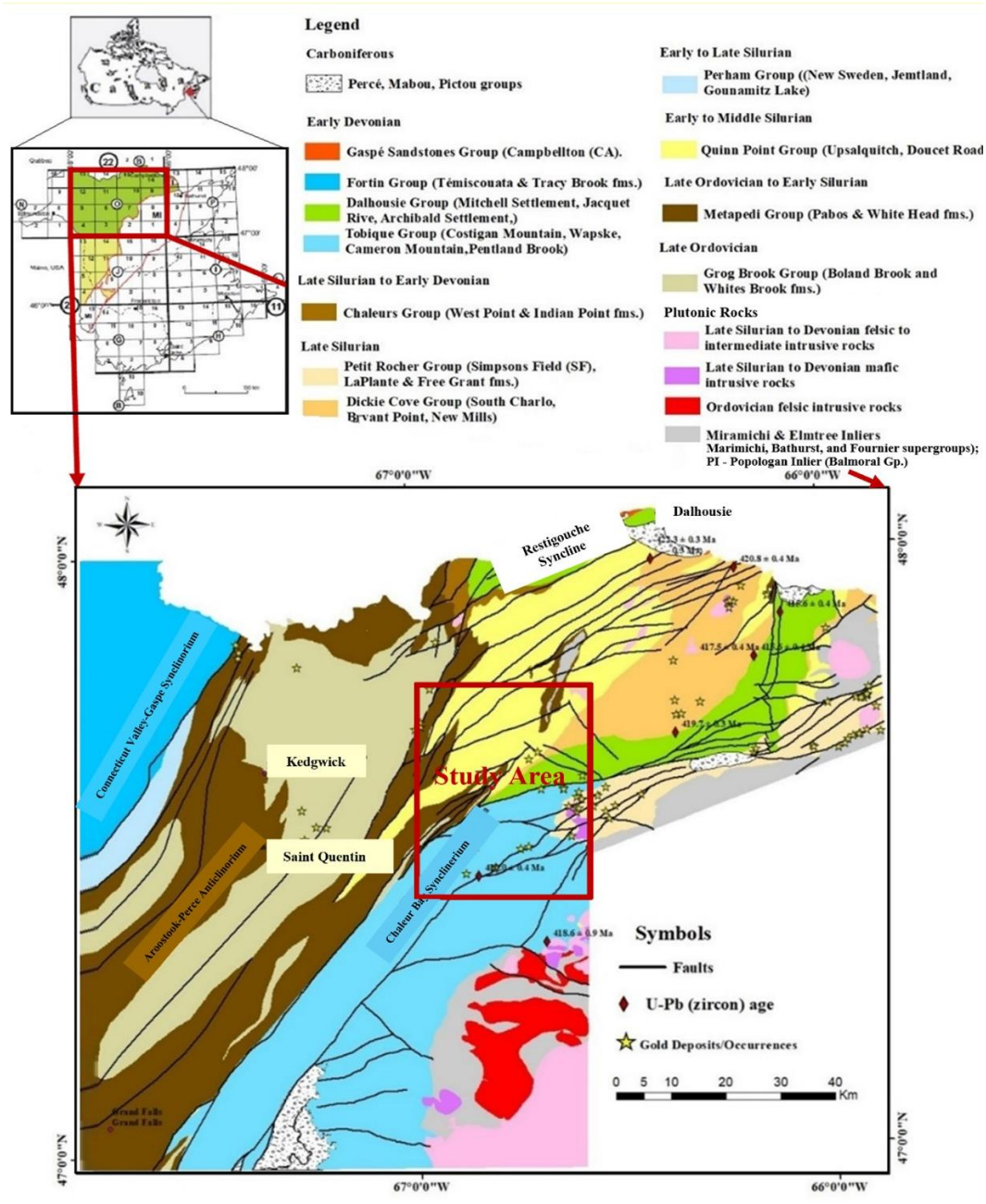

Figure 1-5. Regional geological map of northern New Brunswick showing the location of gold deposits/occurrences investigated in this study (modified from Wilson 2017).

Below is a literature review of several significant gold occurrences in northern New Brunswick, highlighting their geological settings, mineralization styles, and associated structural features.

1.8.1. Williams Brook

Gold mineralization at Williams Brook is hosted in the Siluro-Devonian bimodal volcanic-sedimentary rocks of the Wapske Formation. A sequence of interlayered rhyolite flows, rhyolite porphyries, laminated siltstones, and polymictic rhyolitic breccias, are overlain by basaltic flows. Two styles of mineralization have been identified: 1) early disseminated mineralization hosted in potassically altered rhyolites, characterized by refractory gold in muscovite/illite veinlets, and, 2) later-stage free gold in quartz veins containing hypogene sulfides (e.g., sphalerite, galena, pyrite) and supergene oxyhydroxides. These styles are interpreted to reflect a low-sulfidation epithermal system, with quartz veins formed along extensional fractures related to NE-SW strain, consistent with dextral movement along nearby regional faults (Sánchez- Mora, 2014; Sánchez-Mora et al., 2021).

Petrogenetic and geochronological investigations conducted by Sánchez-Mora (2014) at Williams Brook reveal a complex magmatic and mineralizing history linked to transpressional tectonics during the oblique convergence of Gondwana and Laurentia. U–Pb zircon dating of felsic volcanic rocks yielded ages between 422 ± 3 Ma and 401 ± 9 Ma, whereas Ar–Ar muscovite geochronology indicates hydrothermal activity at approximately 412–408 Ma. The volcanic rocks display A-type geochemical signatures enriched light rare earth elements (LREE), and notable negative anomalies in Nb and Eu, all of which are consistent with an extensional within-plate tectonic setting. Through fluid inclusion analyses and stable isotope studies, Sánchez-Mora demonstrated that gold deposition

occurred at temperatures around 200°C, likely due to mixing of magmatic fluids and meteoric waters. These findings support the interpretation of Williams Brook as a low-sulfidation epithermal gold system and highlight its significance within the northern Appalachian metallogenic framework (Sánchez-Mora, 2014; Sánchez-Mora et al., 2021).

1.8.2. McIntyre Brook

The McIntyre Brook Property, underlain by Devonian volcanic–sedimentary rocks and hosts two gold occurrences, McIntyre Brook and Big Pit, situated roughly 1.5 km apart. The McIntyre Brook occurrence is associated with a 480 m-wide gold-in-soil anomaly, with 40 anomalous grab samples returning values between 0.20 and 41.56 g/t Au over 300 m strike length (Lode Gold Resources Inc, 2019).

Mineralization is hosted by brecciated felsic intrusive and argillitic sedimentary rocks and is interpreted to reflect epithermal gold type mineralization. The Big Pit occurrence consists of a hematite-chalcopyrite vein, with values up to 1.44% Cu and 7.33 g/t Au. Both showings are located near the McIntyre Brook Fault, a splay of the Rocky Brook–Millstream Fault and lie within the Devonian Wapske and Greys Gulch formations (Lode Gold Resources Inc., 2019; Mami Khalifani et al., 2025).

Lode Gold Resources Inc. explored the McIntyre Brook Property through trenching, rock sampling, and diamond drilling. In 2019, two drill holes were completed beneath previously trenched areas, confirming gold mineralization continuity at depth. Drill hole MB019-04 returned 5.73 g/t Au over 2.0 m within a broader interval of 1.20 g/t Au over 20 m (core length; true thickness not determined). Soil geochemical surveys conducted in 2020 (2612 samples) further delineated gold anomalies and supported ongoing exploration.

The local geology comprises felsic and mafic volcanic rocks of the Greys Gulch Formation and sedimentary rocks of the Wapske Formation (Lode Gold Resources Inc, 2019).

1.8.3. Mulligan Gulch

The Mulligan Gulch Porphyry, located in north-central New Brunswick near the Rocky Brook–Millstream Fault, hosts four notable Au–Ag–Pb–Zn occurrences: Mulligan Gulch, Mulligan Gulch South, Humpback, and Mulligan Gulch Southwest. The porphyry intrudes sedimentary sequences of the Petit Rocher and Tobique groups and is interpreted to be a hypabyssal equivalent of regional felsic volcanic rocks. U–Pb zircon dating indicates an emplacement age of ~419 Ma (Bustard and Dahn, 2024). Gold mineralization is spatially associated with quartz ± sericite ± carbonate veins and occurs primarily with arsenopyrite–pyrite ± chalcopyrite ± tennantite ± galena ± acanthite. Alteration assemblages include least-altered porphyry, proximal sericitization, and a late phase resulting from hydrothermal interaction with surface water. These features are consistent with an intermediate-sulfidation epithermal environment (Bustard and Dahn, 2024; Mami Khalifani et al., 2025a, b).

Trenching and diamond drilling at the Mulligan Gulch and Mulligan Gulch Southwest occurrences have revealed multiple vein sets formed during protracted deformation under NW–SE sub-horizontal shortening. Four vein orientations are identified, with Sets 1 and 2 closely associated with mineralization, whereas Set 4 is exclusive to the southwest zone. Fluid mixing is interpreted to have triggered gold precipitation. The presence of cockade-textured quartz and arsenopyrite thermometry support episodic fluid flow. At Mulligan Gulch Southwest, the best drill intersection yielded 844 ppb Au over 0.5 m (GTMG-20-05, 99.9–100.4 m; Forest, 2021). Trenching at the same occurrence produced channel

samples grading up to 32.9 g/t Au and 579 g/t Ag (true thickness not determined; Gold Terra Resource Corp., 2022). The Mulligan Gulch mineral system shares notable geological similarities with Williams Brook and Williams Brook South, suggesting it may be part of a broader regional gold system within the Tobique-Chaleur zone (Bustard and Dahn, 2024).

1.8.4. Simpsons Field

The Simpsons Field gold occurrence is located within the structurally complex Rocky Brook–Millstream Fault Zone. It is hosted by Silurian sedimentary rocks of the Petit Rocher Group, including terrestrial to shallow-water deposits of the Simpsons Field Formation, characterized by brick-red to maroon pebble to boulder conglomerate and lithic sandstone. The mineralized zones occur primarily in calcareous siltstones of the Budworm City Formation and are spatially associated with less-deformed gabbroic dykes and sills. The site lies near the intersection of the Ramsay Brook and Portage Lake faults subsidiary structures of the main fault zone highlighting the importance of structural controls and mafic intrusions in localizing gold mineralization.

Gold at Simpsons Field is hosted in narrow quartz-carbonate veins in intensely silicified and carbonatized siltstone. The alteration assemblage comprises quartz, siderite, pyrite, and hematite, with minor chalcopyrite, arsenopyrite, sericite, and biotite. Gold grains, averaging ~6 μm, are typically enclosed within or situated along the boundaries of sulfide minerals, particularly pyrite, suggesting the presence of refractory gold. The mineralization style, characterized by extensive silicification, sericite-adularia alteration, and sulfide enrichment, supports its classification as a low- to intermediate-sulfidation epithermal gold system.

Since the 1980s, exploration activities including those by Brunswick Mining & Smelting Corp. and Lode Gold Resources Inc have delineated east–west-trending alteration zones with significant assay results. Trenching and drilling have reported grades such as 1.37 g/t Au over 6 meters and up to 6.46 g/t Au in chip samples. Airborne magnetic gradiometer surveys identified prominent magnetic anomalies interpreted as mafic dykes, which correlate with mineralized zones, reinforcing the structural and intrusive controls on mineralization.

Recent geochemical studies conducted by Mami Khalifani et al. (2022, 2023a, b), employing portable and micro-XRF instruments alongside compositional data analysis (CoDA), cluster analysis, and principal component analysis (PCA), have enhanced the understanding of the geochemical characteristics of the Simpsons Field system. The results demonstrate strong correlations between gold and key pathfinder elements, including Cu, K, Zn, Mo, and Fe, with sericitic alteration and sulfide enrichment emerging as significant indicators of mineralization. The integration of geological, structural, geochemical, and geophysical datasets collectively supports the classification of Simpsons Field as an epithermal gold system with substantial exploration potential (Mami Khalifani et al., 2022, 2023a, b).

1.9. Epithermal gold mineralization

Epithermal gold deposits are hydrothermal systems that form at shallow crustal levels, typically within 1–2 km of the paleosurface at temperatures ranging from approximately 150°C to 300°C (John et al., 2018). These systems represent the uppermost levels of vertically zoned magmatic-hydrothermal environments and commonly overlie deeper porphyry Cu-Au systems (Hedenquist and Arribas, 2022). Epithermal deposits are closely

associated with volcanic arcs and extensional tectonic regimes, particularly in settings dominated by calc-alkaline to rhyolitic volcanism, and they constitute important global sources of gold and silver (John et al., 2018). The formation of these deposits is driven by the ascent of metal-rich magmatic fluids through structural conduits, such as faults and fractures, which interact with descending meteoric waters within a complex hydrothermal "plumbing system" (White and Hedenquist, 1995). Two principal mechanisms control ore deposition: boiling, triggered by pressure drops that cause gases like CO_2 and H_2S to exsolve—and fluid mixing, which alters temperature, pH, and redox conditions, favoring the precipitation of precious metals, i.e. gold and silver (White and Hedenquist, 1995).

Epithermal systems are generally classified into low- intermediate, and high-sulfidation types based on fluid chemistry and mineral assemblages. Among these, low-sulfidation (LS) and high-sulfidation (HS) systems are the most distinctive. LS systems are formed from neutral to slightly acidic hydrothermal fluids that are commonly diluted by meteoric water. These systems are structurally controlled and typically precipitate gold and silver within open-space quartz-adularia-calcite veins, often displaying crustiform, colloform, and banded textures indicative of episodic boiling (White and Hedenquist, 1995; Corbett, 2002; John et al., 2018). Ore minerals in LS systems include electrum, native gold, and silver sulfides such as acanthite and naumannite. Alteration zones in LS systems show a characteristic lateral zoning pattern from a core of quartz-adularia±illite outward into illite-smectite and ultimately propylitic assemblages (chlorite-epidote-calcite) (Hedenquist and Arribas, 2022).

In contrast, HS systems are formed by the direct discharge of highly acidic magmatic vapors rich in SO_2, HCl, and HF, with minimal dilution by meteoric waters. These acidic

fluids cause pervasive leaching of the host rocks, producing residual vuggy silica cores and enveloping advanced argillic alteration halos composed of alunite, pyrophyllite, kaolinite, and quartz (White and Hedenquist, 1995; Corbett, 2002; John et al., 2018; Hedenquist and Arribas, 2022). HS mineralization is commonly disseminated- or replacement-type and typically features minerals such as enargite, luzonite, covellite, and gold associated with pyrite halos. Vertical alteration zoning is a diagnostic feature, transitioning from barren vuggy silica to quartz-alunite, then quartz-pyrophyllite, and finally quartz-illite or sericite zones (John et al., 2018).

The gold occurrences in the Tobique–Chaleur Zone of northern New Brunswick represent important examples of epithermal mineral systems spatially and structurally associated with the Rocky Brook–Millstream Fault system and its subsidiary splays. Despite a recent increase in exploration activity, the region's extensive cover and structural complexity continue to present significant challenges for defining the distribution and controls of gold mineralization. This study aims to enhance the understanding and prediction of epithermal gold systems by integrating geoscientific, geochemical, and machine learning approaches into a predictive framework tailored for structurally controlled mineral systems. Building on the geological context of northern New Brunswick and earlier work by Sánchez-Mora et al. (2021) and Mami Khalifani et al. (2022, 2023a), this research employs a multi-scale approach that incorporates geochemical vectoring, mineral system modeling, and supervised machine learning to constrain the processes, pathways, and geospatial expressions of gold mineralization (Sánchez Mora, 2014; Sánchez-Mora et al., 2021; Mami Khalifani et al., 2022, 2023a, b).

A widely accepted conceptual model, originally developed by White and Hedenquist (1995) and refined by Hedenquist and Arribas (2022), provides a comprehensive framework for understanding the spatial and vertical distribution of low- and high-sulfidation (LS and HS) epithermal systems within volcanic environments (White and Hedenquist, 1995; Hedenquist and Arribas, 2022). As illustrated in Figure1-6 of the current guide, LS deposits typically form along structurally controlled pathways such as faults and fractures—that are positioned above or lateral to magmatic intrusions. In contrast, HS systems tend to be localized directly above intrusions, often within volcanic domes or collapse structures like calderas, where the discharge and condensation of acidic magmatic volatiles near the surface generate the extreme chemical conditions required for HS-type mineralization (Corbett, 2002; Hedenquist and Arribas, 2022). This model also underscores the genetic linkage and vertical continuity between epithermal systems and underlying porphyry-style mineralization, emphasizing their coexistence within a single magmatic-hydrothermal system. From an exploration perspective, identifying characteristic alteration halos and mineralogical zonation patterns is of paramount importance, as these features commonly extend well beyond the mineralized zones and provide critical vectors for delineating concealed ore bodies (John et al., 2018).

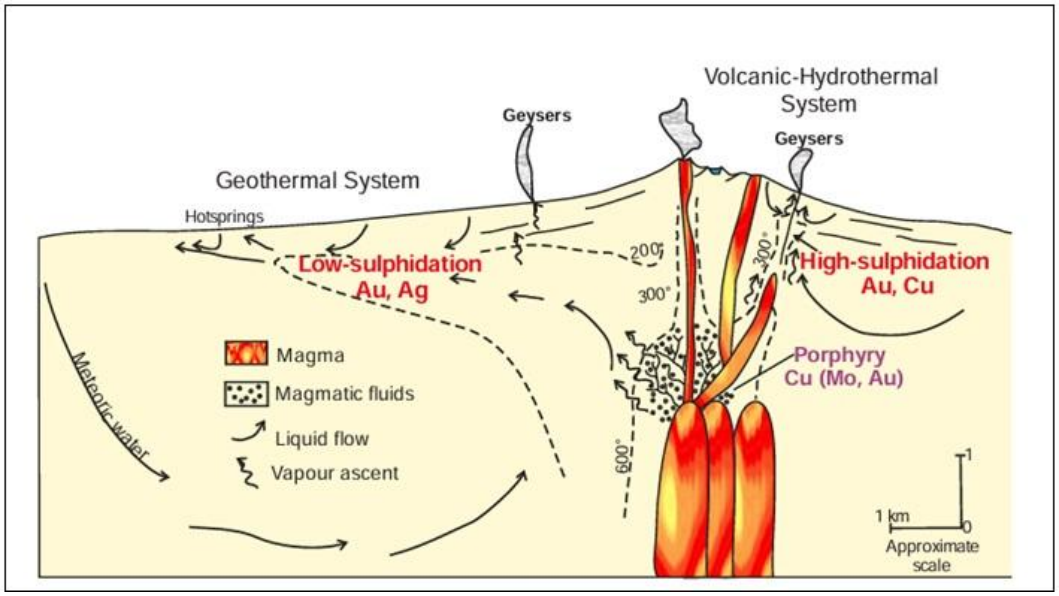

Figure 1-6. Simplified model for porphyry, LS and HS systems (from Hedenquist and Lowenstern, 1994).

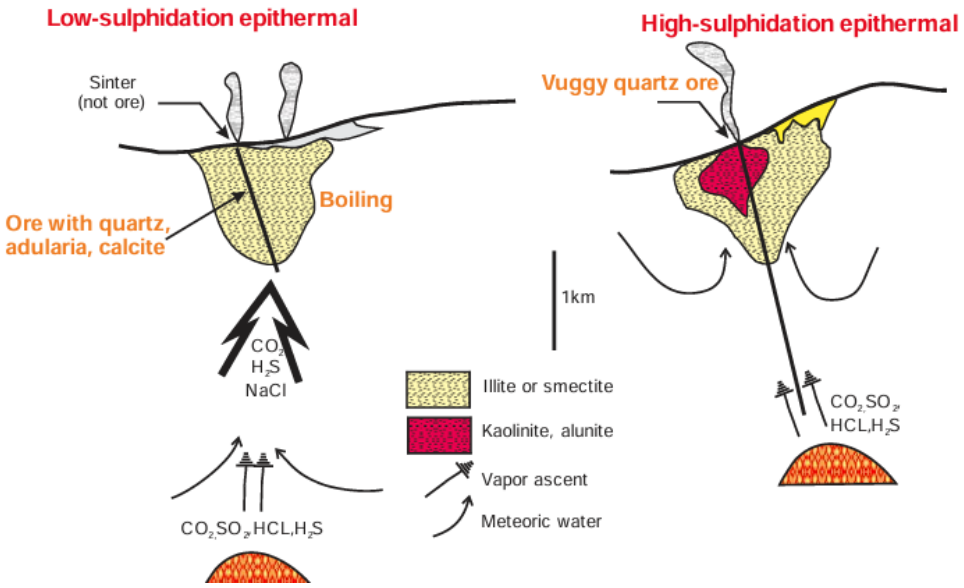

Figure 1-7. Simplified model for fluid types and alteration zoning around LS and HS systems (White and Hedenquist, 1995).

1.10. pXRF Analysis

Portable X-ray fluorescence (pXRF) has emerged as one of the most widely used rapid geochemical techniques in mineral exploration and applied geoscience. The method operates by irradiating a sample with primary X-rays, which causes atoms within the material to emit secondary, element-specific fluorescent X-rays that are detected by an energy-dispersive spectrometer. The intensity of these signals is directly related to elemental concentrations, allowing the device to produce multi-element geochemical data within seconds to minutes (Hall et al., 2011, 2014). Because pXRF analysis is non-destructive and requires little to no preparation, the technique is particularly suited to field deployment, generating immediate results at the outcrop, drill site, or soil grid (Hall et al., 2014; Heidarian et al., 2021). Figure 1-7 illustrates a typical pXRF instrument configuration used in field and laboratory settings.



Figure 1-8. Portable X-ray fluorescence (pXRF) analyzer on a stand with laptop interface for data collection, commonly used in laboratory and field settings.

The two principal calibration strategies that underpin pXRF are fundamental parameters (FP) and empirical calibrations. FP calibrations, generally pre-loaded by manufacturers, apply physics-based algorithms that approximate X-ray interactions in a generalized way, providing semi-quantitative data suitable for reconnaissance surveys (Hall et al., 2014). Empirical, matrix-matched calibrations, in contrast, are built using certified reference materials or in-house standards that reflect the geological matrix of interest, thereby correcting for absorption, enhancement, and inter-element interference effects (Harraden et al., 2025).

Multiple studies have demonstrated that matrix-matched calibrations provide the most accurate results for quantitative geochemistry, whereas FP approaches are sufficient for mapping relative anomalies in early-stage exploration (Hall et al., 2014; Harraden et al., 2025). The use of reference standards is fundamental to ensuring reliable portable X-ray fluorescence (pXRF) analysis. As shown in Figure 2, standards are typically prepared in sample cups and sealed with thin films or bags, containing either certified reference materials (CRMs) or well-characterized in-house materials. These standards are essential for developing empirical, matrix-matched calibrations that correct for absorption and inter-element effects not accounted for in factory fundamental parameter models (Hall et al., 2014; Harraden et al., 2025). By repeatedly analyzing standards alongside unknown samples, users can adjust for systematic biases and improve the quantitative accuracy of pXRF datasets, particularly for trace elements and complex geological matrices. In addition to calibration, standards serve as part of quality assurance and quality control (QA/QC)

protocols, where they are inserted at regular intervals to monitor precision, instrument drift, and contamination (Hall et al., 2014). They also provide a means of determining empirical limits of quantification, which are commonly higher than theoretical detection limits and must be defined to ensure defensible reporting of results (Harraden et al., 2025). In mineral exploration, standards enriched in elements such as As, Cu, and Zn are particularly valuable for validating anomaly maps of gold and base metal pathfinders, while in environmental assessments, Pb- and Zn-rich standards are routinely employed to anchor measurements within regulatory thresholds (Hall et al., 2014; Zhou et al., 2023). Thus, the preparation and consistent use of standards underpin the credibility and reproducibility of pXRF applications across exploration, mining, and environmental monitoring.

Figure 1-9 shows an example of reference standards prepared in sample cups and bags for calibration and quality control.



Figure 1-9. Reference standards in sample cups and bags for pXRF calibration and quality control, used to build empirical calibrations and ensure reliable geochemical data.

The main purpose of employing pXRF is to accelerate data acquisition in mineral exploration while reducing dependence on laboratory turnaround times. Its strengths are most apparent in generating high-density geochemical datasets that reveal geochemical

trends across soil, till, and bedrock sampling grids (Hall et al., 2014). Elements such as arsenic, copper, and zinc are reliably quantified and often show strong correlations with laboratory assays, making them valuable pathfinders for gold and base metal mineralization (Hall et al., 2014; Zhou et al., 2023). In contrast, elements such as antimony, which typically occur near the instrument's limit of detection, may produce noisier datasets and false positives. Nevertheless, large anomalies can still be recognized effectively in the field, underscoring the importance of using laboratory validation to confirm subtle geochemical signatures (Hall et al., 2014; Zhou et al., 2023).

The accuracy and precision of pXRF are also strongly influenced by measurement time and sample preparation. Controlled experiments on nearly one hundred rock powders demonstrated that analytical precision increases significantly between 40 and 80 seconds per beam, but that longer durations yield diminishing returns (Hall et al., 2014). For most exploration contexts, ~80 seconds per condition provides an optimal balance between speed and reproducibility. Major rock-forming elements such as Fe and Si can be quantified in short runs, while trace pathfinders like Cu, As, and Mo require longer acquisition times to minimize relative error (Hall et al., 2011, 2014). Sample preparation is equally critical: flat, clean, and dry surfaces minimize spectral noise, whereas fine fractions in plastic or polyester bags are commonly used for soil analysis. Drift in field campaigns is controlled through quality control protocols that include analysis of blanks, duplicates, and certified reference materials, often inserted at regular intervals (Hall et al., 2014; Zhou et al., 2023).

Case studies from northern Canada illustrate the effectiveness and limitations of pXRF at the property scale. At the Whiskey project in Yukon and Kiyuk Lake in Nunavut, thousands

of soil and till samples were analyzed in the field using factory calibrations, while all samples were also submitted for laboratory ICP-MS assays. The pXRF results successfully reproduced relative patterns of key pathfinder elements such as As and Cu, which guided immediate follow-up in remote field conditions (Hall et al., 2011, 2014). However, Sb measurements were inconsistent, generating noisy maps with false anomalies that required laboratory confirmation. These results demonstrate the concept of "fit-for-purpose" application: for reconnaissance and real-time decision-making, relative anomaly patterns are sufficient, but high-precision data must still rely on laboratory analyses (Hall et al., 2014).

Beyond reconnaissance surveys, pXRF has also been integrated into controlled calibration and methodological studies. Harraden et al. (2025) reviewed more than thirty empirical calibration models and highlighted how regression design, multi-condition configurations, and interference corrections influence accuracy. They emphasized that reliable reporting must be based on empirical limits of quantification, which are often one order of magnitude higher than statistical detection limits. This underscores the necessity of defining project-specific reporting thresholds when using pXRF in quantitative studies.

Applications of pXRF extend across the entire mining cycle. In active operations, properly calibrated pXRF instruments are employed for ore–waste discrimination and grade control, allowing near-instantaneous adjustments to mining faces. In mine closure and environmental monitoring, pXRF has been successfully applied to delineate contaminated soils and waste rock piles, particularly for Pb, Zn, As, and Cu (Barago et al., 2022). These applications show that pXRF is not a replacement for laboratory geochemistry but a powerful complement that accelerates workflows, enables adaptive exploration strategies,

and provides dense spatial datasets otherwise impossible to generate in time- and budget-limited programs.

Overall, the literature demonstrates that pXRF has matured from a reconnaissance tool to a mainstream technique integrated across exploration, mining, and environmental management. Its greatest strength lies in enabling rapid, cost-effective decisions, provided that users clearly define "fit-for-purpose" objectives, employ rigorous QA/QC, and validate results against laboratory benchmarks. With these practices, pXRF delivers reliable, actionable geochemical data that bridges the gap between field efficiency and geoscientific rigor (Hall et al., 2011, 2014; Harraden et al., 2025).

1.11. µXRF Analysis

Micro–X-ray fluorescence (µXRF) is a non-destructive, energy-dispersive XRF imaging technique that focuses an X-ray beam onto an area tens to hundreds of micrometres in diameter to excite characteristic fluorescence from the sample. Detectors then record photon energies and intensities to produce spatially resolved elemental maps over hand-sample to core-scale surfaces. In practice, benchtop instruments raster a polished surface and produce multi-element maps with pixel sizes commonly ~20–100 µm, bridging the scale gap between thin-section petrography/SEM and metre-scale core logging has enabled rapid mapping over cm–dm areas in a few hours while preserving ppm-level sensitivity for many elements. These developments make µXRF well suited to visualize textures (veins, alteration selvages, sulphide dissemination) and to quantify element distributions that are not apparent in hand specimen (Fabre et al., 2022). Figure 1-9 shows a typical benchtop µXRF) system used to raster polished slabs and cores and generate multi-element maps.

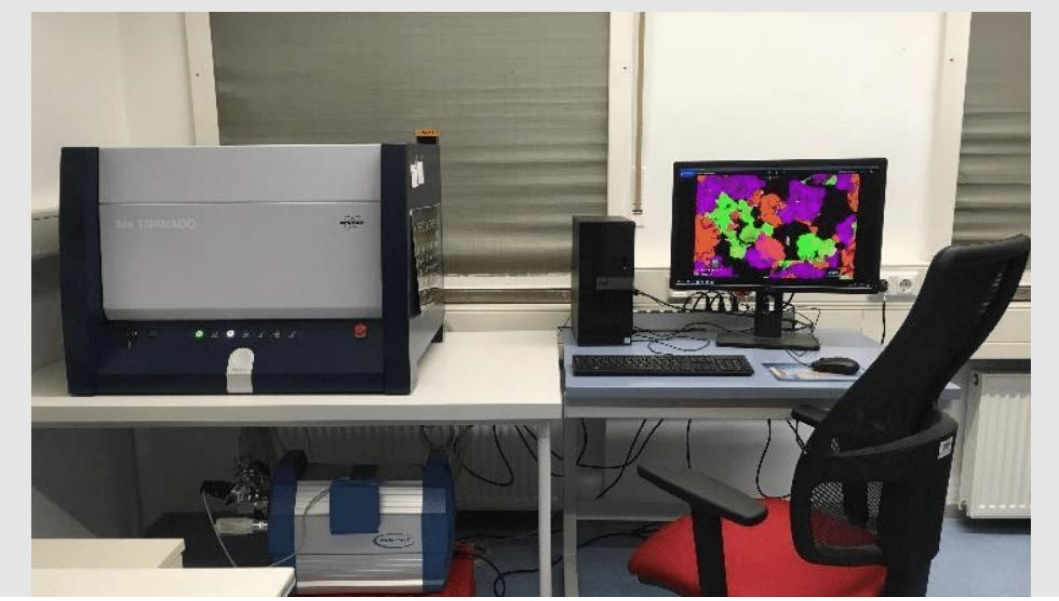

Figure 1-10. µXRF workstation used in this study for quantitative elemental imaging and subsequent mineral mapping, complementing pXRF and bulk geochemical assays.

Methodologically, µXRF maps are acquired as X-ray spectra at each pixel and can be used directly as elemental images or converted to mineral maps through quantitative or machine-learning approaches. A widely adopted workflow quantifies spectra using a fundamental-parameters (FP) model and then estimates per-pixel mineral proportions with optimization (e.g., linear programming) or supervised classification, optionally calibrated to whole-rock to improve accuracy; this has delivered low errors in altered, fine-grained rocks where hand specimen/mineral optics are ambiguous (Barker et al., 2021). Quantitative conversions from multi-element µXRF to mineralogy can also be achieved with automated spectral classification (e.g., spectral angle mapper) or supervised learning; compared across porphyry samples, supervised methods particularly Random Forests showed the lowest normalized errors and faithfully represented mineralogical textures, while unsupervised k-

means is effective for rapid first-pass interpretation (Nikonow and Rammlmair 2017; Harraden et al., 2025).

The purpose of using μXRF in exploration and ore characterization is threefold: first, to map alteration and mineralization footprints at high spatial resolution across large rock or core surfaces, revealing mineral and metal zonation tied to fluid pathways; second, to quantify modal mineralogy and textures (e.g., veining, replacement fronts, sulphide deportment) to inform paragenesis and processing; and third, to link whole-rock or pXRF geochemical anomalies to specific mineral hosts, thereby de-risking interpretations and guiding follow-up work (petrography, geochronology). In VMS exploration, μXRF maps of felsic dome-flow complexes distinguished lateral and vertical alteration zonation (silicification proximal to vents, sericite–chlorite trends distally/vertically), validating whole-rock interpretations when heterogeneity in volcaniclastic facies confounds bulk assays (Genna et al., 2011).

Numerous case studies illustrate capability across commodities and textures. μXRF has been used on pegmatite drill core to characterize element distributions at the centimeter scale with minimal preparation, leveraging large-chamber stages to accommodate diverse sample geometries and to resolve the spatial relationships among major, minor, and some trace elements in zoned pegmatitic textures (Potter and Brand, 2019). Automated μ-XRF mineralogy on plutonic thin sections, using supervised spectral classification, has produced modal mineralogy and mineral distribution maps comparable to SEM-based method but with simpler preparation and faster turnaround, reinforcing μXRF's role as a fast overview tool that guides higher-resolution or destructive analyses (Nikonow and Rammlmair, 2017).

μXRF complements, not replaces, portable XRF (pXRF) and laboratory methods. In integrated workflows, pXRF supplies high-density, rapid, pointwise or small-spot chemistry for anomaly detection across grids and core trays, while μXRF interrogates selected slabs or thin sections to connect those anomalies to textures and mineral hosts. In southern New Brunswick gold systems, pXRF+PCA highlighted alteration versus mineralization element groups, and μXRF maps on the same samples confirmed sericitic/chloritic alteration with sulphides in quartz(-carbonate) veins and located potentially datable phases (titanite, rutile, apatite, monazite) for follow-up chronometry demonstrating how μXRF adds mineralogical and geochronological context to field-scale geochemistry (Heidarian et al., 2021).

Although pXRF reviews focus on field deployment and sample-prep effects, they underscore the strategic value of XRF-based in-situ geochemistry for situational awareness; in that context, μXRF serves as the laboratory-bench analogue that resolves fine-scale spatial questions the handheld cannot address (Young et al., 2016).

In this research, μXRF is warranted as it provides high-resolution, non-destructive elemental and mineralogical mapping that corroborates pXRF geochemical patterns, precisely identifies the sulfide hosts of gold, and characterizes alteration domains critical for interpreting fluid pathways and mineralization processes.

1.12. Mineral Prospectivity Mapping

Exploration targeting is an essential step in any mineral exploration program. Targeting is a scientific endeavor that synthesizes information from multiple geoscience datasets and incorporates those data into spatially referenced data layers. These spatially referenced multi-parameter databases can be queried to create a semi-quantitative ranking of

promising areas at the global, provincial, and local scales. The science of exploration targeting should be employed in all exploration endeavors to reduce risk and provide more cost-effective project exploration through direct detection technologies and methodologies. Mineral prospectivity mapping (MPM) serves as a fundamental tool in modern mineral exploration by identifying areas with elevated potential for undiscovered mineralization. MPM can be utilized to help explorers generate projects, recognize targets, and enhance exploration efficiency by reducing costs and project execution time (Bonham-Carter et al., 1994; Carranza et al., 2008; Hronsky and Groves, 2008). MPM as a multi-criteria decision-making (MCDM) process is commonly applied when exploring for a specific deposit type at a particular geographic scale (Carranza et al., 2008; Hronsky and Groves, 2008; Carranza, 2015), in which multiple exploration datasets are assessed for the purpose of discovering new ore bodies (Zuo et al., 2015).

MPM techniques are broadly categorized into knowledge-driven and data-driven approaches. According to Carranza (2015), knowledge-driven methods are used for predictive MPM in unknown areas (greenfield regions) to identify those areas with the highest potential, which can then be further explored with more detailed exploration techniques such as geochemical or geophysical surveys and drilling. This approach relies on geological knowledge, mineral system models, and expert judgment to assign weights to predictive layers using techniques such as fuzzy logic and index overlay (Liu et al. 2021, 2023; Nykänen et al. 2023; Khammar et al. 2024; Mami Khalifani et al. 2025a, b). While useful for integrating conceptual understanding of ore-forming processes, the subjective nature of these methods may introduce bias and limit reproducibility.

In contrast, data-driven approaches utilize statistical and machine learning (ML) algorithms to uncover spatial relationships among known mineral occurrences and predictive variables derived from geoscientific datasets. These methods reduce subjectivity and increase predictive power by relying on the statistical behavior of the data (Yousefi et al., 2024; Khammar et al., 2024).

Data-driven methods of MPM are utilized to provide predictive models in order to have access to sufficient indicator layers of information in well-explored (brownfield) areas. It should be noted that these indicator layers of information are used as "training data" for identifying correlation among various exploration datasets (i.e., geological, geochemical, and geophysical) and mineral occurrences (Hronsky and Groves, 2008).

To reduce the effects of subjectivity on MPM, McCuaig et al. (2007) proposed a process-oriented mineral systems approach instead of the application of descriptive deposit models, because the latter focuses on the geological features of the deposit scale rather than the geological processes. This approach has been tested and adopted by many researchers as it provides a robust geological framework for translating the expressions of processes critical to the formation of mineral deposits into mappable targeting criteria (Ford et al., 2019; Wei et al., 2020; Davies et al., 2020).

The primary purpose of this research is to produce mineral potential mapping criteria to delimit the promising areas for gold deposit exploration in northern New Brunswick. Structural lineaments have a significant impact on evaluation of gold systems; therefore, accurate recognition of the structural features facilitates mineral exploration targeting of potentially mineralized areas. In addition, structural features (e.g., shear zones, faults, lineaments, or discontinuities) control fluid flow associated with a variety of geological

processes, and is significant in a variety of gold-deposit types (Richards, 2000; Mohebi et al., 2015; Carranza et al., 2015).

In this study, mineral prospectivity maps were generated through the integration of both knowledge-driven and data-driven approaches. The knowledge-driven framework applied fuzzy logic and geometric averaging to translate mineral system criteria into mappable evidence layers, whereas the data-driven framework employed supervised machine learning algorithms, including Random Forest, Support Vector Machine, and XGBoost. A concentration–area fractal model and ensemble methods such as majority voting and a confidence index were further used to refine thresholds, enhance prediction robustness, and quantify uncertainty, ensuring that the resulting maps effectively delineate favorable zones for epithermal gold mineralization.

1.13. Purpose and framework of the study

The dissertation comprises five chapters, each representing a distinct yet interconnected component of the research framework:

Chapter 1 provides the regional and geological framework for this research, focusing on the northern Appalachians and the Tobique–Chaleur Zone of northern New Brunswick, where several epithermal gold occurrences (Williams Brook, McIntyre Brook, Mulligan Gulch, and Simpsons Field) are spatially associated with major fault systems. It reviews the tectonic evolution, stratigraphy, and structural setting of the region, outlines the characteristics of epithermal gold mineralization, and introduces the analytical and methodological approaches employed in this study. These include portable (pXRF) and micro-XRF (μXRF) spectrometry, multivariate statistical analyses, and predictive mineral prospectivity mapping (MPM) using both knowledge-driven and data-driven methods

supported by ensemble and fractal-based approaches. Together, this framework establishes the foundation for integrating geoscience datasets into a robust mineral systems model for predicting favorable zones of gold mineralization.

Chapter 2 focuses on the detection of gold mineralization using portable and micro-X-ray fluorescence (pXRF and μXRF) spectrometry. Selective core intervals from four gold occurrences were analyzed, followed by multivariate compositional data analysis (CoDA), clustering, and principal component analysis to identify pathfinder elements and alteration signatures. These results reveal consistent associations of gold with sulfides and sericitic, potassic, and silicification alteration, providing geochemical and mineralogical constraints on the mineralizing system.

Chapter 3 introduces a mineral systems framework for predictive modeling, integrating knowledge-driven methods (fuzzy logic, geometric average) and a data-driven logistic regression approach. Geospatial evidence layers were generated from geological, geophysical, and geochemical datasets to reflect key ore-forming components (source, pathway, trap). Prospectivity maps were reclassified using a concentration–area fractal method, with the fuzzy logic model yielding the highest accuracy. This hybrid approach demonstrates the viability of combining conceptual and empirical methods for mineral targeting.

Chapter 4 applies supervised machine learning algorithms—Random Forest (RF), Support Vector Machine (SVM), and XGBoost to generate mineral prospectivity maps for epithermal gold in the study area. Using 24 evidence layers derived from multi-source datasets, model performance was evaluated using ROC and prediction–area (P–A)

analyses. Ensemble modeling via majority voting and the development of a confidence index map further refined the predictive outputs and addressed uncertainty.

Chapter 5 synthesizes the findings of the preceding chapters, drawing conclusions about the geological, geochemical, and structural controls on gold mineralization in the Tobique–Chaleur Zone. It also outlines the broader implications of the study for exploration strategies in analogous settings and offers recommendations for future work, including the potential for incorporating geochronological constraints and deep-learning methods in prospectivity modeling.

Together, these integrated investigations present a replicable and data-rich framework for gold exploration in covered terrains and contribute to the growing body of knowledge on machine learning–assisted mineral systems modeling.

1.14. Co-author contributions

This research comprises five chapters and was conducted in collaboration with Prof. David Lentz and Drs. Jim Walker of the New Brunswick Geologic Survey and Dr. Stefan Kruse of Terrane Geoscience.

Prof. Lentz served as supervisor and mentor, providing sustained guidance and support throughout the project, and his role formally included resources, supervision, review and editing, and funding. Dr. Walker contributed field expertise and practical guidance during critical stages, and is credited with resources, review and editing, and funding. Dr. Kruse provided advisory input, constructive critique, and geological perspective that strengthened the dissertation's interpretations.

Paper 1 (Chapter 2): "Advancing Gold Mineralization Detection in Northern New Brunswick Through Portable X-ray and Micro-X-ray Fluorescence Spectrometry with

Multivariate Compositional Data Analysis (CoDA) and Clustering for Pathfinder Elements and Alteration Analysis". This study establishes field-to-lab geochemical validation for four northern New Brunswick Au occurrences using portable XRF (pXRF) and micro-XRF (μXRF), then interprets multivariate signatures with compositional data analysis (biplots, clustering) to link Au to sulfides and alteration (illite/muscovite, silicification, potassic) in felsic–intermediate hosts. It defines practical vectors and element associations that underpin later targeting work.

Co-author contributions: First author led sampling, pXRF analysis/processing, and writing; Prof. Lentz provided conceptualization, supervision, and funding; Dr. Walker provided review and editing. Funding sources acknowledged include UNB and the New Brunswick Department of Natural Resources and Energy Development.

Paper 2 (Chapter 3): "Applying Mineral System Criteria to Develop a Predictive Modelling for Epithermal Gold Mineralization in Northern New Brunswick: Using Knowledge-Driven and Data-Driven Methods." This chapter translates ore-forming processes into mappable criteria using fuzzy logic and geometric average (knowledge-driven) alongside logistic regression (data-driven), then integrates the results via a concentration–area fractal reclassification. The hybrid model partitions the region into favourability zones and achieves strong predictive skill (AUC ≈ 0.97) where high-potential areas align with known Au occurrences.

Co-author contributions: First Author are credited with methodology, software, formal analysis, data curation, original drafting, revision, and visualization; Prof. Lentz with resources, supervision, review/editing, and funding; Dr. Walker with resources,

review/editing, and funding; Fereshteh Khammar with conceptualization of mineral-systems criteria, methodology, validation, and editing.

Paper 3 (Chapter 4): “Applying Random Forest, Support Vector Machine, and XGboost for Mineral Prospectivity Mapping of Epithermal Gold Mineralization: Northern New Brunswick”. Building on the mineral-systems layer design, this paper trains Random Forest, SVM, and XGBoost models on 24 geological, geophysical, and geochemical evidence layers. Model performance is evaluated with ROC and prediction–area curves; an ensemble with a confidence index improves robustness and guides field validation, while recommendations outline extensions.

Co-author contributions: Farzaneh Mami khalifani: Methodology, Analysis, Coding, Data Curation, Writing – Original Draft, and Visualization. Prof. Lentz: Resources, Supervision, Review & Editing, and Funding Acquisition. Dr. Walker: Resources, Review & Editing, and Funding Acquisition.

Paper 1 anchors the geochemical and mineralogical signatures at deposit scale (pXRF/μXRF + CoDA), Paper 2 formalizes those signatures as mineral-systems predictors in a hybrid favourability model, and Paper 3 generalizes targeting with supervised ML and uncertainty-aware ensembles. Together they deliver a coherent exploration framework for structurally complex, partly covered terranes in northern New Brunswick.

I sincerely thank all co-authors of the published paper, the accepted paper, and the manuscript currently under final review, which together form the main components of this thesis. Their contributions were invaluable. The three papers are listed below.

Mami khalifani, F., Lentz, D.R. and Walker, J.A., 2025. Advancing Gold Mineralization Detection in Northern New Brunswick Through Portable X-ray and Micro-X-ray

Fluorescence Spectrometry with Multivariate Compositional Data Analysis (CoDA) and Clustering for Pathfinder Elements and Alteration Analysis. Geochemistry: Exploration, Environment, Analysis, pp.geochem2024-058.

Mami Khalifani, F., Lentz, D.R., Walker, J.A. and Khammar, F., 2025. Applying Mineral System Criteria to Develop a Predictive Modelling for Epithermal Gold Mineralization in Northern New Brunswick: Using Knowledge-Driven and Data-Driven Methods. Minerals, 15(4), p.345.

Mami Khalifani, F., Lentz, D.R. and Walker, J.A., 2025. Machine learning-based mineral prospectivity mapping of epithermal gold mineralization in Northern new brunswick: a comparative study of random forest, support vector machine, and XGboost classifiers. Earth Science Informatics, 18(4), p.553.

References

Azadbakht, Z., Rogers, N., Lentz, D.R., McFarlane, C.R.M., Rogers, N., Initiative, T.G., 2019. Petrogenesis and associated mineralization of Acadian related granitoids in New Brunswick. Geological Survey of Canada. In Targeted Geoscience Initiative, 2018 report of activities, pp. 243−278.

Barago, N., Pavoni, E., Floreani, F., Crosera, M., Adami, G., Lenaz, D., Larese Filon, F. and Covelli, S., 2022. Portable X-ray fluorescence (pXRF) as a tool for environmental characterisation and management of mining wastes: Benefits and limits. Applied Sciences, 12(23), p.12189.

Barker, R.D., Barker, S.L., Wilson, S. and Stock, E.D., 2021. Quantitative Mineral Mapping of Drill Core Surfaces I: A Method for μ XRF Mineral Calculation and Mapping of Hydrothermally Altered, Fine-Grained Sedimentary Rocks from a Carlin-Type Gold Deposit. Economic Geology, 116(4), pp.803−819.

Bernier, M.A. and Webber, G.R., 1989. Mineralogical and geochemical analysis of shallow overburden as an aid to gold exploration in southwestern Gaspésie, Quebec, Canada. Journal of Geochemical Exploration, 34(2), pp.115−145.

Bonham-Carter, G.F., 1994. Geographic information systems for geoscientists-modeling with GIS. Computer Methods in the Geoscientists 13, 398.

Bustard, A.L. and Dahn, D.R.L. 2024. Characteristics and structural setting of veinhostedAu-Ag-Pb-Zn mineralization associated with the Mulligan Gulch Porphyry, northcentral New Brunswick. New Brunswick Department of Natural Resources and Energy Development, Geoscience Report 2024−1, 33 p.

Carranza, E.J.M., 2008. Geochemical Anomaly and Mineral Prospectivity Mapping in GIS. Elsevier.

Carranza, E.J., 2015. Data-driven evidential belief modeling of mineral potential using few prospects and evidence with missing values. Nat. Resour. Res. 24 (3), 291–304.

Carroll, J.I., 2000. Geology and geophysics of the east half of the Kedgwick map area (NTS 21O/11 East), northern New Brunswick. In Current Research 1999. Edited by B.M.W. Carroll. New Brunswick Department of Natural Resources and Energy, Minerals and Energy Division, Mineral Resource Report 2000-4, p. 1–16.

Carroll, J.I., 2003a. Geology of the Kedgwick, Gounamitz River, States Brook and Menneval map areas (NTS 21 O/11, 21 O/12, 21 O/13 and 21 O/14), Restigouche County, New Brunswick. In Current Research 2002. Edited by B.M.W. Carroll. New Brunswick Department of Natural Resources; Minerals, Policy and Planning Division, Mineral Resource Report 2003-4, p. 23– 57.

Carroll, J.I., 2003b. Geology of the Kedgwick area (NTS 21 O/11), Restigouche County, New Brunswick. New Brunswick Department of Natural Resources; Minerals, Policy and Planning Division, Plate 2003−23.

Corbett, G., 2002. Epithermal gold for explorationists. *AIG News*, *67*(2002), pp.1−8.

Davies, R.S., Groves, D.I., Trench, A. and Dentith, M., 2020. Towards producing mineral resource-potential maps within a mineral systems framework, with emphasis on Australian orogenic gold systems. Ore Geology Reviews, 119, p.103369.

Dimitrov, I., McCutcheon, S.R., Williams, P.F., 2003. Progress report: structural investigations in the vicinity of the Rocky Brook – Millstream Fault, Gloucester and Restigouche counties, northern New Brunswick. In Current Research 2002.

Edited by B.M. W. Carroll. New Brunswick Department of Natural Resources; Minerals, Policy and Planning Division, Mineral Resource Report 2003-4, p. 59–71.

Fabre, C., Trebus, K., Tarantola, A., Cauzid, J., Motto-Ros, V. and Voudouris, P., 2022. Advances on microLIBS and microXRF mineralogical and elemental quantitative imaging. Spectrochimica Acta Part B: Atomic Spectroscopy, 194, p.106470.

Ford, A., Peters, K.J., Partington, G.A., Blevin, P.L., Downes, P.M., Fitzherbert, J.A. and Greenfield, J.E., 2019. Translating expressions of intrusion-related mineral systems into mappable spatial proxies for mineral potential mapping: Case studies from the Southern New England Orogen, Australia. Ore Geology Reviews, 111, p.102943.

Forest, R.C. 2021. Mineral Assessment Report July 2020 – December 2020, Rocky Brook Millstream Claim Block 8185, Topographic Map NTS 21 O/10, Gold Matter Corporation.

New Brunswick Department of Natural Resources and Energy Development, Mineral Report of Work 478973, 121 p. plus maps, sections, logs.

Fyffe, L.R., Pajari Jr, G.E., Cherry, M.E., 1981. The Acadian plutonic rocks of New Brunswick. Atlantic Geology, 17, pp. 23−36.

Fyffe, L.R. and Fricker, A., 1987. Tectonostratigraphic terrane analysis of New Brunswick. Maritime Sediments and Atlantic Geology, 23, p. 113–122.

Genna, D., Gaboury, D., Moore, L. and Mueller, W.U., 2011. Use of micro-XRF chemical analysis for mapping volcanogenic massive sulfide related hydrothermal alteration: Application to the subaqueous felsic dome-flow complex of the Cap d'Ours section,

Glenwood rhyolite, Rouyn-Noranda, Québec, Canada. Journal of Geochemical Exploration, 108(2), pp.131−142.

Gold Terra Resource Corp. 2022. Gold Terra Announces High-grade Sampling Results along a 700-Metre-long Epithermal Gold-Silver Corridor with up to 32.9 g/t Gold and 579 g/t Silver, Mulligan Project, New Brunswick. Press Release, October 5, 2022. Accessed from https://goldterracorp.com/news/gold-terra-announces-high-grade-sampling-results-a-4741 [April 2024].

Hall, G., Buchar, A., Bonham-Carter, G., 2011. Quality control assessment of portable XRF analysers: development of standard operating procedures, performance on variable media and recommended uses. In: CAMIRO Project 10E01 Report.

Hall, G.E., Bonham-Carter, G.F. and Buchar, A., 2014. Evaluation of portable X-ray fluorescence (pXRF) in exploration and mining: Phase 1, control reference materials. Geochemistry: Exploration, Environment, Analysis, 14(2), pp. 99−123.

Hatcher, R.D., 2010. The Appalachian orogen: A brief summary. Memoir of the Geological Society of America, 206, 1–19.

Harraden, C.L., Steiner, A.P., Barker, S.L. and Bouzari, F., 2025. Mineralogy from μXRF Elemental Maps: Comparison of Supervised and Unsupervised Methods. Geochemistry: Exploration, Environment, Analysis, pp.geochem 2024–050.

Hedenquist, J.W. and Lowenstern, J.B., 1994. The role of magmas in the formation of hydrothermal ore deposits. *Nature*, *370*(6490), pp.519–527.

Hedenquist, J.W. and Arribas, A., 2022. Exploration implications of multiple formation environments of advanced argillic minerals. Economic Geology, 117(3), pp. 609−643.

Heidarian, H., Lentz, D.R., Thorne, K. and Rogers, N., 2021. Application of portable X-ray and micro-X-ray fluorescence spectrometry to characterize alteration and mineralization within various gold deposits hosted in southern New Brunswick, Canada. Journal of Geochemical Exploration, 229, p.106847.

Hronsky, J.M. and Groves, D.I., 2008. Science of targeting: definition, strategies, targeting and performance measurement. Australian Journal of Earth Sciences, 55(1), 3−12.

John, D.A., Vikre, P.G., du Bray, E.A., Blakely, R.J., Fey, D.L., Rockwell, B.W., Mauk, J.L., Anderson, E.D. and Graybeal, F., 2018. Descriptive models for epithermal gold-silver deposits (No. 2010-5070-Q). US Geological Survey.

Khammar, F., Nykänen, V., Beier, C., and Niiranen, T., 2024. Translating Mineral Systems Criteria into a 891 Prospectivity Model for IOCG Deposits in the Kolari Region, Finland. Ore Geol Rev, 174, 106326, 892.

Kerrich, R., Goldfarb, R., Groves, D. and Garwin, S., 2000. The geodynamics of world-class gold deposits: characteristics, space-time distribution, and origins.

Liu, L., Lu, J., Tao, C., Liao, S. and Chen, S., 2021. GIS-based mineral prospectivity mapping of seafloor massive sulfide on ultraslow-spreading ridges: A case study of Southwest Indian Ridge 48.7–50.5 E. Natural Resources Research, 30(2), 971−987.

Liu, H., Harris, J., Sherlock, R., Behnia, P., Grunsky, E., Naghizadeh, M., Rubingh, K., Tuba, G., Roots, E. and Hill, G., 2023. Mineral prospectivity mapping using

machine learning techniques for gold exploration in the Larder Lake area, Ontario, Canada. Journal of Geochemical Exploration, 253, p.107279.

Mami Khalifani F., Parsa, M., Lentz, D., Walker, J., 2022. Portable XRF-aided pattern recognition for characterization of gold mineralization in Northern New Brunswick. In: Exploration, Mining and Petroleum New Brunswick (EMP 2022) conference.

Mami Khalifani, F., Lentz, D., Parsa, M., Walker, J., 2023a. Recognizing gold mineralization pathfinders with portable XRF and micro-X-ray fluorescence spectrometry in the Williams Brook epithermal system, NB: Analysis of Indicator Elements and Minerals. In: Atlantic Geoscience Society Colloquium Program with Abstracts.

Mami Khalifani, F., Lentz, D.R., Parsa, M., Walker, J.A., 2023b. Recognizing gold mineralization pathfinders with portable XRF and micro-X-ray fluorescence spectrometry in the Williams Brook epithermal system, NB: Analysis of Indicator Elements and Minerals. Atlantic Geoscience Society Colloquium Program with Abstracts.

Mami Khalifani, F., Lentz, D., and Walker, J., 2025a. Machine Learning-Based Framework for Mineral Prospectivity Modeling: Predicting Epithermal Gold Mineralization in Northern New Brunswick, Canada. In: EGU General Assembly 2025, Vienna, Austria.

Mami Khalifani, F., Lentz, D.R., Walker, J.A. and Khammar, F., 2025b. Applying Mineral System Criteria to Develop a Predictive Modelling for Epithermal Gold

Mineralization in Northern New Brunswick: Using Knowledge-Driven and Data-Driven Methods. Minerals, 15(4), p.345.

Massawe, R.J. and Lentz, D.R., 2020a. Evaluation of crystallization and emplacement conditions of the McKenzie Gulch porphyry dykes using chemistry of rock-forming minerals: implications for mineralization potential. Ore Geology Reviews, 116, p.103256.

Massawe, R.J. and Lentz, D.R., 2020b. Petrochemistry and U–Pb (zircon) age of porphyry dykes at the McKenzie Gulch porphyry–skarn Cu–Ag–Au deposit, north-central New Brunswick, Canada: implications for emplacement age, tectonic setting, and mineralization potential. Canadian Journal of Earth Sciences, 57(4), 427−452.

Massawe, R.J. and Lentz, D.R., 2021. Petrogenesis and U–Pb (titanite) age of Cu–Ag skarn mineralization in the McKenzie Gulch area, northern New Brunswick, Canada. Journal of Geochemical Exploration, 232, 106902.

McCuaig, C., Brown, W.M. and Op, K., 2007. Fooling ourselves-dealing with model uncertainty in a mineral system approach to exploration. In: Andrew, CJ et al.(eds.). In 9th Biennial Meeting of the Society for Geology Applied to Mineral Deposits, pp. 1435-1438. Society for Geology Applied to Mineral Deposits.

Mohebi, A., Mirnejad, H., Lentz, D., Behzadi, M., Dolati, A., Kani, A., Taghizadeh, H., 2015. Controls on porphyry Cu mineralization around Hanza Mountain, south-east of Iran: an analysis of structural evolution from remote sensing, geophysical, geochemical, and geological data. Ore Geol. Rev. 69, 187–198.

Malo, M., Moritz, R., Dube, B., Chagnon, A., Roy, F. and Pelchat, C., 2000. Base metal skarns and Au occurrences in the southern Gaspé Appalachians: distal products of

a faulted and displaced magmatic-hydrothermal system along the Grand Pabos-Restigouche fault system. Economic Geology, 95(6), 1297−1318.

Moritz, R. and Malo, M., 1996. Lead isotope signatures of Devonian Acadian structurally controlled mineral occurrences in the Gaspe Peninsula, Quebec Appalachians; constraints on source rocks. Economic Geology, 91(6), pp.1145−1150.

Nikonow, W. and Rammlmair, D., 2017. Automated mineralogy based on micro-energy-dispersive X-ray fluorescence microscopy (μ-EDXRF) applied to plutonic rock thin sections in comparison to a mineral liberation analyzer. Geoscientific Instrumentation, Methods and Data Systems, 6(2), pp.429−437.

Nykänen V, Törmänen T, Niiranen T (2023) Cobalt Prospectivity Using a Conceptual Fuzzy Logic Overlay Method Enhanced with the Mineral Systems Approach. Natural Resources Research 32:2387–2416.

Potter, N. and Brand, N., 2019. Application of micro-XRF to characterise diamond drill-core from lithium-caesium-tantalum pegmatites. ASEG Extended Abstracts, 2019(1), pp.1– 4.

Rodgers, J., 1970. The Tectonics of the Appalachians. John Wiley and Sons, New York, 271 p.

Romer, R.L. and Kroner, U., 2018. Paleozoic gold in the Appalachians and Variscides. Ore Geology Reviews, 92, 475−505.

Sánchez-Mora, D., 2014. Petrogenesis of the low sulfidation gold mineralization in the Williams Brook area, Tobique-Chaleur Zone, New Brunswick. Unpublished M.Sc. thesis, University of New Brunswick, Fredericton, New Brunswick, 172 p.

Sánchez-Mora, D., McFarlane, C.R., Walker, J.A. and Lentz, D.R., 2021. Geochemistry and U–Pb geochronology of the Williams Brook area, Tobique–Chaleur zone, New Brunswick: Stratigraphic and geotectonic setting of gold mineralization. Canadian Journal of Earth Sciences, 58(10), pp.1040−1058.

Sangster, A.L. and Smith, P.K., 2007. Metallogenic summary of the Meguma gold deposits, Nova Scotia. In: Goodfellow, W.D. (Ed.), Mineral Deposits of Canada: A Synthesis of Major Deposit-Types, District Metallogeny, the Evolution of Geological Provinces, and Exploration Methods. Spec. Publ. 5. Geol. Assoc. Can., Min. Depos. Div., pp. 723–732.

St. Peter, C., 1978. Geology of head of Wapske River, map area J−13 (21 J/14): New Brunswick Department of Natural Resources, Mineral Resources Branch Map Report 78−1, 24 p.

Lode Gold Resources Inc., 2019. Assessment report on trench sampling, mapping and diamond drilling McIntyre brook property.

Thorne, K.G., Lentz, D.R., Hoy, D., et al., 2008. Characteristics of Mineralization at the Main Zone of the Clarence Stream Gold Deposit, Southwestern New Brunswick, Canada: Evidence for an Intrusion-Related Gold System in the Northern Appalachian Orogen. Exploration and Mining Geology, 17, 13– 49.

Thorne, K.G., 2011. Gold. New Brunswick Department of Natural Resources; Lands, Minerals and Petroleum Division, Mineral Commodity Profile No. 8, 8 p.

Tremblay, A., Faure, S., Dubé, B., 1993. Gold occurrences of the Rocky Brook – Millstream Fault, northern Appalachians, New Brunswick. In Current Research, Part E, Geological Survey of Canada, Paper 93-1E, p. 337–346.

van Staal, C.R., 2007. Pre-Carboniferous tectonic evolution and metallogeny of the Canadian Appalachians Mineral Deposits of Canada. In: Geological Association of Canada, pp. 793–818.

Walker, J., Gower, S., and McCutcheon, S.R. 1991. Antinouri-Nicholas Project, Gloucester and Restigouche Counties, northern New Brunswick (C-NBCAMD). In Project Summaries for 1991, Sixteenth Annual Review of Activities. Edited by S.A. Abbott. New Brunswick Department of Natural Resources and Energy, Mineral Resources, Information Circular 91-2, pp. 87–100.

Wei, H., Xiao, K., Shao, Y., Kong, H., Zhang, S., Wang, K., Li, Q., Chen, B., Xiang, J. and Wen, C., 2020. Modeling-based mineral system approach to prospectivity mapping of stratabound hydrothermal deposits: A case study of MVT Pb-Zn deposits in the Huayuan area, northwestern Hunan province, China. Ore Geology Reviews, 120, p.103368.

White, N.C. and Hedenquist, J.W., 1995. Epithermal gold deposits: styles, characteristics and exploration. SEG Newsletter, (23), pp. 1−3.

Williams-Jones, A.E., 1982. Patapedia: An Appalachian calc-silicate-hosted copper prospect of porphyry affinity. Canadian Journal of Earth Sciences, 19, pp. 438 – 455.

Williams, H., 1995. Introduction, in Williams. H., ed., Geology of the Appalachian–Caledonian Orogen in Canada and Greenland: Geological Survey of Canada, Geology of Canada, No. 6, pp. 1–19.

Wilson, R.A., Parkhill, M.A. and Carroll, J.I., 2005. Field Trip B8: New Brunswick Appalachian Transect: Bedrock and Quaternary Geology of the Mount Carleton Restigouche River Area.

Wilson, R.A., van Staal, C.R., Kamo, S.L., 2017. Rapid transition from the Salinic to Acadian orogenic cycles in the northern Appalachian Orogen: Evidence from northern New Brunswick, Canada. American Journal of Science, 317(4), pp. 449−482.

Wilson, R.A. 2017. The Middle Paleozoic Rocks of Northern and Western New Brunswick, Canada. New Brunswick Department of Energy and Resource Development; Geological Surveys Branch, Memoir 4, 319 p.

Wilson, R.A. and Kamo, S.L., 2012. The Salinic Orogeny in northern New Brunswick: geochronological constraints and implications for Silurian stratigraphic nomenclature. Canadian Journal of Earth Sciences, 49(1), 222−238.

Zhang, W., Lentz, D.R., Thorne, K.G., and McFarlane, C., 2016. Geochemical characteristics of biotite from felsic intrusive rocks around the Sisson Brook W–Mo–Cu deposit, west-central New Brunswick: An indicator of halogen and oxygen fugacity of magmatic systems. Ore Geology Reviews, 77, 82−96.

Zhou, S., Wang, J., Wang, W. and Liao, S., 2023. Evaluation of portable X-ray fluorescence analysis and its applicability as a tool in geochemical exploration. Minerals, 13(2), p.166.

Zuo, R., Zhang, Z., Zhang, D., Carranza, E.J.M. and Wang, H., 2015. Evaluation of uncertainty in mineral prospectivity mapping due to missing evidence: a case study

with skarn-type Fe deposits in Southwestern Fujian Province, China. Ore Geology Reviews, 71, pp.502−515.

Yang, X.M. and Lentz, D.R., 2005. Chemical composition of rock-forming minerals in gold-related granitoid intrusions, southwestern New Brunswick, Canada: implications for crystallization conditions, volatile exsolution, and fluorine-chlorine activity. Contributions to Mineralogy and Petrology, 150(3), 287−305.

Young, K.E., Evans, C.A., Hodges, K.V., Bleacher, J.E. and Graff, T.G., 2016. A review of the handheld X-ray fluorescence spectrometer as a tool for field geologic investigations on Earth and in planetary surface exploration. Applied Geochemistry, 72, 77−87.

Yousefi, M. and Kreuzer, O., 2024. Towards an effective exploration information system–new concepts and ideas aimed at improving mineral exploration targeting. Applied Geochemistry, 169, p.106053.

2. Advancing Gold Mineralization Detection in Northern New Brunswick Through Portable X-ray and Micro-X-ray Fluorescence Spectrometry with Multivariate Compositional Data Analysis (CoDA) and Clustering for Pathfinder Elements and Alteration Analysis

Farzaneh Mami khalifani[1a], David R Lentz [a], James A Walker[b]

[a] *Department of Earth Science, University of New Brunswick, Fredericton, New Brunswick, E3B 5A3, Canada*

[b] *New Brunswick Department of Natural Resources and Energy Development, South Tetagouche, New Brunswick, Canada*

Abstract

The New Brunswick segment of the Canadian Appalachians contains a variety of gold deposits and occurrences that formed at different stages of the Appalachian orogeny. The Tobique-Chaleur Zone, situated in the northern part of New Brunswick hosts several orogenic and epithermal gold mineralization systems that are spatially related to large-scale crustal faults or their subsidiary splays, e.g., the Rocky Brook-Millstream Fault. Although gold mineralization in northern New Brunswick is hosted by auriferous quartz veins, finding pathfinder elements, indicator minerals, and alteration associated with gold mineralization remains challenging. Herein, the portable X-ray fluorescence (pXRF, Olympus Vanta™) spectrometer, in conjunction with micro-X-Ray Fluorescence (μXRF) Energy Dispersive Spectrometry (EDS), was applied to selected core intervals from four gold systems in the region, namely the Williams Brook, McIntyre Brook, Mulligan Gulch, and Simpsons Field occurrences. We generated pXRF-based multielement datasets from selected intervals, then applied compositional data analysis (CoDA), including principal

component analysis (biplots) and cluster analysis, to interpret them. Although the pXRF analysis and subsequent multivariate compositional data analysis provide geochemical patterns and highlight indicator elements associated with gold mineralization, the study also includes a comprehensive mineralogical analysis. The pXRF geochemical data help the interpretation of the mineralogy, but the explicit mineralogical composition is confirmed through detailed petrographic and μXRF analyses. Gold-bearing minerals were further identified by μXRF-EDS analysis, revealing that gold is mainly associated with sulfide minerals, namely pyrite, chalcopyrite, pyrrhotite, stibnite, and arsenopyrite. In addition to the above, our mineralogical studies further indicate that fine-grained muscovite, illite, potassic, and silicification alteration styles are associated with gold-bearing quartz veins.

Keywords: gold mineralization, pathfinder elements, mineral indicators, alteration, pXRF, μXRF, CODA, Northern New Brunswick

2.1. Introduction

Portable X-ray fluorescence (pXRF) analyzers in the field facilitate rapid and non-destructive analysis of outcrop and drill core samples (Gazley et al., 2014; Bourke and Ross, 2016; Lemiére, 2018; Heidarian et al., 2021; Balaram and Sawant., 2022). Portable XRF is advantageous due to its cost-effectiveness, high efficiency, and stability, and produces results that are reliable to illustrate the spatial distribution of most indicator elements commonly used in mineral exploration (Chen et al., 2013; Zhou et al., 2023; Ross et al., 2014a, b). pXRF reliability is ensured by calibrating matrix-matched certified reference materials, taking multiple measurements per sample to mitigate issues around sample heterogeneity, and employing rigorous QA/QC protocols that monitor and correct

for instrumental drift, as evidenced by high goodness-of-fit metrics in calibration curves. These quality control measures collectively enable precise and accurate spatial mapping of indicator elements, thereby demonstrating that the pXRF data are sufficiently reliable for mineral exploration applications (Ross et al., 2014a, b).

Indicator elements are chemical constituents that can reveal the presence of minerals indicative of specific types of deposits, alteration, or host rock (McClenaghan, 2011). In this study, these elements are utilized both as geochemical exploration vectors to identify prospective mineralized systems, and specific mineralized zones and as lithogeochemical markers to elucidate the host rock, and depositional and alteration processes of those host rocks.

X-ray Fluorescence Spectrometry is a method employed for analyzing the chemical composition of materials and can be applied to various forms, including solids, powders, liquids, and thin films (Scruggs and Ametek, 2010; Kohli, 2012). The ability to swiftly collect numerous analyses facilitates the acquisition of high data density, while conducting replicate analyses ensures reliability and precision (Piercey, 2014; Lemiere, 2018; Ravansari et al., 2020). Various research studies have been conducted to investigate the utility of pXRF instruments to analyze mineralogical and geochemical signatures of mineralization. Arne et al. (2014) showed that key indicator elements for gold exploration, e.g., As, Sb, Bi, and Cu, commonly occur in soils at concentrations near or below the detection thresholds of pXRF instruments. However, pXRF technology can readily ascertain elements characteristic of alteration aureoles (K, Rb, Ba, Sr, P) or lithology (Ca, Fe, K, Ti, Zr) (Lemiere, 2018; Heidarian et al., 2021; Balaram and Sawant, 2022). Balaram and Sawant (2022) employed portable XRF technology to identify indicator minerals and

pathfinder elements for the exploration of platinum group elements, rare earth elements, gold, base metals, and lithium in terrestrial and submarine studies. Heidarian et al. (2021) used pXRF in the Annidale and Clarence Stream areas in southern New Brunswick to analyze gold mineralization by identifying patterns in a diverse suite of associated elements. Barker et al. (2019) indicated that As, which is easily detectable by pXRF, is an effective indicator of Carlin-type gold deposits. Zhang et al. (2017) applied pXRF at the Mount Pleasant deposit in the southern part of New Brunswick, specifically within the W-Mo-Bi Fire Tower Zone and Sn-Zn-In North Zone, to analyze and interpret W-Mo mineralization by identifying different elemental patterns. Lawley et al. (2015) effectively combined pXRF data with lithogeochemical data from whole rock analyses to delineate the hydrothermal footprint at the Meliadine gold deposit. Gazley et al. (2014, 2015) demonstrated that pXRF is a very effective tool in gold exploration by analyzing key associated elements (e.g., As, Cu, K, and V) to identify host rocks and assess sulfide minerals and their abundance, as well as other alteration minerals in hydrothermal alteration zones, thereby mapping geological features that reveal insights into mineralization processes.

This investigation employs an integrated approach to enhance the detection of gold mineralization in northern New Brunswick. It combines pXRF and μXRF to analyze geochemical data from gold-bearing veins and their host rocks at four distinct occurrences. Multi-element datasets were generated from core samples and subsequently examined using multivariate compositional data analysis (CoDA) techniques, including compositional biplots, correlation analysis, and clustering (e.g., Graffelman et al., 2018; Cicchella et al., 2022; Egozcue et al., 2024), to elucidate the compositional characteristics

of the mineralization. Gold-mineralized samples from the Williams Brook (WB), McIntyre Brook (MB), Mulligan Gulch (MG), and Simpsons Field (SF) gold occurrences located in the Wapske and Greys Gulch formations of the Tobique Group, were selected to provide representative geochemical and mineralogical data, which inform future economic assessments of these occurrences.

In addition to the geochemical analysis using pXRF and μ-XRF spectrometry, an extensive mineralogical examination was performed on polished thin sections prepared from core samples. Gold-bearing minerals were analyzed using μ-XRF (Flude et al., 2017) to elucidate their mineralogical and geochemical properties, various alteration types, and the styles of mineralization (e.g., Fritz et al., 2016; Hoehnel et al., 2018). This non-destructive technique, with its high spatial resolution and sensitivity, effectively images key geochemical features, such as fractures and veins, directly associated with gold mineralization. Northern New Brunswick's tectonic framework is characterized by a complex interplay of faults and shear zones that have exerted a first-order control on hydrothermal fluid flow and the localization of auriferous quartz veins. In our study, we highlight the integrated application of pXRF, μXRF, and petrographic-mineralogical analyses, which collectively reveal the relationship between gold mineralization and its associated geochemical and mineralogical signatures.

2.2. Geological setting and gold mineralization

The northern Appalachian belt is a complex collage of suprasubduction zone terranes and microcontinents that formed during the closure of the Iapetus and Rheic oceans between the late Cambrian and the Permian (van Staal, 2007; Romer and Kroner, 2018). The northern part of the Appalachian belt displays systematically younger ages of deformation

from the west to the east, as the remnants of various arcs and microcontinents were accreted (Hatcher, 2010). The Northern Appalachians and Maritime Canada displaying major tectonic units and structures related to the closure of the Iapetus and Rheic oceans, such as the Acadian, NeoAcadian, Variscan, Hercynian, and Alleghanian orogenies (van Staal and Barr, 2012). It should be noted that mainly Devonian intrusions, which are related to post-subduction crustal thickening processes and post-Acadian uplift, are mineralized with granophile and chalcophile elements, such as Sn, W, Mo, Ta, Au, and Sb (Fyffe et al., 1981; McLeod et al., 2008; Azadbakht et al., 2018).

Northern New Brunswick is underlain by three poly-deformed Early Paleozoic inliers, the Popelogan, Miramichi, and Elmtree inliers (Fig 2-1), all of which are overlain by post-Taconic, Middle Paleozoic Matapédia Cover Sequence (MCS) and Carboniferous cover rocks (Wilson, 2000, 2017; Sánchez Mora, 2014). Clastic and carbonate sedimentary rocks of the Ordovician to Silurian Grog Brook and Matapédia groups were deposited in the Matapédia forearc basin, located between the Laurentian margin and the Brunswick Subduction Complex. In contrast, the Upper Silurian to Early Devonian turbiditic sediments and associated volcanic rocks, which are classified as the Dalhousie and Tobique groups in the eastern MCS, either conformably overlie the Matapédia Group or lie unconformably on top of the Miramichi, Elmtree, and Popelogan Inliers (Wilson, 2000; 2017).

The volcanic rocks display geochemical signatures indicative of formation by partial melting of the same subcontinental lithospheric mantle source. Acadian deformation of the MCS in northern New Brunswick occurred in the Early Devonian between 415 and 395 Ma. It was accompanied in its later stages by dextral strike-slip faults on the Rocky Brook

– Millstream, Restigouche – Grand Pabos, and Catamaran Brook faults and several related splays (van Staal et al., 2009; Wilson, 2017). The MCS is divided into three structures that, from northwest to southeast, are: 1) the Connecticut Valley – Gaspé Synclinorium, 2) Aroostook – Percé Anticlinorium, and 3) Chaleur Bay Synclinorium (Rodgers, 1970; Bernier and Webber 1989; Wilson, 2017). The gold occurrences investigated herein, Williams Brook, McIntyre Brook, Mulligan Gulch, and Simpsons Field, are located in the Chaleur Bay Synclinorium and are mainly underlain by Upper Silurian to Early Devonian strata and subordinate lower Silurian strata. The Chaleur Bay Synclinorium has a more diverse and complex geological and tectonic evolution than the Aroostook – Percé Anticlinorium. The uppermost Silurian to Early Devonian sedimentary and volcanic rocks of the Chaleur Bay Synclinorium are divided into the Chaleur, Petit-Rocher, Quinn Point, Dickie Cove, and Dalhousie groups north of the Rocky Brook- Millstream Fault and to the Tobique Group south of the fault (Fig. 2-1; Wilson, 2017). Numerous gold occurrences/deposits occur in and around the Tobique-Chaleur Zone in northern New Brunswick and the adjacent Gaspé Peninsula (Fig. 2-1). In northern New Brunswick, epithermal breccia and vein deposits carrying base metals ± Au and Ag occur in the northeastern part of the Chaleur Bay Synclinorium. They are commonly related to felsic intrusive rocks. The occurrences are spatially associated with significant splays of the Rocky - Brook Millstream Fault, specifically the McCormack Brook and Ramsay Brook faults, and with fine- to medium-grained mafic intrusions (Tremblay et al., 1993; Sánchez Mora, 2014; Wilson, 2017). The Williams Brook property is in the northwestern part of the Chaleur Bay Synclinorium of northern and western New Brunswick (Table 2-1, Fig. 2-1; Wilson, 2017). The McIntyre Brook is situated in northern New Brunswick, approximately

50 km east of Saint-Quentin and 90 km west of Bathurst, located southeast of the trans-crustal Rocky Brook-Millstream Fault (Table 2-1, Fig. 2-1). The Mulligan Gulch is located near the contact between the Greys Gulch and Budworm City formations and the Simpsons Field is located southeast of Upsalquitch River in southern Restigouche country (Table 2-1, Fig. 2-1).

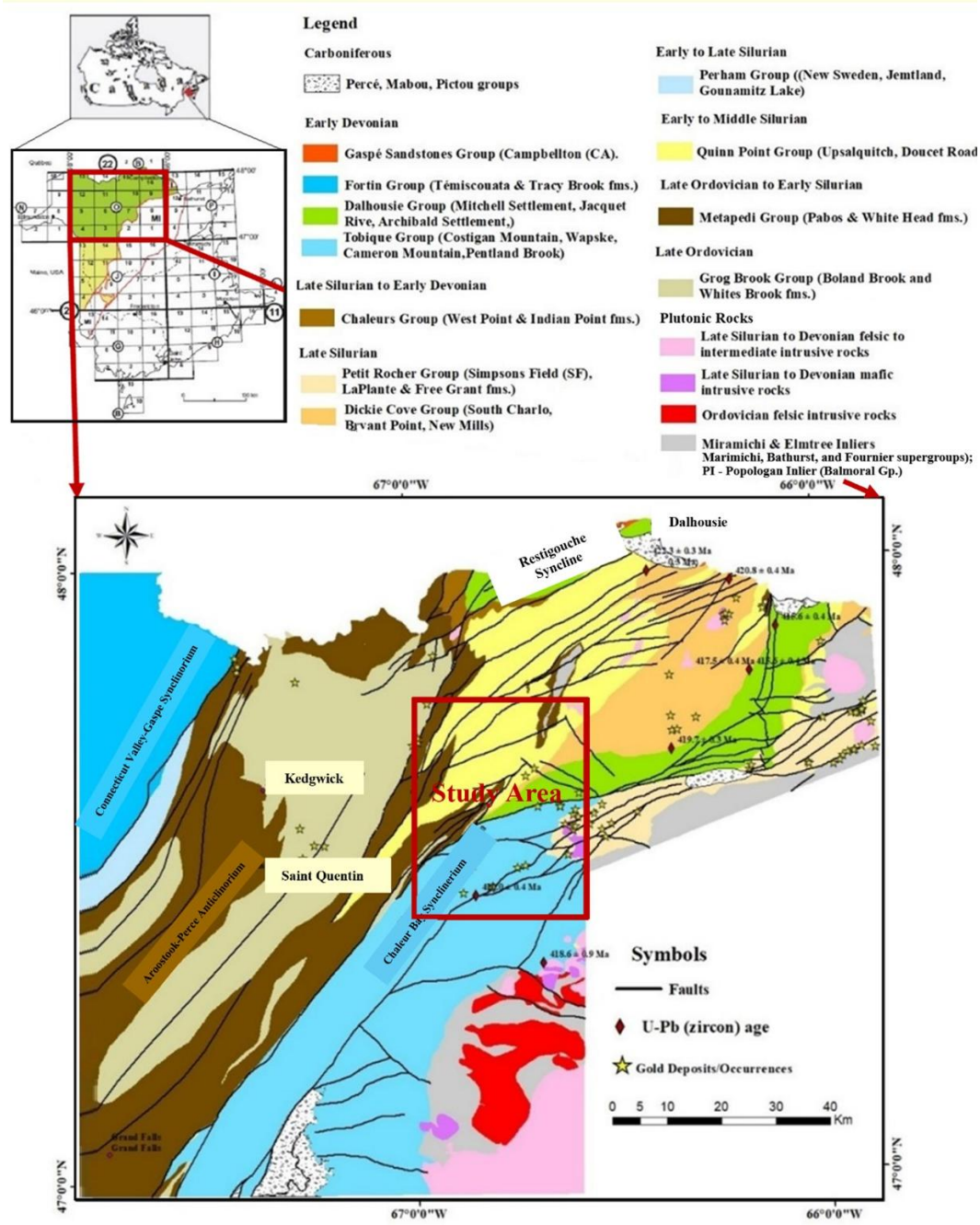

Figure 2-1. Regional geological map of western and northern New Brunswick showing the location of gold deposits/occurrences being examined in this study (modified from Wilson, 2017).

Table 2-1. Overview of property names and commodities in the Tobique-Chaleur belt (New Brunswick computerized mineral occurrence database).

Ref. No	NTS	Property Name	Zone Belt	Commodities
81	21P/12W	Willams Brook	Tobique-Chaleur	Gold
453	21O/10E	McIntyre Brook	Tobique-Chaleur	Gold
142	21O/10E	Mulligan Gulch	Tobique-Chaleur	Arsenic, Gold
438	21O/10E	Simpsons Field	Tobique-Chaleur	Arsenic, Gold

2.3. Epithermal Gold System in Northern New Brunswick

Epithermal deposits primarily contain precious metals such as Au and Ag, but may also include Cu, Pb, and Zn (Taylor, 2007). Epithermal deposits typically form at hydrothermal fluid temperatures ranging between 160 and 270°C (Hedenquist et al., 2000; Goldfarb et al., 2005), although a generally accepted upper limit is <300°C (Bodnar, 2014; Groves et al., 2005). Major structural features, such as faults, shear zones, and thrusts, play a crucial role in the movement and focusing of hydrothermal fluids, particularly in relation to ore deposition. It is known that large-scale fluid movement is associated with steep shear zones due to the focusing of fluids in highly permeable and confined zones (Etheridge et al., 1983).

Epithermal gold deposits commonly can be classified according to sulfide-sulfate mineralogy and alteration character can be categorized into three subtypes: high sulfidation, intermediate sulfidation, and low sulfidation (Sillitoe and Hedenquist, 2003, Chen et al., 2020). The high- and intermediate-sulfidation subtypes are predominantly linked with calc-alkaline volcanic arcs and subvolcanic intrusions, whereas low sulfidation deposits are associated with high-level magmatic systems including both arc volcanism and bimodal volcanism in rift settings (Sillitoe and Hedenquist, 2003). High-sulfidation deposits typically occur close to magmatic sources of heat and volatiles and are associated with boiling acidic fluids. In contrast, low-sulfidation deposits are formed from near-neutral fluids, primarily consisting of mixed meteoric and magmatic waters (Hedenquist et al., 2000; Taylor, 2007).

Epithermal gold mineralization in New Brunswick, although not extensive, is of considerable geological significance (Fig. 2-2). Figure 2-2 presents a regional geological map of the Chaleur Bay Synclinorium in northern New Brunswick, highlighting the distribution of epithermal gold occurrences and deposits. While the primary focus of this study is on northern NB, it is useful to consider other epithermal systems in the province as analogues for genetic processes and exploration criteria.

In the south, the Chambers Settlement deposit in the Avalon Zone hosts high-sulfidation mineralization in altered Neoproterozoic felsic volcanic rocks with gold and silver. In the southwest, the Evandale Granodiorite intrusion is linked to distal low-sulfidation mineralization, with veins containing pyrite, chalcopyrite, molybdenite, and arsenopyrite, and nearby occurrences (e.g., Clarence Stream) supporting its genetic association (Heidarian et al., 2021).

In northern New Brunswick, the northeastern Chaleur Bay Synclinorium contains several epithermal breccia and vein systems enriched in both base metals and precious metals. These deposits are associated with felsic hypabyssal rocks and mafic intrusions near major fault splays, such as the McCormack Brook and Ramsay Brook faults. For instance, the Williams Brook area exhibits low-sulfidation epithermal gold mineralization in Siluro-Devonian volcanic and sedimentary rocks formed under a transpressive tectonic regime during Gondwana–Laurentia convergence. Early mineralization is indicated by muscovite/illite ± adularia veinlets with gold and galena, followed by later quartz veins containing native gold, sulfide minerals, and oxyhydroxide minerals, with geochemical evidence pointing to a magmatic origin for the fluids (Sánchez Mora, 2014; Sánchez Mora et al., 2021). Further studies in northern New Brunswick have examined the Williams Brook, McIntyre Brook, Mulligan Gulch, and Simpsons Field occurrences (Mami Khalifani et al., 2025). At Mulligan Gulch, an low sulfidation system is indicated by multiple quartz veins, from early deformation-related to later structural-controlled, coupled with alterations such as sericite (Massawe and Lentz, 2022). At McIntyre Brook, structural controls along fault zones and lithological boundaries result in gold-bearing brecciated felsic rocks and quartz-carbonate veins, commonly accompanied by Ci, Pb, Zn, and Co. Simpsons Field, located in low-grade metamorphic rocks, features quartz-carbonate veins and pyritic alteration zones that exhibit silicification and carbonatization. Gold is primarily associated with pyrite, chalcopyrite, and arsenopyrite, commonly found near faults and gabbroic contacts.

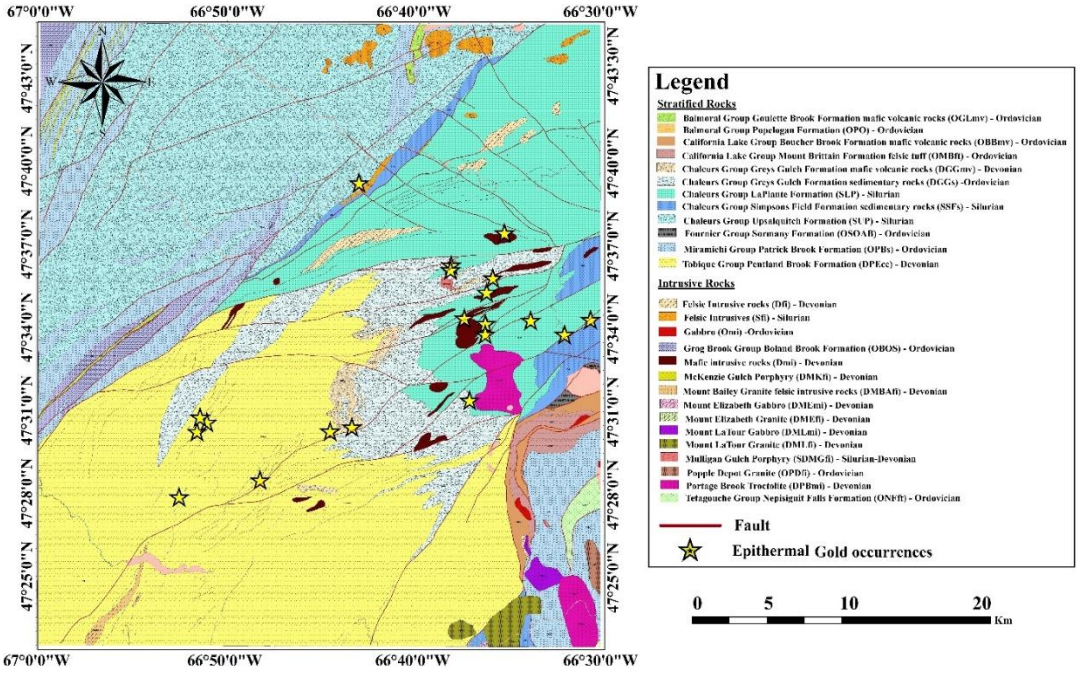

Figure 2-2. Regional geological map of the Chaleur Bay Synclinorium in northern New Brunswick, highlighting the locations of gold deposits (modified after Wilson, 2017).

2.4. Alteration, veins, host rock, structures, and mineralization

The types of hydrothermal alteration are influenced by fluid composition, host rock lithology, temperature, and pressure, leading to different mineral assemblages (Sánchez Mora et al., 2021). Fine-grained muscovite is found within and around quartz veins in all studied deposits/occurrences. Quartz is the primary host for gold-bearing sulfide mineralization that occurs in quartz-carbonate veins. There is spatial variability of sulfide mineral concentrations within the Williams Brook, McIntyre Brook, Mulligan Gulch, and Simpsons Field occurrences.

Gold mineralization in the Williams Brook area exhibits features typical of low-sulfidation epithermal systems occurring within the bimodal volcanic and sedimentary rocks of the Siluro-Devonian Wapske Formation (Sánchez Mora, 2014; Sánchez Mora et al., 2021).

Two stages of gold mineralization have been identified in the Williams Brook area. The first, considered early, consists of gold and galena with pyrite found as disseminations along muscovite/illite ± adularia veinlets in slightly potassically altered porphyritic rhyolite and flow-layered rhyolite. The second type consists of quartz veins with minor supergene oxyhydroxide minerals (jarosite, goethite) and hematite, along with hypogene sulfide minerals (sphalerite, galena), and native gold. Uranium-Pb dating suggests gold mineralization occurred in discrete events; the first formed at ~422–416 Ma, whereas the second was emplaced at 410–408 Ma (Sánchez Mora, 2014; Sánchez Mora et al., 2021). Quartz veins that crosscut the rhyolitic breccias are oblique to the regional (NW-SE) trend of the host rocks and are consistent with a dextral movement (contraction NW-SE and extension NE-SW). Dextral movement of the regional Rocky Brook-Millstream Fault and its splay, the McCormack Brook Fault, appears to have influenced the development of folds in felsic units at Williams Brook and the localization and orientation of quartz veins. This movement may have facilitated enhanced fluid flow within local extensional dilatant openings (Sánchez Mora, 2014). Most gold-bearing veins occur within the rhyolite, specifically near the contact with interlayered sedimentary rocks (siltstone), although quartz veins also occur in the sedimentary rocks (Dahn et al., 2021). Hydrothermal alteration in the Williams Brook area is characterized by a weak potassic alteration, where there is a minor depletion in Na_2O and enrichment in K_2O (Sánchez Mora, 2014; Sánchez Mora et al., 2021). Fine-grained muscovite alteration occurs as disseminations within the various felsic volcanic units and in the quartz veins. The prominent fine grained muscovite alteration is accompanied by secondary supergene limonite and goethite. The prominent fine-grained muscovite alteration is indicative of intense hydrothermal activity and is

commonly observed in host rocks associated with both gold-bearing and barren quartz veins (Sánchez Mora, 2014). In contrast, secondary supergene minerals such as limonite and goethite formed later through weathering (or paleoweathering) of sulfide-bearing rocks. The spatial association of hydrothermal muscovite with these supergene products reflects overprinting by near-surface oxidation processes rather than formation from the same fluid.

The western McIntyre Brook area is dominated by Devonian sedimentary rocks of the Wapske Formation; the northeastern region features felsic volcanic rocks bordered by mafic basalt flows, and the southern part comprises interbedded sedimentary rocks from the Greys Gulch and Wapske Formations. Gold mineralization at McIntyre Brook is classified as epithermal . At McIntyre Brook gold is associated with hematite- and sulfide mineral-bearing quartz veins within potassically altered feldspar phyric rhyolite (Mami Khalifani et al., 2025). Quartz veins in this area occur in an altered portion of a mafic intrusion. Trenching revealed an east-west striking shear zone with more quartz veining and silicification alteration. Quartz-hematite, magnetite, and siderite were identified within this shear zone, along with significant gold mineralization. Hematite-bearing veins are commonly cut by irregular feldspar and calcite-bearing quartz veins containing pyrite. The alteration associated with mineralization in sedimentary rocks is characterized by iron-rich carbonate minerals, such as ankerite, and iron oxide minerals (Stratabound Minerals Corp., 2019; Mami Khalifani et al., 2025).

The Mulligan Gulch occurrence is in a feldspar (± quartz) porphyry, which is a hypabyssal felsic intrusion into upper Silurian sedimentary rocks (McCutcheon and Bevier, 1990). The mineralization at Mulligan Gulch exhibits similarities with the gold occurrences at

Williams Brook, suggesting that the Mulligan Gulch mineralization could be part of a broader regional-scale system (Bustard and Dahn, 2024). At Mulligan Gulch, the mineralization represents an Au–Ag epithermal system that evolved towards a low-sulfidation Au–Cu setting. The veinlets cut extensively sericitized Silurian feldspar porphyry, which intrudes into Silurian siltstone. Faure et al. (1992) described two sets of quartz-carbonate mineral veins at Mulligan Gulch. The first comprises foliation-parallel shear veins, whereas the second comprises extensional veins. Both sets are associated with movement along a splay of the Rocky Brook-Millstream Fault. In this area, the porphyry contains wide zones of argillic alteration, silicification, minor carbonatization, and locally quartz-stockwork and breccia containing pyrite, sphalerite, and chalcopyrite. Two phases of quartz were noted: one is milky-white and sulfide mineral-free, and the other is grey and mildly sulfide mineral-bearing. Gold occurs in both sets of quartz veins. In the sulfide-bearing veins, Au is associated with pyrite, whereas in the sulfide mineral-free veins, it is found along the margins of the veins and in stockworks developed within fractures and shear zones (Bustard and Dahn, 2024). At Mulligan Gulch, gold occurs primarily in an assemblage of arsenopyrite, pyrite, chalcopyrite, galena, bornite, and acanthite within quartz, fine-grained muscovite, and carbonate mineral veins (Bustard and Dahn, 2024; Lavoie, 2018).

The Simpsons Field occurrence is situated within the Rocky Brook-Millistream fault and is underlain by Silurian terrestrial to shallow-water deposits of brick red, maroon, or green pebble to boulder conglomerate and grey, green, or red lithic and sandstone of the Simpsons Field Formation (Mami Khalifani et al., 2025). Simpsons Field is hosted by calcareous siltstone of the Budworm City Formation and lesser deformed gabbroic dykes and sills and

is located near the junction of the Ramsay Brook and Portage Lake faults. The gold mineralization at Simpsons Field can be categorized as epithermal. This classification is supported by the gold being located within narrow quartz veins that cut through the Simpsons Field Formation, as well as the notable concentration of gold in highly silicified and pyritic zones (Wilson, 2017; Puma Exploration Inc., 2021). The gold occurrences in this area are located along subsidiary faults of the Rocky Brook-Millstream Fault Zone (Faure et al.,1992; Puma Exploration Inc., 2021). Mineralized zone and altered rock consist primarily of quartz, siderite, pyrite, and hematite/carbonate minerals, with a minor amount of chalcopyrite, fine-grained muscovite, and biotite (Puma Exploration Inc, 2021). Gold is hosted in narrow quartz-carbonate minerasl veins that are closely associated with quartz, iron-carbonate, and minor potassic (muscovite-adularia) minerals, and grab samples confirm the presence of gold mineralization.

2.5. Materials and Methods

Figure 2-3 shows the flowchart outlining the identifying indicator minerals and elements related to gold mineralization.

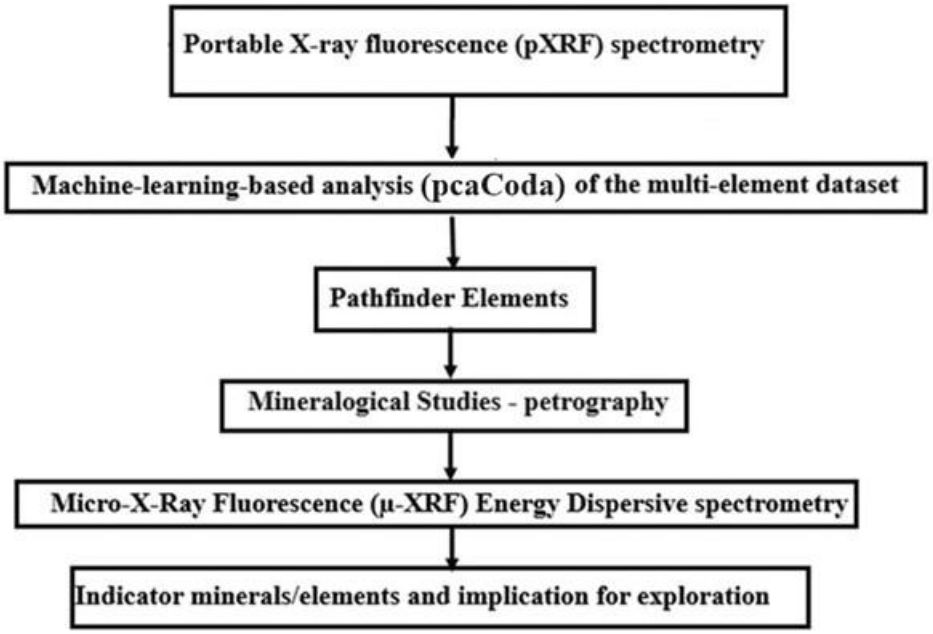

Figure 2-3. A flowchart illustrates the steps for identifying indicator minerals and elements associated with gold mineralization through pXRF and μ-XRF analysis.

2.5.1 Sampling

Gold-bearing samples from the four occurrences (WB, MB, MG, and SF) were collected from drill cores stored at the provincial core repository at Madran, New Brunswick and Puma Exploration's Saint Quentin core storage facilities. The sample set includes 305 samples from WB, 225 samples from MB, 93 samples from MG, and 62 samples from SF. Sampling was based on gold concentration as determined by reported/published assay data and drill core accessibility, i.e. there is a larger collection of samples from occurrences with better access or those with higher concentrations of gold (Stratabound Minerals Corp, 2019; Puma Exploration Inc., 2021; Bustard and Dahn, 2024).

Figure 2-4 shows core photographs from Williams Brook and McIntyre Brook that illustrate key mineralization features, including quartz-carbonate veins hosted in altered

rhyolite, zones of sericite–limonite–chlorite alteration, visible gold (VG), and brecciated felsic dykes. Gold mineralization is associated with quartz, hematite, and pyrite fracture-fill textures, with circles marking high-grade zones and locations selected for pXRF analysis.

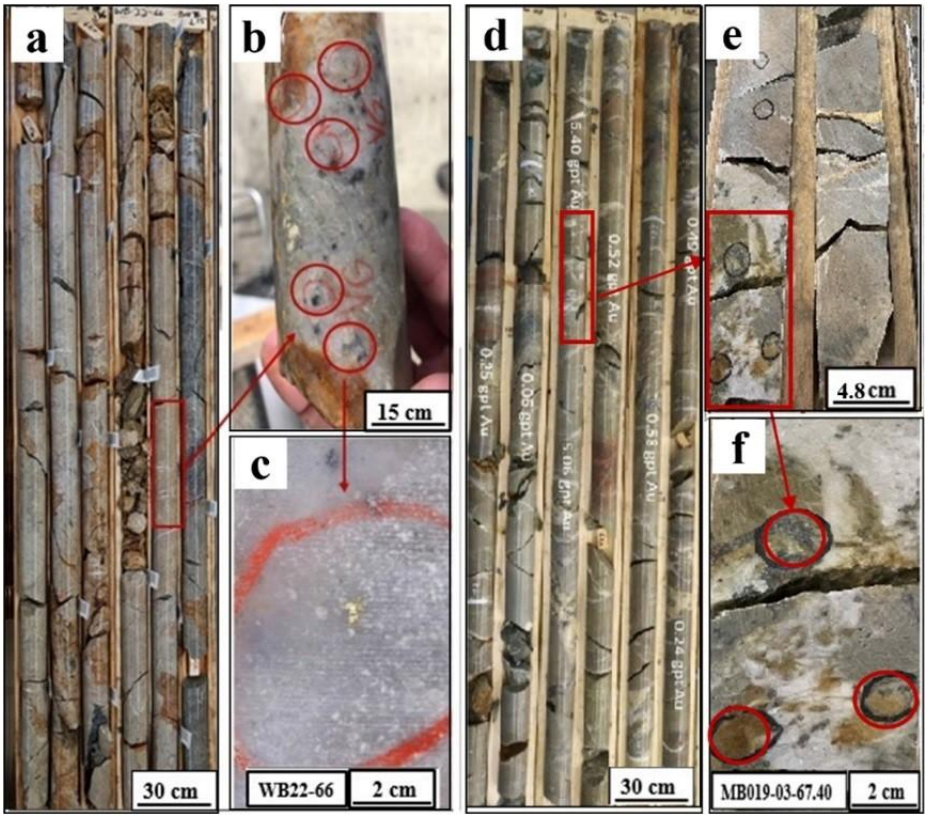

Figure 2-4. a) Photo of quartz-carbonate veins in the altered rhyolite host rock in Williams Brook, showing the samples chosen for pXRF analysis. b) Sericite, limonite, and chlorite are alteration typess within and around the quartz veins (Williams Brook).

2.5.2 p-XRF Data Analysis

Selected core samples consisting of quartered cores were washed, and then three or four flat surfaces containing gold-bearing quartz and associated minerals were analyzed using pXRF (Olympus Vanta™). Brand and Brand (2014) highlighted that using multiple pXRF

instruments can lead to substantial discrepancies due to variations in calibration and detector performance; consequently, this study utilized a single pXRF unit throughout the analyses to maintain consistent and reliable data. This sample preparation methodology offers a consistent and controlled environment for analysis, thereby reducing potential variations that could affect the accuracy and reliability of the data collected (Gray and van Rythoven, 2020; Heidarian et al., 2021, Khammar et al., 2022). To address the issue of heterogeneity, a particular problem for grain sizes exceeding 1 mm, three or four closely located points were analyzed to obtain an averaged representative value. Additionally, matrix-matched certified reference materials (CRMs) were regularly included to address matrix effects. Matrix effects occur when differences in the physical and chemical properties between the sample and the calibration standards cause inaccuracies in the measurement. Using CRMs that closely resemble the analyzed samples' composition can minimize these effects, resulting in more reliable data.

2.5.3 QA/QC

In all applications, it is crucial to implement robust QA/QC plans and systematic laboratory controls on selected samples to ensure reliable measurements (Lemiere, 2018). Assessing the precision and accuracy of analytical sessions is vital in analytical geochemistry. By implementing QA/QC procedures, analysts can confidently assess the significance of their results (Hall et al. 2011; Piercey, 2014; Lemiere, 2018; Ravansari et al., 2020). These procedures help identify and rectify potential errors and track the reliability and consistency of analytical data over time (Piercey, 2014; Garcelon et al., 2016, 2018). In this research, we utilized the pXRF in "GeoChem" mode. Vanta’s GeoChem mode employs a dual-beam system, with the primary beam operating at 50 kV and a secondary beam at

10 kV. Each beam is integrated for 120 seconds, totaling 240 seconds per measurement point (see also Heidarian et al., 2021). The Geochem mode, primarily optimized for typical rock major elemental analysis, can also be effectively utilized for trace-element analysis when calibrated with standards of comparable element concentrations and matrices (Heidarian et al., 2021). In this study, the QA/QC procedures utilized were based on methods developed by Hall et al. (2011). In various technical examinations of pXRF, a notable concern is the potential for instrumental drift observed across multiple measurements (Fischer et al., 2017; Hall et al., 2011; Le Vaillant et al., 2016; Bourke and Ross, 2014). To address this issue, the common approach involves periodically analyzing CRMs to monitor and correct for drift, as Hall et al. (2011) and Bourke and Ross (2016) emphasized. In this study, at the beginning and end of each analytical session, various powdered certified reference materials (CRMs) were analyzed, including SY-4 (diorite gneiss), DS-1 (gold ore), NIST-2711a (Montana II soil), MA-2C (gold ore), NIST-2710a (Montana I soil), and OREAS 620 (Rhyodacite (VHMS ore)), as well as a SiO_2 blank. This process was repeated after every batch of seven analyses of unknown samples (Jochum et al., 2005). This rigorous protocol verifies the instrument's performance, ensuring the accuracy and reliability of the analytical results; any potential drift or bias is subsequently corrected through a calibration curve constructed using all the analyzed CRMs. In our study, instrument performance was evaluated by plotting measured element concentrations against those of certified reference materials (CRMs) and documenting calibration metrics such as slope, intercept, and the goodness-of-fit (r^2). Here, r^2 was calculated as the square of the Pearson Product correlation coefficient, as the proportion of variance in the CRM data explained by our calibration model, distinguishing it from R^2,

which is commonly used in multiple regression contexts (cf. Hall et al., 2011; Heidarian et al., 2021).

2.5.4 Log-ratio approach to compositional data

The family of log-ratio transformations consists of the Centered Log-Ratio (CLR) transformation, Isometric Log-Ratio (ILR) transformation, and Additive Log-Ratio (ALR) transformation (Aitchison, 1986; Reimann et al., 2008; Zuo et al., 2013; Carranza, 2017; Khammar et al., 2021; Vasilopoulos et al., 2023). In the CLR method, the logarithm of each variable is initially specified and subsequently divided by the geometric mean of the variables (Eq. 1).

clr (x)= [$\ln\frac{X_1}{g_{m\,(X)}}$, $\ln\frac{X_2}{g_{m\,(X)}}$, …, $\ln,\frac{X_D}{g_{m\,(X)}}$],

The CLR transformation is commonly used in compositional data (CoDA) analysis to handle data that sum to a constant value (closed data). It transforms compositional data from a simplex to real Euclidean space, making it suitable for statistical analysis techniques that assume normality and linearity, such as PCA (Buccianti and Grunsky, 2014; Pawlowsky-Glahn et al., 2015). This study utilized the CLR-transformed values obtained from CoDaPack software version 2.03.01 for PCA analysis. The results can be directly applied to other methods that depend on subspace estimation, including Principal Component Analysis (PCA) and cluster analysis.

2.5.5 CoDA-Compositional Data Analysis

Geochemical datasets consist of compositional variables where the individual components represent fractions of a whole (Cicchella et al., 2022). Ignoring this compositional nature can lead to misleading results due to outliers and data closure. To address these issues,

various multivariate techniques, such as principal components analysis (PCA), cluster analysis, and discriminant analysis, have been adapted specifically for the analysis of compositions (Buccianti and Grunsky, 2014; Barak et al., 2021; Cicchella et al., 2022, Vasilopoulos et al., 2023; Khalifani et al., 2019, 2023c). The function pcaCoda is used for performing the robust principal component analysis (PCA) on compositional data (Braga and Braga, 2020). It applies statistical methods less sensitive to outliers and deviations from normality, making it suitable for handling the unique characteristics of compositional datasets, such as closure constraints and non-normal distributions (Filzmoser et al. 2009; Pawlowsky-Glahn et al., 2015). The goal of PCA is to reduce the dimensions of large data sets by converting interrelated variables into new, uncorrelated variables called principal components, arranged in decreasing order of importance (Jolliffe, 2002; Filzmoser et al., 2009; Cicchella et al., 2022). A biplot is a 2D visualization of singular value decomposition (SVD), where data points are represented as dots and variables as rays (Otero et al., 2005). The length of each ray reflects the variable's standard deviation, and closely aligned rays suggest a strong association between variables. If multiple rays align, a potential compositional linear relationship may exist. The angle between rays represents the correlation between the simple log ratios of variables, with a 90-degree angle indicating likely noncorrelation (Egozcue and Pawlowsky-Glahn, 2005; Hron and Filzmoser., 2014).

2.5.6 Cluster analysis

Cluster analysis can be utilized to categorize samples and generate insights into the multivariate geochemistry of the given dataset. An effective cluster analysis will produce clusters in which the observations within each group are highly similar whereas the differences between the clusters are maximized. Cluster analysis automatically determines

the optimal number of classes using data-driven criteria and assigns each observation to the most appropriate group (Templ et al., 2008). It is essential to consider appropriate data transformations to "open" the data before conducting cluster analysis (Aitchison, 1986, Barak et al., 2021;). As previously discussed, the CLR transformation was employed to open the data and facilitate their analysis in real space.

2.5.7 µ-XRF mapping

For in situ investigations of texture, mineral chemistry, and mineral and elemental indicators of gold, polished thin sections were analyzed using µ-XRF mapping, with details of the analytical methods described in Flude et al. (2017). µ-XRF allows for high-resolution elemental mapping at a microscopic scale, with a spatial resolution of ~20 µm, revealing variations in elemental composition within mineral grains.

This technique is valuable for studying the distribution and concentration of S, Fe, Cu, Zn, and other elements within sulfide minerals. By analyzing element zonation, we can gain insights into mineral formation processes, composition, alteration, and mineralogical associations, aiding in interpreting geological and metallurgical phenomena. 2D µ-XRF-Energy Dispersive Spectrometry (EDS) mapping enables high spatial resolution and nondestructive textural analysis of dominant mineralogy in polished thin sections (Genna et al., 2011; Heidarian et al., 2021; Mami khalifani et al., 2023a, b). This technique involves placing polished thin sections inside a vacuum chamber for EDS mapping analysis.

X-rays were generated using a rhodium (Rh) tube (30–50 kV, 300–400 µA; Flude et al., 2017) and analyzed with a static spot size of 20 µm to create raster multi-element maps (Guilherme et al., 2012; Heidarian et al., 2021). These maps, constructed from pixel intensities linked to X-ray spectra, provide clear visualization of elemental distributions.

Color-coded μ-XRF maps enhance the interpretation of elemental distributions and interrelationships. Heidarian et al. (2021) demonstrated their utility by identifying a systematic association between visible gold and sulfide minerals (pyrite, chalcopyrite, arsenopyrite, and sphalerite), thereby providing important insights into the geochemical processes governing the formation of auriferous pyritic quartz ± carbonate vein deposits.

2.6. Results

2.6.1 Mineralogy Studies

Polished thin sections prepared from drill core samples at Williams Brook (Fig. 2-5a, b) display minerals and alteration, including fine-grained muscovite and limonite. Rhyolite in the hanging wall of quartz veins has a well-developed cream coloured alteration, likely due to kaolinization along with muscovite (Figs. 2-5a, b, 2-6a). This suggests significant chemical weathering, where kaolinite locally forms as a result of the breakdown of feldspar and muscovite (Sánchez Mora et al., 2021). Chlorite, fine-grained muscovite, and secondary limonite are the most prevalent alteration types in the Williams Brook samples, and chlorite, muscovite, and recrystallized quartz are the primary hypogene silicate minerals in altered veins in the Williams Brook area (Fig. 2-5a, b, 2-6a). These hypogene gold-bearing quartz veins commonly contain minor amounts of sphalerite, chalcopyrite, galena, and visible gold. Sphalerite adjacent to chalcopyrite within the quartz veins is red under transmitted light due to moderate iron content and has been observed at the O'Neil vein in the Williams Brook area (Puma Exploration Inc. 2021).

Disseminated sulfide mineral (pyrite and sphalerite) occur locally within the rhyolite host rocks. Pyrite is the primary sulfide mineral in this region, comprising 1 to 5% of the host

rock. Native gold occurs within pyrite and minor galena (Fig. 2-7a). In some quartz veins, sphalerite is the dominant sulfide mineral, followed by galena (1-2%) and trace amounts of pyrite (Fig. 2-7b). Drill core samples, such as DDH WB22-66-66.50B and WB22-66-68.05 (Fig. 2-7a, b), contain visible gold, galena, and sphalerite as indicator minerals. Previous studies indicate that most of the gold occurs on pyrite rims, according to ore mineral chemistry; however, this is not exclusive, as gold mineralization can also be associated with different generations of quartz (Sánchez Mora, 2014; Sánchez Mora et al., 2021, Mami khalifani et al., 2022, 2025). The highest gold concentrations recorded in the cores are 183 and 134.5 g/t Au from samples WB22-25 and WB22-66.

Polished thin sections derived from drill core samples at McIntyre Brook (Fig. 2-5c, d) exhibit alteration such as muscovite and chlorite. Muscovite, with high-grade gold mineralization, is the most prevalent alteration in this area. Additionally, low-grade gold occurs with zones of silicification and hematization (Fig. 2-6b). The gold mineralization in the MB area was noted to be localized within two parallel bands of hematite, pyrite, and lesser amounts of silica-cemented breccia. These mineralized zones occur within and around the boundaries of sub-vertical dykes cutting argillic altered siltstone host rocks. The gold-associated mineral assemblage, in addition to native gold, includes pyrite, pyrrhotite, chalcopyrite, hematite, magnetite, stibnite, and elevated rare earth metals (cf. Wood 1987; Fig. 7c, d). Based on Lode Gold Resources Inc. (2019) report, grab sample assays yielded up to 43.1 g/t Au from hematite-magnetite veins cutting altered sedimentary rocks of the Wapske Formation.

Drill core samples from Mulligan Gulch show a variety of alteration minerals, including ankerite, muscovite, and biotite (Fig. 2-5e, f). These alteration styles, together with

hematization and silicification, are present in both low-and high-grade gold zones, with silicification being the most dominant and laterally extensive (Fig. 2-6c). Evidence from polished thin sections prepared from a gold-bearing interval in this area further highlights the spatial association of pyrite and pyrrhotite with gold (Fig. 2-7e, f).

Simpsons Field displays carbonatization, silicification, and sericitization with minor hematitic and argillic alteration types (Fig. 5g, h). Gold-bearing veins comprise quartz-siderite and minor pyrite, arsenopyrite, and hematite. Gold occurs as isolated grains within pyrite or along grain boundaries. Polished thin-section analyses of mineralized and altered rock samples from SF revealed quartz as the dominant mineral, along with sericite-muscovite alteration (Fig. 2-5g, h). Sericitation, carbonatization, and hematization are prevalent alteration types in this area and are associated with high-grade gold mineralization (Fig. 6d). Pyrite and pyrrhotite are identified as crucial indicators of sulfide minerals for gold mineralization in the SF gold occurrence (Fig. 2-7g, h).

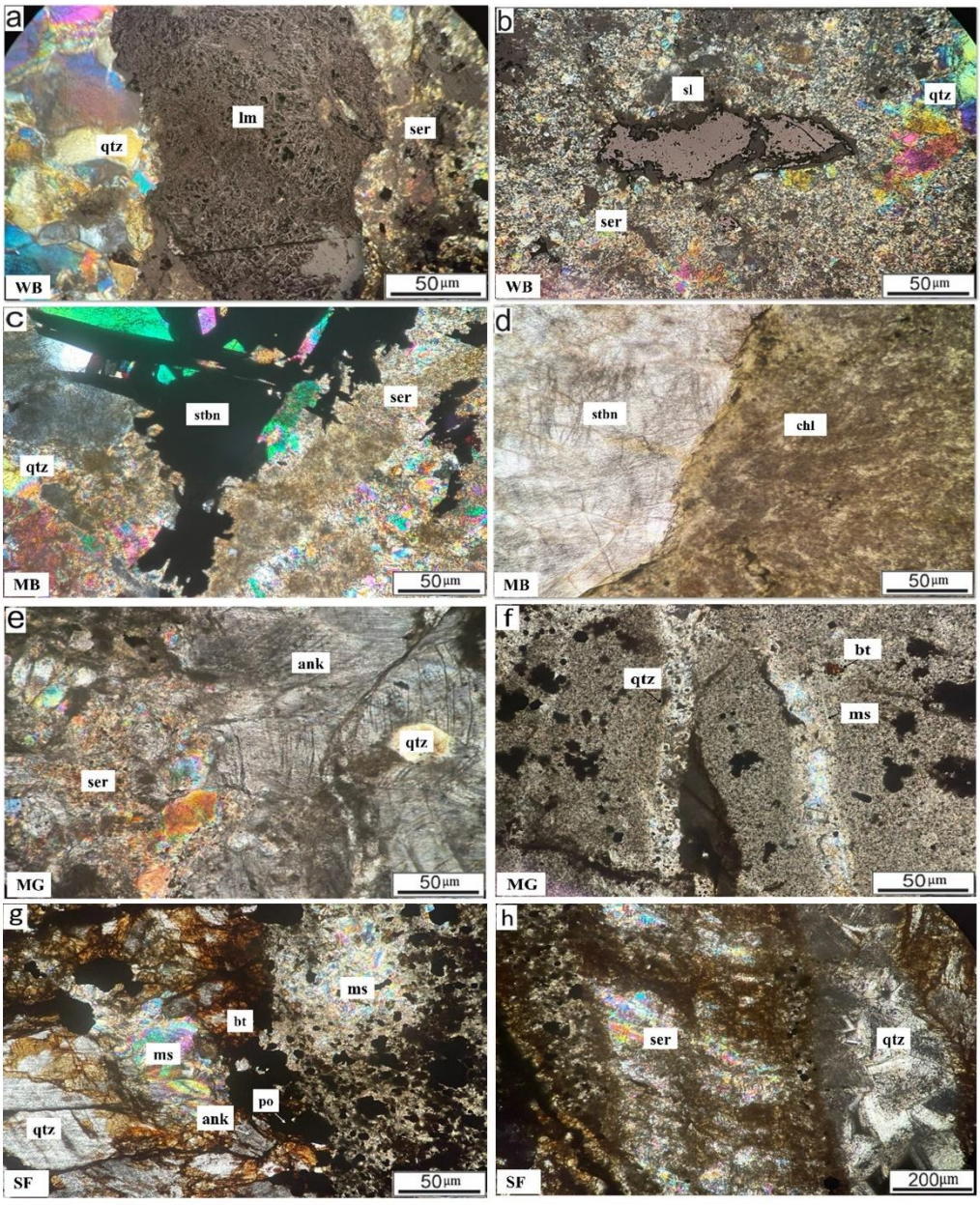

Figure 2-5. Photomicrograph images (crossed polarized light, CPL) of minerals in altered host rocks from quartz-carbonate veins in the Williams Brook, McIntyre Brook, Mulligan Gulch, and Simpsons Field areas. a) Sericite alteration, accompanied by limonite in the altered margin of quartz veins. (sample WB22-66-68.50A, from the Williams Brook gold occurrence). b) Sphalerite in the center of the Sericite alteration in the margin of quartz veins. (sample WB22-66-68.05, from the Williams Brook gold occurrence). c) Stibnite and

sericite alteration are observed near an altered quartz vein. Sericite constitutes the prevalent altered mineral in the vein (sample MBO19-03-70A, from the McIntyre Brook gold occurrence). d) Stibnite is found in proximity to chlorite alteration. (Sample MBO19-03-70, from the McIntyre Brook gold occurrence). e) Quartz veinlet is present within ankerite and sericite in an altered porphyry host rock (sample Mg1-35.70 A, from the Mulligan Gulch occurrence). f) Samples from Mg1-35.70 B show the presence of a quartz vein along with biotite and muscovite alteration. g) Alteration assemblage of sericite and muscovite with biotite and quartz (qtz) surrounding pyrrhotite (po) (sample SF2-14.70, from the Simpsons Field). h) Sericite alteration appears along the margins of the quartz vein (sample SF2-18.34, from the Simpsons Field). All images are in transmitted crossed polarized light. Abbreviations are sericite (ser), limonite (lm), quartz (qtz), sphalerite (sl), stibnite (stbn), chlorite (chl), ankerite (ank), biotite (bt), muscovite (ms), pyrrhotite (po).

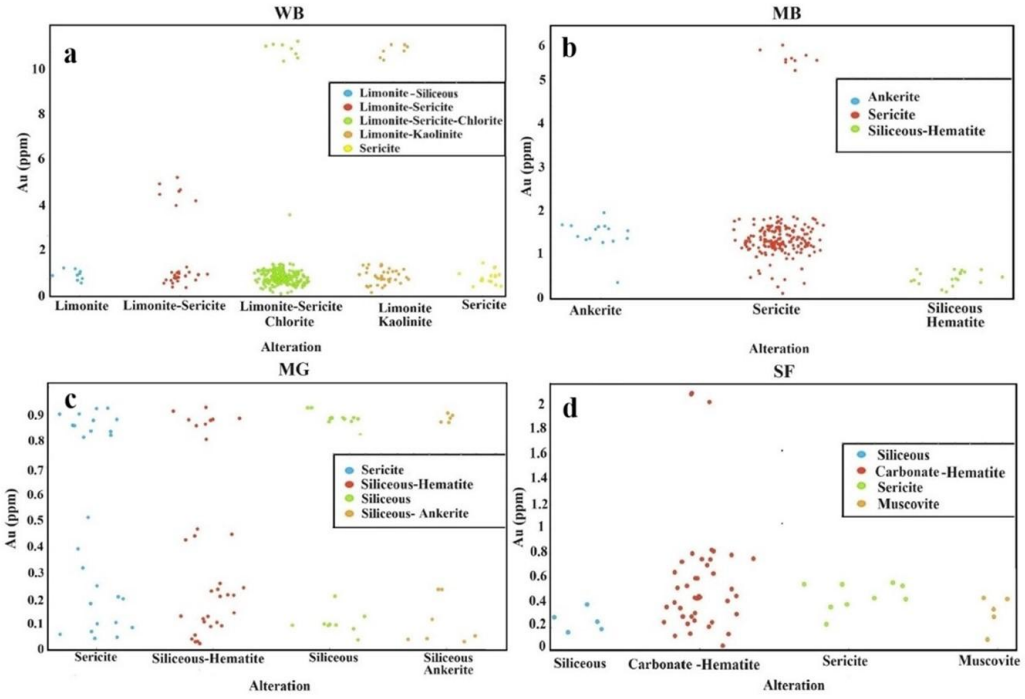

Figure 2-6. Variation plots of core samples from gold mineralization that illustrate the alteration types associated with gold deposits and occurrences in four areas: a) Williams Brook (Limonite-Siliceous, Limonite-Sericite, Limonite-Sericite-Chlorite, Limonite-Kaolinite, and Sericite), b) McIntyre Brook (Ankerite, Sericite, Siliceous, and Siliceous-Hematite), c) Mulligan Gulch (Sericite, Siliceous-Hematite, Siliceous, and Siliceous-Ankerite), d) Simpsons Field (Siliceous, Carbonate-Hematite, Sericite, and Muscovite).

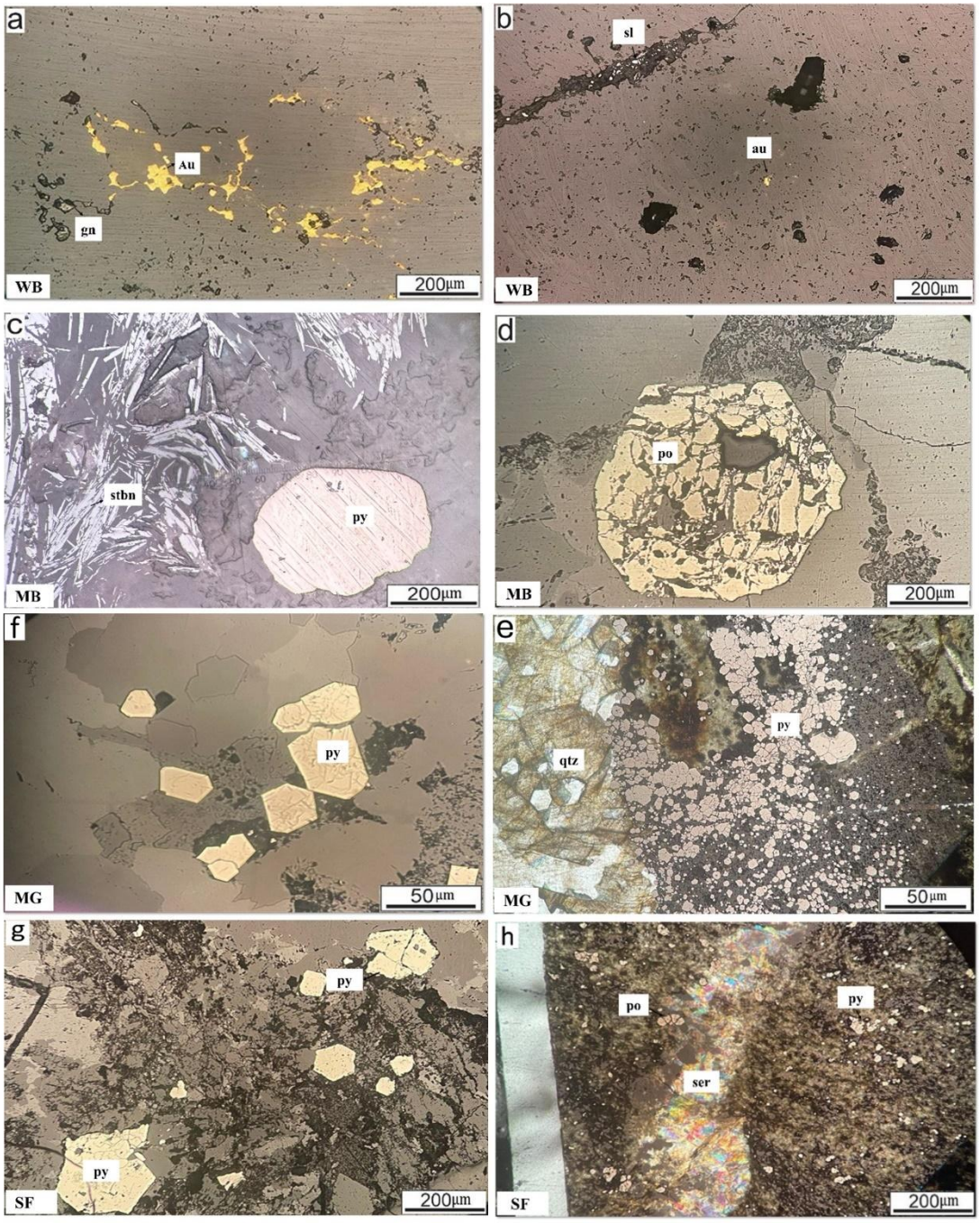

Figure 2-7. Photomicrographs reflect light plane polarized light of various sulphides and electrum (gold) within various gangue phases. a) Gold with some sulphide minerals, such as pyrite (py), and galena (gn) (sample WB22-66-66.50B, from the Williams Brook occurrence). b) Gold with minor sphalerite (sl) in the quartz vein (sample WB22-66-

66.50A, from the Williams Brook occurrence). c) Massive of acicular stibnite (stbn) around pyrite (py) (sample MBO19-03-81, from the McIntyre Brook occurrence). d) A sieve-textured pyrrhotite (po) (sample MBO19-03-66.70B, from the McIntyre Brook occurrence). e) pyrrhotite-rich (po) close to quartz vein; (sample Mg-55.82, from Mulligan Gulch). f) Pyrite (py) within rhyolite (sample MG-35.70, from Mulligan Gulch). g) pyrite (py) with sulphide inclusions, such as pyrrhotite (po) (sample SF2-18.74, from Simpsons Field). h) pyrrhotite (po) and pyrite (py) surrounded by sericitic (ser) alteration (sample SF2-14.70, from the Simpsons Field). Abbreviations are pyrite (py), galena (gn), sphalerite (sl), stibnite (stbn), pyrrhotite (po), sericitic (ser).

2.6.2 . Portable X-Ray Fluorescence (pXRF) Spectrometry data analysis

As described above, drill core samples from epithermal gold occurrences were examined using pXRF to study the quartz vein gold-bearing mineralization and associated host rock alteration. Summarized slope and R^2 values for various elements are presented in Tables 2-2 and 2-3 for the Williams Brook, McIntyre Brook, Mulligan Gulch, and Simpsons Field occurrences, respectively. For each element, calibration 'accuracy' is defined as the absolute difference between the observed slope and the ideal value of 1 (i.e. $|\text{slope} - 1|$) and precision, as indicated by the r^2 value. A higher composite score reflects both a slope closer to 1 (indicating higher accuracy) and a higher r^2 (indicating greater precision and repeatability). We further integrated these two metrics into a single composite score to rank the reliability of the pXRF measurements for each element, as per the criteria outlined by Hall et al. (2011) and Heidarian et al. (2021).

Table 2-2. Element accuracy and precision for Williams Brook (left) and McIntyre Brook (right) according to Hall et al. (2011) criteria.

Element	Accuracy |m-1|	Precision (R^2)	Score
S	0.55	0.71	1
K	0.61	1.00	6
Ca	0.83	0.99	3
Ti	0.80	0.09	0
Mn	0.93	0.98	3
Fe	0.78	0.91	4
Cu	0.42	0.94	5
Zn	0.52	1.00	6
As	0.80	0.99	4
Rb	0.84	0.88	3
Sr	1.01	0.99	2
Zr	0.75	0.81	5
Mo	1.00	0.92	4
Ag	0.69	0.96	5
Sn	0.30	0.89	5
Sb	0.47	0.91	5
Ba	1.10	0.95	3
W	0.65	0.78	2
Pb	0.90	0.99	4

Element	Accuracy |m-1|	Precision (R^2)	Score
S	0.53	0.69	0
K	0.69	0.92	5
Ca	0.80	0.90	3
Ti	0.30	0.70	1
Mn	0.84	0.98	4
Fe	0.47	0.88	4
Cu	0.69	0.92	6
Zn	0.62	0.99	6
As	0.74	0.95	4
Rb	0.83	0.89	3
Sr	1.10	0.99	4
Zr	0.78	0.81	3
Mo	1.00	0.99	4
Ag	0.77	0.96	5
Sn	0.21	0.87	5
Sb	0.51	0.97	5
Ba	1.08	0.95	4
W	0.24	0.78	2
Pb	1.10	0.99	5

Table 2-3. Element accuracy and precision for Mulligan Gulch (left) and Simpsons Field (right) according to Hall et al. (2011) criteria.

Element	Accuracy $[m^{-1}]$	Precision (R^2)	Score
S	1.70	0.94	3
K	0.75	0.95	5
Ca	0.90	0.83	3
Ti	0.10	0.06	0
Mn	0.38	0.19	1
Fe	0.63	0.75	3
Cu	0.73	1.00	6
Zn	0.68	0.99	5
As	0.75	1.00	5
Rb	1.24	0.60	3
Sr	0.84	0.52	3
Zr	0.75	0.87	4
Mo	0.51	0.99	5
Ag	0.83	0.88	4
Sn	1.02	0.89	3
Sb	0.56	0.99	6
Ba	0.25	0.24	2
W	0.10	0.06	0
Pb	0.34	0.97	5

Element	Accuracy $[m^{-1}]$	Precision (R^2)	Score
S	0.93	0.96	4
K	0.72	0.96	5
Ca	0.94	0.85	3
Ti	1.23	0.52	3
Mn	0.95	0.97	4
Fe	0.66	0.90	5
Cu	0.74	1.00	6
Zn	1.21	0.99	4
As	0.78	1.00	5
Rb	1.29	0.63	1
Sr	0.85	0.61	0
Zr	0.92	0.84	4
Mo	0.53	1.00	5
Ag	0.99	0.97	4
Sn	1.17	1.00	4
Sb	0.85	1.00	5
Ba	0.67	0.99	5
W	1.69	0.32	2
Pb	0.78	0.99	5

Certain elements, such as Zn, Cu, Sb, Pb, and K, demonstrate stronger scores, indicating higher reliability, whereas W, Ti, Ba, Mn, and Sr are predominantly below detection. The initial data were adjusted using pXRF with CRM-based correction curves. In this study, CRMs were primarily employed to construct correction curves and to monitor and correct

for instrumental drift; they were not reused as independent validation standards. Accuracy was instead evaluated through the consistency of corrected values with expected geochemical ranges and comparative datasets, while precision was measured through replicate analyses and correlation coefficients. These adjustments collectively improve the accuracy and precision of the elemental composition data by compensating for systematic errors and biases in the measurements. The statistical summaries of the corrected pXRF data are detailed in Tables 2-4 and 2-5 for the Williams Brook, McIntyre Brook, Mulligan Gulch, and Simpsons Field occurrences. Due to poor precision, accuracy, and low concentration (below detection), specific elements, such as Ni, Nb, Ta, and Y, were excluded from the pXRF dataset.

Table 2-4. Statistical summary of corrected pXRF Data for Williams Brook and McIntyre Brook samples.

Element		WB		MB	
		n = 93		n = 62	
		Mean	SD	Mean	SD
Au	ppb	2900	15700	1018.1	904.4
S	%	0.22	0.45	2.24	17.83
K	%	3.42	3.33	2.87	3.02
Ca	%	0.71	3.26	1.67	5.82
Ti	%	0.17	0.20	0.14	0.31
Mn	%	0.06	0.30	0.26	0.85
Fe	%	2.78	5.43	4.90	6.96
Cu	ppm	18	31	81	346
Zn	ppm	69	541	19	59
As	ppm	39	395	413	1705
Rb	ppm	140	133	97	83
Sr	ppm	73	121	41	252
Zr	ppm	366	231	220	159
Mo	ppm	13.2	38.8	60	121
Ag	ppm	3.6	3.7	33	78
Sn	ppm	257	78	14	4
Sb	ppm	41	29	14	11
Ba	ppm	449	326	326	145
W	ppm	13	26	38	66
Pb	ppm	35	136	11	19

Note: Au assays from the assessment file.

Table 2-5. Statistical summary of corrected pXRF Data for Mulligan Gulch and Simpsons Field samples.

Element		MG		SF	
		n = 93		n = 62	
		Mean	SD	Mean	SD
Au	ppb	390800	354400	321400	429000
S	%	0.50	1.15	1.78	2.10
K	%	0.25	0.26	0.27	0.22
Ca	%	2.51	3.69	2.78	3.67
Fe	%	1.07	0.98	9.12	8.89
Cu	ppm	6	22	4	1
Zn	ppm	383	2817	179	19
As	ppm	48	120	39	41
Zr	ppm	388	282	78	45
Mo	ppm	4.7	5.7	2.2	2.0
Ag	ppm	1.5	1.1	1.2	1.0
Sb	ppm	6.6	10.3	8.3	5.8
Ba	ppm	89	88	38	22
Pb	ppm	53	110	27	12

Scatter plots of Fe, Sb, S, Cu, and As highlight geochemical patterns characteristic of sulfide mineralization, which serve as key indicators of gold mineralization (Fig. 2-8a–f). The S–Fe diagram reveals a strong, statistically significant positive correlation (Pearson's $r = 0.72$, $p < 0.01$) in the Williams Brook and Mulligan Gulch datasets, while a moderate correlation is observed in the Simpsons Field and McIntyre Brook areas (Fig. 2-8a). The Sb vs. S plot shows that the Williams Brook and McIntyre Brook datasets display relatively high Sb values compared to S, indicating the occurrence of Sb-bearing sulfides (Fig. 2-8b). In contrast, the Mulligan Gulch and Simpsons Field datasets are characterized by low Sb and relatively high S concentrations. In the Fe vs. Cu plot, Fe values are consistently higher than Cu across all study areas (Fig. 2-8c). Among them, McIntyre Brook displays relatively elevated Cu contents, while Williams Brook, Mulligan Gulch, and Simpsons Field remain strongly Fe-dominated. In the S vs. Cu plot (Fig. 2-8d), Mulligan Gulch shows a strong and statistically significant positive correlation ($r = 0.78$, $p < 0.001$). By contrast, Williams Brook, McIntyre Brook, and Simpsons Field exhibit weak to negligible correlations, indicating variable relationships between sulfur and copper.

In the Fe vs. As diagram, McIntyre Brook shows the highest As contents, whereas Williams Brook has moderate As and both Mulligan Gulch and Simpsons Field are As-poor, with the latter also marked by elevated Fe (Fig. 2-8e). A comparable trend is observed in the S vs. As diagram, where McIntyre Brook is enriched in As across a wide S range, Williams Brook records moderate levels, and Mulligan Gulch and Simpsons Field remain As-poor (Fig. 2-8f).

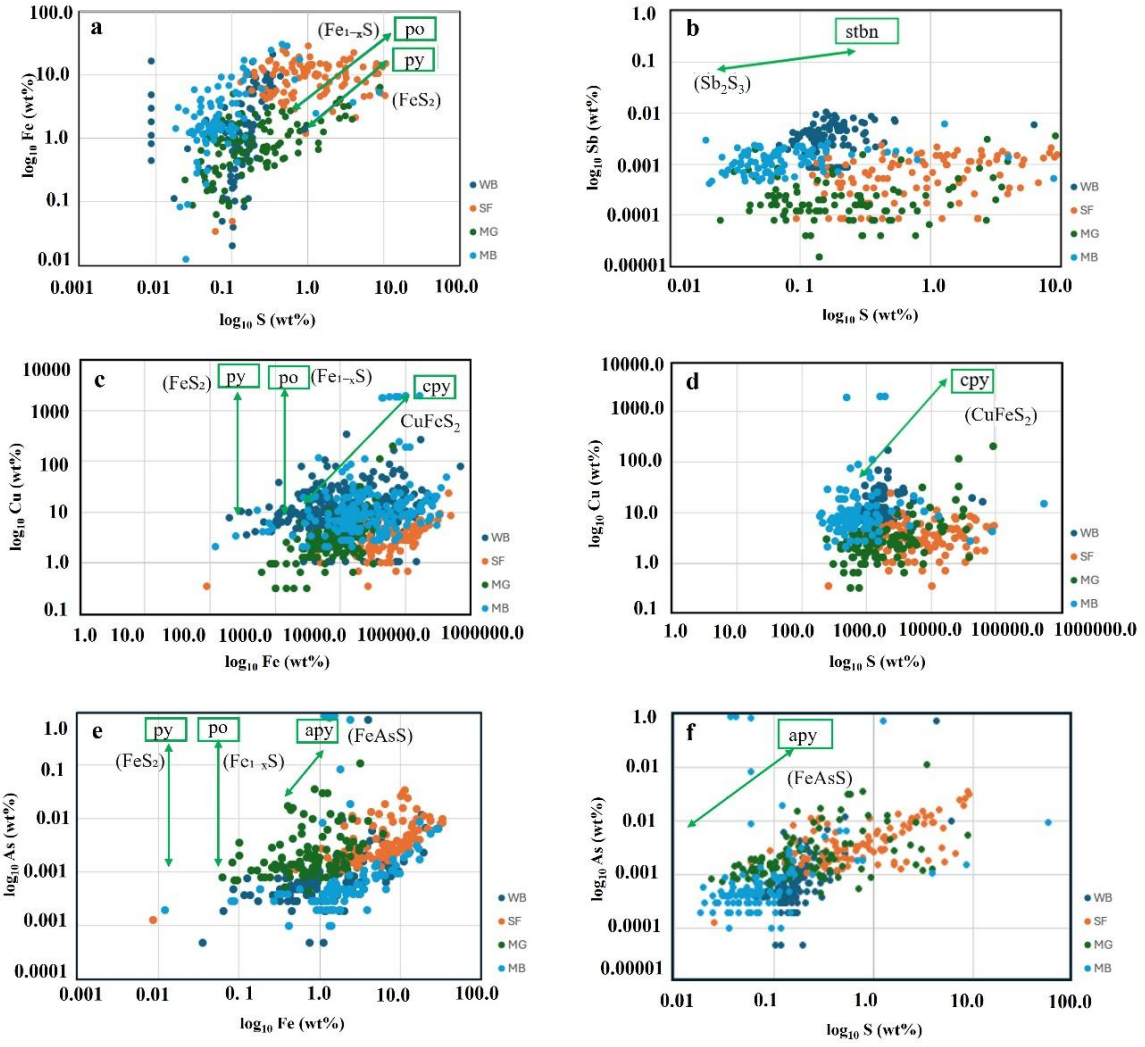

Figure 2-8. Scatter plots of pXRF data for gold occurrences from Williams Brook, McIntyre Brook, Mulligan Gulch, and Simpsons Field areas include a) S vs. Fe; b) S vs. Sb c) Fe vs. Cu; d) S vs. Cu; e) Fe vs. Au; f) S vs. As.

2.6.3 . Principle Component Analysis (PCA) of pXRF data

After performing PCA, the ILR-transformed data, including loadings, scores, and eigenvalues, were back-transformed into CLR-space to facilitate interpretation using a compositional biplot (Cicchella et al., 2022). PCA efficiently identifies groups of variables and highlights their importance in relation to gold mineralization. When the scree plot

shows that the largest variances are concentrated in the first few components, typically only two or three components are selected for further analysis or visualization because they capture the most significant patterns and relationships in the data. The dataset comprises three main components, each having eigenvalues greater than one (Heidarian et al., 2021). In the Williams Brook dataset, the first principal component (PC1; 38.35% of the variance) is characterized by strong positive loadings for S, Cu, and Sb, which show a close alignment with Au in the biplots (Fig. 2-9a, b). The PC1 vs. PC2 biplot further emphasizes this strong association, with Au clustering closely with S, Cu, and Sb. (Fig. 2-9a). The PC1 vs. PC3 biplot further shows Au clustering with S, Sb, and Cu, while also displaying a weaker affinity with W and Ag. PC2 and PC3 are characterized by elevated contributions from W, Sn, Mo, and Ag, distinguishing them from the Au, S, Cu, Sb association along PC1 (Fig. 2-9b). In the McIntyre Brook occurrence, Au is closely associated with Ag, Pb, Sn, Sb, and Cu, which consistently group together across the principal components, defining a multi-element pathfinder suite for Au mineralization (Fig. 2-9c, d). In the PC1 vs. PC2 biplot, Au occurs with Cu, Sb, Sn, Ag, and Pb (Fig. 2-9c). In the PC1 vs. PC3 biplot, Au correlates with Sr, Pb, and Ag. The same diagram also shows strong loadings of K, Rb, and Ti, together with a negative relationship to Ca (Fig. 2-9d). The Mulligan Gulch data show a positive correlation between Au, Sb, and Ba in PC1 vs. PC2 (Fig. 2-9e). In the PC1 vs. PC3 biplot, Au is associated with K (Fig. 2-9f). Using the data from Simpsons Field, PC1 vs. PC2 reveals a positive correlation between Au, Cu, Ba, Mo, Zn, and K (Fig. 2-9g). In the PC1 vs. PC3 biplot, Au is associated with Cu, Zn, Fe, Sb, and K (Fig.2-9h).

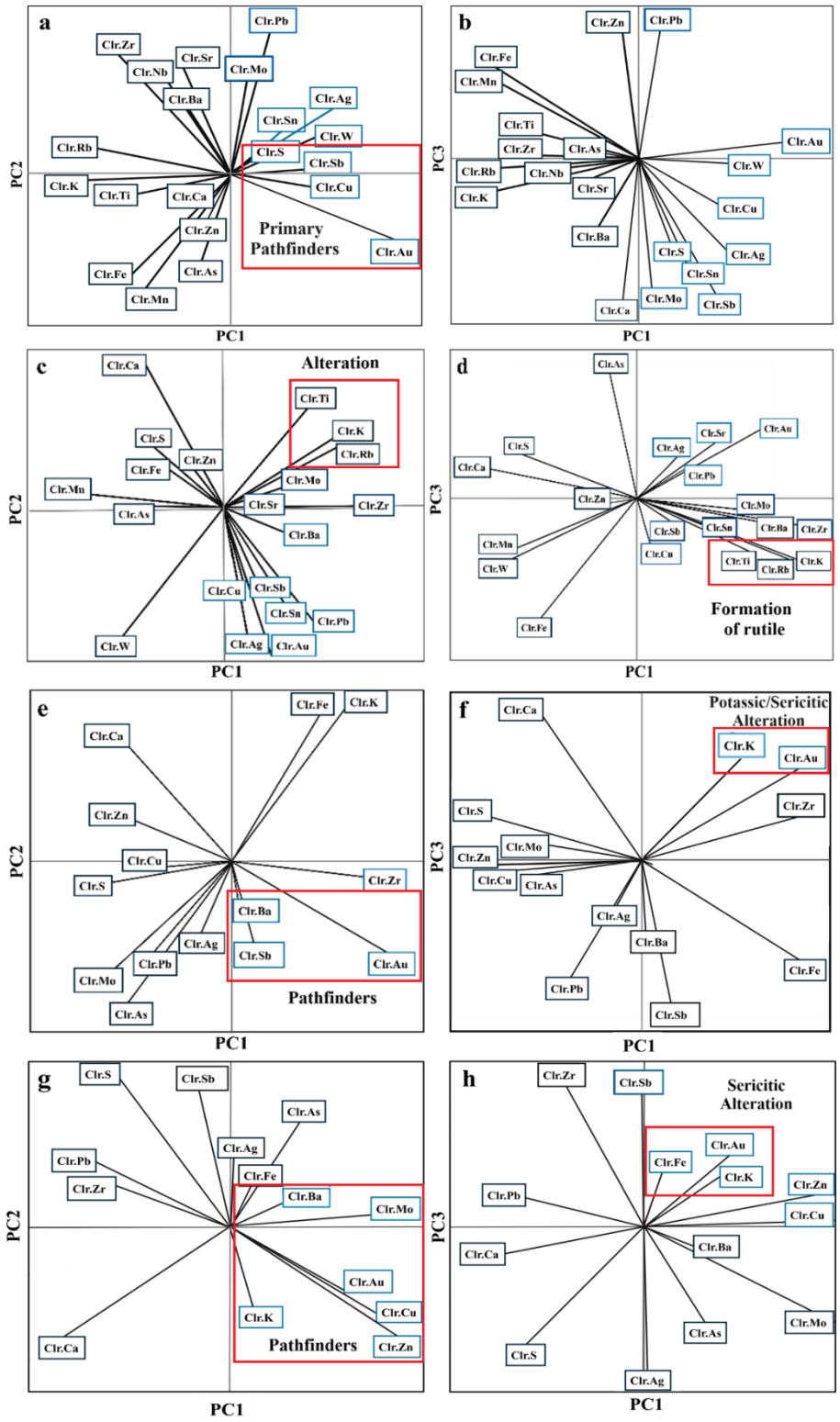

Figure 2-9. Biplots of principal component analysis (PCA) for pXRF data of all areas. a, b) Williams Brook; c, d) McIntyre Brook; e, f) Mulligan Gulch; g, h) Simpsonss Field.

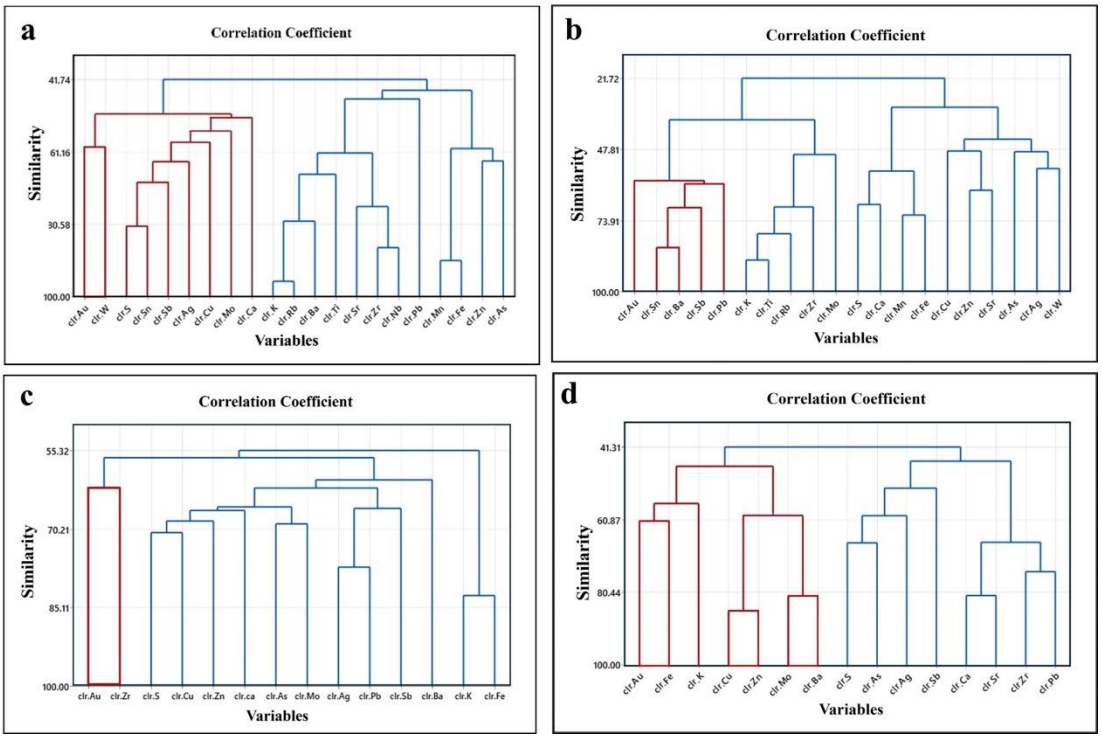

Figure 2-10. Cluster analysis (dendrogram) diagrams based on the opened pXRF data by CLR transformation for areas. a) Williams Brook; b) McIntyre Brook; c) Mulligan Gulch; d) Simpsons Field.

2.6.4 . Micro (µXRF) X-ray Fluorescence (µXRF) Spectrometry

Micro-XRF EDS mapping analysis was employed to support pXRF and petrography to help identify sulfide minerals within quartz veins and alteration phases (Heidarian et al., 2021). The distribution of sulfide minerals, including pyrite, pyrrhotite, chalcopyrite, galena, and sphalerite, all of which can be indicators of quartz vein hosted gold mineralization, were determined through mineralogical studies and by plotting variations in pathfinder elements. µXRF-EDS mapping verifies that gold is associated with specific sulfide minerals in all areas studied, consistent with the elemental associations of gold

pathfinder elements (S, Sb, Cu, As, Ag, Zn, and Fe) illustrated by the principal components and cluster analyses (Figs. 2-9, 10).

At the Williams Brook area, images from samples WB22-66-68.05 (Zn, Au, Pb, W) and WB22-66-66.50b (Fe, Au, Pb) confirms the presence of native gold within sulfide-bearing quartz veins (Fig. 2-11a, b). μXRF analysis also confirms the presence of the same suite of pathfinder-indicator Au-associated elements as identified through compositional-based multivariate techniques applied to pXRF data. Figure 2-11b illustrates the iron oxide vein located next to the gold, confirming that gold mineralization is associated with iron oxide and quartz veins. According to μXRF analysis (Fig. 2-11c, d), a high concentration of Fe, S, and Ca at McIntyre Brook is linked to hematite- and sulfide mineral-bearing quartz veins, whereas the presence of S, Sb, and Ca further suggests the occurrence of sulfide minerals in the area.

In the Mulligan Gulch, μXRF imaging highlights the occurrence of S, Pb, Ca, and As, indicating the formation of sulfide minerals in the quartz veins (Fig. 2-11e). Figure. 2-11f depicts a quartz vein (a red spot outlined with a white boundary), with previous studies have shown that gold mineralization at Mulligan Gulch is associated with fine-grained arsenopyrite, and pyrite either hosted within or adjacent to quartz veins (McCutcheon and Bevier, 1990; Forest, 2021).

At Simpson Field, sample SF-18.34 (Fig. 2-11g) shows stibnite (A purple spot bordered by a white outline) adjacent to sulfide-bearing quartz (-carbonate) veins, while Fig. 2-11h reveals the presence of Fe and Ca in sample SF-14.70, suggesting the presence of carbonate minerals, such as siderite and ankerite (a green spot outlined with a white boundary).

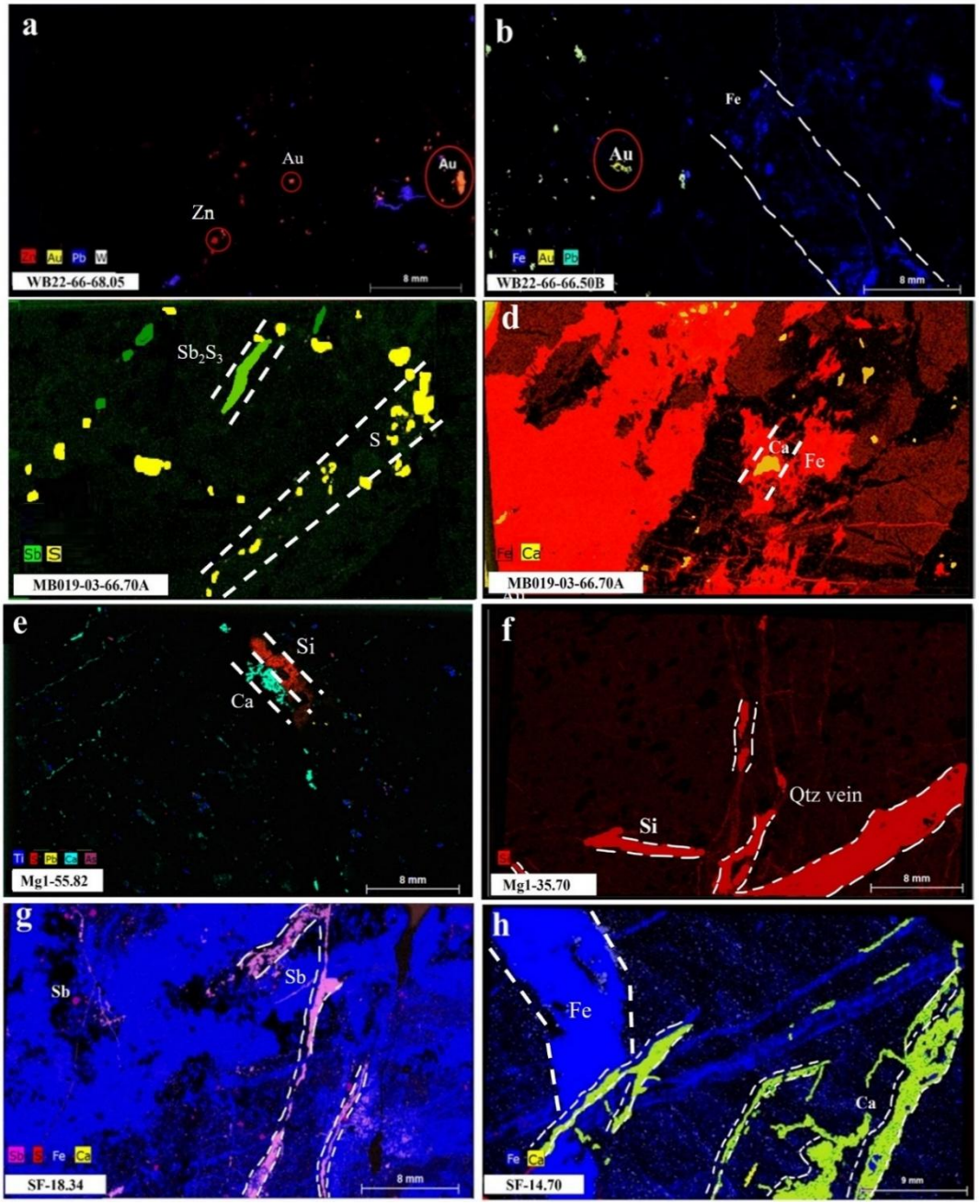

Figure 2-11. Multielement μXRF- Energy Dispersive Spectrometry (EDS) maps depict the distribution of gold and sulfide minerals, and key elements such as W, Fe, Ti, Ca, and Si in polished thin sections from WB (a, b), MB (c, d), MG (e, f), and SF (g, h), respectively.

2.7. Discussion

As shown in Fig. 2-8a, the strong S–Fe correlations at Williams Brook and Mulligan Gulch reflect the dominance of Fe-sulfide minerals, particularly pyrite and pyrrhotite, as the principal hosts of both sulfur and iron. In contrast, weaker correlations at Simpson Field and McIntyre Brook suggest that additional mineral phases or alteration processes influence S–Fe distributions in these areas. Elevated Sb at Williams Brook and McIntyre Brook (Fig. 2-8b) indicates the presence of Sb-bearing sulfides such as stibnite and tetrahedrite, whereas low Sb and higher S at Mulligan Gulch and Simpson Field imply sulfur is primarily hosted in common sulfides, including pyrite, arsenopyrite, chalcopyrite, or sphalerite. This distinction between Sb-rich and S-rich sulfide assemblages is supported by Fe-based plots (Figs. 2-8a, c), which highlight the role of iron sulfides in controlling sulfur distribution. The relatively higher Cu at McIntyre Brook points to localized chalcopyrite mineralization, while the strong Fe dominance at Williams Brook, Mulligan Gulch, and Simpson Field reflects pyrite- and pyrrhotite-rich assemblages with minor Cu contributions. Similarly, the strong S–Cu correlation at Mulligan Gulch (Fig. 2-8d) is consistent with chalcopyrite ($CuFeS_2$), in contrast to weaker associations at the other areas. Elevated As contents at McIntyre Brook reflect arsenopyrite enrichment, whereas moderate As at Williams Brook and the As-poor character of Mulligan Gulch and Simpson Field (Figs. 2-8e, f) indicate limited or negligible arsenopyrite in those areas.

In this study, the first three components are interpreted as having geological significance (Fig. 2-9a-h). At Williams Brook, the strong alignment of Au with S, Cu, and Sb along PC1 suggests control by sulfide assemblages, including pyrite, chalcopyrite, and Sb-bearing phases such as stibnite and tetrahedrite, whereas the elevated contributions of W,

Sn, Mo, and Ag to PC2 and PC3 likely reflect secondary or late-stage hydrothermal processes (Figs. 2-9a, b). At McIntyre Brook, the clustering of Au with Cu, Sb, Sn, Ag, and Pb in the PC1 vs. PC2 biplot indicates an association with chalcopyrite, stibnite, and galena (Fig 2-9c). In the PC1 vs. PC3 biplot, the positive loadings of K, Rb, and Ti, coupled with a negative relationship to Ca, suggest titanite breakdown and rutile formation during CO_2-rich fluid interaction, producing calcite and quartz (see equation; , Fig 2-9d, and MacKenzie and Craw, 2007; Heidarian et al., 2021).

$$CaTiSiO5(titanite)+CO2(influid)=TiO2(rutile)+CaCO3(calcite)+SiO2(hydrothermal\ quartz) \quad (1)$$

At Mulligan Gulch, Au clusters with Sb and Ba (PC1 vs. PC2), reflecting control by Sb-bearing sulfides and barite, whereas the Au with K in the PC1 vs. PC3 biplot points to muscovite-rich (locally adularia-bearing) alteration characteristic of epithermal systems (Figs, 2-9e, f). At Simpson Field, the PC1 vs. PC2 biplot (Fig. 2-9g) shows Au clustering with Cu, Zn, Mo, Ba, and K, defining a polymetallic pathfinder suite indicative of sulfide-related mineralization with hydrothermal alteration. The PC1 vs. PC3 biplot (Fig. 2-9h) further links Au with K and Fe, consistent with sericitic alteration adjacent to quartz veins, as corroborated by petrographic observations (Figs. 2-4 and 2-5). Further geochemical relationships are elucidated by the expanded element Au associations shown in Fig. 2-10. At Williams Brook (Fig. 2-10a), Au clusters with S, Sb, Cu, Mo, Sn, W, and Ag, reflecting sulfide assemblages (pyrite, chalcopyrite, stibnite, tetrahedrite) with a potential hydrothermal overprint from Mo–Sn–W–Ag. At McIntyre Brook (Fig. 10b), Au is associated with Sb, Pb, Ba, and Sn, consistent with a polymetallic vein system dominated by stibnite, tetrahedrite, and galena, and distinguished from Williams Brook by the absence

of Cu. At Mulligan Gulch (Fig. 2-10c), Au–Zr clustering indicates lithological control through zircon-rich host rocks, whereas As- and Pb-bearing quartz veins suggest arsenopyrite and pyrite as key hosts. At Simpson Field (Fig. 2-10d), Au occurs with alteration indicators (K, Ba) and sulfide-related elements (Fe, Cu, Zn, Mo), pointing to fine-grained muscovite alteration and sulfide mineralization in pyrite, chalcopyrite, sphalerite, and molybdenite, with stibnite in quartz–carbonate veins and Fe–Ca signatures highlighting siderite/ankerite alteration.

The μXRF data (Fig. 2-11) provide essential mineralogical context to the pXRF geochemical patterns, showing that Au mineralization is controlled by both sulfide assemblages and alteration processes. At Williams Brook, Au is associated with sulfide- and Fe-oxide–bearing quartz veins, indicating structurally and mineralogically controlled deposition consistent with multivariate geochemical signatures. At McIntyre Brook, the coexistence of hematite, sulfides, and Sb-bearing phases reflects the interplay of sulfide deposition and fluid-driven alteration. At Mulligan Gulch, arsenopyrite- and pyrite-bearing quartz veins accompanied by Pb- and As-bearing sulfides highlight the polymetallic nature of the system, while at Simpson Field, the link between stibnite and carbonate alteration (siderite, ankerite) emphasizes the role of both fluid chemistry and wall-rock interaction. Collectively, these results show that Au mineralization across the study areas is controlled by contrasting but systematic mineralogical and alteration frameworks, ranging from sulfide-dominated to polymetallic and carbonate-influenced systems.

The methodological framework developed in this study, combining pXRF, μXRF, and multivariate statistical analyses, demonstrates broad applicability beyond the northern New Brunswick case study. Comparable approaches in southern New Brunswick have

demonstrated the effectiveness of these techniques in distinguishing between orogenic and intrusion-related gold systems, where the integration of geochemical and mineralogical data provided key insights into alteration signatures and pathfinder associations (Heidarian et al. 2021). Similarly, trace-element studies of pyrite and arsenopyrite at the Golden Ridge deposit in southwestern New Brunswick revealed how "invisible" gold is partitioned within sulfide lattices and inclusions, thereby constraining ore-forming processes and fluid evolution (Cardenas-Vera et al. 2023). Beyond New Brunswick, the mineralogical and geochemical patterns identified here parallel exploration criteria in other major gold provinces such as the Andes, the Tethyan belt, and the Central Asian orogenic systems (e.g., Goldfarb et al., 2014). This emphasizes the capability of the multi-scale geochemical and mineralogical methodology to advance exploration by providing rapid, high-density datasets suitable for application in structurally complex terranes.

2.8. Summary and conclusions

Although the fundamental processes driving ore-metal deposition are similar across various systems, local geological variations lead to differences in grade, shape, and geochemical and geophysical characteristics of individual deposits. Understanding the variation in these unique features is crucial for successful exploration. Although pathfinder elements have been and will continue to be used to guide gold exploration, pinpointing an unequivocal suite of indicator elements for gold mineralization remains challenging.

In this study, drill cores containing auriferous quartz veins from epithermal gold systems were sampled to identify elements, minerals, and alteration indicators. Auriferous mineralization and alteration characteristics from four areas (Williams Brook, McIntyre

Brook, Mulligan Gulch, and Simpson Field) were assessed and compared. All occurrences have characteristics of epithermal gold systems.

Pyrite and chalcopyrite are the main sulfide minerals associated with epithermal gold mineralization at Williams Brook, McIntyre Brook, Mulligan Gulch, and Simpson Field. In Williams Brook, additional minerals include secondary (supergene) jarosite, goethite, with hypogene hematite, sphalerite, and galena. At McIntyre Brook, pyrrhotite, hematite, magnetite, and occasional stibnite occur with pyrite and chalcopyrite, whereas Mulligan Gulch hosts arsenopyrite, galena, and bornite. Simpson Field hosts a sulfide assemblage dominated by pyrite, sphalerite, arsenopyrite, galena, and chalcopyrite, with minor amounts of pyrrhotite. Pyrite occurs both in quartz-rich veins and in the sericite-rich alteration haloes around them. Gold systems examined here are consistently marked by fine-grained muscovite and siliceous alteration; notably, fine-grained muscovite is observed both within and along the margins of quartz veins in all investigated deposits and occurrences (Figs. 2-3, 2-5). In the Williams Brook gold occurrence, fine-grained muscovite is found as disseminations within various felsic volcanic units and quartz veins, where it is prominently altered. In the McIntyre Brook area, the presence of quartz veining, silicification, and minerals such as hematite, magnetite, and siderite are closely associated with significant gold mineralization. Extensive quartz-carbonate vein systems in the Mulligan Gulch area, influenced by movement along the Rocky Brook-Millstream Fault, include both foliation-parallel and extensional veins. The pXRF data were utilized to create an accurate depiction of mineralization across various epithermal gold occurrences. The various principal components, correlation coefficients, and binary plots of p-XRF data are interpreted to indicate pathfinder elements, mineralization trends, and alteration types that

align with petrographic mineralogical observations supported by μ-XRF-EDS elemental mapping of polished thin sections.

PCA and correlation analyses across Williams Brook, McIntyre Brook, Mulligan Gulch, and Simpson Field consistently highlight Au–Sb associations, supported by cluster dendrograms and indicative of Sb-bearing sulfides (e.g., stibnite, tetrahedrite) as key pathfinders for gold. Additional associations with Cu, Pb, Sn, Ba, Mo, Zn, and K vary by locality, while Fe is persistently enriched, reaching maxima of ~69 wt.% at Williams Brook and ~42 wt.% at McIntyre Brook, with more uniform levels at Mulligan Gulch and Simpson Field. These results demonstrate that integrated pXRF–μXRF and petrographic methods effectively identify elemental pathfinders, mineral indicators, and alteration styles linked to gold mineralization, providing a robust framework for exploration of epithermal systems in northern New Brunswick.

2.9. Future Work and Recommendations

Future research should extend the integrated pXRF–μXRF–CoDA framework to additional gold occurrences across northern New Brunswick and adjacent terranes to test the transferability of pathfinder associations. High-precision geochronology (U–Pb, Re–Os, Ar–Ar) is needed to better constrain the timing of mineralization and its relationship to tectonomagmatic events. Detailed mineral chemistry of sulfides (e.g., LA-ICP-MS of pyrite, arsenopyrite) will help validate multivariate geochemical associations. Integration with geophysical and hyperspectral datasets, coupled with advanced machine learning algorithms, represents a promising direction for predictive prospectivity modeling in structurally complex terranes.

Exploration strategies should prioritize Au–Sb associations, supported by Cu, Pb, Zn, Ba, and Fe, as key pathfinder elements. Illite/fine-grained muscovite and siliceous alteration haloes, consistently observed adjacent to mineralized quartz veins, should be targeted as vectors to mineralization. The combined use of pXRF–μXRF and petrography is recommended as a cost-effective workflow for rapid characterization of mineralization styles and alteration. This methodology should be applied not only in northern New Brunswick but also to analogous Appalachian systems (e.g., Gaspé Peninsula, southern NB) to refine regional exploration criteria and enhance efficiency by reducing reliance on more time-consuming laboratory assays.

Credit authorship contribution statement

Farzaneh Mami Khalifani: Sampling, pXRF analysis, processing, and writing the manuscript.

David Lentz: Conceptualization, Supervision, Reviewing, and applying for providing funding.

James A. Walker: Reviewing, and Editing.

Declaration of competing interest:

The authors declare that they have no known competing financial interests or personal relationships that could have appeared to influence the work reported in this paper.

Acknowledgments

This research is part of Farzaneh Mami khalifani's PhD studies at the University of New Brunswick and was supported by a UNB graduate scholarship and funding from the New Brunswick Department of Natural Resources and Energy Development. Additional support was provided through a Natural Sciences and Engineering Research Council Discovery

Grant to David Lentz. The authors gratefully acknowledge Prof. Matthew Leybourne, Editor-in-Chief, and the reviewers for their constructive feedback, which significantly improved the manuscript. All authors have reviewed and approved the final version.

References

Aitchison, J., 1986. The statistical analysis of compositional data. Monographs on statistics and applied probability. Chapman and Hall, London, 416 p ISBN: 0412280604 9780412280603.

Arne, D.C., Mackie, R.A. and Jones, S.A., 2014. The use of property-scale portable X-ray fluorescence data in gold exploration: advantages and limitations. Geochem. Explor. Environ. Anal. 14, 233–244.

Azadbakht, Z., Lentz, D.R. and McFarlane, C.R., 2018. Apatite chemical compositions from Acadian-related granitoids of New Brunswick, Canada: implications for petrogenesis and metallogenesis. Minerals, 8(12), 598.

Balaram, V. and Sawant, S.S., 2022. Indicator minerals, pathfinder elements, and portable analytical instruments in mineral exploration studies. Minerals, 12(4), p.394.

Barak, S., Imamalipour, A., Abedi, M., Bahroudi, A. and Khalifani, F.M., 2021. Comprehensive modeling of mineral potential mapping by integration of multiset geosciences data. Geochemistry, 81(4), p.125824.

Barker, S.L.L., Hood, S., Rosie, M., Richards, H. and Richards, S., 2019. The lithogeochemical signatures of hydrothermal alteration in the Waihi epithermal district, New Zealand. N. Z. J. Geol. Geophys. 62, 513–530.

Bernier, M.A. and Webber, G.R., 1989. Mineralogical and geochemical analysis of shallow overburden as an aid to gold exploration in southwestern Gaspésiesie, Quebec, Canada. Journal of Geochemical Exploration 34(2), 115−145.

Bodnar, R.J., Lecumberri-Sanchez, P., Moncada, D. and Steele-Macinnis, M. 2014. Fluid in Hydrothermal Ore Deposits. In Treatise on Geochemistry. Edited by H.D. Holland, K.K. Turekian. Oxford, Elsevier, 13: 119−142.

Bourke, A. and Ross, P.S., 2016. Portable X-ray fluorescence measurements on exploration drill-cores: comparing performance on unprepared cores and powders for 'whole-rock' analysis. Geochem. Explor. Environ. Anal. 16, 147–157.

Braga, L.P. and Braga, J., 2020. Mapping gold pathfinder metal ratios in Northern Nevada, USA: A compositional analysis approach. Journal of Geochemical Exploration, 219, p.106616.

Buccianti, A.and Grunsky, E., 2014. Compositional data analysis in geochemistry are we sure to see what really occurs during natural processes. Journal of Geochemical Exploration 141, 1−5.

Bustard, A.L. and Dahn, D.R.L., 2024. Characteristics and structural setting of veinhosted Au-Ag-Pb-Zn mineralization associated with the Mulligan Gulch Porphyry, northcentral New Brunswick. New Brunswick Department of Natural Resources and Energy Development, Geoscience Report 2024−1, 33 p.

Brand, N.W. and Brand, C.J., 2014. Performance comparison of portable XRF instruments. Geochem. Explor. Environ. Anal. 14, 125–138.

Carranza, E.J.M., 2017. Geochemical mineral exploration: should we use enrichment factors or log-ratios?. Natural Resources Research 26, 411−428.

Cardenas-Vera, A., MacDonald, M., Lentz, D.R. and Thorne, K.G., 2023. Trace element characteristics of pyrite and arsenopyrite from the Golden Ridge gold deposit, New Brunswick, Canada: Implications for ore genesis. Minerals, 13(7), p.954.

Chen, Z., Williams, P.N. and Zhang, H., 2013. Rapid and nondestructive measurement of labile Mn, Cu, Zn, Pb and As in DGT by using field portable-XRF. Environmental Science: Processes & Impacts 15(9), 1768−1774.

Chen, M.T., Wei, J.H., Li, Y.J., Shi, W.J. and Liu, N.Z., 2020. Epithermal gold mineralization in Cretaceous volcanic belt, SE China: Insight from the Shangshangang deposit. Ore Geology Reviews, 118, p.103355.

Cicchella, D., Ambrosino, M., Gramazio, A., Coraggio, F., Musto, M.A., Caputi, A., Avagliano, D. and Albanese, S., 2022. Using multivariate compositional data analysis (CoDA) and clustering to establish geochemical backgrounds in stream sediments of an onshore oil deposits area. The Agri River basin (Italy) case study. Journal of Geochemical Exploration, 238, p.107012.

Dahn, D.R.L., Bustard, A.L., Terekhova, A.M. and Hanley, J.J., 2021. Gold-bearing Quartz Veins at the Williams Brook South Occurrence; a Description and Structural Analysis of Veins and Fractures. In Geological Investigations in New Brunswick. Edited by E. Keith. New Brunswick Department of Natural Resources of Natural Resources and Energy Development. Geological Surveys Branch, Mineral Resource Report 2021−1, 39-64.

Egozcue, J.J., Gozzi, C., Buccianti, A. and Pawlowsky-Glahn, V., 2024. Exploring geochemical data using compositional techniques: A practical guide. Journal of Geochemical Exploration 258, p.107385.

Egozcue, J.J. and Pawlowsky-Glahn V.,2005. Groups of parts and their balances in compositional data analysis. Math Geol 37(7):795–828.

Etheridge, M.A., Wall, V.J. and Vernon, R.H., 1983. The role of the fluid phase during regional metamorphism and deformation. Journal of metamorphic Geology, 1(3), pp.205−226.

Faure, S., Tremblay, A. and Dubé, B., 1992. Structural study of relationships between gold occurrences and the Rocky Brook-Millstream Fault zone in the Upsalquitch Forks area, northern New Brunswick. Current Research, Part D. Geological Survey of Canada, Paper 92-1D, 101–109.

Filzmoser, P., Hron, K. and Reimann, C., 2009. Principal component analysis for compositional data with outliers. Environmetrics: The Official Journal of the International Environmetrics Society 20(6), 621−632.

Fischer, C. and Hsieh, E., 2017. Export Chinese blue-and-white porcelain: compositional analysis and sourcing using non-invasive portable XRF and reflectance spectroscopy. Journal of Archaeological Science 80, 14−26.

Flude, S., Haschke, M. and Storey, M., 2017. Application of benchtop micro-XRF to geological materials. Mineral. Mag. 81 (4), 923–948.

Forest, V., 2021. Combined effects of nanoparticles and other environmental contaminants on human health-an issue often overlooked. NanoImpact 23, p.100344.

Fritz, J., Tagle, T., Ashworth, L., Schmitt, R.-T., Hofmann, A., Luais, B., Harris, P.D., Hoehnel, D., Ozdemir, S., Mohr-Westheide, T. and Koeberl, C., 2016. Nondestructive spectroscopic and petrochemical investigations of paleoarchean SLs from the ICDP drill core BARB5, Barberton Mountain Land, South Africa. Meteorit. Planet. Sci. 51, 2441e2458.

Fyffe, L.R., Pajari Jr, G.E. and Cherry, M.E., 1981. The Acadian plutonic rocks of New Brunswick. Atlantic Geology, 17, pp. 23−36.

Garcelon, E.A., Lentz, D.R. and Walker, J.A., 2016. Portable X-ray fluorescence spectroscopy applied to volcanic rocks hosting VMS deposits of the California Lake Group, Bathurst Mining Camp, New Brunswick. In: Geoscience Report 2016-5. New Brunswick Department of Energy and Resource Development, Geological Surveys Branch, 25 p.

Garcelon, E.A., Lentz, D.R. and Walker, J.A., 2018. California Lake Group massive sulfide chemistry. In: Geoscience Report 2018-1. New Brunswick Department of Energy and Resource Development, Geological Surveys Branch, 12 p.

Gazley, M.F., Tutt, C.M., Fisher, L.A., Latham, A.R., Duclaux, G., Taylor, M.D. and de Beer, S.J., 2014. Objective geological logging using portable XRF geochemical multi-element data at Plutonic Gold Mine, Marymia Inlier, Western Australia. Journal of Geochemical Exploration 143, 74−83.

Gazley, M.F., Duclaux, G., Fisher, L.A., Tutt, C.M., Latham, A.R., Hough, R.M., De Beer, S. J. and Taylor, M.D., 2015. A comprehensive approach to understanding ore deposits using portable X-ray fluorescence (pXRF) data at the Plutonic Gold Mine, Western Australia. Geochem. Explor. Environ. Anal. 15, 113–124.

Genna, D., Gaboury, D., Moore, L. and Mueller, W.U., 2011. Use of micro-XRF chemical analysis for mapping volcanogenic massive sulfide related hydrothermal alteration: Application to the subaqueous felsic dome-flow complex of the Cap d'Ours section, Glenwood rhyolite, Rouyn-Noranda, Québec, Canada. Journal of Geochemical Exploration 108(2), 131−142.

Goldfarb, R., Baker, T., Dube, B., Groves, D.I., Hart, C.J. and Gosselin, P. (2005) Distribution, character and genesis of gold deposits in metamorphic terranes. Economic geology 100th Anniversary volume. Society of Economic Geologists, Littleton, Colorado, USA.

Goldfarb, R.J., Taylor, R.D., Collins, G.S., Goryachev, N.A. and Orlandini, O.F., 2014. Phanerozoic continental growth and gold metallogeny of Asia. Gondwana Research, 25(1), pp.48−102.

Graffelman, J., Pawlowsky-Glahn, V., Egozcue, J.J. and Buccianti, A., 2018. Exploration of geochemical data with compositional canonical biplots. Journal of Geochemical Exploration 194, 120−133.

Gray, C.A. and Van Rythoven, A.D., 2020. A comparative study of porphyry-type copper deposit mineralogies by portable X-ray fluorescence and optical petrography. Minerals 10.

Groves, D., Condie, K.C., Goldfarb, R.J., Hronsky, J.M.A. and Vielreicher, R., 2005. Secular changes in global tectonic processes and their influence on the temporal distribution of gold-bearing mineral deposits. Economic Geology, 100(2), 203−224.

Guilherme, A., Buzanich, G. and Carvalho, M.L., 2012. Focusing systems for the generation of X-ray micro beam: An overview. Spectrochimica Acta Part B: Atomic Spectroscopy 77, 1–8.

Hatcher, J.r., 2010. The Appalachian orogen: A brief summary. In: Tollo, R.P., Bartholomew, M.J., Hibbard, J.P., Karabinos, P.M. (Eds.), From Rodinia to

Pangea: The Lithotextonic Record of the Appalachian Region. vol. 206. Geol. Soc. Am., Memoir, pp. 1–19.

Hall, G., Buchar, A. and Bonham-Carter, G., 2011. Quality control assessment of portable XRF analysers: development of standard operating procedures, performance on variable media and recommended uses. In: CAMIRO Project 10E01 Report.

Hedenquist, J.W., Arribas, A. and Gonzalez-Urien, E. 2000. Exploration for epithermal gold deposits. SEG reviews 13: 245−277.

Heidarian, H., Lentz, D.R., Thorne, K. and Rogers, N., 2021. Application of portable X-ray and micro-X-ray fluorescence spectrometry to characterize alteration and mineralization within various gold deposits hosted in southern New Brunswick, Canada. Journal of Geochemical Exploration, 229, p.106847.

Hoehnel, D., Reimold, W.U., Altenberger, U., Hofmann, A., Mohr-Westheide, T., Özdemir, S. and Koeberl, C., 2018. Petrographic and Micro-XRF analysis of multiple archean impact-derived spherule layers in drill core CT3 from the northern Barberton Greenstone Belt (South Africa). Journal of African Earth Sciences, 138, 264−288.

Hron, K. and Filzmoser, P., 2014. Exploring Compositional Data with the Robust Compositional Biplot. In Advances in Latent Variables: Methods, Models and Applications (pp. 219-226). Cham: Springer International Publishing.

Jochum, K.P., Nohl, U., Herwig, K., Lammel, E., Stoll, B. and Hofmann, A.W., 2005. GeoReM: a new geochemical database for reference materials and isotopic standards. Geostandards and Geoanalytical Research, 29(3), pp.333−338.

Jolliffe, I., 2011. Principal component analysis. In International encyclopedia of statistical science (pp. 1094-1096). Springer, Berlin, Heidelberg.

Khammar, F., Yousefi, S. and Joonaghani, S.A., 2021. Analysis of lithogeochemical data using log-ratio transformations and CA fractal to separate geochemical anomalies in Tak-Talar, Iran. Arabian Journal of Geosciences, 14, pp.1−15.

Khammar, F., Alborzian Joonaghani, S., Abadi, L.J., Boomeri, M. and Lentz, D.R., 2022. Investigation of geochemical characteristics and hydrothermal alteration zone mapping supported by remote sensing of a porphyry copper prospect, southeastern Iran: integrated applications to exploration. Geochemistry: Exploration, Environment, Analysis, 22(4), pp. geochem2022-014.

Kohli, R., 2012. Methods for monitoring and measuring cleanliness of surfaces. In Developments in Surface Contamination and Ccleaning (pp. 107−178). William Andrew Publishing.

Lavoie, T. 2018. Assessment Report, Rocky Brook-Millstream, May 2017 to November 2017 for Stephane LeBlanc: New Brunswick Department of Natural Resources and Energy Development, Mineral Report of Work 478329, 25 p.

Lawley, C.J.M., Dubé, B., Mercier-Langevin, P., Kjarsgaard, B., Knight, R. and Vaillancourt, D., 2015. Defining and mapping hydrothermal footprints at the BIF-hosted Meliadine gold district, Nunavut, Canada. J. Geochem. Explor. 155, 33–55.

Le Vaillant, M., Barnes, S.J., Fiorentini, M.L., Santaguida, F. and T¨orm¨anen, T., 2016. Effects of hydrous alteration on the distribution of base metals and platinum group elements within the Kevitsa magmatic nickel sulphide deposit. Ore Geol. Rev. 72, 128–148.

Lemiére, B., 2018. A review of pXRF (field portable X-ray fluorescence) applications for applied geochemistry. Journal of Geochemical Exploration 188, 350−363.

MacKenzie, D.J. and Craw, D., 2007. Contrasting hydrothermal alteration mineralogy and geochemistry in the auriferous Rise & Shine Shear Zone, Otago, New Zealand. J. Geol. Geophys. 50 (2), 67–79.

Mami Khalifani, F., Bahroudi, A., Aliyari, F., Abedi, M., Yousefi, M. and Mohammadpour, M., 2019. Generation of an efficient structural evidence layer for mineral exploration targeting. Journal of African Earth Sciences, 160, p.103609.

Mami Khalifani, F., Parsa, M., Lentz, D., Walker, J., 2022. Portable XRF-aided pattern recognition for characterization of gold mineralization in Northern New Brunswick. In: Exploration, Mining and Petroleum New Brunswick, EMP conference.

Mami Khalifani, F., Lentz, D., Parsa, M., Walker, J., 2023a. Recognizing gold mineralization pathfinders with portable XRF and micro-X-ray fluorescence spectrometry in the Williams Brook epithermal system, NB: Analysis of Indicator Elements and Minerals. In: Atlantic Geoscience Society Colloquium Program with Abstracts.

Mami Khalifani, F., Lentz, D.R., Parsa, M., Walker, J.A., 2023b. Recognizing gold mineralization pathfinders with portable XRF and micro-X-ray fluorescence spectrometry in the Williams Brook epithermal system, NB: Analysis of Indicator Elements and Minerals. Atlantic Geoscience Society Colloquium Program with Abstracts.

Mami Khalifani, F., Imamalipour, A., Barak, S., Abedi, M., Jozanikohan, G. and Bahroudi, A., 2023c. The application of various mineral prospectivity modeling in the exploration of orogenic gold deposit in Saqez-Sardasht region, northwest Iran. Lithology and Mineral Resources, 58(4), pp.368-386.

Mami Khalifani, F., Lentz, D.R., Walker, J.A. and Khammar, F., 2025. Applying Mineral System Criteria to Develop a Predictive Modelling for Epithermal Gold Mineralization in Northern New Brunswick: Using Knowledge-Driven and Data-Driven Methods. Minerals, 15(4), p.345.

Massawe, R.J. and Lentz, D.R., 2022. Petrogenesis and UPb (titanite) age of CuAg skarn mineralization in the McKenzie Gulch area, northern New Brunswick, Canada. Journal of Geochemical Exploration, 232, .106902.

McCutcheon, S. and Bevier, M., 1990. Implications of field relations and U-Pb geochronology for the age of gold mineralization and timing of Acadian deformation in northern New Brunswick. Atlantic Geology 26(3), 237-246.

McClenaghan, M.B., 2011. Overview of common processing methods for recovery of indicator minerals from sediment and bedrock in mineral exploration. Geochem. Explor. Environ. Anal. 11, 265–278.

McLeod, M.J., Hoy, D., Thorne, K.G., 2008. History, Tectonic setting, and models for intrusion-related Gold deposits in southwestern New Brunswick, Canada: examples from the Clarence Stream area. Explor. Min. Geol. 17, 1–12.

Otero, N., Tolosana-Delgado, R., Soler, A., Pawlowsky-Glahn, V. and Canals, A., 2005. Relative vs. absolute statistical analysis of compositions: a comparative study of surface waters of a Mediterranean river. Water research, 39(7), pp.1404-1414.

Pawlowsky-Glahn, V., Egozcue, J.J. and Tolosana-Delgado, R., 2015. Modeling and Analysis of Compositional Data. John Wiley & Sons.

Piercey, S.J., 2014. Modern analytical facilities 2: a review of Quality Assurance and Quality Control (QA/QC) procedures for lithogeochemical data. Geoscience Canada 41(1), 75-88.

Puma Exploration Inc. 2021. Report on a helicopter-borne versatile time domain electromagnetic (VTEM™ Plus) and horizontal magnetic gradiometer geophysics-survey.

Ravansari, R., Wilson, S.C. and Tighe, M., 2020. Portable X-ray fluorescence for environmental assessment of soils: Not just a point and shoot method. Environment International 134, p.105250.

Reimann, C., Filzmoser, P. and Garrett R, Dutter G., 2008. Statistical Data Analysis Explained Applied Environmental Statistics with R. Wiley, New York, pp 269–275 ISBN: 0470985816.

Rodgers, J., 1970. The Tectonics of the Appalachians. John Wiley and Sons, New York, 271.

Romer, R.L. and Kroner, U., 2018. Paleozoic gold in the Appalachians and Variscides. Ore Geology Reviews 92, 475-505.

Ross, P.S., Bourke, A. and Fresia, B., 2014a. Improving lithological discrimination in exploration drill-cores using portable X-ray fluorescence measurements:(1) testing three Olympus Innov-X analysers on unprepared cores, 171-185.

Ross, P.S., Bourke, A. and Fresia, B., 2014b. Improving lithological discrimination in exploration drill-cores using portable X-ray fluorescence measurements:(2)

applications to the Zn-Cu Matagami mining camp, Canada. Geochemistry: Exploration, Environment, Analysis 14(2), 187-196.

Sánchez Mora, D., 2014. Petrogenesis of the low sulfidation gold mineralization in the Williams Brook area, Tobique-Chaleur Zone, New Brunswick. Unpublished M.Sc. thesis, University of New Brunswick, Fredericton, New Brunswick, 172 p.

Sánchez-Mora, D., McFarlane, C.R., Walker, J.A. and Lentz, D.R., 2021. Geochemistry and U/Pb geochronology of the Williams Brook area, Tobique-Chaleur zone, New Brunswick: stratigraphic and geotectonic setting of gold mineralization. Canadian Journal of Earth Sciences 58, 1040–1058.

Scruggs, B. and Ametek, E.D.A.X., 2010. The Orbis Micro-XRF Analyzer Series.

Sillitoe, R.H. and Hedenquist, J.W. 2003. Linkages between volcanotectonic settings, ore-fluid compositions, and epithermal precious metal deposits: Society of Economic Geologists Special Publication, 10: 315-343.

Lode Gold Resources Inc, 2019. Assessment report on trench sampling, mapping and diamond drilling McIntyre brook property.

Taylor, B.E., 2007. Epithermal gold deposits. Mineral Deposits of Canada: A synthesis of major deposit-types, district metallogeny, the evolution of geological provinces, and exploration methods: Geological Association of Canada, Mineral Deposits Division, Special Publication, 5, 113-139.

Templ, M., Filzmoser, P. and Reimann, C., 2008. Cluster analysis applied to regional geochemical data: problems and possibilities. Applied geochemistry, 23(8), pp.2198-2213.

Tremblay, A., Faure, S. and Dubé, B., 1993. Gold occurrences of Rocky Brook – Millstream Fault, northern Appalachians, New Brunswick. In Current Research, Part E, Geological Survey of Canada, Paper 93-1E, 337–346.

van Staal, C.R. and Barr, S.M., 2012. Lithospheric architecture and tectonic evolution of the Canadian Appalachians and associated Atlantic margin. In: Percival, J., Cook, F., Clowes, R. (Eds.), Tectonic Styles in Canada – The LITHOPROBE Perspective. Spec. Pap. 49. Geol. Assoc. Can., pp. 41–95.

van Staal, C.R., Whalen, J.B., Valverde-Vaquero, P., Zagorevski, A. and Rogers, N., 2009. Pre-Carboniferous, episodic accretion-related, orogenesis along the Laurentian margin of the northern Appalachians. Geological Society, London, Special Publication 327(1), 271-316.

van Staal, C.R. 2007. Pre-Carboniferous tectonic evolution and metallogeny of the Canadian Appalachians. In Mineral Deposits of Canada: A Synthesis of Major Deposit-types, District Metallogeny, the Evolution of Geological Provinces, and Exploration Methods. Edited by W.D. Goodfellow. Geological Association of Canada, Mineral Deposit Division, Special Publication, 5: 793-818.

Vasilopoulos, M., Molnár, F., Ranta, J.P. and O'Brien, H., 2023. Mineralogical, lithogeochemical and sulfide trace element characteristics of the Hirvilavanmaa Au-only and the base metal-rich Naakenavaara orogenic gold deposits in the Central Lapland belt, northern Finland. Journal of Geochemical Exploration, 244, p.107132.

Wilson, R.A., 2000. Geology of the Popelogan Lake – Lost Pine Lake area (NTS 21 O/15a and b), Restigouche County, New Brunswick. In Current Research 1999. Edited by

B.M.W. Carroll. New Brunswick Department of Natural Resources and Energy, Minerals and Energy Division, Mineral Resource Report 2000-4, p. 91–136.

Wilson, R.A., van Staal, C.R. and Kamo, S.L., 2017. Rapid transition from the Salinic to Acadian orogenic cycles in the northern Appalachian Orogen: Evidence from northern New Brunswick, Canada. American Journal of Science 317(4), 449-482.

Wood, S. A., 1987. Application of a multiphase ore mineral solubility experiment to the separation of base metal and gold mineralization in Archean greenstone terrains. Economic Geology, 82(4), 1044-1048.

Zhang, W., Lentz, D.R. and Charnley, B.E., 2017. Petrogeochemical assessment of rock units and identification of alteration/mineralization indicators using portable X-ray fluorescence measurements: applications to the Fire Tower Zone (W-Mo-Bi) and the North Zone (Sn-Zn-In), Mount Pleasant deposit, New Brunswick, Canada. J. Geochem. Explor. 177, 61–72.

Zhou, S., Wang, J., Wang, W. and Liao, S., 2023. Evaluation of portable X-ray fluorescence analysis and its applicability as a tool in geochemical exploration. Minerals 13(2), p.166.

Zuo, R., Xia, Q. and Wang H.,2013. Compositional data analysis in the study of integrated geochemical anomalies associated with mineralization. Appl Geochem 28:202–211.

3. Applying Mineral System Criteria to Develop a Predictive Modelling for Epithermal Gold Mineralization in Northern New Brunswick: Using Knowledge-Driven and Data-Driven Methods

Farzaneh Mami khalifani[1*], David R. Lentz[1], Jim Walker[2], Fereshteh Khammar[3]

[1]Department of Earth Science, University of New Brunswick, Fredericton, New Brunswick, E3B 5A3, Canada; farzaneh.mamikhalifani@anb.ac (F.MK), and dlentz@unb.ca (D.L)

[2]New Brunswick Department of Natural Resources and Energy Development, South Tetagouche, New Brunswick, Canada; jim.walker@gnb.ca (J.W)

[3]Department of Geosciences and Geography, Research Programme of Geology and Geophysics (GeoHel), University of Helsinki, Helsinki, Finland; fereshteh.khammar@helsinki.fi (F.Kh)

* Correspondence: farzaneh.mamikhalifani@anb.ac (F.MK)

Abstract

Using mineral prospectivity modeling (MPM), the mineral systems approach enables the identification of geological indicators linked to ore formation. This approach streamlines exploration by minimizing the time and cost required to identify areas with the highest mineral potential. With its extensive till cover and dense forests limiting bedrock exposure, New Brunswick provides an ideal environment to test this approach. The New Brunswick portion of the Canadian Appalachians hosts a diverse range of gold deposits and occurrences that formed during various stages of the Appalachian orogeny.

These deposits include intrusion-related, orogenic, and epithermal types, with many being in part structurally controlled by faults. In northern New Brunswick and the adjacent Gaspé Peninsula, the Tobique-Chaleur Zone contains several orogenic and epithermal gold systems that are closely associated with a large-scale crustal fault and its offshoots, i.e., long-lived trans-crustal Rocky Brook-Millstream Fault system. This study applied mineral prospectivity modeling (MPM) to identify promising areas for epithermal gold mineralization in northwestern New Brunswick. Key mineral system elements, including sources of ore metals and sulfur, fluid pathways, traps, and geological factors affecting deposit formation, were translated into mappable criteria for a regional-scale assessment. In this research, the data were modeled through an integration of knowledge-based and data-driven methods, including fuzzy logic, geometric average, and logistic regression approaches. The concentration-area (C-A) fractal model was applied to reclassify the MPM maps based on prospectivity values obtained from fuzzy logic, geometric average, and logistic regression methods. This approach segmented the mineral prospectivity maps into six distinct classes, with threshold values emphasizing high-favorability zones. The fuzzy overlay model had the highest predictive accuracy (AUC 0.97), followed by the geometric average model (AUC 0.93), whereas the logistic regression identified more tightly constrained high-potential zones. In the prospectivity models, known epithermal gold mineralization consistently overlaps with regions of high favorability. This suggests a positive result from the use of MPM, indicating that this approach could be applicable to other regions and types of ore deposits.

Keywords: Mineral prospectivity mapping, Epithermal gold mineralization, Fuzzy logic, Geometric average, Logistic regression

3.1. Introduction

Mineral Prospectivity Mapping (MPM) is a multi-criteria decision-making process that aims to assist mineral explorationist in identifying mineral targets using existing geological datasets (Khalifani et al. 2019; Liu et al. 2021; Khammar et al. 2024; Li et al. 2024). It achieves this by identifying areas that share geological features with known mineral deposits or occurrences. This process involves integration of various types of geospatial data, such as geochemical, geophysical, geological (Josso et al. 2023). MPM implicitly is faced with challenges, particularly in ensuring the validity and interpretability of predictive results (Barak et al. 2021; Khalifani et al. 2023; Mami Khalifani et al. 2023c; Roshanravan et al. 2023). One significant source of uncertainty is the limited interpretation of the correlation between final potential maps and deposit models, which reduces the reliability of predictions (Yu et al. 2024). To address this, researchers have translated mineral system models for specific mineral deposit types to link geological features to prospectivity models (Khammar et al. 2024). MPM follows one of two methodologies, i.e., data-driven techniques that use training points to identify patterns directly from geospatial data, making them suitable when there is a large dataset of known mineral occurrences (brown fields). In contrast, knowledge-driven approaches depend on geological expertise, which is particularly valuable in areas with limited data (green fields). Knowledge-driven methods are efficient in translating mineral system components to mappable criteria and the production of potential maps (Liu et al. 2024). These techniques have demonstrated their effectiveness in leveraging expert knowledge to test mineral system models and support MPM (Nykänen et al. 2023; Khammar et al. 2024). Recently, in the Kolari region, Finland, Khammar et al. (Khammar et al. 2024) modified the integration of proxies using the

mineral system approach and integration of evidence layers to generate four components, namely: source, energy, pathway, and trap. These components were analyzed using fuzzy logic overlay, geometric average, fuzzy inference system, and logistic regression to create prospectivity maps, which successfully delineated areas of high potential for iron oxide-copper-gold deposits. Likewise, Skirrow et al. (Skirrow et al. 2019) described a method of MPM based on the mineral systems concept and mapped iron oxide copper gold mineral potential in Australia using knowledge driven methodology (Skirrow et al. 2019). They concluded that the approach is most appropriately applied at cartoon- to regional-scale analysis (Nykänen et al. 2023) effectively applied a knowledge-based fuzzy logic approach to delineate potential areas for Co across Finland. This method integrated parameters derived from mineral systems models to identify Co as either a primary commodity or a by-product. Kim et al. (Kim et al. 2019) applied fuzzy logic and geometric average to create a mineral potential map for Cu sulfide deposits in the Kapsan Basin, DPR Korea. These approaches aimed to identify areas of high prospectivity for Cu sulfide mineralization (Kim et al. 2019).

In Canada, MPM studies have addressed various mineral systems, utilizing advanced mapping techniques to uncover mineralization patterns specific to structural geology. Also, there has been extensive MPM research focusing on mineral-rich areas and leveraging geostatistical and machine-learning models to identify economically viable deposits (Bonham-Carter and Agterberg 1990; Harris JR. et al. 2015; Lawley et al. 2021; Parsa et al. 2023; Lauzon and Gloaguen 2024). However, a comprehensive study on translating mineral system criteria for gold epithermal systems is still lacking. Therefore, the novelty

of this study lies in translating these components and interpreting potential models based on geological features that influence gold mineralization.

The aim of this study is to investigate the geological criteria controlling the formation of gold mineralization and translate them to mappable criteria and evidence layers. This was accomplished by employing various geological, geochemical, and geophysical datasets. Following this, three integration techniques were employed to generate prospectivity maps. This study applies fuzzy logic overlay and geometric average, in the light of recent advancements in knowledge-driven approaches (Nykänen et al. 2023; Khammar et al. 2024). Moreover, the study incorporates an empirical approach using logistic regression (LR), enabling a direct comparison between knowledge-driven and data-driven methods trained on known occurrences, thereby improving the accuracy in the identification of prospective areas. A case study is conducted in New Brunswick, a region recognized for its gold potential. Twenty-one evidence layers are created based on the conceptual model of the targeted deposit-type, which were then utilized to produce prospectivity maps. This study applied the concentration-area fractal method to define threshold limits for various types of mineral prospectivity maps (Yousefi M and Carranza E J M 2015; Keykhay-Hosseinpoor et al. 2024). Finally, the effectiveness of the maps was evaluated using success rate under curves (ROC) and mineralogy and petrology studies (Khammar et al. 2024).

3.2. Geology of the study area

The northern Appalachian belt as a complex collage of supra subduction zone terranes and microcontinents formed during the closure of the Iapetus and Rheic oceans between the late Cambrian and the Permian (van Staal 2007; Romer and Kroner 2018). The northern

part of the Appalachian belt displays systematically younger ages of deformation from the west to the east, as the remnants of various arcs and the microcontinents were accreted (Hatcher 2010). Appalachians include rocks affected by various orogenies, representing the combination of folding, faulting, metamorphism, and plutonism (Van Wagoner 2002) (Figure 1a). Siluro-Devonian bimodal volcanic and interbedded sedimentary rocks of the Northern Appalachians in eastern Canada and Maine (USA) are exposed in three major belts: the Piscataquis, Tobique-Chaleur zone, and Coastal volcanic belts. The study area is located within the Tobique-Chaleur zone, which stretches from southwestern New Brunswick to Gaspé Peninsula of Québec (Van Wagoner 2002; Sánchez-Mora et al. 2021) (Figure 1b, c).

The Canadian Appalachians hosts gold mineralization which formed during various stages of the Appalachian orogeny and subsequent episodes of exhumation and erosion (Wilson et al. 2017; Romer and Kroner 2018). These include a wide range of gold-bearing mineral deposit types, including orogenic (Watters 1993), volcanogenic massive sulphide (Goodfellow et al. 2003; McClenaghan et al. 2003), skarn (Morrissy 1991; Lentz 2002), and epithermal systems (Corbett 2002).

According to Fyffe and Fricker (Fyffe and Fricker 1987), the Middle Paleozoic Matapédia Cover Sequence (MCS) is a Late Ordovician to Middle Devonian basin fill sequence. The Matapedia Cover Sequence is divided into three structures that from northwest to southeast, are: 1) the Connecticut Valley – Gaspé Synclinorium, 2) Aroostook – Percé Anticlinorium, and 3) Chaleur Bay Synclinorium (Rodgers 1970; Bernier and Webber 1989). The southern limit of the Fortin Formation, the Matapedia fault, marks the boundary between the

Connecticut Valley-Gaspé Synclinorium and the Aroostook-Percé Anticlinorium to the south (Bernier and Webber 1989).

In Northern New Brunswick (Figure 1), Late Silurian volcanic rocks are divided into the Petit Rocher, Dickie Cove, and Chaleurs groups, whereas Early Devonian volcanic rocks are included in the Tobique and Dalhousie groups (Wilson and Kamo 2012b). In the study area (Figure 1b, c) three Early Paleozoic inliers—Popelogan, Miramichi, and Elmtree—are overlain by Middle Paleozoic rocks of the Tobique Chaleurs zone and Carboniferous rocks. Estimates suggest that the Acadian deformation in northern New Brunswick took place during the Early Devonian, between 415 and 395 Ma. In its later stages, this deformation was characterized by dextral, primarily strike-slip faulting, along the Rocky Brook–Millstream, Restigouche–Grand Pabos, and Catamaran Brook fault systems, as well as several associated satellite faults (Van Staal et al. 2009; Wilson et al. 2017). The gold occurrences investigated in this study are located in the Chaleur Bay Synclinorium and are hosted primarily by Upper Silurian to Early Devonian strata and subordinate lower Silurian strata (Figure 1b, c). The area investigated encompasses two 1:50,000 scale map sheets, covering approximately 1,560 km² and containing 20 gold occurrences (Figure 1c). The Chaleur Bay Synclinorium exhibits more varied geology and a more intricate tectonic history than the adjacent Aroostook–Percé Anticlinorium. Its uppermost Silurian to Early Devonian sedimentary and volcanic rocks are divided into the Chaleurs, Petit-Rocher, Quinn Point, Dickie Cove, and Dalhousie groups north of the Rocky Brook–Millstream Fault, whereas south of the fault, early Devonian rocks are included in the Tobique Group (Wilson et al. 2017).

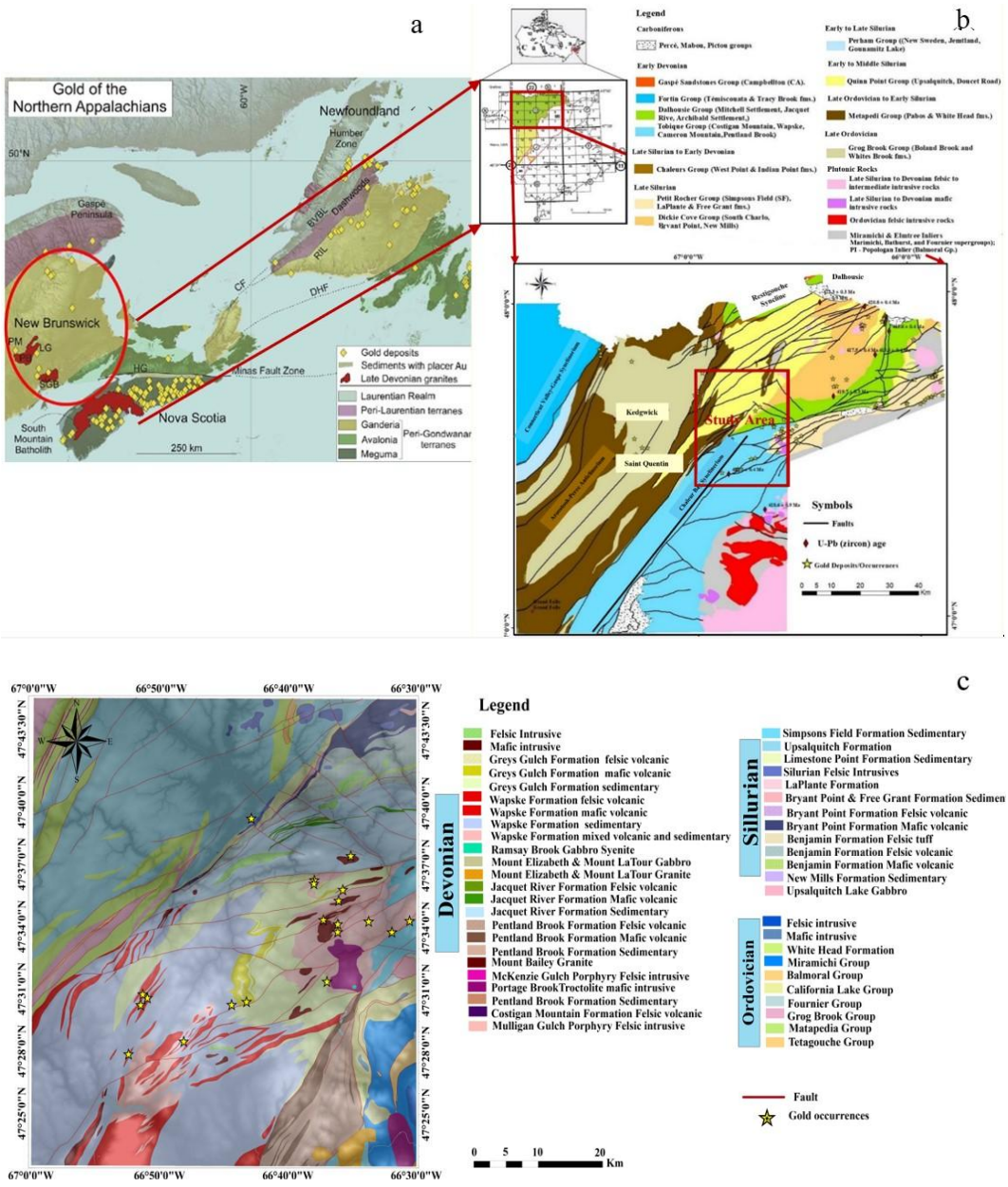

Figure 3-1. Location and geology of the study area. a) Map of the northern Appalachians and Maritime Canada representing major tectonic zones, and distribution of Au mineralization (Romer and Kroner 2018), b) A regional geological map of western and northern New Brunswick displaying the gold deposits and occurrences under investigation in this study (modified from Wilson 2017), c) Detailed geological map of the area investigated showing locations of gold mineralization (adapted from Wilson (Wilson 2017).

3.3. Epithermal Gold System

Epithermal gold systems are shallow (1–2 kilometers below surface), hydrothermally formed deposits that commonly form in volcanic and geothermally active settings (John et al. 2018). These systems result from the interaction of hot fluids, either magmatic or meteoric, with surrounding host rocks. The deposits are characterized by formation in a temperature range of approximately 150° to 300°C (Corbett 2002; John et al. 2018). Depending on fluid chemistry and alteration patterns, epithermal systems are divided into two types: high-sulfidation and low-sulfidation systems. High-sulfidation systems are linked to acidic, oxidized fluids derived from magmatic processes, whereas low-sulfidation systems are associated with near-neutral pH and reduced fluids, often equilibrated with host rocks (White and Hedenquist 1995b; John 2018; Aminu et al. 2024). The alteration patterns and mineralization styles differ significantly between the two deposit types. In high-sulfidation systems, acidic fluids cause extensive rock leaching, creating advanced argillic alteration zones characterized by minerals like quartz, alunite, and kaolinite. The leached rocks may later be mineralized with gold and other metals through magmatic fluid activity. Low-sulfidation systems, on the other hand, exhibit zonal alteration from quartz-adularia veins to argillic and propylitic assemblages (White and Hedenquist 1995b; John 2018). These systems commonly form in structurally controlled vein networks where gold and silver precipitate due to fluid boiling and mixing. Epithermal gold deposits are highly variable in terms of grade and tonnage and are significant exploration targets globally. Epithermal systems occur in a range of tectonic settings characterized by high geothermal gradients, e.g., subduction zones, rift zones, and continental hot spots. Their mineral assemblages commonly include electrum, silver sulfides, and selenides in low-sulfidation

systems, whereas high-sulfidation systems host minerals like enargite and luzonite. The understanding of alteration zoning, structural controls, and fluid dynamics within these systems is essential for effective exploration and resource assessment (White and Hedenquist 1995b; John 2018).

3.4. Epithermal Gold Mineralization in New Brunswick

Epithermal gold mineralization in New Brunswick is limited but geologically significant. The only confirmed high-sulfidation epithermal occurrence is at Chambers Settlement, in the Avalon Zone of southern NB and is hosted by intensely altered Neoproterozoic felsic volcanic rocks. The alteration assemblage includes topaz, pyrophyllite, kaolinite, and quartz, with gold and silver as the primary metals. Yousefi et al. (Yousefi et al. 2023) investigated the potential for distal, low-sulfidation epithermal gold mineralization within the Evandale porphyry Cu-Mo-(Au) system in southwestern New Brunswick (Yousefi et al. 2023). The research highlighted the significance of the Middle Devonian Evandale Granodiorite, an oxidized I-type intrusion with adakitic characteristic, as a fertile magmatic source for such epithermal systems. Here, mineralization occurs in veins containing pyrite, chalcopyrite, molybdenite, and arsenopyrite, with anomalous gold, and is structurally controlled by regional fractures and faults. Additionally, the proximity of gold occurrences, such as those in the Clarence Stream area, supported the genetic link between the Evandale system and epithermal gold systems, establishing the Evandale Granodiorite as a significant exploration target for epithermal gold mineralization (Yousefi et al. 2023). In northern New Brunswick, the northeastern part of the Chaleur Bay Synclinorium hosts several occurrences of epithermal breccias and veins containing base metals, along with gold and silver. These are commonly associated with felsic hypabyssal rocks as well as

fine- to medium-grained mafic intrusions that are spatially associated with major splays of the Rocky Brook–Millstream Fault, e.g., the McCormack Brook and Ramsay Brook faults (Sánchez Mora D 2014; Wilson et al. 2017). Sanchez Mora et al. (Sánchez Mora D 2014; Sánchez-Mora et al. 2021) studied the Williams Brook area in northern New Brunswick, which hosts low-sulfidation epithermal gold mineralization hosted by Siluro-Devonian bimodal volcanic and sedimentary rocks, deposited in a transpressive tectonic setting during the convergence of Gondwana and Laurentia (Sánchez Mora D 2014; Sánchez-Mora et al. 2021). Gold mineralization is associated with felsic units and is associated with early-stage gold and galena in muscovite/illite veinlets and later-stage quartz veins containing native gold, sulfides, and oxyhydroxides. Geochemical and stable isotope analyses indicate a magmatic origin for the mineralizing fluids, supporting their classification as a low-sulfidation epithermal system. Khalifani et al. (Mami Khalifani et al. 2023b) investigated the Williams Brook epithermal gold mineralization, which is hosted in Siluro-Devonian volcanic-sedimentary rocks of the Wapske Formation and controlled by the Rocky Brook–Millstream Fault. This low-sulfidation system is characterized by gold hosted in quartz veins and stockworks within rhyolite (Mami Khalifani et al. 2022b). Additionally, they investigated epithermal gold mineralization at the McIntyre Brook (MB), Mulligan Gulch (MG), and Simpson Field occurrences in northern New Brunswick and conducted pXRF and Micro-XRF analyses on drill cores from these occurrences (Mami Khalifani et al. 2022b). Epithermal gold mineralization in the Mulligan Gulch area is associated with an intermediate sulfidation system and occurs primarily within quartz veins containing arsenopyrite, pyrite, and other sulfide minerals. Multiple generations of quartz veining, ranging from early deformation-related phases to later fault-controlled

emplacement, indicate a protracted mineralizing event. Alteration phases such as sericite and smectite reflect varying thermal and chemical conditions within the hydrothermal system, with high-temperature alteration overprinted by lower-temperature assemblages. Gold precipitation is interpreted to result from fluid mixing, as evidenced by sulfide textures and the absence of boiling features and the presence of Ag, Pb, and Zn suggests a complex mineralizing fluid. Comparisons with nearby occurrences, such as Williams Brook, reveal similar structural controls and hydrothermal processes, though variations in temperature and mineral assemblages highlight local geological differences (Bustard 2024). The McIntyre Brook epithermal gold mineralization is structurally controlled, occurring along the McIntyre Brook Fault, and at lithological boundaries between felsic and sedimentary units. Gold is found in brecciated felsic rocks and quartz-carbonate veins and is associated with hematite, potassic feldspar, and albite alteration and is commonly associated with base metals such as copper, zinc, and cobalt. The Simpson Field occurrence is recognized as an epithermal gold system, distinguished by its development within low grade metamorphic rocks. In this area, gold mineralization predominantly occurs in quartz-carbonate veins and is associated with wall rocks altered to biotite or actinolite. The Simpson Field epithermal gold mineralization is associated with pyritic quartz-carbonate alteration zones, which are locally silicified and carbonatized. Gold is primarily linked with pyrite and minor amounts of chalcopyrite and arsenopyrite in sedimentary rocks and mafic intrusions. In addition, some gold mineralization occurs along fault zones and contacts with gabbroic intrusions. Figure 2 illustrates drill core samples from norther New Brunswick occurrence showing examples of gold mineralization in quartz veins, felsic porphyritic and mafic intrusions with sulphide mineralization and alteration.

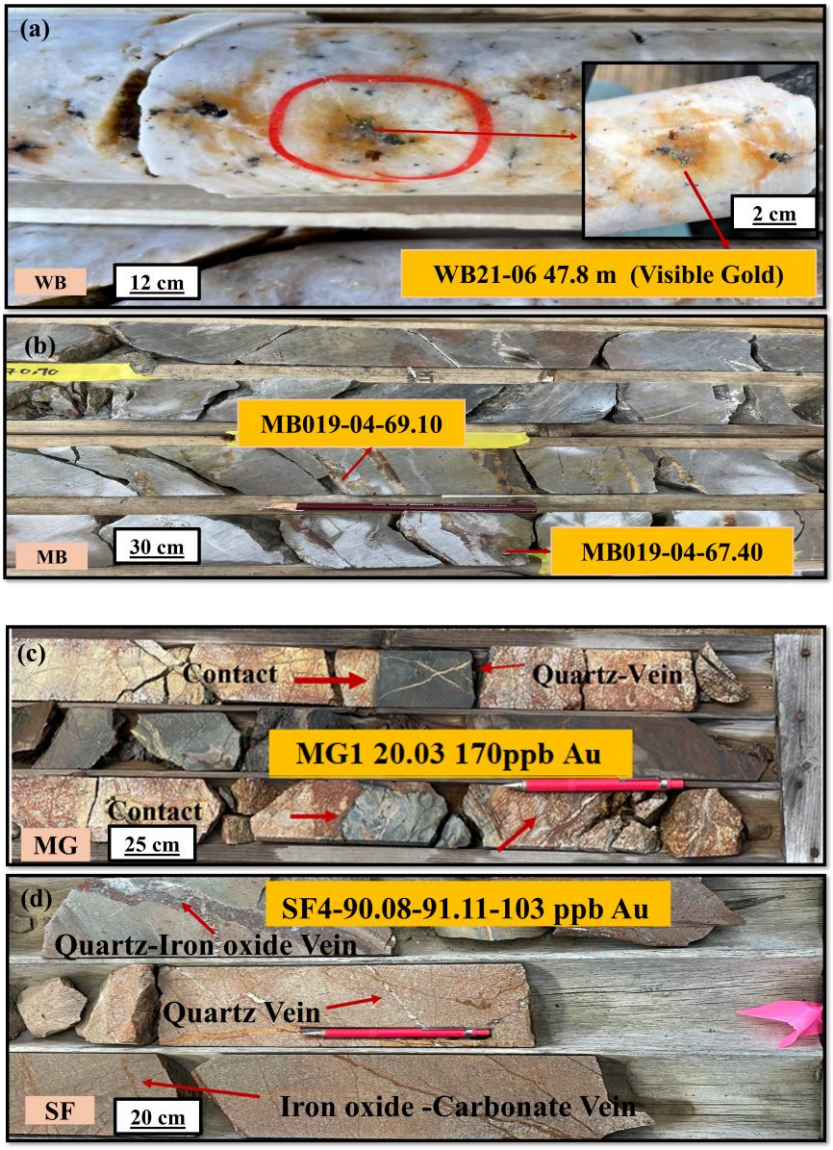

Figure 3-2. Drill core samples from epithermal gold occurrences in the northern New Brunswick (a) Quartz vein with visible gold from Williams Brook, (b) Felsic intrusive with pyrrhotite, pyrite, and gold from McIntyre Brook, (c) Altered Feldspar Porphyry and dark grey siltstone including pyrite, and pyrrhotite in Mulligan Gulch, (d) Altered mafic intrusive rock and siltstone with pyrrhotite, pyrite, and gold in Field.

3.5. Materials and Methods

3.5.1. Framework of Model

To model epithermal gold mineralization, theoretical criteria for ore formation and associated geological processes must be established. Then a database is created and structured to capture key parameters of the mineral system. Figure 3-3 presents the methodological flowchart employed in this study to process geospatial data and develop a mineral model for epithermal gold mineralization in Northern New Brunswick. Geological, geochemical, and geophysical layers were initially generated using suitable analytical methods. Logistic transformation functions were applied to normalize and assign continuous weights to spatial evidence layers. Subsequently, knowledge-driven and data-driven approaches were applied, namely, fuzzy logic, geometric average, and logistic regression.

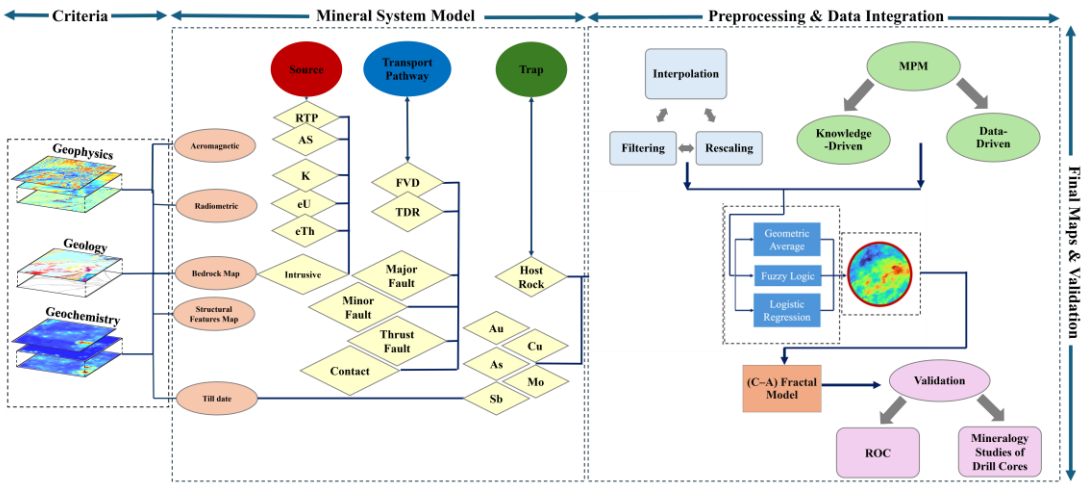

Figure 3-3. The workflow utilized in this study to produce mineral prospectivity maps for epithermal gold mineralization.

We employed the concentration–area fractal model, originally proposed by Cheng et al. (Cheng et al. 1994), to establish thresholds for classifying values in mineral prospectivity mapping. The C-A fractal model enables the identification of distinct mineralization patterns and spatial distributions by delineating thresholds based on the relationship between concentration and area (Yousefi and Carranza 2016). These thresholds were then applied to enhance the classification of values derived from fuzzy logic, geometric average, and logistic regression methods. Finally, a receiver operating characteristics (ROC) curve was used to evaluate the effectiveness of the prospectivity models developed using fuzzy logic and geometric average. Furthermore, the findings of the mineralogy and petrology studies corroborate the results of the mineral prospectivity analysis.

3.5.2. Dataset

3.5.2.1. Geological data

Geological data used as evidence layers in this study include lithological map units (polygons) and structural features such as faults. These features provide critical insights into the geological processes controlling mineralization and are used to define mappable criteria for mineral prospectivity analysis. The geological data for this study were obtained from the 1:50,000 bedrock geology map published by the New Brunswick Department of Natural Resources (2008). Specifically, a digitized compilation of lithological rock unit maps for National Topographic System map sheets (21O/10 and 21O/07). Examining geological units and faults in these maps enables exploration geologists to better understand and interpret geophysical and geochemical data in terms of epithermal gold mineralization.

3.5.2.2. Surficial geochemical till data

The till geochemical data provided by the New Brunswick Department of Natural Resources (2014) encompasses samples collected at 2000-meter intervals, providing a comprehensive geochemical foundation that facilitates an understanding of the distribution of geologic units, mineralization, and alteration in the subsurface. A dataset of 460 samples analyzed using inductively coupled plasma mass spectrometry (ICP-MS) and instrumental neutron activation analysis (INAA) was extracted from the provincial dataset to generate geochemical evidence layers, following standard preparation and Coda-based procedures.

3.5.2.3. Geophysical data

Geophysical data, specifically airborne magnetometry, provides crucial information on both surface and subsurface geological units and lineaments (Mami Khalifani et al. 2019, 2023c). In this study, the aeromagnetic geophysical datasets from Campbelltown (GSC 1986) and Bathurst (GSC 1987a) surveys were utilized to detect faults, contacts and intrusive bodies associated with mineralization. The Campbelltown dataset features a line spacing of 1000 meters and a cell size of 200 meters, whereas the Bathurst dataset was collected using 300 m line spacing and a cell size of 75 meters, making the two surveys complementary. Merging these datasets ensured full coverage of the study area, creating a unified geophysical framework to highlight key geological and structural features, critical for a well-founded MPM study. Various processing techniques have been crafted to delineate the boundaries of magnetic anomalies that are commonly associated with mineralization-related intrusions (Cooper and Cowan 2008; Mami Khalifani et al. 2023c). In this research, the total magnetic intensity data were reduced to the north magnetic pole (RTP) with an inclination of 72.96° and a declination of -20.65 2° (Baranov 1957). To delineate lineaments from aeromagnetic data, several filters are used, including the RTP (Mami Khalifani et al. 2019; Feizi et al. 2021), the analytic signal (AS) and the tilt derivative (TDR) (Golshadi et al. 2016; Mami Khalifani et al. 2019) , and the first vertical derivative (FVD) (Almasi et al. 2018; Mami Khalifani et al. 2019). These tools are instrumental in enhancing the definition of geological structures within magnetic data, thereby improving the identification of faults, contacts, and other boundaries (Mami Khalifani et al. 2019). Airborne radiometric surveys can be especially useful for detecting hydrothermally altered areas close to gold deposits. Additionally, they can help to identify

and pinpoint felsic intrusions and volcanic rocks, which commonly contain high concentrations of potassium (K), equivalent uranium (eU), and equivalent thorium (eTh) (Almasi et al. 2018; Mami Khalifani et al. 2023c). In this research, radiometric data from Campbelltown (GSC 1976) and Campbelltown (GSC 1986) surveys were used to help identify lithological boundaries and alteration zones associated with mineralization.

3.5.3. Methods

3.5.3.1. Log-ratio Approach and Principal Component Analysis

Geochemical data is inherently compositional, meaning that its chemical components always sum to a fixed total, thereby forming a closed system (Braga and Braga 2020; Khammar et al. 2021). Geochemical data requires preprocessing and normalizing prior to use in any MPM application. The closed system features and related challenges, and the necessity and importance of converting closed systems to open data have been discussed in many studies (Mohammadpour et al. 2019; Braga and Braga 2020; Heidarian et al. 2021; Mami Khalifani F et al. 2022). Here, we employ a central log-ratio transformation (CLR), a form of log-ratio family, to properly handle the closed and compositional nature of the geochemical dataset (Aitchison 1986; Imamalipour et al. 2020; Khammar et al. 2021). This transformation converts compositional data from classical to Aitchison geometry, facilitating the identification of underlying patterns. Among several multivariate analysis techniques, principal component analysis (PCA) was applied to the geochemical data, enabling a more precise interpretation of the interrelationships among the dataset's variables (Braga and Braga 2020; Khammar et al. 2021; Mami Khalifani et al. 2023c).

3.5.3.2. Logistic transformation

Logistic transformation is a mathematical technique used to normalize continuous spatial data into a range of [0, 1], making it useful for integrating diverse datasets in MPM (Yousefi and Nykänen 2016; Keykhay-Hosseinpoor et al. 2024). The transformation employs a logistic function, a sigmoid-shaped curve, to assign fuzzy weights to evidence values. These weights represent the relative importance of each data point in identifying mineralization potential. This approach avoids the discretization of data into arbitrary classes, a common practice in traditional methods, reducing exploration bias and allowing for a more accurate representation of the underlying evidence (Yousefi and Nykänen 2016; Keykhay-Hosseinpoor et al. 2024).

This study utilizes the logistic function previously applied by Yousefi et al. (Yousefi et al. 2012) and Yousefi and Carranza (Yousefi and Carranza 2015b) to standardize the values of various evidential datasets into a unified space (Yousefi et al. 2012; Yousefi and Carranza 2015b; Yousefi and Nykänen 2016). The function is expressed as:

$$F_{Ev}=\frac{1}{1+e^{-s(Ev-i)}}$$

Here, F_{Ev} represents the fuzzy weight in logistic space, ranging between 0 and 1. The parameters i and s correspond to the inflection point and slope of the logistic function, respectively, while Ev is the evidential value at each pixel in the input map (e.g., fault density or proximity to specific features).

3.5.3.3. Fuzzy logic

Fuzzy logic is a mathematical framework built on the principles of fuzzy set theory, first introduced by Zadeh (Zadeh 1965). Fuzzy logic overlay entails using fuzzy logic principles

within geographic information system (GIS) environment to effectively address uncertainty in spatial data (Zadeh 1965; Nykänen et al. 2023; Khammar et al. 2024).

The method transforms evidential data using functions such as the logistic sigmoid or Gaussian functions, enabling normalization and comparability of diverse input layers. The logistic sigmoid function is expressed as:

$$F_x = \frac{1}{1 + e^{-k(x-c)}}$$

where X is the input variable (e.g., a geochemical value or a geophysical reading), C is the inflection point, i.e. the value of x at which the function's output is 0.5, and K is the steepness (or slope) parameter, which controls how quickly the function transitions from values near 0 to values near 1 (Porwal et al. 2003; Yousefi et al. 2012; Behera and Panigrahi 2021).

Evidential layers are combined using fuzzy operators like fuzzy AND, fuzzy OR, or gamma operators to produce a unified prospectivity map (Bonham-Carter and Agterberg 1990). In this study, the final fuzzy overlay prospectivity map was created using a fuzzy gamma of 0.90.

3.5.3.4. Geometric average

The geometric average method is a knowledge-driven approach used for mineral prospectivity mapping to integrate multiple evidential layers effectively. The geometric average is calculated by taking the nth root of the product of the values, where n is the total number of values. For dataset v1, v2, ..., vn}, the geometric average (GA), is computed accordingly (Yousefi and Carranza 2015b; Kim et al. 2019; Khammar et al. 2024).

$$G_A(v_1, v_2, \ldots, v_n) = \left(\prod_{i=1}^{n} v_i\right)^{1/n} = \sqrt[n]{v_1 v_2 \ldots v_n}$$

GA is particularly useful for handling uncertainties and combining diverse geological, geochemical, and geophysical datasets into a unified prospectivity model (Yousefi and Carranza 2015b; Kim et al. 2019).

In this study, 21 evidential layers were multiplied together, and the 21st root of the resulting product was calculated (Yousefi and Carranza 2015b).

3.5.3.5. Logistic regression

Logistic regression (LR) is a versatile multivariate statistical technique especially suited to binary classification tasks, utilizing a logistic function to model the probability of a categorical outcome (Kost et al. 2021; Khammar et al. 2024). This method is particularly advantageous for mineral prospectivity mapping (MPM), where the presence of minerals, categorized distinctly as either present or absent, serves as the dependent variable. In this study, LR assesses and quantifies the relationships between multiple independent variables (e.g., source, pathways, traps), which function as evidential layers (Porwal et al. 2010). These variables are integral in predicting favorable mineralized zones, making LR a widely applied and powerful data-driven tool in MPM. The model effectively describes how these independent variables relate to the dependent variable mineral deposits or occurrences thereby providing statistically interpretable results that aid in identifying mineral prospectivity areas. The probability of mineral occurrence is determined using the following equation (Khammar et al. 2024):

$$Z = b_0 + b_{1 \times 1} + b_2x_2 + \ldots + b_nx_n$$

where:

Z = logit (linear transformation of the dependent variable).

b_0 = intercept.

b_1, b_2…, bn = regression coefficients.

x_1, x_2…, x_n = independent predictor variables.

Probability Calculation: the probability (P) of mineral occurrence is derived from equation (2) (Zhao et al. 2023; Khammar et al. 2024).

$$P=\prod_{k=1}^{n} A_k$$

This equation maps the linear combination Z into a range between 0 and 1(Nykänen V and Salmirinne H 2007; Porwal et al. 2010; Khammar et al. 2024).

3.5.3.6. Fractal-based discretization of MPM maps

In geosciences, fractal models have been employed to describe the spatial distributions of geological features (Cheng and Agterberg 1995; Raines 2008). Numerous fractal models have been created and successfully implemented to analyze spatial features associated with mineralization, such as geochemical anomalies (Yousefi M and Carranza E J M 2015), structural elements (Zhao et al. 2011), and geological units (Wang et al. 2011). In this study, we applied the concentration area (C–A) fractal model (Cheng et al. 1994) to establish thresholds on MPM maps through both knowledge-driven and data-driven approaches. Specifically, we derive threshold values by identifying breakpoints or inflection points on the resulting multifractal curve; these thresholds effectively partition the MPM maps into discrete classes that reflect varying levels of mineral prospectivity. This classification not only enhances our ability to differentiate high-favorability zones from background noise but also improves the interpretation of spatial mineralization patterns, as demonstrated in previous studies (Yousefi M and Carranza E J M 2015; Keykhay-Hosseinpoor et al. 2024).

3.5.3.7. Receiver Operating Characteristic

The Receiver operating characteristic (ROC) curve is a widely used statistical method for evaluating the predictive accuracy of MPM. The ROC curve uses the true positive rate (sensitivity) versus the false positive rate (1-specificity). Sensitivity measures the proportion of actual positive instances correctly identified by the model. It is calculated as TP/(TP + FN), where TP is true positive, and FN is false negative. The 1-specificity measures the proportion of actual negative instances incorrectly classified as positive by the model. It is calculated as FP/(FP + TN), where FP is false positive, and TN is true negative.

The ROC curve is generated by varying the decision threshold of the classifier. As the threshold changes, the true and false positive rates also change, resulting in various points along the ROC curve. AUC-ROC quantifies the overall performance of the classifier. A model with perfect discrimination has an AUC-ROC of 1, whereas a random classifier has an AUC-ROC of 0.5. Higher AUC-ROC values indicate better discriminative ability. The closer the ROC curve is to the upper-left corner, the better the model's performance (Khammar et al. 2024; Mantilla-Dulcey et al. 2024).

A diagonal line represents random guessing (no discrimination), whereas points below this line indicate a less reliable model performance. The method supports selecting an appropriate threshold for a given application based on the desired balance between sensitivity and specificity (Fawcett 2006; Nykänen et al. 2017, 2023). The ROC analysis not only validates the precision of the models but also enables comparisons among different approaches, ensuring more reliable delineation of exploration targets. This study utilizes

20 mineral occurrences, classified as gold epithermal mineralization, to develop fuzzy overlay and geometric average models (Khammar et al. 2024).

3.6. Mineral system approach

The concept of a mineral system approach was introduced by (Wyborn et al. 1994; Hagemann et al. 2016; McCuaig and Hronsky 2017). It includes all geological factors that influence the information and deposition of mineral deposits, such as the processes responsible for transferring and concentrating mineral constituents from their source via the migration pathway to the depositional site.

The mineral systems approach involves the following concepts: (1) trigger: tectonic events that initiate a mineralization event e.g. subduction of an oceanic ridge. (2) source regions: any geochemical and tectonic processes that increase concentrations of metals and fluids. (3) pathways: any structural elements or basinal architecture that leads to the formation of conduits that facilitate the flow of fluids or magma, and operating at the lithospheric, crustal, province, and district scales. (4) driver: processes that trigger the movement of fluids within these conduits. (5) throttle: any mechanical and structural event that directs and guides the flow of fluids or magma into specific locations where concentrated mineral deposition can occur, commonly known as “trap” sites. (6) trap: any chemical and physical processes such as fractional crystallization, fluid–rock interaction, density separation, etc. which is responsible for the deposition of metals. (7) dispersion: geochemical and geophysical processes that can alter mineralized material and leave detectable features like geochemical and geophysical anomalies. (8) preservation: the mechanisms that enhance mineralized material (Wyborn et al. 1994). It also is a conceptual framework that helps map the geological processes (Wyborn et al. 1994; Hronsky and Groves 2008; Kreuzer et

al. 2008; McCuaig et al. 2010). In practice, there is an updated conceptual framework that simplifies the mineral system components from eight to three crucial components: source, pathway, and trap (Wyborn et al. 1994; McCuaig and Hronsky 2017).

3.6.1. Mapping components to targeting criteria

3.6.1.1. Source

Epithermal deposits are often associated with magmatic systems. Magmatic fluids originate from volcanic arcs or other tectonic settings that generate significant heat and magma (Gabo-Ratio et al. 2020; Li et al. 2020; Yousefi et al. 2023). Fluids and metals, including gold, are derived from a magmatic source (Gabo-Ratio et al. 2020). The bimodal volcanic rocks and their hypabyssal equivalents of the Tobique and Chaleurs groups are assumed to be the magmatic source for gold and associated metals in the study area. Likewise, the magmas responsible for the formation of these rocks likely supplied the necessary heat and fluids crucial for the formation of epithermal gold systems (Sánchez Mora D 2014). The close spatial association of intrusions with mineralized zones implies their importance as a heat (and metal) source to drive these gold mineralizing systems (Groves et al. 2000; Goldfarb et al. 2001).

3.6.1.2. Pathway

The pathway component of mineral systems for gold mineralization describes the critical role of transporting ore-forming fluids from their source to the site of deposition (Corbett 2002). According to Gabo-Ratio et al. (Gabo-Ratio et al. 2020), structural pathways are critical for facilitating the migration of ore-forming fluids in epithermal gold systems. Major fault systems, such as the Rocky Brook Millstream Fault in the northern New

Brunswick area, act as primary conduits for hydrothermal fluids in the study area (Wilson et al. 2017; Gahlan et al. 2022).

These faults, once formed, may be episodically reactivated during episodic tectonic activity, repeatedly creating zones of high permeability that facilitate the ascent of mineralizing fluids. In epithermal gold systems, fracture networks associated with extensional tectonic regimes further enhance fluid flow. These networks provide interconnected pathways for fluid migration, often linked to localized stress regimes and dilation zones, which are crucial for hosting gold mineralization. The structural evolution of the study area, combined with evidence of vein formation and reactivation, underscore the importance of fault and fracture systems as dynamic pathways for hydrothermal processes (Corbett 2002; Sánchez Mora D 2014; John et al. 2018).

3.6.1.3. Trap

Gold and associated metals are commonly deposited in veins and breccias in a number of favorable settings including faults and fault intersections, volcanic domes, and contacts between lithologic units of contrasting rheology. In many cases gold-bearing fluids mix with meteoric waters, reducing temperature and triggering precipitation of gold and associated minerals. Physico-chemical processes, such as boiling, cooling, and fluid mixing, further enhance the trapping potential by changing fluid chemistry (e.g., pH, redox state), leading to further gold precipitation. Stable isotopic analyses (O, H, S) and fluid inclusion studies in the Williams Brook area indicate gold deposition occurred at ~200°C and was likely triggered by fluid mixing (Sánchez Mora D 2014). The trap component in the mineral system approach for epithermal gold mineralization integrates the spatial distribution (enrichment and depletion) patterns of key elements (e.g., Au, As, Cu, Mo, Pb,

Sb, and Zn) as critical evidence layers. These elements act as proxies for hydrothermal processes and can delineate zones where fluids were focused and gold was deposited. Multi-element anomalies of As, Sb, Pb, and Zn can outline hydrothermal alteration zones that function as chemical traps (Hafezi et al. 2024). In this study, the relationship between the first two principal components (PC1 and PC2) highlights the important relationship among several elements (Fig. 3-4).

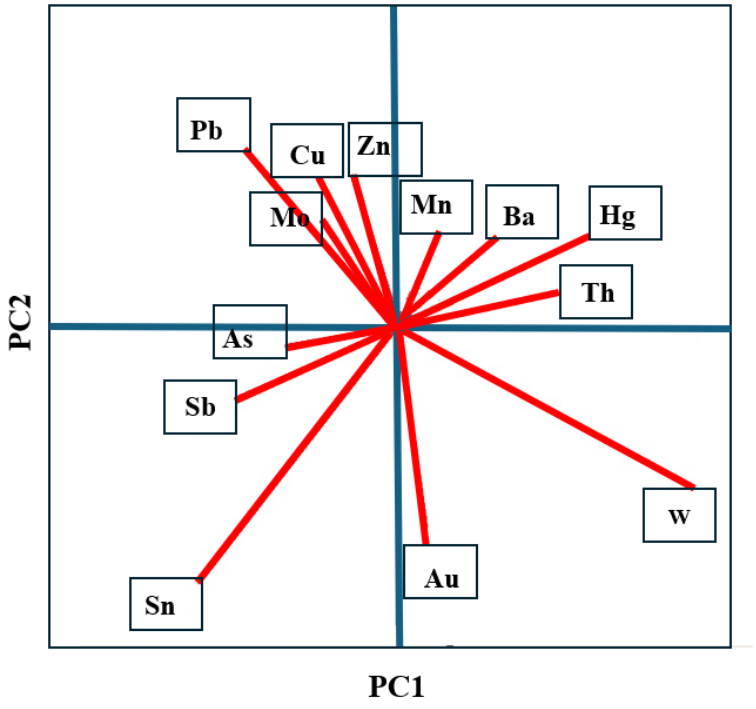

Figure 3-4. Biplots of principal component analysis (PCA) for till data used in this study.

3.7. Results and discussion

MPM applied in this study effectively identified high-favorability zones for epithermal gold mineralization in northern New Brunswick. In the study area, there are 20 occurrences of epithermal gold mineralization. Table 1 provides a summary of the evidence layers utilized in this study, whereas each layer is shown individually in Figure 3-5a-u. The

evidence layers indicating the likely source of mineralization in the study area encompass the Late Devonian Ramsay Brook Gabbro, Mount LaTour Granite and related gabbro, Mount Elizabeth Granite and related gabbro, Mount Bailey Granite, Portage Brook Troctolite, various unnamed Silurian felsic intrusions, and the Silurian-Devonian Mulligan Gulch Porphyry, any of which may have provided a magmatic contribution to these systems (Fig. 3-5a). Based on RTP and AS maps (Fig. 3-5b, c), rock units exhibiting high aeromagnetic anomalies are identified as felsic and mafic intrusions, both of which contain magnetite minerals (Mami Khalifani et al. 2019).

In the study region, felsic volcanic rocks of the Benjamin and Wapske formations are associated with several Au occurrences in the study area and exhibit high K, eU, and eTh (Fig. 3-5d, e, and f). These combined geological and geophysical layers demonstrate the critical role of magmatic processes in generating mineralizing fluids and metals (Mami Khalifani et al. 2019).

Pathways for epithermal gold mineralization in the study area are often evidenced by geological structures and geophysical indicators that facilitate the movement of hydrothermal fluids. Proximity to major and minor, faults and magnetic lineaments serve as critical evidence layers for identifying fluid conduits (Fig. 3-5g, h, and i). Faults create zones of high permeability that channel fluids through the crust. Likewise, proximity to lithological contacts (Fig. 3-5l), where rocks of contrasting rheology provide fluid pathways by enhancing structural complexity and fluid flow. Geophysical evidence such as high values of first vertical derivative (FVD) and total tilt derivative (TDR) can further delineate areas of increased structural favorability, highlighting potential pathways (Fig. 3-5j-k). These combined structural and geophysical evidence layers are essential for mapping

and understanding the features formed by hydrothermal fluid migration and gold deposition.

Geochemical zonation, exemplified by the proximal distribution of elements such as Au, As, Sb, Zn, Pb, Cu, Mo, and W, serves as an indicator for mineralized traps and reflects the dynamic evolution of fluid conditions and depositional environments (Fig. 3-5.m-t). Pathfinder elements identified through till data analyses strongly correlated with high-potential zones. These anomalies align with zones of hydrothermal alteration, particularly sericitization, and silicification, indicating their reliability as proxies for epithermal gold mineralization. For example, the Williams Brook area's geochemical signatures exhibit elevated As and Pb, which correlated with high-potential zones delineated by the models. Alteration patterns, including sericitization, silicification, and chloritization, provided further insights into mineralizing processes (Sánchez Mora D 2014; Sánchez-Mora et al. 2021) These features, often concentrated near major fault zones, are critical indicators of hydrothermal activity. Drill core samples from Williams Brook and Mulligan Gulch highlighted multiple phases of quartz veining, pyrite mineralization, and alteration halos, reinforcing the presence of active hydrothermal systems. The models' ability to predict areas with such alteration patterns validated their effectiveness in delineating epithermal gold systems. Furthermore, the Devonian mafic and felsic volcanic host rocks of the Wapske Formation, along with the mafic volcanic rocks of the Greys Gulch Formation, play a crucial role as vectors to mineralize traps and the depositional environment (Fig. 3-5).

Table 3-1. Evidence layers employed in this study.

Fundamental Processes of the Gold Mineralization	Outline of Targeting Criteria	Predictor maps	Source of data	Practices employed	Figure
Source	Tobique Group and Chaleurs Group mafic and felsic intrusive rocks with Silurian-Devonian aged	Ramsay Brook Gabbro, Upsalquitch Lake Gabbro, Silurian Felsic Intrusive, Portage Brook Troctolite mafic intrusive, Mulligan Gulch Porphyry felsic intrusive, Mount Bailey Granite, Mount LaTour Gabbro, Mount Elizabeth Gabbro, Mount Elizabeth Granite	1:50,000 bedrock geology maps (21O/10 & 21O/07) (2008)	The Euclidean distance was calculated using intrusive rocks, including both Granite and Gabbro units.	Fig. 3-5a

		High values of RTP and Analytic Signal	Campbelltown aeromagnetic data with 200-meter resolution (GSC) Bathurst aeromagnetic data with 75-meter resolution (GSC 1987b)	After applying the Reduction to the Pole (RTP) and Analytic Signal (AS) filter, the Euclidean distance was determined from the RTP anomalous regions (Keykhay-Hosseinpoor et al. 2024).	Fig. 3-5b-c
		High values of K, eU, and eTh,	Campbelltown radiometric data with 100-meter resolution (GSC) Campbelltown radiometric data	The Euclidean distance was computed using the radiometric K, eU, and eTh elements.	Fig. 3-5d-f

			with 1000-meter resolution (1976)		
Pathway of hydrothermal fluid	Faults, lineament and lithological contacts	Proximity to mapped major, minor, and thrust faults	1:500,000-scale bedrock geology map (2008)	Major, minor, and thrust faults were identified through geological map analysis, and the Euclidean distance from these fault structures was subsequently calculated.	Fig. 3-5g-i
		Proximity to extracted Magnetic lineament features using the value of tilt derivative (TDR) and first vertical derivative (FVD)	Campbelltown aeromagnetic data with 200-meter resolution (GSC) Bathurst aeromagnetic data with 75-meter resolution	Shallow and deep magnetic structures were highlighted using various derivative-based techniques, including the tilt derivative and first vertical derivative. Following this enhancement, the Euclidean distance to the identified structures was	Fig. 3-5j-k

			(GSC 1987b)	calculated (Keykhay-Hosseinpoor et al. 2024).	
		Proximity to lithological contacts	1:500,000-scale bedrock geology map (2008)	Faults were identified through the analysis of geological maps, and the Euclidean distance to these fault structures was then calculated.	Fig. 3-5l
Trap & metal deposition and emplacement	Geochemical indicator elements	Anomalous signature of Au, As, Cu, Mo, Pb, Sb, Zn and W elements	Geochemical till data collected at 2000m sampling intervals (2014)	Gold pathfinder geochemical signatures were analyzed after applying a central log-ratio transformation, and Euclidean distances to anomalous basins were calculated.	Fig. 3-5m-t
	Host rocks	Proximity to Greys Gulch Formation felsic, mafic volcanic and sedimentary rocks, Wapske Formation	1:50,000 bedrock geology maps (21O/10 & 21O/07)	Euclidean distances to felic and mafic volcanic rocks were calculated.	Fig. 3-5u

		felsic and mafic volcanic, Wapske Formation mixed volcanic and sedimentary, Free Grant Formation sedimentary rocks	(2008)		

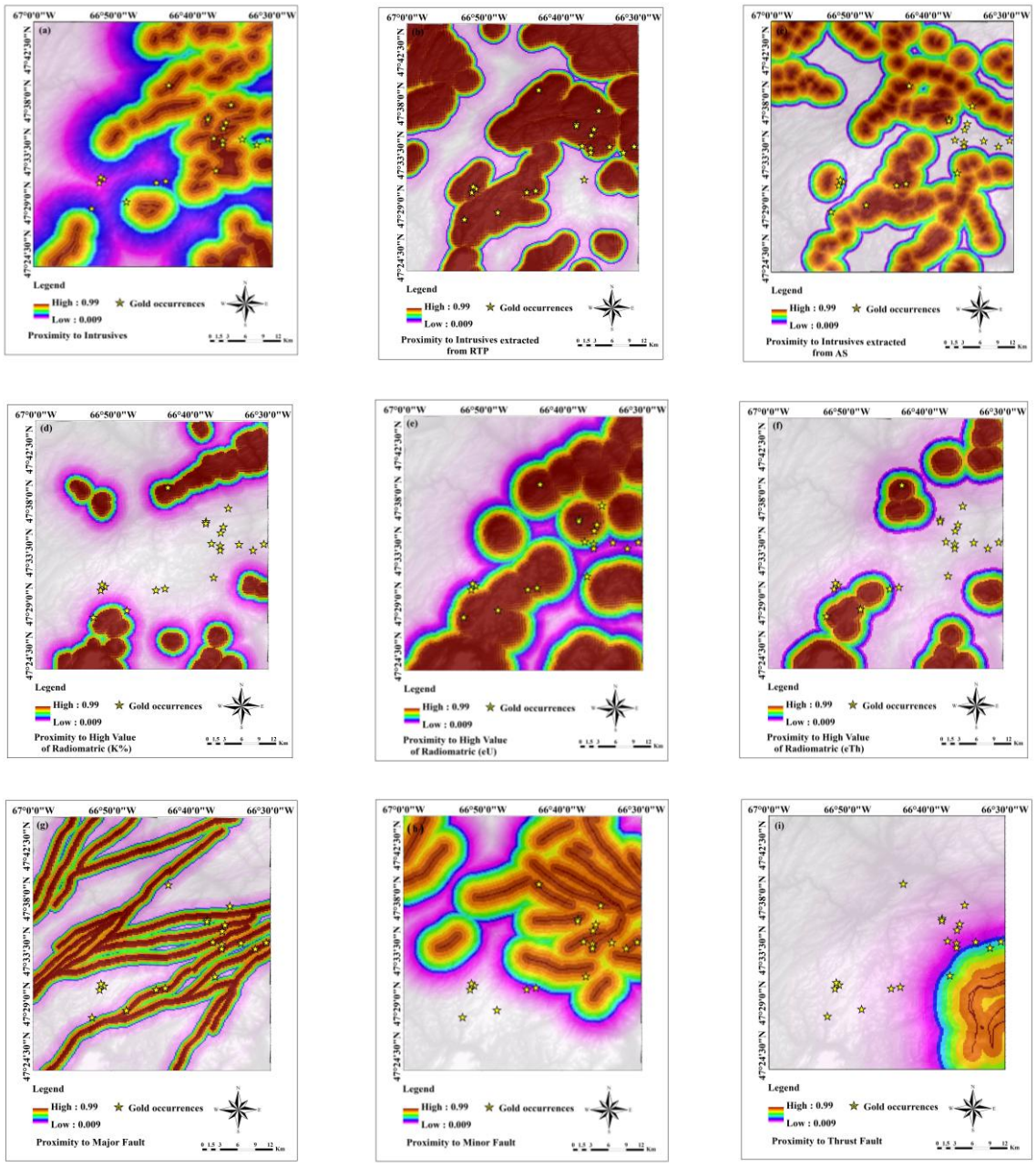

Figure 3-5. Fuzzified input evidence layers for MPM: (a) proximity to intrusions, (b) proximity to intrusions extracted from RTP, (c) proximity to intrusions extracted from AS, (d) proximity to high value of K(%), (e) proximity to high value of eU (ppm), (f) proximity to high value of eTh (ppm), (g) proximity to major faults, (h) proximity to minor faults, and (i) proximity to thrust faults.

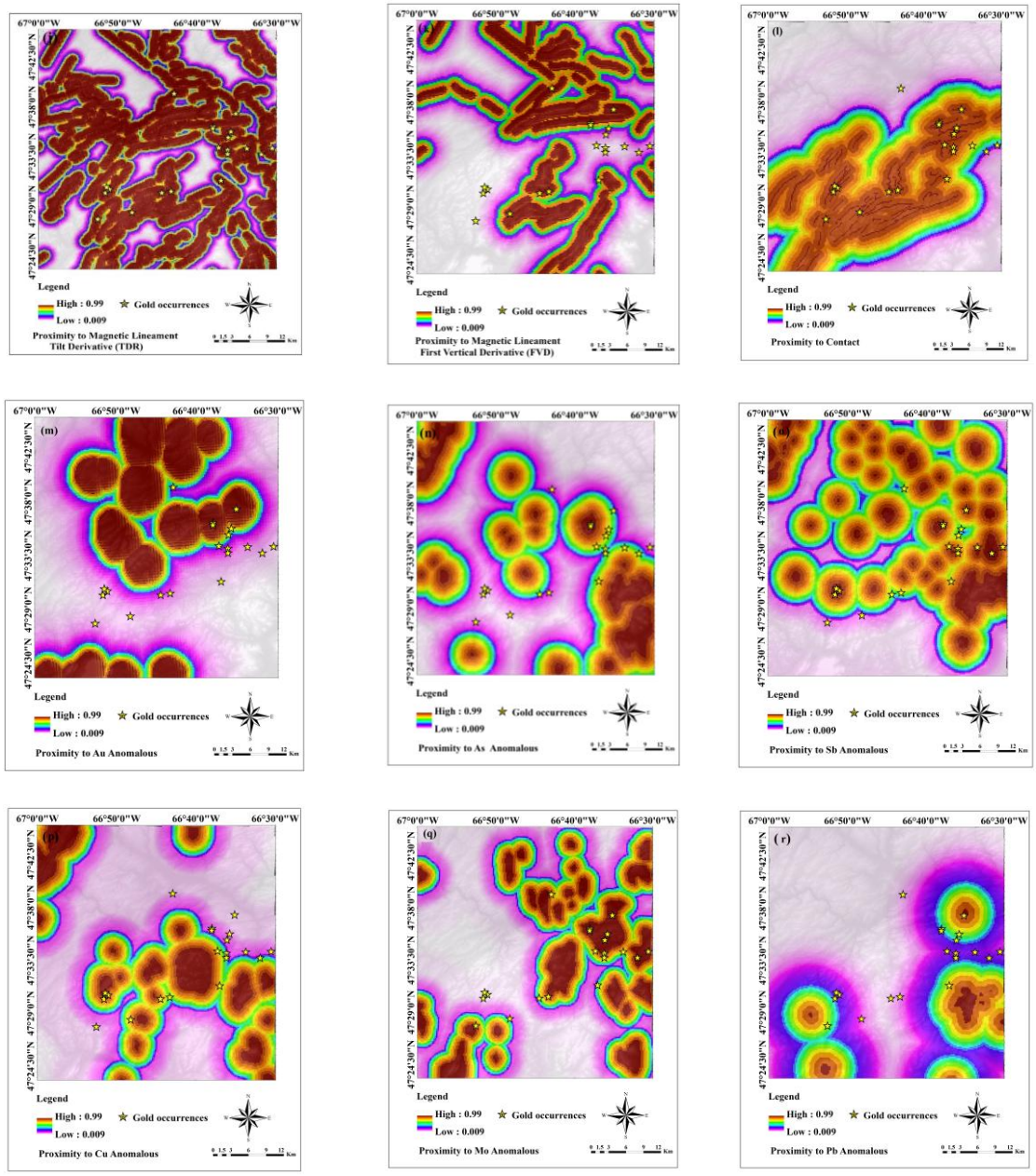

Figure 3-6. Fuzzified input evidence layers for MPM: (j) proximity to magnetic lineament derived from tilt derivative, (k)) proximity to magnetic lineament derived from first vertical derivative, (l) proximity to contact, (m) proximity to old anomalies, (n) proximity to As anomalies, (o) proximity to Sb anomalies, (p) proximity to Cu anomalies, (q) proximity to Mo anomalies, and (r) proximity to Pb anomalies.

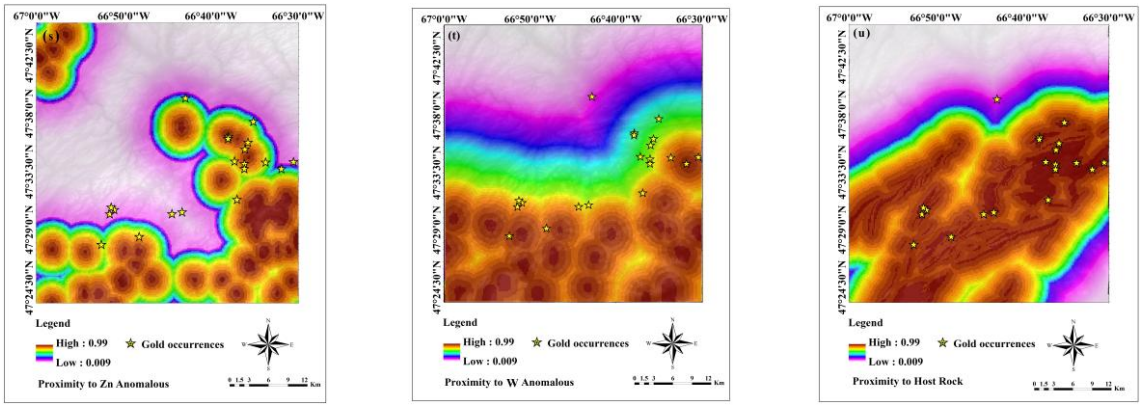

Figure 3-7. Fuzzified input evidence layers for MPM: (s) proximity to Zn anomalies, (t) proximity to W anomalies, and (u) proximity to felsic and mafic volcanic rocks.

This study applied the concentration area fractal method to classify and evaluate various MPM maps using fuzzy logic, geometric average, and logistic regression, as shown in Figure 3-6a, c, and e (Yousefi M and Carranza E J M 2015). Based on the C-A fractal method, we discretized the mineral prospectivity maps for fuzzy logic, geometric average, and logistic regression models (Fig. 3-6b, d, and f). Here, the MPM result was categorized into six classes according to the relevant C-A multifractal curve (Figs. 3-6). The first and second thresholds for fuzzy logic (0.90 and 0.94), geometric average (0.92 and 0.95), and logistic regression (0.86 and 0.94), depicted in deep red and orange, signify high favorability on three MPM maps derived from fuzzy logic, geometric average, and logistic regression (Fig. 3-6b, d, and f). Yellow stars indicate the locations of epithermal gold mineralization in the study area and closely align with the highly favorable areas identified. This suggests that the prospectivity map effectively identifies high favorability values at known gold occurrences while highlighting areas of potential. The identification of favorable areas near known gold mineralization suggests accurate identification of zones

exhibiting similar characteristics to the known occurrences. The fuzzy gamma map identifies broader, more continuous zones of high potential, whereas the geometric average method produced somewhat more localized but still relatively diffuse areas of potential. In contrast, the logistic regression map identifies more sharply defined high-potential zones closely aligned with known gold occurrences. Exploration efforts should focus on areas with the highest prospectivity, irrespective of the modeling method employed (Nykänen et al. 2023).

In this study, we utilized the ROC curve, which compares the true positive rate with the false positive rate across various classification thresholds. With an area under the curve (AUC) exceeding 0.9, the model demonstrates strong discriminative capability, effectively distinguishing between classes. Furthermore, its ROC curve lies predominantly in the top-left portion of the plot, indicative of both high sensitivity and specificity, reinforcing the model's overall robustness. The ROC curves and corresponding mean AUC values for the two knowledge-driven models are presented, with results indicating that the fuzzy overlay model achieved the highest AUC (0.97), followed by the geometric average model (0.93). These findings demonstrate exceptionally favorable performance (Fig. 3-7 a-b).

To validate the mineral prospectivity map derived from the logistic regression model, the mineralogical and petrological characteristics of the identified promising zones were examined. Figure 3-8 illustrates the presence of gold and common pathfinder minerals, including pyrite, galena, and pyrrhotite, in gold occurrences such as Williams Brook, McIntyre Brook, Mulligan Gulch, and the Simpson field. The mineral indicators, observed within the high-potential areas identified by the model, provide confidence in the accuracy of the prospectivity predictions. The models demonstrated a strong alignment with known

gold occurrences within the Tobique Chaleur Zone, which is characterized by its complex geology and significant structural controls. A major focus of this study was the development of meaningful geological, geochemical, and geophysical evidential layers to model using a mineral system approach (Hagemann et al. 2016; Khammar et al. 2024). These layers highlight the critical role of faults as fluid pathways, the significance of felsic and mafic intrusive rocks as source components, and geochemical signatures, as well as the importance of felsic and mafic volcanic trap rocks. The MPM maps (Fig. 3-6), further illustrate the effectiveness of comparing knowledge-driven methods (fuzzy logic and geometric average) with a data-driven method (logistic regression). This two-pronged approach ensures that both expert insights and statistical analyses contribute to the delineation of prospective areas.

The data-driven modeling approach demonstrated significant advantages in terms of reducing the exploration area while maintaining high predictive accuracy. Logistic regression is used to make robust predictions by efficiently processing large datasets and identifying meaningful patterns that traditional methods might miss, thereby improving predictive accuracy. This method provides a systematic and quantitative framework for decision-making. For example, Figure 3-6 reveals that known occurrences consistently overlap regions of high predicted favourability, with new target areas identified in underexplored areas. This capability not only enhances exploration efficiency but helps to mitigate risks associated with greenfield exploration.

Fuzzy logic and geometric average both draw on expert geological insights to assign weights to evidence layers, making them particularly suitable for areas with limited data. In this study, they identified extensive zones of high mineral potential, with fuzzy logic

demonstrating higher predictive accuracy (AUC = 0.97) than the geometric average method (AUC = 0.93). By contrast, data-driven logistic regression relies on training data from known occurrences, capturing complex relationships among variables and generating more narrowly defined high-potential areas. However, it demands a sufficiently large dataset and risks overfitting when data are scarce. Integrating these approaches combines the breadth of expert-based knowledge with rigorous statistical mapping, improving the efficiency and reliability of exploration targeting. In addition, all three methods fuzzy logic, geometric average, and logistic regression prove adaptable in addressing uncertainties from sparse or variable data, underscoring their value in complex geological terrains.

These methods significantly reduced the search area, thereby streamlining exploration efforts and reducing costs. Figure 3-8 presents a 3D view of the study area, showing the distribution of gold occurrences and the high-potential areas identified in this study. Overall, this study underscores the importance of integrating geological knowledge with advanced computational methods to address the challenges of mineral prospectivity mapping.

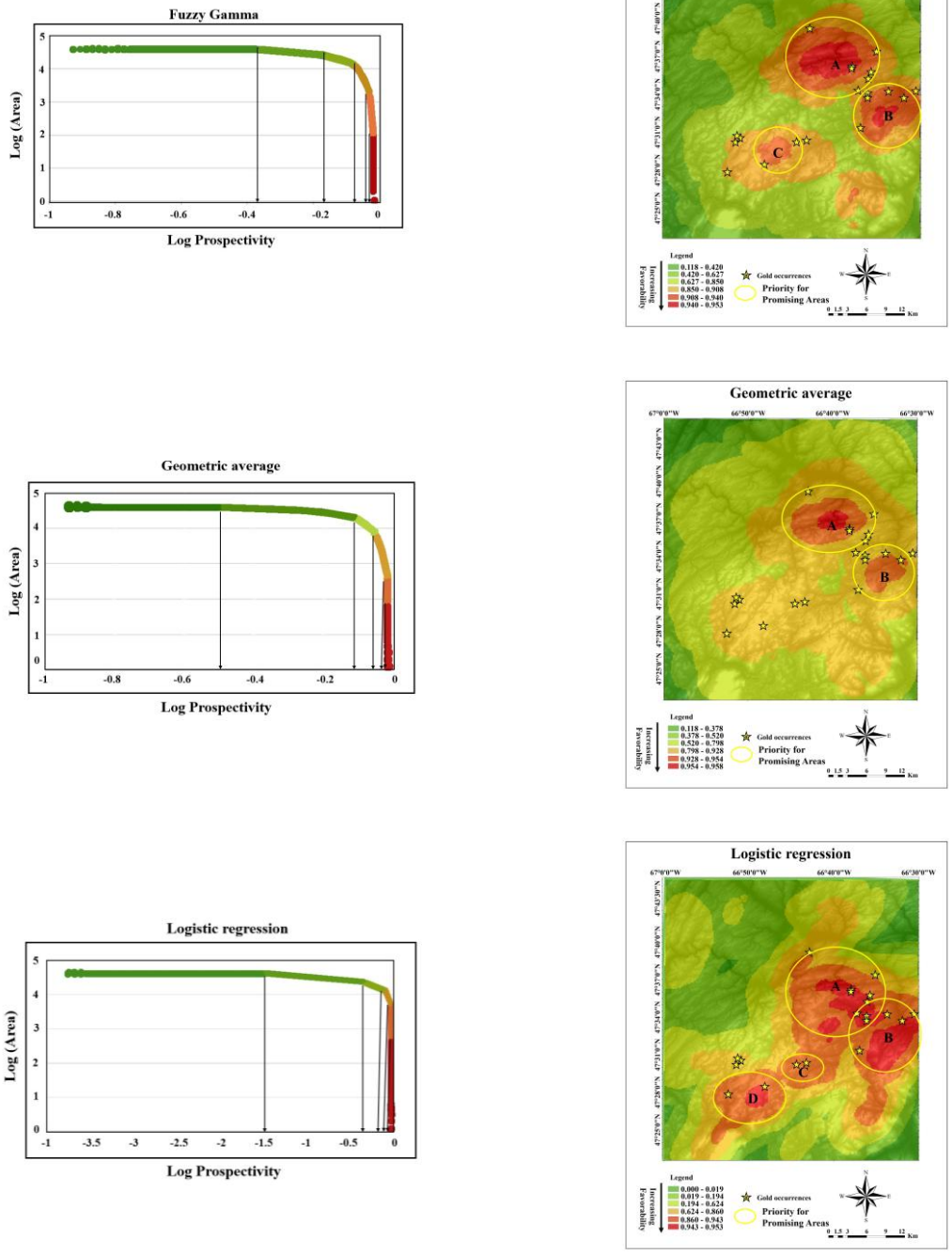

Figure 3-8. MPM assessment of the study area. (a), (c) and (e) are fractal-based curves relevant for reclassifying the MPM maps for b) fuzzy logic, d) geometric average, and f) logistic regression prospectivity values, respectively.

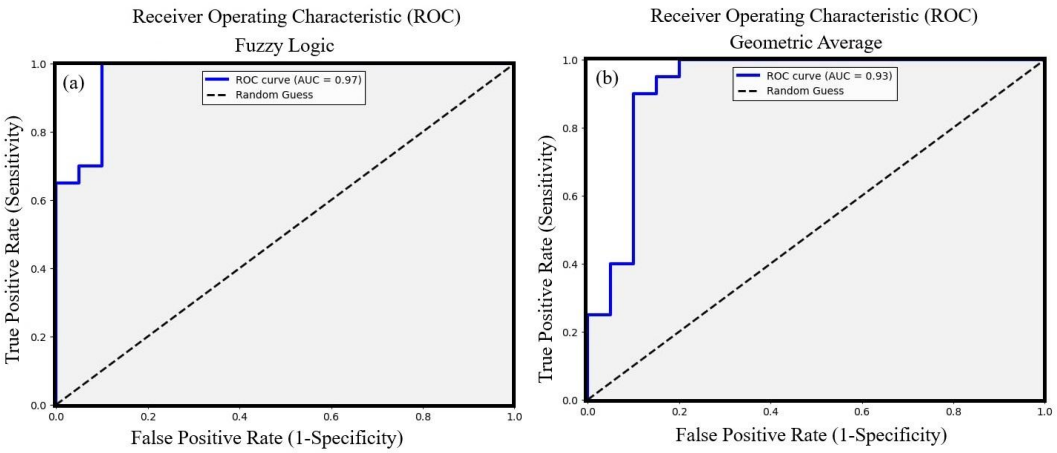

Fig. 3-7. Receiver operating characteristic validation graphs of knowledge-driven prospectivity models, a) fuzzy logic overlay, b) geometric average.

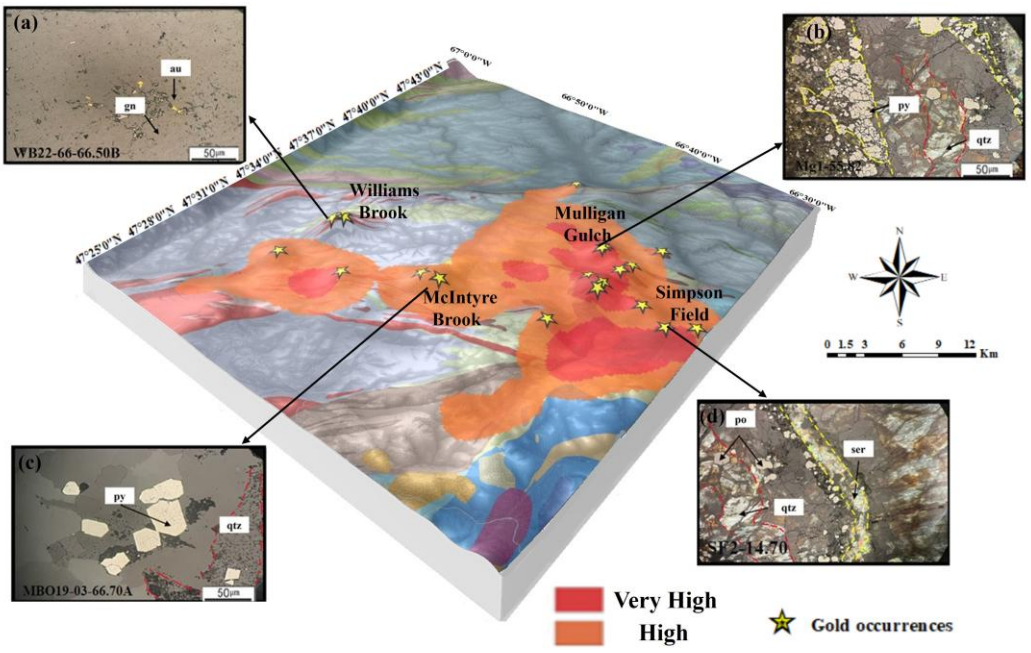

Figure 3-9. Geology of the study area showing areas of high to very high mineral prospectivity for gold mineralization (as determined by the LR method) overlain on the digital elevation model (DEM) map and showing occurrences of gold mineralization including four occurrences represented by photomicrographs (a to d). Plane-polarized reflected-light photomicrographs displaying a range of sulfide phases and electrum (native gold) hosted in various gangue phases. a) Gold accompanied by galena (gn), in sample WB22-66-66.50B from the Williams Brook occurrence. b) Pyrite-rich (py) zone adjacent to a quartz vein, sample Mg-55.82 from Mulligan Gulch. c) Pyrite (py) in sample MBO19-03-70A from the McIntyre Brook occurrence. d) Pyrite (py) located next to quartz, enveloped by sericitic (ser) sample SF2-14.70, from Simpson Field.

3.8. Conclusions and recommendations

The major accomplishments of this study can be summarized as follows:

1. This study applied an MPM technique to identify high-favorability zones for epithermal gold mineralization in Northern New Brunswick. By integrating geological expertise with advanced computational methods, namely fuzzy logic, geometric averaging, and logistic regression, it achieved a high level of predictive accuracy. The identified zones strongly correlated with known gold occurrences, especially in the structurally controlled Tobique Chaleur Zone.

2. Geological, geochemical, and geophysical datasets were crucial in defining evidence layers that represented the mineral system components. The alignment of high-favorability zones with key structural features, such as the Rocky Brook Millstream Fault system, demonstrated the importance of faults as fluid pathways. The study also underscored the role of felsic and mafic intrusive rocks as essential magmatic sources, contributing to gold mineralization.

3. The fuzzy gamma model delineated extensive, continuous zones with high potential. The geometric average method identified more localized but somewhat dispersed areas of interest. The logistic regression model generated sharply defined high-potential zones that closely corresponded with known occurrences. Integrating knowledge-driven approaches (fuzzy logic and geometric average) with a data-driven method (logistic regression) enhanced the accuracy and effectiveness of the prospectivity analysis.

4. The high area under the curve (AUC) values obtained from the receiver operating characteristic (ROC) curves validate the robustness and reliability of the MPM methods used in this study. Specifically, the fuzzy overlay model achieved the highest AUC (0.97), followed by the geometric average model (0.93). These values indicate strong predictive

accuracy, confirming that the models effectively delineate high-favorability zones for epithermal gold mineralization in Northern New Brunswick.

5. The study identified indicator minerals and pathfinder elements that strongly correlate with high-potential zones. Drill core analysis confirmed the presence of gold-bearing quartz veins and associated mineralization, further reinforcing the accuracy of the MPM models.

In addition, future work might include the following:

6. Incorporate field-based validation (e.g., additional drilling or detailed mapping) in the newly identified high-favorability zones to confirm the presence of epithermal gold mineralization.

7. Explore machine-learning techniques beyond logistic regression (e.g., random forests or support vector machine) to capture nonlinear relationships and optimize predictive accuracy.

8. Acquire or integrate higher-resolution geophysical and geochemical datasets—where it is feasible to further reduce uncertainty and improve spatial resolution of prospectivity maps.

9. Apply the presented methodology to related mineral deposit styles (e.g., orogenic gold, base-metal skarns) within the Appalachian or other structurally complex terrains, assessing model adaptability and limitations.

Acknowledgments: This research forms part of the first author's PhD thesis. We acknowledge the Department of Geosciences and Geography, Research Programme of Geology and Geophysics (GeoHel) at the University of Helsinki, Finland, and the New

Brunswick Department of Natural Resources and Energy Development, for their financial valuable support, as well as a scholarship to FMK from the University of New Brunswick. All authors have read and agreed to the published version of the manuscript.

Funding: University of New Brunswick.

Conflicts of Interest: The authors declare no conflicts of interest.

References

Abdelrady M, Moneim MA, Alarifi SS, et al (2023) Geophysical investigations for the identification of subsurface features influencing mineralization zones. J King Saud Univ Sci 35(7)−102809.

Abedi M, Torabi SA, Norouzi GH, et al (2012) PROMETHEE II: A knowledge-driven method for copper exploration. Comput Geosci 46:255-263.

Aitchison J (1986) The Statistical Analysis of Compositional Data, Monographs on Statistics and Applied Probability. 1 publ edn, Chapman and Hall, London [u.a]

Almasi, A., Yousefi, M. and Carranza, E.J.M., 2017. Prospectivity analysis of orogenic gold deposits in Saqez-Sardasht goldfield, Zagros orogen, Iran. Ore Geology Reviews, 91, pp.1066-1080.

Aminu MB, Adiat KAN, Akinlalu AA, et al (2024) A review on the applications of airborne geophysical and remote sensing datasets in epithermal gold mineralisation mapping. Geosystems and Geoenvironment 3:100284.

Barak S, Imamalipour A, Abedi M, et al (2021) Comprehensive modeling of mineral potential mapping by integration of multiset geosciences data. Geochemistry 81.

Baranov, V., 1957. A new method for interpretation of aeromagnetic maps: pseudo-gravimetric anomalies. Geophysics, 22(2), pp.359−382.

Behera S, Panigrahi MK (2021) Mineral prospectivity modelling using singularity mapping and multifractal analysis of stream sediment geochemical data from the auriferous Hutti-Maski schist belt, S. India. Ore Geol Rev 131:104029.

Behnia P, Harris J, Liu H, et al (2023) Random forest classification for volcanogenic massive sulfide mineralization in the Rouyn-Noranda Area, Quebec. Ore Geol Rev 161, 105612.

Bernier MA, Webber GR (1989) Mineralogical and geochemical analysis of shallow overburden as an aid to gold exploration in southwestern Gaspésie, Quebec, Canada. J Geochem Explor 34.

Bonham-carter GF, Agterberg FP (1999) Arc-WofE: a GIS tool for statistical integration of mineral exploration datasets. Bulletin of the International Statistical Institute 52, pp.497−500.

Bonham-Carter GF, Agterberg FP (1990) Application of a Microcomputer-based Geographic Information System to Mineral-Potential Mapping. Microcomputer Applications in Geology 2 49–74.

Bonham-Carter GF, Agterberg FP, Wright DF (1990) Integration of geological datasets for gold exploration in Nova Scotia. Introductory readings in geographic information systems 10, pp.15-23.

Braga LPV, Braga J (2020) Mapping gold pathfinder metal ratios in Northern Nevada, USA: A compositional analysis approach. J Geochem Explor 219:106616.

Bustard AL, Dahn DRL (2024) Characteristics and structural setting of vein hosted Au-Ag-Pb-Zn mineralization associated with the Mulligan Gulch Porphyry, north central

New Brunswick. New Brunswick Department of Natural Resources and Energy Development, Geoscience Report.

Bustard AL, DDRL, (2024) Characteristics and structural setting of veinhosted Au-Ag-Pb-Zn mineralization associated with the Mulligan Gulch Porphyry, northcentral New Brunswick.

Byberg T, Kim Tyler R (2020) Assessment Report on Trench Sampling, Mapping and Diamond Drilling McIntyre Brook Property.

Cardenas-Vera A, MacDonald M, Lentz DR, Thorne KG (2023) Trace Element Characteristics of Pyrite and Arsenopyrite from the Golden Ridge Gold Deposit, New Brunswick, Canada: Implications for Ore Genesis. Minerals 13.

Carranza EJM (2009) Objective selection of suitable unit cell size in data-driven modeling of mineral prospectivity. Comput Geosci 35(10), pp.2032-2046.

Carranza EJM, Hale M, Faassen C (2008) Selection of coherent deposit-type locations and their application in data-driven mineral prospectivity mapping. Ore Geol Rev 33:33(3–4), pp.536-558.

Carranza EJM, Sadeghi M, Billay A (2015) Predictive mapping of prospectivity for orogenic gold, Giyani greenstone belt (South Africa). Ore Geol Rev 71, pp.703-718.

Cheng H, Zhenge Y, Wu S, et al (2023) GIS-based mineral prospectivity mapping using machine learning methods: a case study from Zhuonuo ore district, Tibet. 161, 105627.

Cheng Q, Agterberg FP (1995) Multifractal modeling and spatial point processes. Math Geol 27.

Cheng Q, Agterberg FP, Ballantyne SB (1994) The separation of geochemical anomalies from background by fractal methods. J Geochem Explor 51.

Cooper GRJ, Cowan DR (2008) Edge enhancement of potential-field data using normalized statistics. Geophysics 73.

Corbett, G., 2002. Epithermal gold for explorationists. AIG News, 67(2002), pp.1-8.

Corbett GJ, Leach TM (1998) Southwest Pacific Rim gold-copper systems: structure, alteration, and mineralization. Society of Economic Geologists.

Cox DP, Singer DA (1988) Distribution of gold in porphyry copper deposits.

Dimitrov I, McCutcheon SR,, Williams PF, 2003 (2003) Progress report: structural investigations in the vicinity of the Rocky Brook – Millstream Fault, Gloucester and Restigouche counties, northern New Brunswick. In Current Research 2002. Edited by B.M. W. Carroll. New Brunswick Department of Natural Resources; Minerals, Policy and Planning Division

Einaudi F, Godard M, Pezard P, et al (2003) Magmatic cycles and formation of the upper oceanic crust at spreading centers: Geochemical study of a continuous extrusive section in the Oman ophiolite. Geochemistry, Geophysics, Geosystems 4(6).

Esmaeiloghli S, Tabatabaei SH, Carranza EJM (2021) Spatio-Geologically Informed Fuzzy Classification: An Innovative Method for Recognition of Mineralization-Related Patterns by Integration of Elemental, 3D Spatial, and Geological Information. Natural Resources Research 30, pp.989-1010.

Fawcett T (2006) An introduction to ROC analysis. Pattern Recognition Letters. Pattern Recognit Lett 27:

Feizi F, Amir Abbas Karbalaei-Ramezanali, Farhadi S (2021) Application of multivariate regression on magnetic data to determine further drilling site for iron exploration. Open Geosciences 13.

Fyffe LR, Fricker A (1987) Tectonostratigraphic terrane analysis of New Brunswick. Atlantic Geology 23(3), pp.113-122.

Gabo-Ratio JA, Buena AE, Villaplaza BRB, et al (2020) Epithermal mineralization of the Bonanza-Sandy vein system, Masara Gold District, Mindanao, Philippines. Journal of Asian Earth Sciences: X 4:100041.

Gahlan HA, Azer MK, Asimow PD, Al-Kahtany KM (2022) Formation of gold-bearing listvenite in the mantle section of the Neoproterozoic Bir Umq ophiolite, Western Arabian Shield, Saudi Arabia. Journal of African Earth Sciences 190.

Ghezelbash R, Daviran M, Maghsoudi A, (2025a) Combination of Machine Learning and Fractal approaches for AI-MPM: Identifying Low-Risk Exploration Targets associated with Porphyry-Cu Deposits in the Kerman Belt, Iran. Remote Sens Appl p.101596.

Ghezelbash R, Daviran M, Maghsoudi A, Hajihosseinlou M (2025b) Density based spatial clustering of applications with noise and fuzzy C-means algorithms for unsupervised mineral prospectivity mapping. Earth Sci Inform 18(2), 217.

Goldfarb RJ, Baker T, Dubé B, et al (2005) Distribution, character, and genesis of gold deposits in metamorphic terran.

Goldfarb RJ, Groves DI, Gardoll S (2001) Orogenic gold and geologic time: A global synthesis. Ore Geol Rev 18.

Golshadi Z, Ramezanali AK, Kafaei K (2016) Interpretation of magnetic data in the Chenar-e Olya area of Asadabad, Hamedan Iran, using analytic signal, Eulerdeconvolution, horizontal gradient and tilt derivative methods. Bollettino di Geofisica Teorica ed Applicata 57.

Goodfellow WD, McCutcheon SR, Peter JM (2003) Massive Sulfide Deposits of the Bathurst Mining Camp, New Brunswick, and Northern Maine: Introduction and Summary of Findings. Massive Sulfide Deposits of the Bathurst Mining Camp, New Brunswick, and Northern Maine.

Groves DI, Goldfarb RJ, Knox-Robinson CM, et al (2000) Late-kinematic timing of orogenic gold deposits and significance for computer-based exploration techniques with emphasis on the Yilgarn Block, Western Australia. Ore Geol Rev 17.

GSC (1986) Geological Survey of Canada (GSC) (1986). Aeromagnetic Data 300m Campbelltown. Retrieved from 1027 Https://Geophysical-Data.Canada.ca/Portal/Results?MinLong=-69.19&maxLong=-1028 63.42&minLat=44.19&maxLat=49.59.

GSC (1987a) Geological Survey of Canada (GSC) (1987). Aeromagnetic data 300m Campbelltown. Retrieved from https://geophysical-data.canada.ca/Portal/Results?minLong=-69.19&maxLong=-63.42&minLat=44.19&maxLat=49.59.

GSC (1976) Geological Survey of Canada (GSC) (1976). Airborne radiometric data 1000m national-scale maps. Retrieved from https://geophysical-data.canada.ca/Portal/Results?minLong=-69.19&maxLong=-63.42&minLat=44.19&maxLat=49.59

GSC Geological Survey of Canada (GSC) (1986). Aeromagnetic data 1000m Campbelltown. Retrieved from https://geophysical-data.canada.ca/Portal/Results?minLong=-90067.868&maxLong=-66.7775&minLat=45.4768&maxLat=46.4425.

GSC (1987b) Geological Survey of Canada (GSC) (1987). Aeromagnetic data 300m Campbelltown. Retrieved from https://geophysical-data.canada.ca/Portal/Results?minLong=-69.19&maxLong=-63.42&minLat=44.19&maxLat=49.59.

Hafezi A, Asadi Haroni H, Tabatabaei SH, Esmaeiloghli S (2024) Adopting a cell-based method to identify mineralized geological structures in support of mineral prospectivity mapping at the Kuh–Lakht epithermal gold deposit, Central Iran. Ore Geol Rev 171:106175.

Hagemann SG, Lisitsin VA, Huston DL (2016) Mineral system analysis: Quo vadis. Ore Geol Rev 76

Harris JR., Grunsky E, Behnia P, Corrigan D (2015) Data- and knowledge-driven mineral prospectivity maps for Canada's North. Ore Geol Rev 71, pp.788-803.

Hatcher RD (2010) The Appalachian orogen: A brief summary. Memoir of the Geological Society of America 206:1–19.

Hedenquist JW, Arribas A (2022) Exploration Implications of Multiple Formation Environments of Advanced Argillic Minerals. Economic Geology 117:609–643.

Heidarian H, Lentz DR, Thorne K, Rogers N (2021) Application of portable X-ray and micro-X-ray fluorescence spectrometry to characterize alteration and mineralization

within various gold deposits hosted in southern New Brunswick, Canada. J Geochem Explor 229.

Hronsky JMA, Groves DI (2008) Science of targeting: definition, strategies, targeting and performance measurement. Australian Journal of Earth Sciences 55:3–12.

Imamalipour A, Barak S, Khalifani FM (2020) Quantifying mass changes during hydrothermal alteration in listwaenite-type mercury mineralization, tavreh area, northwestern iran. Geochemistry: Exploration, Environment, Analysis 20.

J. Massawe R, Lentz DR (2020) Evaluation of crystallization and emplacement conditions of the McKenzie Gulch porphyry dykes using chemistry of rock-forming minerals: Implications for mineralization potential. Ore Geol Rev 116.

John D, VPG, du BEA, BRJ, FDL, RBW, MJL, AED and GF, (2018) Descriptive models for epithermal gold-silver deposits

John DA, Vikre PG, du Bray EA, et al (2018) Descriptive models for epithermal gold-silver deposits. Scientific Investigations Report.

Josso P, Hall A, Williams C, et al (2023) Application of random-forest machine learning algorithm for mineral predictive mapping of Fe-Mn crusts in the World Ocean. Ore Geol Rev 162, 105671.

Karbalaeiramezanali A, Parsa M, Lentz DR, Thorne KG (2025) Prospectivity Modeling of Devonian Intrusion-Related W–Mo–Sb–Au Deposits in the Pokiok Plutonic Suite, West-Central New Brunswick, Canada, Using a Monte Carlo-Based Framework. Natural Resources Research 1-34.

Keykhay-Hosseinpoor M, Alok P, Kalimuthu Rajendran (2024) Targeting porphyry Cu deposits in the Chahargonbad region of Iran: A joint application of deep belief networks and random forest techniques. Geochemistry 126155.

Khalifani F, Bahroudi A, Barak S, Abedi M (2019) An integrated Fuzzy AHP-VIKOR method for gold potential mapping in Saqez prospecting zone, Iran. Earth Observation and Geomatics Engineering 3.

Khalifani FM, Imamalipour A, Barak S, et al (2023) The Application of Various Mineral Prospectivity Modeling in the Exploration of Orogenic Gold Deposit in Saqez-Sardasht Region, Northwest Iran. Lithology and Mineral Resources 58:368–386.

Khammar F, Nykänen V, Beier C, Niiranen T (2024) Translating mineral systems criteria into a prospectivity model for IOCG deposits in the Kolari region, Finland. Ore Geol Rev p.106326.

Khammar F, Yousefi S, Joonaghani SA (2021) Analysis of lithogeochemical data using log-ratio transformations and C-A fractal to separate geochemical anomalies in Tak-Talar, Iran. Arabian Journal of Geosciences 14.

Kim Tyler. R (2020) MCINTYRE BROOK PROPERTY SOIL SAMPLING SURVEY

Kim Y-H, Choe K-U, Ri R-K (2019) Application of fuzzy logic and geometric average: A Cu sulfide deposits potential mapping case study from Kapsan Basin, DPR Korea. Ore Geol Rev 107:239–247.

Kost S, Rheinbach O, Schaeben H (2021) Using logistic regression model selection towards interpretable machine learning in mineral prospectivity modeling. Geochemistry 81.

Kreuzer OP, Etheridge MA, Guj P, et al (2008) Linking Mineral Deposit Models to Quantitative Risk Analysis and Decision-Making in Exploration. Economic Geology 103:829–850.

Lauzon D, Gloaguen E (2024) Quantifying uncertainty and improving prospectivity mapping in mineral belts using transfer learning and Random Forest: A case study of copper mineralization in the Superior Craton Province, Quebec, Canada. Ore Geol Rev 166, 105918.

Lawley CJM, Tschirhart V, Smith JW, et al (2021) Prospectivity modelling of Canadian magmatic Ni (±Cu ± Co ± PGE) sulphide mineral systems. Ore Geol Rev 132:103985. https://doi.org/10.1016/j.oregeorev.2021.103985.

Lentz DR, TK, YX and CBMW, (2002) Preliminary analysis of the controls on the various episodes of gold mineralization at the Lake George antimony deposit, New Brunswick. Mineral Resource Report, MRR 55–79

Li C, Xiao K, Sun L, et al (2024) CNN-Transformers for mineral prospectivity mapping in the Maodeng–Baiyinchagan area, Southern Great Xing'an Range. Ore Geol Rev 167:106007.

Li T, Xia Q, Zhao M, et al (2020) Prospectivity Mapping for Tungsten Polymetallic Mineral Resources, Nanling Metallogenic Belt, South China: Use of Random Forest Algorithm from a Perspective of Data Imbalance. Natural Resources Research 29.

Liu B, Zheng W, Wang L, et al (2024) Mineral exploration model for Lhasa Area, eastern Gangdese metallogenic belt: Based on knowledge-driven compositional data analysis and catchment basin division. Journal of Geochemical Exploration. J Geochem Explor.

Liu L, Lu J, Tao C, et al (2021) GIS-based Mineral Prospectivity Mapping of Seafloor Massive Sulfide on Ultraslow-spreading Ridges: A Case Study of Southwest Indian Ridge 48.7°–50.5° E. Natural Resources Research 30:971–987.

Malo M, Moritz R, Dube B, et al (2000) Base metal skarns and Au occurrences in the Southern Gaspe Appalachians: Distal products of a faulted and displaced magmatic-hydrothermal system along the grand pabos-restigouche fault system. Economic Geology 95.

Mami Khalifani F, Bahroudi A, Aliyari F, et al (2019) Generation of an efficient structural evidence layer for mineral exploration targeting. Journal of African Earth Sciences 160, 103609.

Mami Khalifani F, Lentz D, Parsa M, Walker J (2023a) Recognizing gold mineralization pathfinders with portable XRF and micro-X-ray fluorescence spectrometry in the Williams Brook epithermal system, NB: Analysis of Indicator Elements and Minerals. In: Atlantic Geoscience Society

Mami khalifani F, Lentz D, Walker J (2025a) Machine Learning-Based Framework for Mineral Prospectivity Modeling: Predicting Epithermal Gold Mineralization in Northern New Brunswick, Canada. In: EGU General Assembly 2025, Vienna, Austria.

Mami Khalifani F, Lentz D, Walker J (2024) Gold Prospectivity Mapping and Exploration Targeting in Northern New Brunswick, Canada: Combined Application of Random Forest (RF) and Fuzzy Inference System (FIS). In: American Geophysical Union (AGU), Washington. DC.

Mami khalifani F, Lentz D, Walker J (2025b) A Machine Learning-Based Framework for Mineral Prospectivity Modeling: Predicting Epithermal Gold Mineralization in Northern New Brunswick, Canada. In: EGU General Assembly 2025, Vienna, Austria

Mami Khalifani F, Lentz D, Walker J, Khammar F (2025) Applying Mineral System Criteria to Develop a Predictive Modelling for Epithermal Gold Mineralization in Northern New Brunswick: Using Knowledge-Driven and Data-Driven Methods. Minerals 15(4), 345.

Mami Khalifani F, Lentz DR, Parsa M, Walker JA (2023b) Recognizing gold mineralization pathfinders with portable XRF and micro-X-ray fluorescence spectrometry in the Williams Brook epithermal system, NB: Analysis of Indicator Elements and Minerals. Atlantic Geoscience Society Conference.

Mami Khalifani F, Parsa M, Lentz D, Walker J (2022a) Portable XRF-aided pattern recognition for characterization of gold mineralization in Northern New Brunswick. In: Exploration, Mining and Petroleum New Brunswick (EMP 2022)

Mami Khalifani F, Parsa M, Lentz D, Walker J (2021) Magnetic and radiometric signatures of gold mineralization in northern New Brunswick: constraints from numerical and spatial techniques. GAC-MAC Conference.

Mami Khalifani FM, Barak S, Abedi M, Yousefi S (2023c) Gold prospectivity mapping through generation and integration of geophysical, geochemical, remote sensing, and geological evidence layers in Saqez area, NW Iran. International Journal of Mining and Geo-Engineering 57.

Mami Khalifani, Lentz D.R, Parsa M, Walker J (2022b) Portable XRF-aided pattern recognition for characterization of gold mineralization in Northern New Brunswick

Mantilla-Dulcey A, Goyes-Peñafiel P, Báez-Rodríguez R, Báez-Rodríguez R (2024) Porphyry-type mineral prospectivity mapping with imbalanced data via prior geological transfer learning. Gondwana Research

Massawe RJR, Lentz DR (2022) Petrogenesis and U–Pb (titanite) age of Cu–Ag skarn mineralization in the McKenzie Gulch area, northern New Brunswick, Canada. J Geochem Explor 232.

McClenaghan SH, Goodfellow WD, Lentz DR (2003) Gold in Massive Sulfide Deposits, Bathurst Mining Camp: Distribution and Genesis. Massive Sulfide Deposits of the Bathurst Mining Camp, New Brunswick, and Northern Maine.

McCuaig TC, Beresford S,, Hronsky J (2010) Translating the mineral systems approach into an effective exploration targeting system. Ore Geol Rev 38(3), pp.128-138.

McCuaig TC, Hronsky J (2017) The mineral systems concept: the key to exploration targeting. Applied Earth Science 126.

Mccutcheon S R, Anderson H E, Robinson P T (1997) Detection of Mineralization Zones Using Aeromagnetic Data. Applied Sciences. Geol Mag 12(18), 9078.

Mohamed A, Abdelrady M, Alshehri F, et al (2022) Detection of Mineralization Zones Using Aeromagnetic Data. Applied Sciences.

Mohammadpour M, Bahroudi A, Abedi M, et al (2019) Geochemical distribution mapping by combining number-size multifractal model and multiple indicator kriging. J Geochem Explor 200.

Morrissy C (1991) Gold assessment at the Lake George mine, York County, New Brunswick

NBDNR (2014) NBDNR (2014) New Brunswick Department of Natural Resources. https://www2.gnb.ca/content/gnb/en/departments/erd/open.

Nykänen V, Niiranen T, Molnár F, et al (2017) Optimizing a Knowledge-driven Prospectivity Model for Gold Deposits Within Peräpohja Belt, Northern Finland. Natural Resources Research 26:. https://doi.org/10.1007/s11053-016-9321-4

Nykänen V, Salmirinne H (2007) Prospectivity analysis of gold using regional geophysical and geochemical data from the Central Lapland Greenstone Belt, Finland. Special Paper of the Geological Survey of Finland 44, pp.251-269.

Nykänen V, Törmänen T, Niiranen T (2023) Cobalt Prospectivity Using a Conceptual Fuzzy Logic Overlay Method Enhanced with the Mineral Systems Approach. Natural Resources Research 32:2387–2416.

Nykänen Vesa, Lahti Ilkka, Niiranen Tero, Korhonen Kimmo (2015) Receiver operating characteristics (ROC) as validation tool for prospectivity models — A magmatic Ni–Cu case study from the Central Lapland Greenstone Belt, Northern Finland. Ore Geol Rev 71, pp.853-860.

Parsa M, Lentz DR, Walker JA (2023) Predictive Modeling of Prospectivity for VHMS Mineral Deposits, Northeastern Bathurst Mining Camp, NB, Canada, Using an Ensemble Regularization Technique. Natural Resources Research 32.

Porwal A, Carranza EJM, Hale M (2003) Artificial neural networks for mineral-potential mapping: A case study from Aravalli Province, Western India. Natural Resources Research 12:155–171.

Porwal A, Carranza EMJ (2015) Introduction to the Special Issue: GIS-based mineral potential modelling and geological data analyses for mineral exploration. Ore Geol Rev 71, pp.477-483.

Porwal A, González-Álvarez I, Markwitz V, et al (2010) Weights-of-evidence and logistic regression modeling of magmatic nickel sulfide prospectivity in the Yilgarn Craton, Western Australia. Ore Geol Rev 38:184–196.

Raines GL (2008) Are fractal dimensions of the spatial distribution of mineral deposits meaningful? Natural Resources Research 17.

Rodgers J (1970) The Tectonics of the Appalachians. John Wiley and Sons, New York, 271.

Romer RL, Kroner U (2018) Paleozoic gold in the Appalachians and Variscides. Ore Geol Rev 92:475–505.

Roshanravan B, Kreuzer OP, Buckingham A, et al (2023) Mineral potential modelling of orogenic gold systems in the granites-tanami Orogen, Northern Territory, Australia: A multi-technique approach. Ore Geol Rev 152:.

Sánchez Mora D (2014) Petrogenesis of the low sulfidation gold mineralization in the Williams Brook area, Tobique-Chaleur Zone, New Brunswick.

Sánchez-Mora D, McFarlane CRM, Walker JA, Lentz DR (2021) Geochemistry and U–Pb geochronology of the Williams Brook area, Tobique–Chaleur zone, New Brunswick: stratigraphic and geotectonic setting of gold mineralization. Can J Earth Sci 58(10), pp.1040-1058.

Sibson RH (1990) Deformation Mechanisms, Rheology and Tectonics.

Sillitoe RH, Hedenquist JW (2003) Linkages between volcanotectonic settings, ore-fluid compositions, and epithermal precious metal deposits. In: pubs.geoscienceworld.org.

Silva dos Santos V, Gloaguen E, Hector Abud Louro V, Blouin M (2022) Machine learning methods for quantifying uncertainty in prospectivity mapping of magmatic-hydrothermal gold deposits: A case study from Juruena mineral province, northern Mato Grosso, Brazil. Minerals (pp. 207-235). Boston, MA: Springer US.

Skirrow RG, Murr J, Schofield A, et al (2019) Mapping iron oxide Cu-Au (IOCG) mineral potential in Australia using a knowledge-driven mineral systems-based approach. Ore Geol Rev 113.

St Peter C (1978) Geology of parts of Restigouche.

Suthaharan S (2016) Support vector machine. In Machine learning models and algorithms for big data classification: thinking with examples for effective learning. Boston, MA: Springer US., p (pp. 207-235).

Taylor BE (2007) Epithermal gold deposits. Mineral Deposits of Canada: A synthesis of major deposit-types, district metallogeny, the evolution of geological provinces, and exploration methods. Geological Association of Canada, Mineral Deposits Division, Special Publication, 5, pp.113-139.

Thorne KG (2011) Gold in New Brunswick, Canada

Thorne KG, Lentz DR, Hoy D, et al (2008) Characteristics of Mineralization at the Main Zone of the Clarence Stream Gold Deposit, Southwestern New Brunswick, Canada: Evidence for an Intrusion-Related Gold System in the Northern Appalachian Orogen. Exploration and Mining Geology 17(1–2), pp.13-49.

Tremblay A, Faure S,, Dubé B, (1993) Gold occurrences of the Rocky Brook – Millstream Fault, northern Appalachians, New Brunswick. In Current Research, Part E, Geological Survey of Canada. Paper 93-1E 337–346

van Staal C R, de Roo J A, Hibbard J P, Cawood P A (1995) Mid-Paleozoic tectonic evolution of the Appalachian Central Mobile Belt in northern New Brunswick, Canada: collision, extensional collapse and dextral transpression. Current Perspectives in the Appalachian-Caledonian Orogen. Geological Association of Canada Special Paper 41, pp.367-389.

van Staal CR (2007) Pre-Carboniferous tectonic evolution and metallogeny of the Canadian Appalachians Mineral Deposits of Canada. In: Geological Association of Canada. pp 793–818

Van Staal CR, Whalen JB, Valverde-Vaquero P, et al (2009) Pre-Carboniferous, episodic accretion-related, orogenesis along the Laurentian margin of the northern Appalachians. Geol Soc Spec Publ 271-316.

Van Wagoner NA, LMI, DKA, BDK and MW, (2002) Late Silurian bimodal volcanism of southwestern New Brunswick, Canada: Products of continental extension. Geol Soc Am Bull 400–418

Walker J, Gower S,, McCutcheon SR (1993) Geology of the Nigadoo Lake area (NTS 21P/12e), Gloucester and Restigouche counties. New Brunswick Department of Natural Resources and Energy, Mineral Resources Division

Wang G, Zhang S, Yan C, et al (2011) Mineral potential targeting and resource assessment based on 3D geological modeling in Luanchuan region, China. Comput Geosci 37.

Wang J, Zuo R, Xiong Y (2020) Mapping mineral prospectivity via semi-supervised random forest. Natural Resources Research 29, pp.189-202.

Watters S (1993) Structure and alteration related to Hercynian gold deposition, Cape Spencer, New Brunswick, Canada.

White NC, Hedenquist JW (1995a) Epithermal gold deposits: styles, characteristics and exploration. SEG newsletter. (23), pp.1-13.

White NC, Hedenquist JW (1995b) Epithermal Gold Deposits: STYLES, CHARACTERISTICS AND EXPLORATION. SEG Discovery 1–13.

Wilson RA (2017) The Middle Paleozoic Rocks of Northern and Western New Brunswick, Canada.

Wilson RA, Kamo SL (2012a) The Salinic Orogeny in northern New Brunswick: geochronological constraints and implications for Silurian stratigraphic nomenclature. Can J Earth Sci 49:222–238

Wilson RA, Kamo SL (2012b) The Salinic Orogeny in northern New Brunswick: Geochronological constraints and implications for Silurian stratigraphic nomenclature. Can J Earth Sci 49:222–238.

Wilson RA, van Staal CR, Kamo SL (2017) Rapid transition from the salinic to Acadian orogenic cycles in the northern Appalachian Orogen: Evidence from northern New Brunswick, Canada. Am J Sci 317:449–482.

Wyborn LAI, Heinrich CA, Jaques AL (1994) Australian Proterozoic Mineral Systems: Essential Ingredients and Mappable Criteria. Australian Institute od Mining and Metallurgy Annual Conference

Yin J, Li N (2022) Ensemble learning models with a Bayesian optimization algorithm for mineral prospectivity mapping. Ore Geol Rev 145, 104916.

Yousefi F, White T, Lentz DR, et al (2023) Middle Devonian Evandale porphyry Cu-Mo (Au) deposit, southwestern New Brunswick, Canada: Analysis of petrogenesis to potential as a source for distal intrusion-related epithermal gold mineralization. Ore Geol Rev 162:105716.

Yousefi M, Carranza E J M (2015) Prediction–area (P–A) plot and C–A fractal analysis to classify and evaluate evidential maps for mineral prospectivity modeling. Comput Geosci 79, pp.69-81.

Yousefi M, Carranza EJM (2015a) Fuzzification of continuous-value spatial evidence for mineral prospectivity mapping. Comput Geosci 97-109.

Yousefi M, Carranza EJM (2016) Data-Driven Index Overlay and Boolean Logic Mineral Prospectivity Modeling in Greenfields Exploration. Natural Resources Research 25:. https://doi.org/10.1007/s11053-014-9261−9

Yousefi M, Carranza EJM (2015b) Geometric average of spatial evidence data layers: A GIS-based multi-criteria decision-making approach to mineral prospectivity mapping. Computers & Geosciences 83:72–79.

Yousefi M, Kamkar-Rouhani A, Carranza EJM (2012) Geochemical mineralization probability index (GMPI): A new approach to generate enhanced stream sediment geochemical evidential map for increasing probability of success in mineral potential mapping. J Geochem Explor 115:24–35.

Yousefi M, Lindsay M, Kreuzer O (2024) Mitigating uncertainties in mineral exploration targeting: Majority voting and confidence index approaches in the context of an exploration information system (EIS). Ore Geol Rev 165, 105930.

Yousefi M, Nykänen V (2016) Data-driven logistic-based weighting of geochemical and geological evidence layers in mineral prospectivity mapping. J Geochem Explor 164:94–106.

Yu Z, Li B, Wang X (2024) Mineral prospectivity mapping susceptibility evaluation based on interpretable ensemble learning. Ore Geol Rev 106248:

Zadeh LA (1965) Fuzzy sets. Information and Control 8:338–353.

Zhang N, Zhou K, Du X (2017) Application of fuzzy logic and fuzzy AHP to mineral prospectivity mapping of porphyry and hydrothermal vein copper deposits in the Dananhu-Tousuquan island arc, Xinjiang, NW China. Journal of African Earth Sciences 128, pp.84−96.

Zhang Q, Chen J, Xu H, et al (2022) Three-dimensional mineral prospectivity mapping by XGBoost modeling: A case study of the Lannigou gold deposit, China. Natural Resources Research 31(3), pp.1135-1156.

Zhao J, Chen S, Zuo R, Carranza EJM (2011) Mapping complexity of spatial distribution of faults using fractal and multifractal models: Vectoring towards exploration targets. Comput Geosci 37.

Zhao J, Sui Y, Zhang Z, Zhou M (2023) Application of Logistic Regression and Weights of Evidence Methods for Mapping Volcanic-Type Uranium Prospectivity. Minerals 13:608.

Zheng C, Yuan F, Luo X, et al (2023) Mineral prospectivity mapping based on Support vector machine and Random Forest algorithm–A case study from Ashele copper–zinc deposit, Xinjiang, NW China. Ore Geol Rev 159, 105567.

Zuo R (2020) Geodata Science-Based Mineral Prospectivity Mapping: A Review. Natural Resources Research 29:3415–3424

Zuo R, Carranza EJM (2011) Support vector machine: A tool for mapping mineral prospectivity. Comput Geosci 1967−1975.

(2008) New Brunswick Department of Natural Resources (NBDNR) (2008). Bedrock Geology of New Brunswick. Minerals. Policy and Planning Division. Map NR-1 (2008 Edition). Scale 1:500000 (Revised 2008).

(2014) New Brunswick Department of Natural Resources (NBDNR) (2014). Till geochemistry data of New Brunswick.

Geological Survey of Canada (GSC) (1976). Airborne radiometric data 1000m national-scale maps. Retrieved from https://geophysical-data.canada.ca/Portal/Results?minLong=-69.19&maxLong=63.42&minLat=44.19&maxLat=49.59.

4. Machine Learning-Based Mineral Prospectivity Mapping of Epithermal Gold Mineralization in Northern New Brunswick: A Comparative Study of Random Forest, Support Vector Machine, and XGboost Classifiers

Farzaneh Mami khalifani[1*], David R Lentz [1], James A Walker[2]

[1]Department of Earth Science, University of New Brunswick, Fredericton, New Brunswick, E3B 5A3, Canada, School of Mining.

[2]New Brunswick Department of Natural Resources and Energy Development, South Tetagouche, New Brunswick, Canada[3]

***Corresponding Author:**

Farzaneh Mami khalifani

Email: farzaneh.mamikhalifani@unb.ca

Abstract

The Tobique-Chaleur Zone (TCZ), located in northern New Brunswick and the neighboring Gaspé Peninsula, hosts a number of gold occurrences. Gold mineralization in TCZ is spatially associated with large-scale crustal structures or their subsidiary splays (e.g., the Rocky Brook-Millstream Fault system). The gold occurrences in the Chaleur Bay Synclinorium, are hosted primarily underlain by Upper Silurian to Early Devonian strata, with some lower Silurian strata also present. This study applies three supervised machine learning algorithms—Random Forest (RF), Support Vector Machine (SVM), and Extreme Gradient Boosting (XGBoost) to generate mineral prospectivity mapping (MPM) for epithermal gold mineralization in the Tobique–Chaleur Zone of northern New Brunswick. A total of 24 evidence layers, derived from geological, geochemical, and geophysical

datasets, were selected based on a mineral systems framework to represent key ore-forming processes including source, pathway, and trap components. Model performance was evaluated using Receiver Operating Characteristic (ROC) curves, with RF achieving the highest AUC (0.93), followed by SVM (0.92) and XGBoost (0.91). Additionally, prediction–area (P–A) plot analysis revealed that XGBoost was the most efficient model in terms of spatial targeting. A majority voting ensemble and confidence index map were employed to enhance robustness and quantify model uncertainty. The spatial correlation of high-prospectivity zones with known gold occurrences and key geological features validates the applied approach. These results demonstrate the effectiveness of integrated machine learning and mineral systems modeling in generating reliable and interpretable prospectivity maps for mineral exploration.

Keywords: Random Forest, Support Vector Machine, XGboost, Epithermal gold mineralization, northern New Brunswick, Prediction-Area, Majority voting, Confidence index.

4.1. Introduction

Mineral resources are essential for the sustaining advancement of society. The outcomes of mineral prospecting are inherently uncertain due to the diversity of deposit types, complex ore formation processes, ambiguous ore-controlling factors, and varying interpretations of geoscience datasets. Consequently, improving the objectivity, quantification, and refinement of the mineral prospecting process remains a leading subject in the field of metallogenic prediction science (Josso et al. 2023; Mami Khalifani et al. 2025a). Mineral prospectivity mapping (MPM) helps geologists focus on areas that are

considered promising for specific types of mineral deposits (Carranza et al. 2008; Ghezelbash et al. 2025a). The concept of MPM was first introduced in the late 1980s by geoscientists as a statistical approach to integrate and analyze spatial patterns in geoscience data (Bonham-Carter et al. 1990). The objective is to determine connections among multiple geoscience datasets, such as geology, geophysics, remote sensing, and geochemistry, to identify promising areas for mineralization. Mineral prospectivity mapping can be categorized into two primary methodologies: knowledge-based modeling and data-based modeling. Knowledge-based methods rely on expert judgment to assign weights to evidence layers using techniques such as index overlay, fuzzy logic, and geometric averaging. Conversely, data-driven methods like weights-of-evidence and logistic regression employ statistical techniques to evaluate the spatial associations between various geological features and known mineral occurrences, thereby assigning weights to individual layers (Zheng et al. 2023).

The emergence of machine learning has significantly enhanced the application of classification methods in data-driven mineral prospectivity mapping (Liu et al., 2018; Lou and Liu, 2023; Lauzon and Gloaguen, 2024). Liu et al. (2018) demonstrated the effectiveness of the Maximum Entropy (MaxEnt) model in mineral prospectivity mapping, highlighting its ability to handle presence-only data and limited training samples. Lou and Liu (2023) conducted a comparative study of multiple machine learning algorithms including logistic regression, suport vector machine, random forest, convolutional neural networks, and Light Gradient Boosting Machine (LGBM) for tungsten polymetallic prospectivity mapping in the Gannan region, China, highlighting the advantages of deep learning and ensemble methods in improving prediction accuracy and spatial efficiency.

This is primarily due to its ability to uncover complex and nonlinear spatial relationships between known mineral deposits and their associated geospatial features, thereby increasing the effectiveness of MPM. By utilizing these advanced methodologies, researchers are better equipped to analyze vast datasets, thereby facilitating more informed decision-making processes and improving predictive accuracy in resource evaluation and exploration strategies (Yu et al. 2024). This approach classifies geographic areas as prospective or non-prospective and presents results in binary maps or confidence-based prospectivity maps. Classification techniques are broadly categorized into unsupervised and supervised methods. Unsupervised methods identify patterns by clustering data based on intrinsic similarities within the spatial dataset, offering insights into mineral prospectivity without prior labels (Esmaeiloghli et al. 2021; Cheng et al. 2023; Ghezelbash et al. 2025b). In contrast, supervised methods rely on labeled training samples to guide the learning process and improve predictive accuracy. It should be recognized that most advanced methodologies for MPM are primarily distinguished by the implementation of supervised machine learning techniques and deep learning algorithms within a data-driven framework. These approaches leverage substantial datasets to enhance predictive accuracy and model complex geological relationships, thereby facilitating more effective mineral exploration strategies (Zuo 2020; Yu et al. 2024). Supervised machine learning methods utilize labeled datasets comprising known mineralized (positive) and non-mineralized (negative) locations to train predictive models. These methods, when properly trained, can more accurately delineate prospective zones by capturing the relationships between exploration variables and deposit presence, often surpassing manual data-driven approaches (Liu et al., 2018; Silva dos Santos et al. 2022; Lou and Liu, 2023; Lauzon and

Gloaguen 2024). It is essential to recognize that, despite the emergence of diverse and robust techniques for MPM, no single model consistently performs best across all geological settings or exploration scenarios. As a result, combining multiple data-driven methods can provide a more comprehensive and reliable framework for generating MPM, as it allows for the integration of different analytical strengths and better accommodates the complexity of mineralization processes (Porwal and Carranza 2015; Yu et al. 2024). For example, Zheng et al. (2023) integrated SVM and RF algorithms to generate mineral prospectivity maps for copper-zinc deposits. Similarly, Wang et al. (2020) combined RF, SVM, and MaxEnt models to evaluate the potential of stacked ensemble learning techniques in MPM (Liu et al., 2018; Wang et al. 2020; Lou and Liu, 2023). Lauzon and Gloaguen (2024) applied transfer learning in conjunction with the RF algorithm to quantify uncertainty and enhance the accuracy of prospectivity mapping within mineral belts. Furthermore, Yin and Li (2022) established an ensemble learning framework for mineral exploration by integrating XGBoost and RF models, with hyperparameter optimization conducted through the Bayesian Optimization Algorithm (BOA) to improve predictive performance (Yin and Li 2022).

In light of these challenges, this study develops an integrated MPM framework for epithermal gold mineralization in northern New Brunswick by combining multi-source geoscience datasets within a mineral systems and machine learning approach. The research addresses the difficulty of accurately predecting potential mineralization in structurally complex and geologically heterogeneous terrains, where conventional exploration techniques often fail to capture the nonlinear relationships among geological, geochemical, geophysical, and remote sensing variables. The novelty of this work lies in the comparative

application of three advanced algorithms (RF, SVM, and XGBoost) coupled with mineral systems–based predictor selection, geochemical analysis, and detailed structural interpretation. Furthermore, an ensemble and confidence-based integration of the models is employed to enhance targeting reliability, reduce uncertainty, and provide geologically plausible exploration targets that can guide efficient field validation.

Expanding upon previous research in which Mami Khalifani et al. (2025a, b) applied mineral system criteria to construct a predictive model using both knowledge- and data-driven approaches for epithermal gold mineralization in northern New Brunswick, the present study advances mineral prospectivity mapping by integrating supervised machine learning techniques within a data-driven framework (Mami Khalifani et al. 2025a, b). While knowledge-driven approaches are valuable in early-stage greenfield exploration due to their reliance on expert interpretation and conceptual models, they are inherently subjective and may not fully capture complex, nonlinear relationships among geological features. With the availability of refined exploration datasets and a growing number of documented mineral occurrences in the area, the application of machine learning algorithms such as RF, SVM, and XGBoost, offers an opportunity to enhance prediction accuracy and reduce bias by utilizing objectively learning patterns from the data. This transition aims to build a more robust and reproducible prospectivity model, leveraging the strengths of both prior knowledge and advanced data analytics. The predictive model exhibits strong generalization and robustness in handling complex, high-dimensional datasets with correlated features (Zheng et al. 2023). SVM models are widely recognized for their high predictive accuracy and strong classification capabilities (Zheng et al. 2023). Moreover, the RF model, an ensemble learning algorithm, demonstrates fast training

efficiency, strong resilience to noise, and superior generalization performance relative to many other machine learning techniques. The XGBoost algorithm, an enhanced version of the Gradient Boosting Decision Tree model, has been extensively applied across various disciplines owing to its high computational efficiency and its effectiveness in mitigating overfitting (Zheng et al. 2023). A majority voting ensemble was used to combine predictions from multiple prospectivity models, and a confidence index was introduced to address uncertainty by measuring the variation in predictions for each cell. Together, these methods enable consistent and reliable identification of exploration targets using an integrated model ensemble. Finally, the performance of the prospectivity models generated using RF, SVM, and XGBoost was assessed using a Receiver Operating Characteristic (ROC) curve and Prediction-Area (P-A).

4.2. Geology of the study area

4.2.1. Regional geology

The Post-Taconic, Middle Paleozoic Matapédia Cover Sequence (MCS) in northern and western New Brunswick unconformably overlies deformed Early Paleozoic inliers located to the northwest (Popelogan) and southeast (Miramichi and Elmtree) (Fig. 4-1). The Acadian deformation of the Matapédia Cover Sequence (MCS) in northern New Brunswick occurred during the Early Devonian, between approximately 415 and 395 Ma, and was accompanied by dextral strike-slip faulting along major (regional) structures such as the Rocky Brook–Millstream, Restigouche–Grand Pabos, and Catamaran Brook faults, as well as numerous associated subsidiary faults (local) (van Staal et al. 2009; Wilson 2017; Mami Khalifani et al. 2023b). Gold mineralization in the study area occurs predominantly as

epithermal breccia and veins enriched in base metals ± Au and Ag, particularly in the northeastern Chaleur Bay Synclinorium. These occurrences are commonly associated with felsic intrusions and spatially correlated with major splays of the Rocky Brook–Millstream Fault system, including the McCormack Brook and Ramsay Brook faults, as well as mafic intrusions (van Staal et al. 2009; Wilson 2017; Mami Khalifani et al. 2023b).

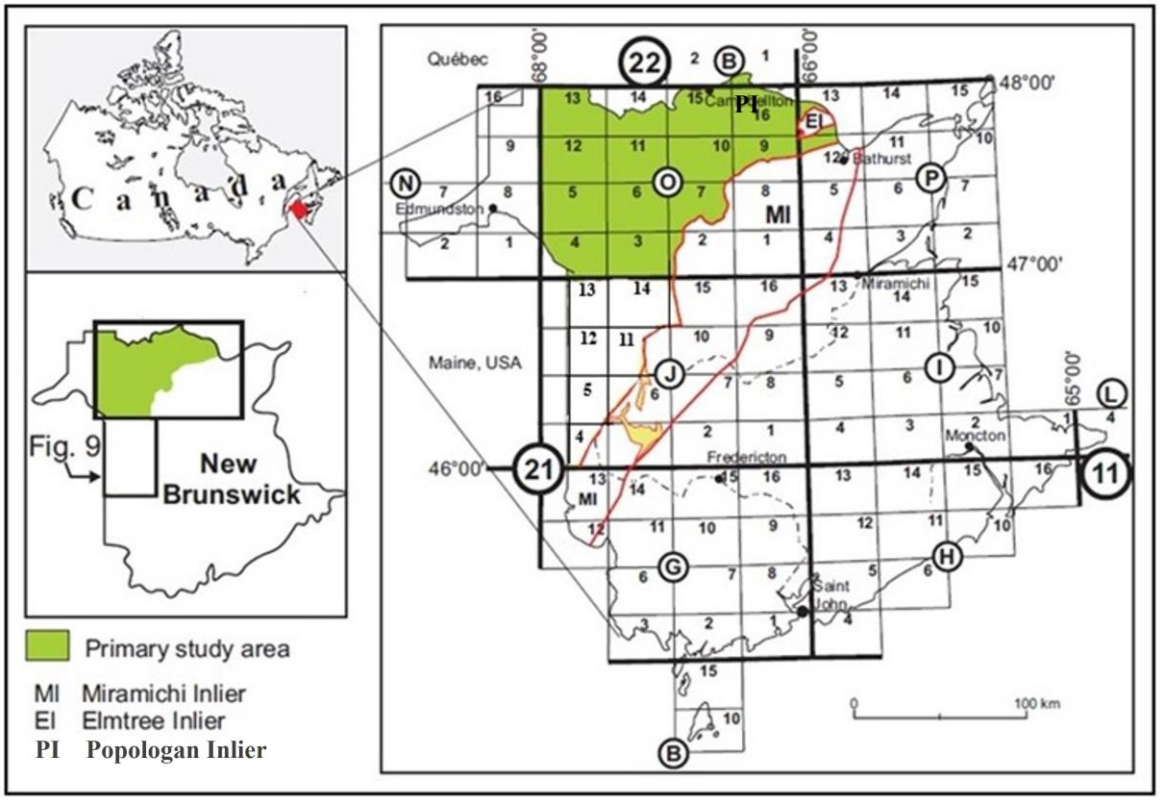

Figure 4-1 Location of study area and National Topographic System (NTS) grid for New Brunswick (Wilson 2017).

4.2.2. Tectonic Setting

The Middle Paleozoic succession of northern and western New Brunswick, referred to as the Matapédia Cover Sequence (MCS) by Fyffe and Fricker (1987), represents a post-Taconic to broadly syn-Acadian stratigraphic package spanning the Late Ordovician to

Middle Devonian (Fyffe and Fricker 1987). This cover sequence unconformably overlies deformed Cambrian to Middle Ordovician rocks of the Humber and Notre Dame zones to the west and the Ganderian terrane to the east (van Staal et al. 1995). The MCS extends from the eastern Gaspé Peninsula, southwest through northern New Brunswick and into northern and central Maine (Fig. 4-2). The Matapédia Cover Sequence (MCS) comprises three main structural divisions that, from northwest to southeast are: the Connecticut Valley–Gaspé Synclinorium, the Aroostook–Percé Anticlinorium, and the Chaleur Bay Synclinorium (Fig. 4-2). The Aroostook–Percé-Anticlinorium is underlain by a range of sedimentary rocks, including Devonian strata of the Fortin Group in New Brunswick and equivalent formations indeeper waterwell as well as deeper-water turbidites and fine-grained siliciclastic rocks of Ordovician to Silurian age (Wilson 2017). The older strata of the MCS include Upper Ordovician to Lower Silurian deep-water sedimentary rocks of the Grog Brook and Matapédia groups, which dominantly occur in the Aroostook – Percé Anticlinorium. The Chaleur Bay Synclinorium is mainly underlain by Upper Silurian to Lower Devonian volcanic and sedimentary strata, along with subordinate Lower Silurian strata. The geological complexity of the region reflects the interplay of multiple transgressive-regressive cycles in the Aroostook-percé Anticlinorium, which is expressed through unconformities, disconformities, widespread magmatic activity. These features are associated with tectonic events linked to the Silurian Salinic and Devonian Acadian orogenies, corresponding to the accretion of the trailing edge of Ganderia and Avalonia, respectively, onto composite Laurentia (Wilson and Kamo 2012a) as shown in Fig. 4-2.

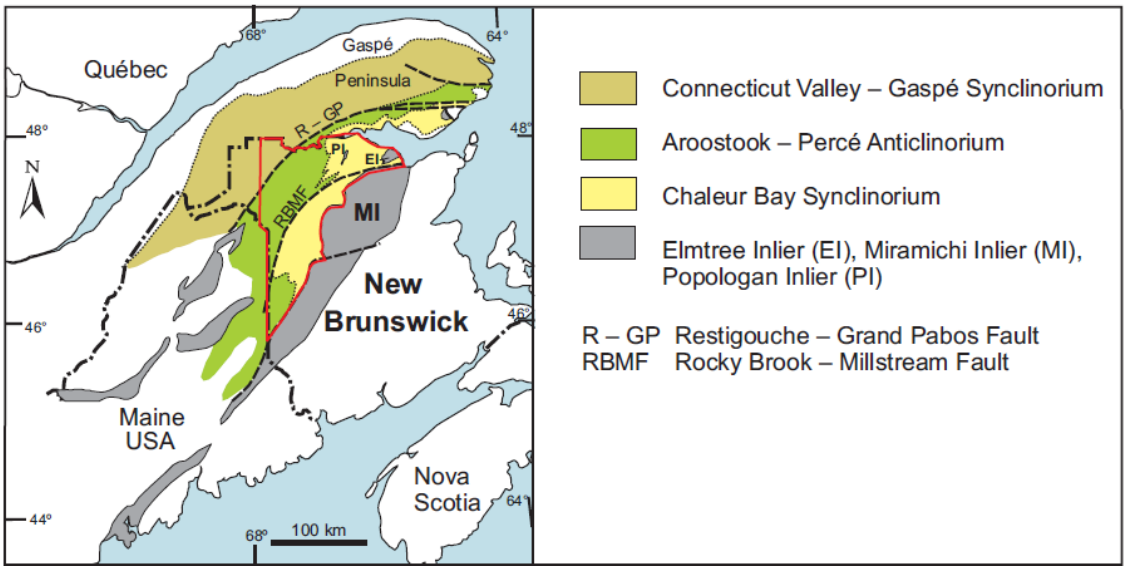

Figure 4-2. Subdivisions of the Matapédia Cover Sequenc (modified from Wilson (2017). Study area outlined in red (Wilson 2017).

Early Paleozoic inliers consist of sedimentary and volcanic rocks of the Popelogan Arc and Tetagouche Backarc Basin (Fig 4-2). The descriptions of Middle Paleozoic stratigraphy and constituent lithostratigraphic units in northern and western New Brunswick are arranged according to group and formation, generally from oldest to youngest.

4.3. Epithermal Gold in Northern New Brunswick

Gold occurrences within and adjacent the Tobique-Chaleur Zone (Fig. 4-3) are characterized as epithermal gold mineralization types, many of which occur in close spatial association with the Rocky Brook-Millstream and Restigouche-Grand Pabos fault systems (Mami Khalifani et al. 2025a). Epithermal deposits, as described by Lindgren (1933), form at shallow crustal levels. Epithermal systems typically consist of veins and disseminated mineralization formed at shallow depths, generally around 1.5 km below the surface. They

are primarily hosted in volcanic and sedimentary rocks, as well as unconsolidated sediments, with less common occurrences in metamorphic rocks (Taylor 2007). These deposits are commonly linked to hot spring activity and regions of recent volcanism (typically Tertiary to Quaternary in age), with ore compositions primarily consisting of precious metals (gold and silver) with containing some base metals i.e. copper, lead, and zinc (Taylor 2007). Epithermal deposits generally form at temperatures ranging from 160° to 270°C (White and Hedenquist 1995a) although a broader upper limit of 300°C is also widely accepted (Bodnar et al., 2014). Epithermal gold deposits are classified on the basis of sulfide mineral content into three main subtypes: high-sulfidation, intermediate-sulfidation, and low-sulfidation (Einaudi et al. 2003; Sillitoe and Hedenquist 2005).

Although epithermal gold deposits are relatively uncommon in New Brunswick, they are of considerable geological significance (Wilson 2017; Mami Khalifani et al. 2023b). In northern New Brunswick, Sanchez Mora (2014) and Sanchez Mora et al. (2021) studied the Williams Brook area, where low-sulfidation epithermal gold mineralization is hosted in Siluro-Devonian volcanic and sedimentary rocks formed during Gondwana-Laurentia collision. Here the earliest, gold appears in muscovite/illite veinlets with galena, and later quartz veins containing native gold, sulfides, and oxyhydroxides (Sánchez-Mora 2014; Sánchez-Mora et al. 2021). The bulk of the quartz vein associated gold mineralization at Williams Brook is hosted within rhyolite (Mami Khalifani et al. 2025a, b). Mami Khalifani et al. (2022, 2023a, b) conducted pXRF and micro-XRF analyses on drill core from the Williams Brook, McIntyre Brook, Mulligan Gulch, and Simpson Field occurrences in northern New Brunswick to aid in mineral prospectivity mapping for epithermal gold mineralization (Mami Khalifani et al. 2022; 2023a). The 20 gold occurrences examined in

this study are predominantly hosted by Upper Silurian to Early Devonian rocks, with subordinate Lower Silurian hosted occurrences. The investigated area covers two 1:50,000 map sheets (~1560 km²) (see Fig. 4-3).

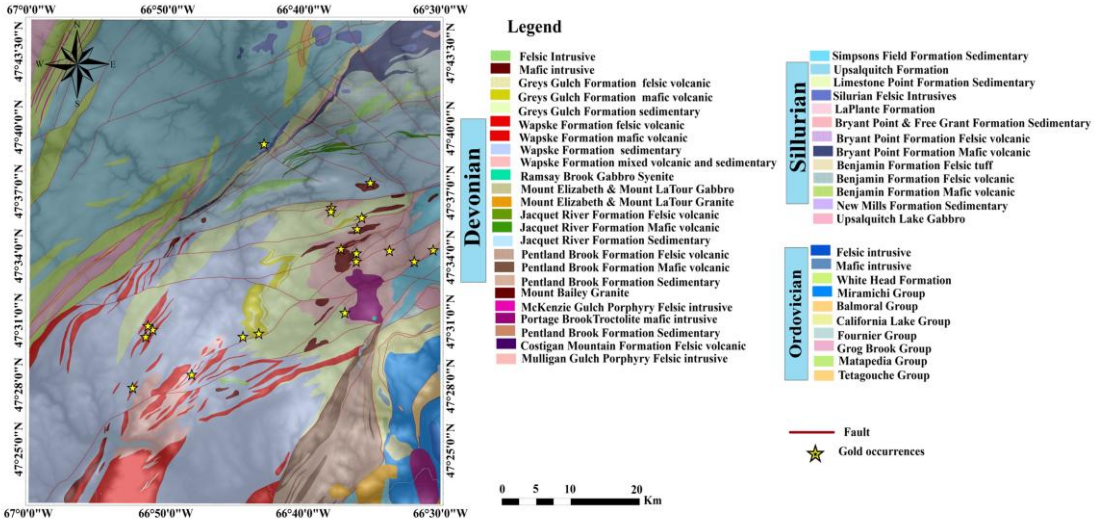

Figure 4-3. Regional-scale geological map of the investigated area illustrating the locations of gold mineralization (modified from Wilson 2017; Mami Khalifani et al. 2025a, b).

Rock and drill core samples from Williams Brook, McIntyre Brook, Mulligan Gulch, and Simpson Field occurrences in northern New Brunswick are presented in Figures 4-4 and 4-5 and highlight the style of gold mineralization within quartz veins, as well as in felsic porphyritic and mafic intrusive host rocks containing sulfide mineralization and associated alteration.

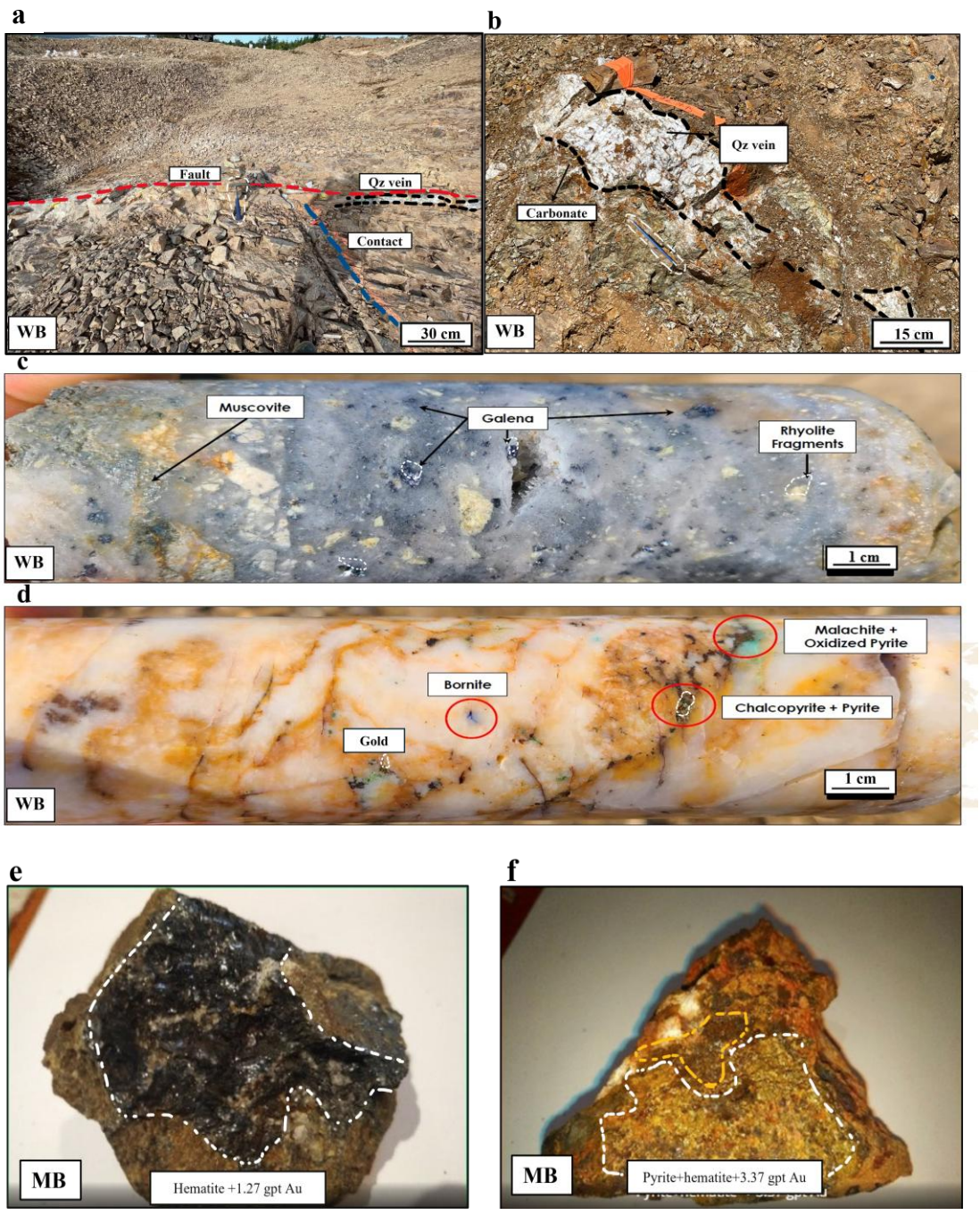

Figure 4-2. Photographs of selected rock and drill core samples from epithermal gold occurrences in the study a) Photograph depicting the Williams Brook highlighting a quartz vein, the contact between rhyolite and sedimentary rocks, and a fault. b) outcrop from the Williams Brook, displaying a quartz-carbonate (Qz-carbonate) vein hosted within altered

volcanic rocks. The vein is highlighted by dashed lines and shows a clear textural contrast with the surrounding host rock in c) Drill core sample from the Williams Brook area, showing mineralized zones with visible muscovite, galena, and rhyolite fragments. The texture and mineral assemblage are characteristic of low-sulfidation epithermal gold systems. Scale bar = 1 cm. d) Drill core sample from the Williams Brook area displaying epithermal-style mineralization including native gold, bornite, chalcopyrite, pyrite, malachite, and oxidized pyrite hosted within a quartz vein. The presence of copper-bearing minerals and oxidized textures suggests late-stage hydrothermal alteration. Scale bar = 1 cm. e) Sample from the McIntyre Brook area showing hematite-rich mineralization with associated gold. The outlined area represents hematite, which is commonly linked to epithermal alteration and gold mineralization. f) Sample from McIntyre Brook showing pyrite and hematite mineralization associated with gold mineralization. The outlined zones highlight areas enriched in iron oxide and sulfide minerals, typical of epithermal mineralization.

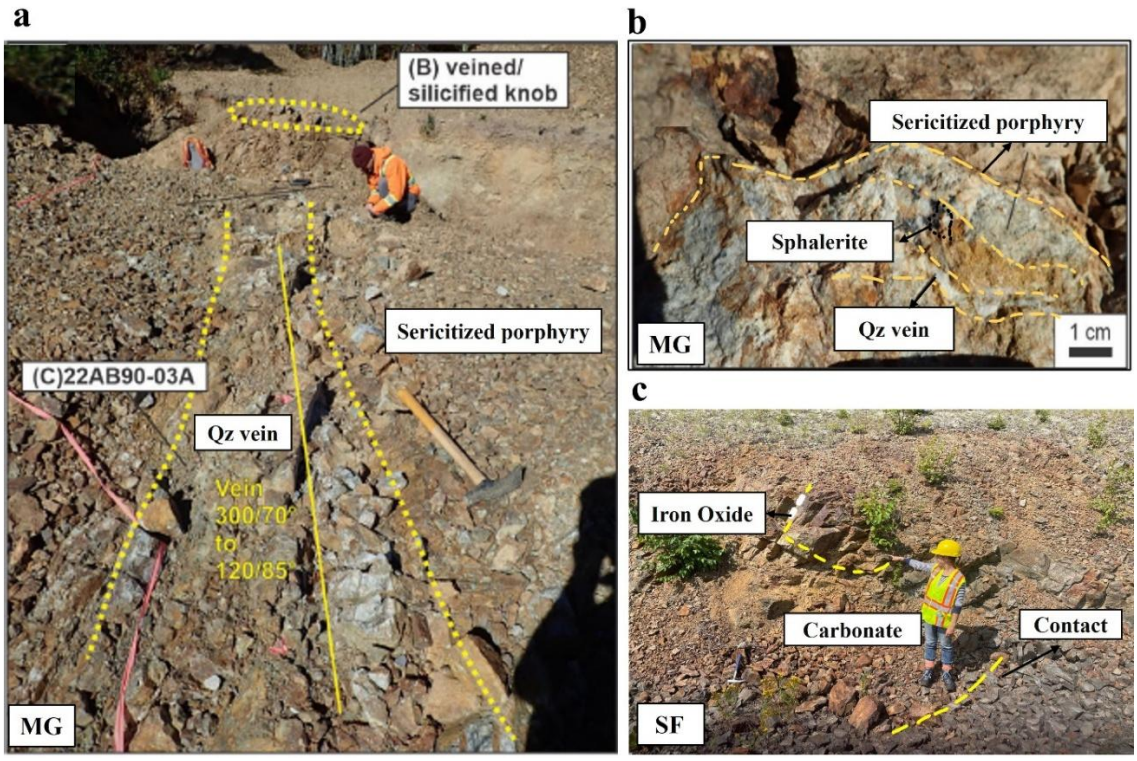

Figure 4-3. Rock and drill core samples from epithermal gold occurrences in the study area g) An outcrop photograph from the Mulligan Gulch (MG) occurrence showing a prominent quartz (Qz) vein hosted within sericitized porphyry. The vein trends from 300°/70° to 120°/85°. Field mapping and structural orientation highlight features typical of low-sulfidation epithermal gold systems. h) sample from the Mulligan Gulch (MG) occurrence showing a quartz (Qz) vein hosted by sericitized porphyry with sphalerite mineralization. The assemblage is characteristic of low-sulfidation epithermal systems. Scale bar = 1 cm. i) Outcrop at the Simpson Field (SF) occurrence showing iron oxide and carbonate alteration at lithological contact. The contact zone, highlighted by dashed lines, marks a transition between distinct rock units, with iron oxide staining indicative of hydrothermal alteration related to epithermal gold mineralization.

4.4. Methodologies

4.4.1. Modelling workflow

To effectively model epithermal gold mineralization, it is essential to first establish theoretical criteria that reflect the fundamental geological processes and conditions responsible for the formation of this type of mineralization. This involves understanding the structural, lithological, geochemical, and hydrothermal control on the deposition of gold in epithermal systems. Once defined, a comprehensive and structured database must be developed to capture the key parameters of the mineral system. This database typically includes several spatial controlled datasets such as lithology, hydrothermal alteration zones, structural features, geochemical anomalies, and geophysical signatures, all of which are critical for accurately characterizing the mineralized zone and supporting predictive modeling (Mami Khalifani et al. 2025a). Figure 4-6 illustrates the methodological workflow used in this study to process geospatial data and construct a mineral prospectivity map for epithermal gold mineralization in Northern New Brunswick. Initially, geological, geochemical, and geophysical layers were produced using appropriate analytical techniques. Structural and geological features were derived from geological and geophysical data, whereas gold anomalies and associated pathfinder elements were identified through geochemical analysis. As outlined by (Mami Khalifani et al. 2025a), logistic transformation functions were then applied to normalize and assign continuous weights to the spatial evidence layers. Finally, supervised machine learning techniques specifically Random Forest, Support Vector Machine, and XGBoost were utilized for MPM.

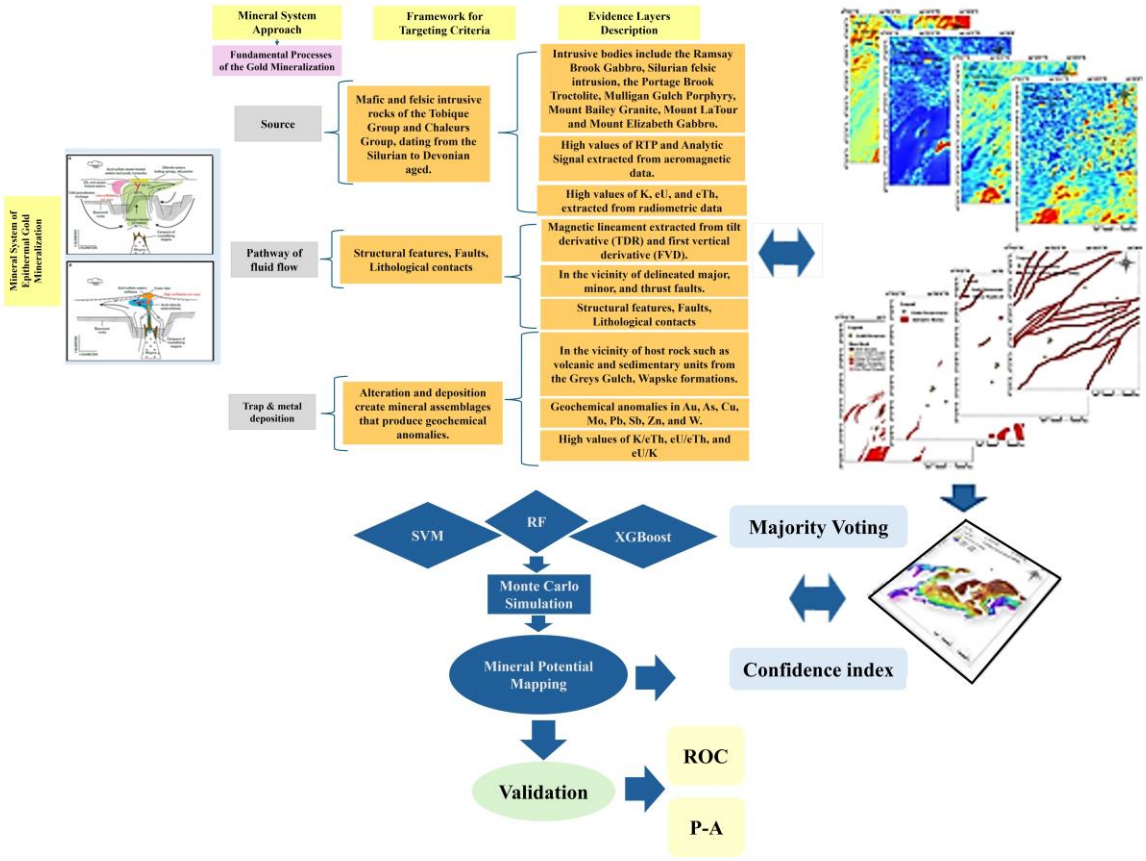

Figure 4-4. The workflow used in this study outlines the process for generating mineral prospectivity maps (MPM) for epithermal gold mineralization. On the left, the mineral system approach and targeting criteria framework are illustrated in gray and light orange, respectively. On the right, all evidence layers are integrated to develop the MPM using data-driven methods, including Random Forest (RF), Support Vector Machine (SVM), and XGBoost, which are represented in gray and blue tones. The majority voting and Confidence Index methods are highlighted in light blue, while the validation process is shown in light yellow.

To enhance the reliability of the mineral prospectivity results, a majority vote model was generated by integrating the outputs of individual prospectivity models. To produce an integrated map, this ensemble approach combines predictions from multiple data-driven methods, such as Random Forest, Support Vector Machine, and XGBoost. By considering areas consistently identified as prospective across models, the majority vote model reduces individual model bias and improves overall prediction robustness (Khammar et al. 2024; Yousefi et al. 2024). Additionally, a Confidence Index was employed to quantify model uncertainty by assessing the consistency of predictions across the applied algorithms, thereby enhancing the reliability and interpretability of the prospectivity maps. Finally, the effectiveness of the prospectivity models developed using Random Forest (RF), Support Vector Machine (SVM), and XGBoost were assessed through Receiver Operating Characteristic (ROC) curve analysis. This statistical tool provides a quantitative measure of model performance by evaluating the true positive rate against the false positive rate. A Prediction–Area (P–A) analysis was performed to evaluate the spatial efficiency of the predictive models, allowing comparison of how effectively each algorithm captures known mineral occurrences within the smallest possible favorable area an essential criterion for cost-effective exploration targeting.

4.4.2. Methods

4.4.2.1. Random Forest

Random Forest (RF; Breiman, 2001) is an ensemble of decision trees built on bootstrap replicates of the training data (bagging) with random subsets of features considered at each

split (random subspace). Roughly one-third of samples in each replicate are “out-of-bag” and provide an internal estimate of generalization error. Splits are chosen to minimize node impurity measured by the Gini index:

$$G = 1 - \sum_{j=1}^{m} p_j^2 \quad (1)$$

where p_j is the proportion of class j in the node and m is the number of classes. Final labels are obtained by majority voting across trees. For mineral prospectivity mapping, this scheme handles high-dimensional, nonlinear predictors while reducing variance and overfitting. Figure 4-7 illustrates the workflow: the training set is resampled into k bootstrap subsets, a tree is grown on each subset with random feature tests, and the k outputs are aggregated by majority vote to yield the final classification.

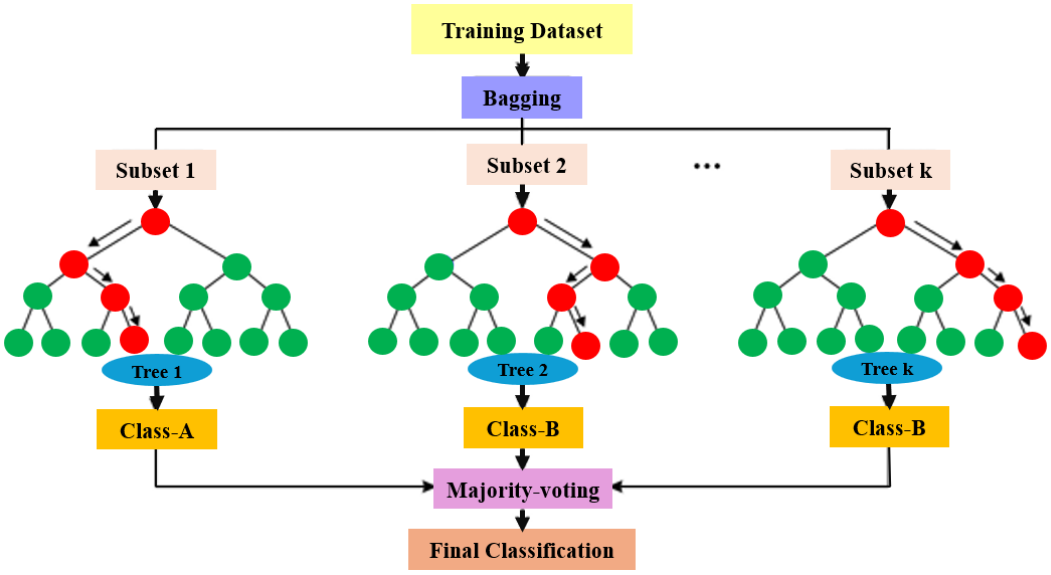

Figure 4-5. Flowchart of classification using RF algorithm.

4.4.2.2. Support Vector Machine

SVM is a supervised method for classification (and nonlinear regression) that maps data into a higher-dimensional space so a simple linear boundary can separate the data (Zuo and Carranza 2011). SVM estimates a separating hyperplane that maximizes the interclass margin, with the decision function determined solely by the support vectors that lie on the margins. Owing to this sparse representation, SVMs are relatively robust to noise and perform effectively in high-dimensional feature spaces (Suthaharan 2016).

As shown in Figure 4-8, many separating hyperplanes (e.g., $\mathbf{H_0}$, $\mathbf{H_1}$, and $\mathbf{H_2}$,) are possible, but the optimal one is the maximum-margin hyperplane. In R^d, a hyperplane is written (Wang et al. 2020; Zheng et al. 2023):

$$w^T x + b = 0 \tag{2}$$

$$r = \frac{|w^T + b|}{||w||} \tag{3}$$

Where, wis the hyperplane's normal vector, b its offset, and the (signed) margin for sample $\boldsymbol{x_i}$ is $\boldsymbol{y_i}\,(\boldsymbol{w^T x_i} + \boldsymbol{b})/\big|\big|\boldsymbol{w}\big|\big|$. Under perfect separation, each training point satisfies Equation (4).

$$\begin{cases} \boldsymbol{w^T x_i} + \boldsymbol{b} \geq +\mathbf{1}, \boldsymbol{y_i} = +\mathbf{1} \\ \boldsymbol{w^T x_i} + \boldsymbol{b} \leq -\mathbf{1}, \boldsymbol{y_i} = +\mathbf{1} \end{cases} \tag{4}$$

In this method, kernel functions are used to map low-dimensional data into higher-dimensional space for linear separation. This study employed four kernels: linear, polynomial, radial basis, and sigmoid (Zhang et al. 2017; Zheng et al. 2023). Additional explanations of the mathematical foundations of SVM algorithms have been discussed in prior studies (Zuo and Carranza 2011; Wang et al. 2020).

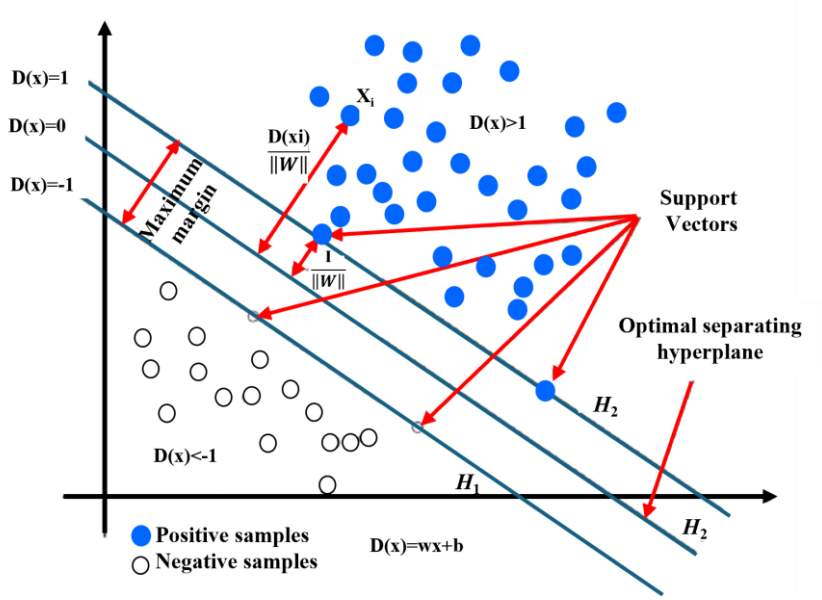

Figure 4-6. Schematic diagram of the SVM model.

4.4.2.3. Extreme Gradient Boosting XGBoost

XGBoost is a gradient-boosted decision-tree method that optimizes an objective combining data-fit and model complexity (Chen and Guestrin 2016):

$$\text{Obj}=\sum_{i=1}^{n} l(y_i, \hat{y}_i)+\sum_{k=1}^{k} \Omega(f_k) \quad (6)$$

$$\Omega(f_k)=\gamma T+\frac{1}{2}\lambda\sum_{j=1}^{T} \omega_i^2 \quad (7)$$

In the equation, Obj represents the objective function, where yi and ŷi are the true and predicted values for the i-th sample, and l denotes the loss function. fk refers to the weak classifier, ωj is the weight of leaf node j, and T is the total number of leaf nodes. The regularization term Ω includes γ and λ, which control the model. We used XGBoost with the gbtree base learner: 300 boosting trees, learning rate = 0.1, subsample = 0.70 (each tree

fits on 70% of samples), max_depth = 7, and the minimum required sum of sample weights in each leaf node is 3.

4.4.2.4. Majority voting

In mineral prospectivity mapping, majority voting is used as an ensemble technique to enhance the consistency and reliability of targeting exploration by integrating multiple prospectivity models. Each model may utilize different techniques, which can result in variations in the predicted favorable zones (Khammar et al. 2024; Yousefi et al. 2024). The majority voting approach consolidates these outputs by assigning a final prospectivity class to each spatial unit based on the most frequently occurring class across all input models. This method reduces individual model bias, smooths prediction variability, and strengthens spatial agreement between methods. As implemented by Khammar et al. (2024) and described by Yousefi et al. (2024), this approach provides a more stable and interpretable map, particularly when followed by additional uncertainty quantification techniques such as the Confidence Index (Khammar et al. 2024; Yousefi et al. 2024). An ensemble approach was applied by combining the prospectivity maps generated from Random Forest, Support Vector Machine, and XGBoost models.

4.4.2.5. Confidence index (CI) to measure uncertainty

The Confidence Index (CI) is a quantitative metric introduced to address uncertainties that arise from combining multiple mineral prospectivity models. This index measures the consistency of prospectivity predictions across different models by computing the ratio of the mean to the standard deviation of prospectivity values for each cell in the study area. A higher CI value indicates higher agreement among the models and greater confidence in

the prediction, whereas lower values suggest variability and uncertainty in model outputs. By applying CI alongside ensemble techniques such as majority voting, exploration targets can be more reliably delineated, reducing false positives and enhancing decision-making. Yousefi et al. (2024) and Khammar et al. (2024) emphasize that CI supports the interpretation of ensemble outputs by identifying regions with consistently high prospectivity and low variation, thus mitigating the risks associated with model disagreement. This approach not only strengthens the robustness of mineral targeting but also facilitates clearer prioritization of follow-up exploration efforts (Khammar et al. 2024; Yousefi et al. 2024).

4.5. Experiment and analysis

4.5.1. Targeting criteria

In a recent study, Mami Khalifani et al. (2025a) generated geological, geochemical, and geophysical evidence layers by applying logistic transformation functions to normalize and assign continuous weights to spatial datasets. These processed evidence layers serve as key targeting criteria for mineral prospectivity mapping in the current study, which employs machine learning algorithms including Random Forest (RF), Support Vector Machine (SVM), and Extreme Gradient Boosting (XGBoost). To support a mineral system's approach to gold exploration, the following sections provide a detailed explanation of each dataset and evidence layer. This includes the extraction and interpretation of geological, geochemical, and geophysical signatures that define the critical components of mineralization systems namely, the source, pathway, and trap for epithermal gold mineralization in the study area. Table 4-1 outlines the set of predictor variables utilized in

this study to characterize the key attributes of epithermal gold mineralization within the study area.

Table 4-1. Predictor variables used to characterize the geological processes responsible for the deposition and concentration of epithermal gold mineralization. (RTP=Reduction to the pole), (AS=Analytic Signal), (TDR=Tilt Derivative), (FVD=First Vertical Derivative), (K%= Potassium concentration), (eU= equivalent Uranium), (eTh=equivalent Thorium).

Geological Predictor Variables	Geophysical Predictor Variables	Geochemical Predictor Variables
	RTP	
Host rocks	AS	Au
Intrusive rocks	TDR	As
Major (regional) faults	FVD	Sb
Minor (local) faults	K%	Cu
Thrust faults	eU	Mo
Contacts	eTh	Zn
	K/eTh	Pb
	eU/eTh	W
	eU/K	

4.5.1.1. Geological criteria

The geological data used in this study consist of lithological units and faults derived from 1:50,000 bedrock geology maps for NTS sheets 21O/10 and 21 O/7 maps provided by the New Brunswick Department of Natural Resources (Mami Khalifani et al. 2025a, b). These

maps provide the basis for mineral prospectivity analysis of epithermal gold mineralization and supported by geophysical and geochemical data. Figure 4-9 shows the distribution of host volcanic and sedimentary rocks and intrusions, alongside key structural features, such as major regional, minor local, and major thrust-faults. Figure 4-9a highlights key host rock units associated with epithermal gold mineralization in the study area, including the volcanic rocks of the Wapske (Mami Khalifani et al. 2025a, b). Figure 4-9b shows the distribution of mafic and felsic intrusions that represent potential magmatic sources contributing to epithermal gold mineralization within the study area. Devonian mafic intrusions are associated with gold occurrences at Dalhousie Road, McCormack Brook, and Jonpol. Significant felsic and mafic intrusions, i.e., the Mount Elizabeth Granite and Gabbro, Mount LaTour Granite, Mount Bailey Granite, Mulligan Gulch Porphyry, Ramsay Brook Gabbro, and Upsalquitch Lake Gabbro, are spatially and genetically linked to gold mineralization in the study area. Additionally, Silurian felsic intrusions are proximal to gold mineralization at Upsalquitch Forks, whereas the Portage Brook Troctolite is associated with the Ramsay Brook gold mineralization. The Mulligan Gulch Porphyry underlies the Mulligan Gulch gold occurrence, and the Upsalquitch Lake Gabbro is interpreted as a source for gold mineralization at the Simpson Field occurrence. These intrusive bodies likely played a significant role in driving hydrothermal systems responsible for gold deposition in the region (Mami Khalifani et al. 2025a, b; Fig. 4-9a). Major (regional) faults (with 300-meter buffer), such as the Rocky Brook–Millstream, McCormack Brook, McIntyre Brook, Rocky Gulch, and Portage Lake faults, can serve as primary conduits for hydrothermal fluid flow. These structures play a critical role in controlling the migration of mineralizing fluids and are key components of the regional

structural framework associated with gold mineralization in the study area (Mami Khalifani et al. 2025a, b) (refer to Fig. 4-9c). Figure 4-9d illustrates the spatial relationship between minor (local) faults and gold occurrences in the study area. Minor faults and associated lineaments were extracted from integrated geological and geophysical datasets and provide insight into the relationship between structures and gold mineralization. In epithermal gold systems, minor faults and lineaments play a fundamental role as conduits that focus and channel mineralizing fluids from deeper magmatic or metamorphic sources toward upper crustal depositional environments (Corbett and Leach 1998). Their spatial correlation with gold occurrences, as shown in Figure 4-9d, highlights their significance as structural controls in ore mineralization. The distribution pattern of gold occurrences along and near the minor faults further supports the mineral systems approach, where these structures act as not only fluid pathways but also sites of increased permeability, favoring gold precipitation due to pressure drops or chemical interactions with host rocks (Cox and Singer 1988). Figure 4-10a shows the distribution of thrust faults in relation to gold occurrences in the study area. The clustering of gold showings along the eastern margin of the study area, in close proximity to thrust faults, indicates a possible link to gold mineralization. Thrust faults in northern New Brunswick are typically associated with compressional tectonic regimes and crustal shortening events, have acted as major fluid conduits for epithermal systems (McCutcheon et al. 1997; Thorne et al. 2008; Mami Khalifani et al. 2021). These structures commonly juxtapose contrasting lithologies and generate zones of enhanced permeability, creating favorable conditions for hydrothermal fluid flow and subsequent gold precipitation. In epithermal gold systems, thrust faults serve as critical pathways for ascending mineralizing fluids and commonly represent reactivated

deep-seated faults linked to broader tectono-magmatic processes. Their association with gold mineralization in the study area reinforces their potential as first-order controls within the mineral system framework (Sibson 1990; Goldfarb et al. 2005). The association of gold occurrences with lithological contacts indicates that these boundaries may have served as preferential pathways for hydrothermal fluid migration, enhancing the potential for ore deposition. The contacts between contrasting lithologies, particularly those between volcanic and sedimentary units, likely acted as fluid conduits, focusing mineralizing solutions and contributing to localized gold enrichment (refer to Fig. 4-10b). Lithological contacts juxtapose rocks of different rheological and permeability characteristics that promote hydrothermal fluid flow and epithermal gold mineralization. The spatial association of gold occurrences with lithological contacts underscores the role of contacts as structural and lithological pathways that facilitated fluid flow during mineralization events.

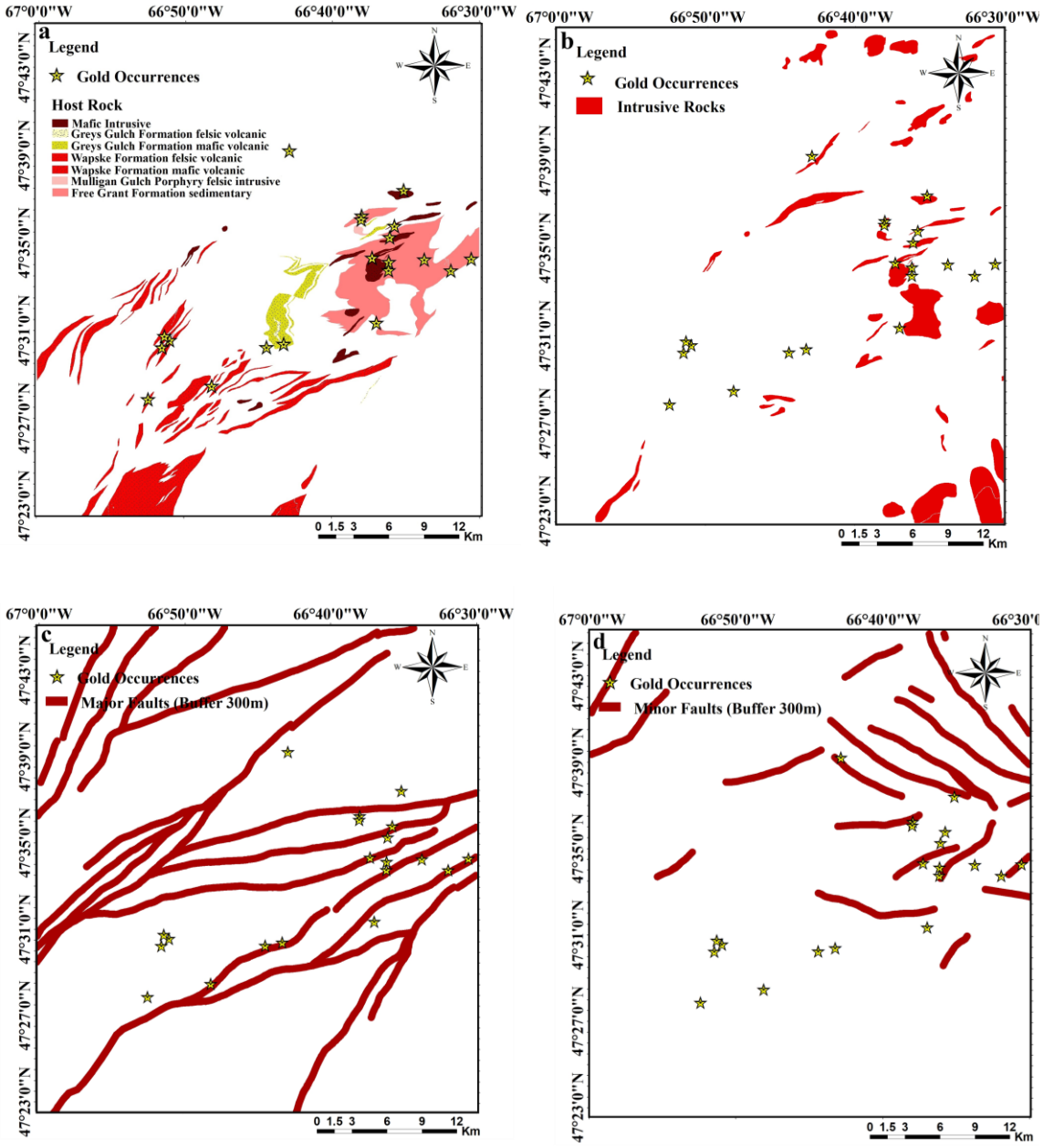

Figure 4-7. Targeting Criteria used in this study (a) host rocks, (b) intrusive rocks, (c) major faults, (d) minor faults.

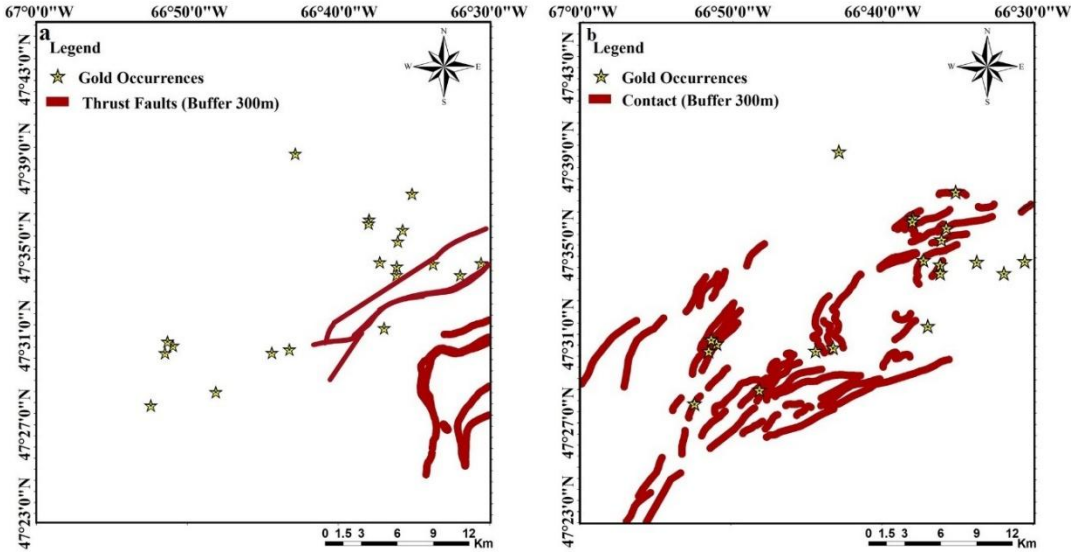

Figure 4-8. Targeting Criteria used in this study (a) thrust faults, and (b) contact.

4.5.1.2. Geophysical criteria

Airborne magnetic and radiometric data from the Campbelltown and Bathurst area (Geological Survey of Canada (GSC 1976, 1986, 1987) surveys were integrated to provide comprehensive coverage of the study area, enabling the detection of faults, contacts, and intrusive bodies linked to mineralization (Sánchez-Mora et al. 2021). The magnetic data were processed using techniques such as Reduced-to-Pole (RTP), Analytic Signal (AS), Tilt Derivative (TDR), and First Vertical Derivative (FVD) to enhance the interpretation of structural and geological features. Complementary radiometric data were employed to identify hydrothermal alteration zones and felsic intrusions based on elevated K, eU, and eTh, aiding in mineral prospectivity analysis.

4.5.1.3. Geomagnetic data

RTP and AS filters are essential geophysical techniques for interpreting aeromagnetic data in mineral exploration, particularly for identifying intrusive and extrusive bodies associated with hydrothermal mineral systems (Mami Khalifani et al. 2019; Karbalaeiramezanali et al. 2025; Mami Khalifani et al. 2025a). Application of RTP and AS filtering highlights magnetic anomalies that align with several Devonian intrusions, include the Ramsay Brook and Upsalquitch Lake gabbros, and Silurian intrusions, i.e. Portage Brook Troctolite, Mulligan Gulch Porphyry, Mount Bailey Granite, Mount LaTour Gabbro, and Mount Elizabeth Gabbro and Granite (Mami Khalifani et al. 2025a, b) (refer to Fig. 4-11a, b). These features coincide spatially with known epithermal gold occurrences, particularly along the Rocky Brook–Millstream Fault system. TDR and FVD sharpen aeromagnetic data to delineate structures features, faults, fractures, and lineaments critical for fluid flow and gold mineralization. TDR highlights shallow source edges independent of magnetization direction, while FVD emphasizes near-surface, high-gradient anomalies, improving detection of subtle faults, lineaments, and contacts (Mami Khalifani et al. 2019; Mohamed et al. 2022; Abdelrady et al. 2023; Mami Khalifani et al. 2025a) (refer to Fig. 4-11c, d). In northern New Brunswick, the application of these derivatives to aeromagnetic data has revealed a network of linear features aligned NW-SE and NE-SW directions consistent with the regional tectonic fabric and known gold-bearing shear zones. These structures serve as conduits for hydrothermal fluids and are commonly associated with Devonian intrusions that supplied the thermal and metallogenic drivers for epithermal gold mineralization (Mami Khalifani et al. 2024; Mami khalifani et al. 2025a, b).

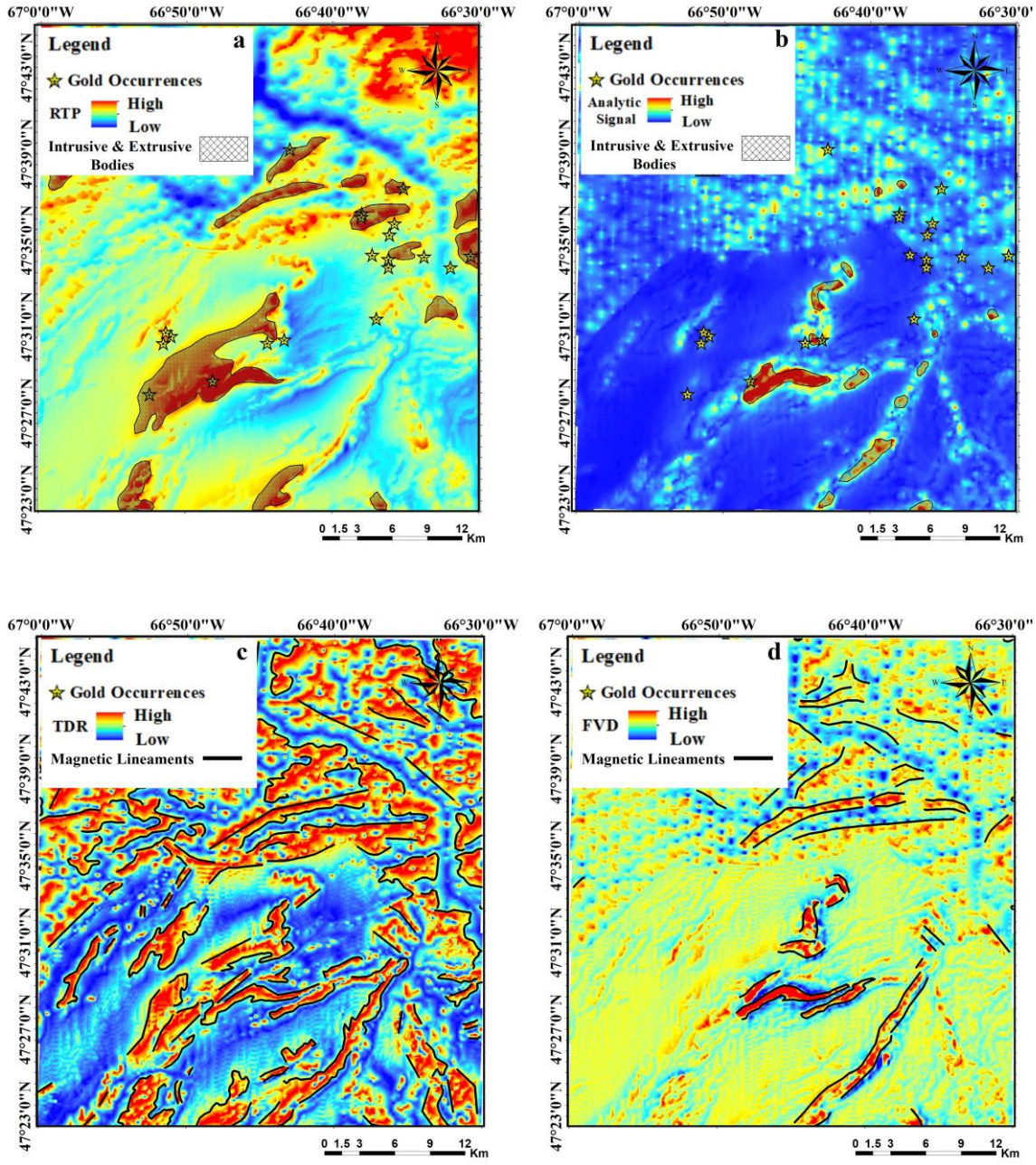

Figure 4-9. Targeting Criteria of intrusive and extrusive bodies extracted from geomagnetic data: (a) RTP, (b) AS, and magnetic lineaments extracted from (c) TDR, and (d) FVD.

4.5.1.4. Radiometric data

Radiometric data is critical in mineral exploration, particularly for identifying hydrothermally Volcanic and felsic rocks associated with gold mineralization. In northern New Brunswick, the combined interpretation of potassium (K), equivalent uranium (eU), and equivalent thorium (eTh) radiometric maps indicate a strong spatial association between felsic intrusions and gold occurrences. Elevated K, eU, and eTh are prominent in the southern part of the study area and correspond to the felsic volcanic rocks of the Wapske Formation. However, it is important to acknowledge a key limitation of radiometric data: gamma-ray attenuation due to overburden thickness and moisture content, particularly in areas with dense vegetation, water saturation, or glacial cover. These shielding effects can reduce the measured gamma signal, potentially masking radiometric anomalies. Despite this limitation, radiometric anomalies in this study align well with exposed felsic units and geophysical signatures, increasing confidence in their geological relevance.

High levels of potassium, typically linked to K-feldspar alteration and silicification, may indicate areas of significant hydrothermal alteration, which may be indicators of epithermal gold mineralization. Petrographic and field studies in the Williams Brook area have identified localized K-feldspar alteration within the felsic volcanic units of the Wapske Formation (Sánchez-Mora et al. 2021). However, this potassic alteration is relatively limited, with silicification and sericitization representing the dominant hydrothermal alteration styles in the system. Therefore, elevated potassium anomalies observed in radiometric data likely reflect a combination of primary lithological contributions particularly from rhyolitic volcanic rocks, and localized potassic alteration associated with synvolcanic magmatic-hydrothermal processes (Sánchez-Mora et al. 2021).The

radiometric anomalies especially those with high K/eTh and K/eU highlight potential alteration zones on the margins of intrusions, indicating areas where magmatic fluids may have interacted with the surrounding country rock, promoting mineral deposition. Furthermore, radiometric anomalies often overlap with structurally complex regions identified through magnetic derivatives and lineament extraction, reinforcing their genetic connection to mineralized systems (refer to Fig. 4-12a-d, and 4-13a, b). The TDR and FVD are magnetic filtering techniques that enhance the interpretation of aeromagnetic data by delineation (Mami Khalifani et al. 2019, 2021; Mohamed et al. 2022; Abdelrady et al. 2023). The eU/eTh and eU/K maps provide complementary insights into uranium mobility and the redox state of alteration systems. High eU/eTh values typically mark zones of uranium enrichment or thorium depletion and may be linked to oxidizing conditions in hydrothermal fluids. These anomalies, especially when aligned with faults or structural corridors, suggest areas where fluids have mobilized uranium, indicating potential pathways for mineralizing systems. In contrast, elevated eU/K commonly highlights felsic volcanic terrains and silicified zones where potassium has been depleted relative to uranium due to leaching. These patterns are especially useful when integrated with magnetic and structural data, as they help distinguish between primary lithologic and secondary alteration effects. The spatial overlap of radiometric anomalies with interpreted lineaments and magnetic highs enhances confidence in their association with gold-bearing hydrothermal systems in the Tobique–Chaleur Zone (Mami Khalifani et al. 2025a, b).

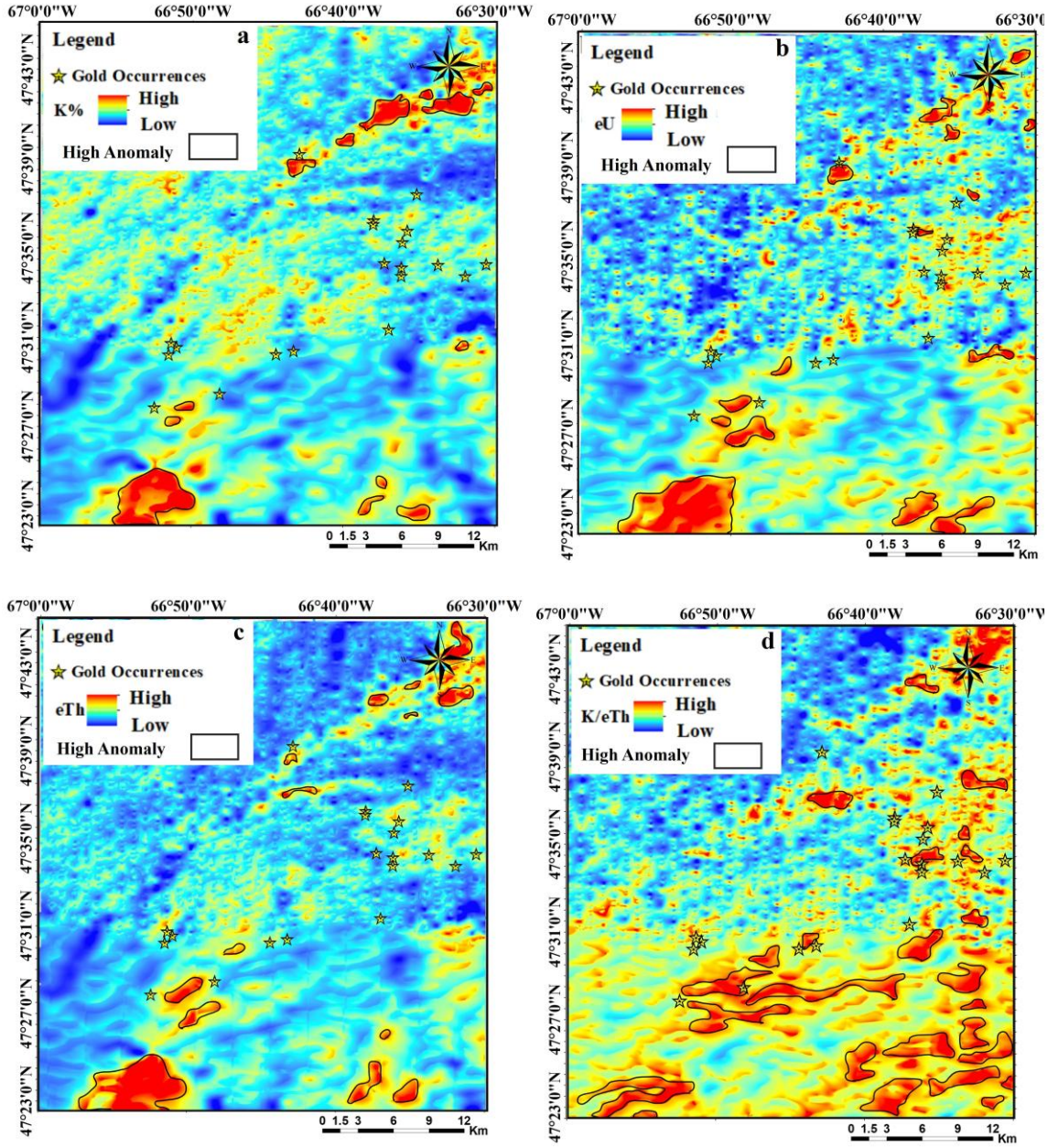

Figure 4-10. Radiometric targeting Criteria used in this study: (a) K%, (b) eU, (c) eTh, (d) K/eTh.

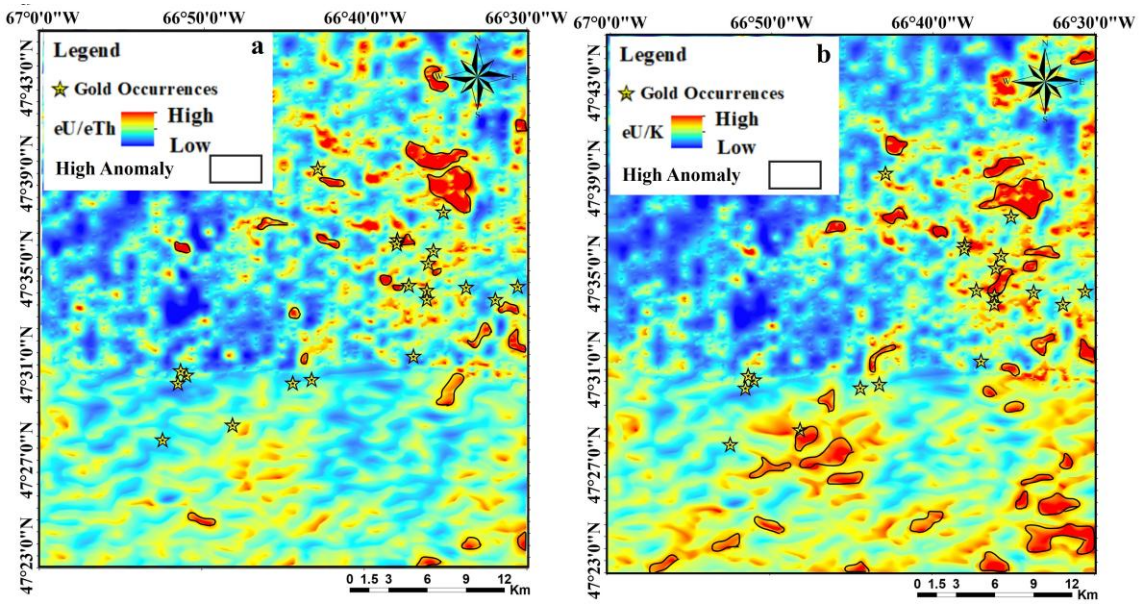

Figure 4-11. Radiometric targeting Criteria used in this study: (a) eU/eTh, and (b) eU/K.

4.5.1.5. Geochemical criteria

Till geochemical data from the study area (NBDNR 2014) were analyzed to delineate geochemical anomalies associated with epithermal gold mineralization in the study area. The samples were analyzed through advanced and precise whole-rock analytical methods, including Inductively Coupled Plasma- Mass Spectrometry (ICP-MS) and Instrumental Neutron Activation Analysis (INAA) (Mami Khalifani et al. 2025a).

Given the regional glacial history, southeast-directed ice flow from the northern Maine–Notre Dame divide indicates that tills at Williams Brook chiefly sample proximal up-ice bedrock (Wilson et al., 2005; Wu & Kruse, 2022). The Late Wisconsinan till is thin and discontinuous (<0.5 m), implying limited transport; thus the observed till-geochemical anomalies are interpreted as locally derived and closely tied to underlying lithologies. Before integration into RF, SVM, and XGBoost models, the till geochemistry was CLR-

transformed to address compositional closure and then summarized by PCA to capture element associations and reduce dimensionality(Mami Khalifani et al. 2024; Mami Khalifani et al. 2025a, b). The trap component for epithermal gold mineralization in the mineral system approach uses spatial elements such as Au, As, Cu, Mo, Pb, Sb, and Zn, as key indicators of hydrothermal activity and gold deposition zones. Multi-element anomalies, particularly As, Sb, Pb, and Zn, mark hydrothermal alteration zones and chemical traps. As demonstrated by Mami Khalifani et al. (2025a, b), the relationships among these elements are effectively illustrated through principal component analysis, highlighting their importance in identifying prospective mineralization zones. Following preprocessing, the geochemical datasets were normalized via logistic transformations, ensuring compatibility and optimal performance within machine learning frameworks. Geochemical maps generated from these transformed datasets served as critical input layers for the application of RF, SVM, and XGBoost methods. Based on the interpretation of geochemical maps, i.e. Au, As, Sb, Cu, Mo, Pb, Zn, and W, the distribution and correlation of pathfinder elements demonstrate the strong spatial relationships with gold occurrences, reflecting hydrothermal processes within epithermal systems (Figs 4-14 and 4-15). The geochemical maps reveal multi-element anomalies (elevated As, Sb, Pb and Zn) that delineate zones of hydrothermal alteration. These pathfinder elements are commonly enriched around faults, which serve as chemical traps where gold-bearing fluids precipitate due to physio-chemical changes, such as fluid mixing or temperature drop. Notably, As and Sb have a strong spatial correlation with gold occurrences, particularly in the southeastern parts of the study area (Figs. 4-14 and 4-15), indicating a proximal alteration halo of those associated with low-sulfidation epithermal systems. Additionally, Cu and Mo

anomalies in the same area may indicate deeper magmatic-hydrothermal contributions associated with intrusion-related systems.

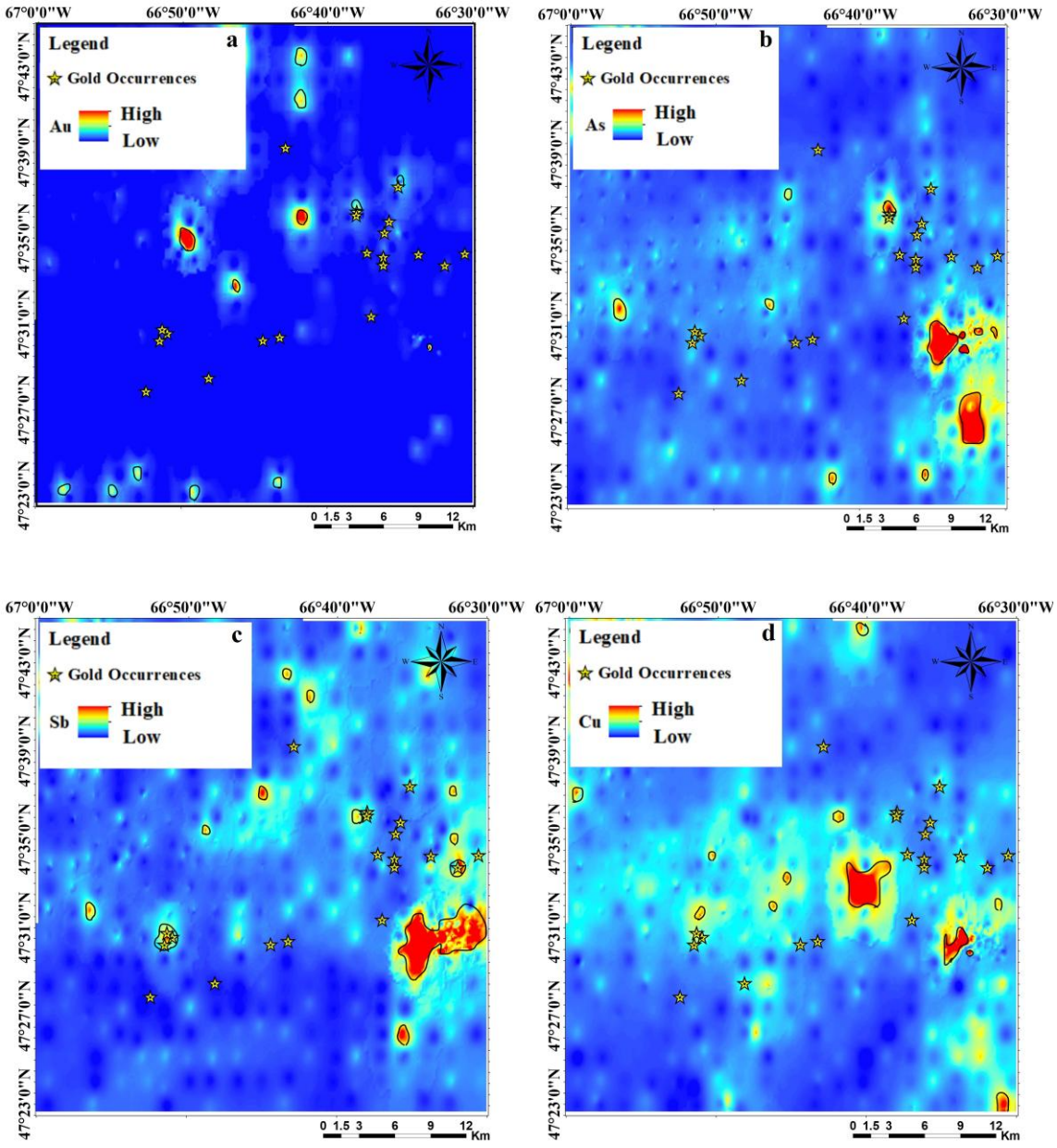

Figure 4-12. Targeting Criteria based on the till geochemical data, (a) Au, (b) As, (c) Sb, and (d) Cu.

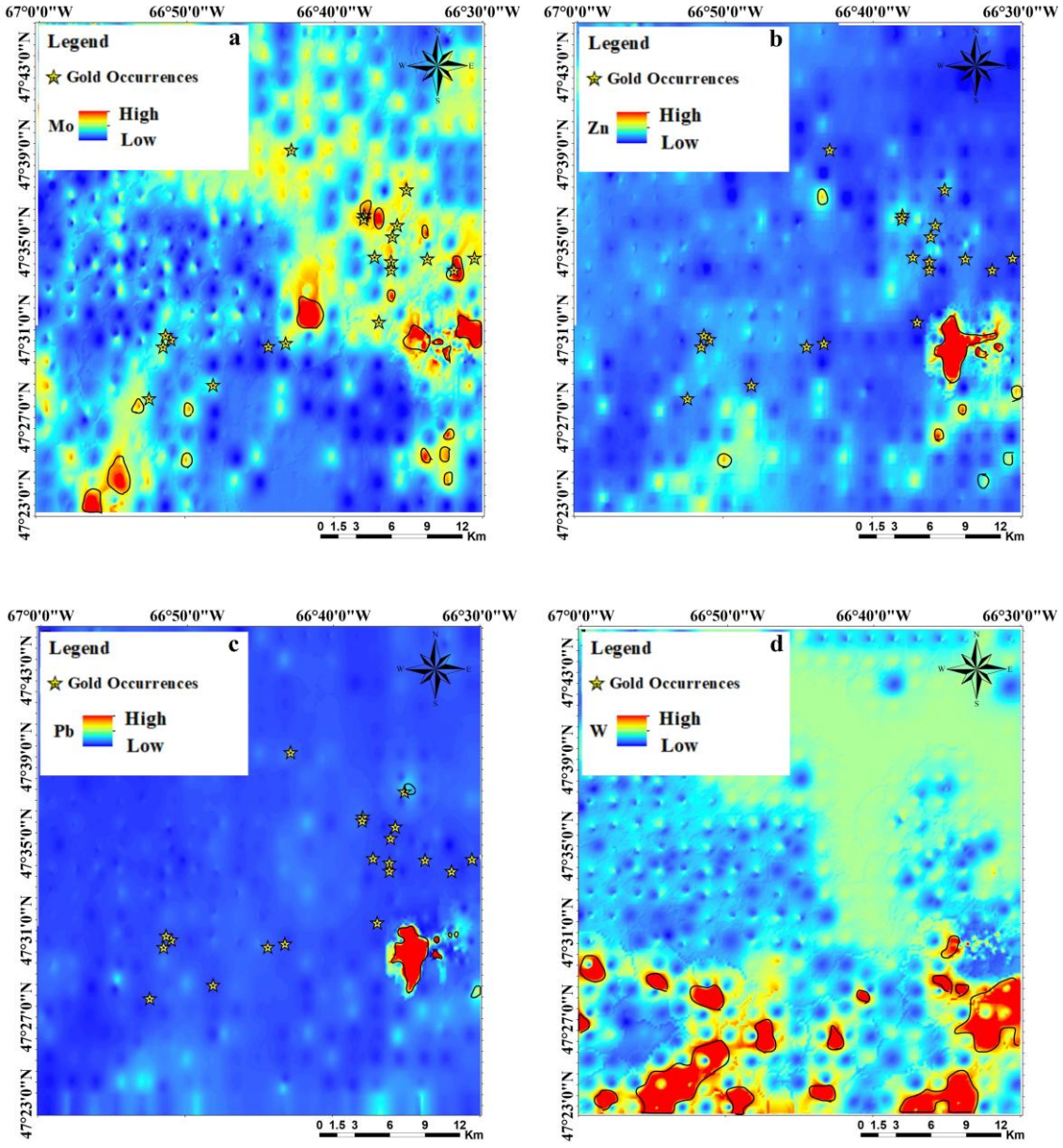

Figure 4-13. Targeting Criteria based on till geochemical data of (a) Mo, (b) Zn, (c) Pb, and (d) W.

4.5.2. Selection of Training and Testing Samples

In supervised machine learning methods, two types of data are required: positive data, representing known mineralized locations, and negative data, representing non-mineralized

areas (Bonham-Carter and Agterberg 1999; Nykänen and Salmirinne 2007; Abedi et al. 2012; Carranza et al. 2015; Harris et al. 2015; Lauzon and Gloaguen 2024). Known mineral deposits and occurrences can be selected as positive training samples for supervised mineral prospectivity modeling (Behnia et al. 2023; Josso et al. 2023; Khammar et al. 2024). Identifying non-mineralized areas is challenging because regions close to mineralized zones often share similar characteristics, which can reduce the accuracy of model predictions. Previous studies have shown that randomly generated negative datasets may not accurately represent true non-deposit locations (Carranza 2009). Nevertheless, several approaches have been proposed to reduce this uncertainty. One involves the identification of areas with a low probability of a deposit based on the spatial distribution of known mineralization (Carranza et al. 2008), whereas another limits the selection of negative samples to lithological units deemed unfavorable for mineralization (Nykänen Vesa et al. 2015). A combination of these techniques may enhance model accuracy (Silva dos Santos et al. 2022). Furthermore, selection of negative samples from the location of mineral deposits unrelated to the target commodity has been shown to provide less uncertainty than purely random selection (Lauzon and Gloaguen 2024). This study focuses on careful selection of training and testing datasets, and determination of the most appropriate input variables for the selected classification algorithms. In this study, an equal number of deposit and non-deposit samples were utilized to balance the positive and negative classes, thereby enhancing model performance and achieving optimal results.

4.5.2.1. Sampling positive data

For this study, 20 epithermal gold occurrences were used as positive training samples, sourced from the New Brunswick Mineral Occurrence database with 70% used for model training and 30% used for testing performance. Drill core samples were collected and analyzed for use in the Prediction-Area testing diagram to assess the model's effectiveness.

4.5.2.2. Sampling of Negative Data

The training dataset was assembled from 20 positive and 30 negative instances, reflecting the paucity of well-documented epithermal gold occurrences and the deliberate exclusion of ambiguous sites to minimize label noise. For the negative class, 100 candidate locations were first generated across the study area; from these, 30 were retained on the basis of lithologic unfavorability, absence of corroborating geochemical and geophysical anomalies, and separation from known occurrences by distance buffers. To mitigate overfitting with this limited sample size, we (i) rigorously vetted all labels using consistent geological, geochemical, and geophysical criteria; (ii) employed bootstrapping (10 resamples) together with stratified 10-fold cross-validation preserving the 20:30 class ratio to assess model stability; (iii) optimized model complexity via randomized search for RF and grid search for SVM and XGBoost; and (iv) integrated the three classifiers by majority voting with a confidence index to temper the influence of any single model and quantify uncertainty. Diagnostic plots (Fig. 4-16) show training and testing loss curves that converge without notable divergence, and ROC curves (Fig. 4-17) for both training and testing that indicate strong generalization.



Figure 4-14. Loss vs. epoch (trees for XGBoost; bootstrap steps for SVM) for the training (blue) and testing (orange) sets.

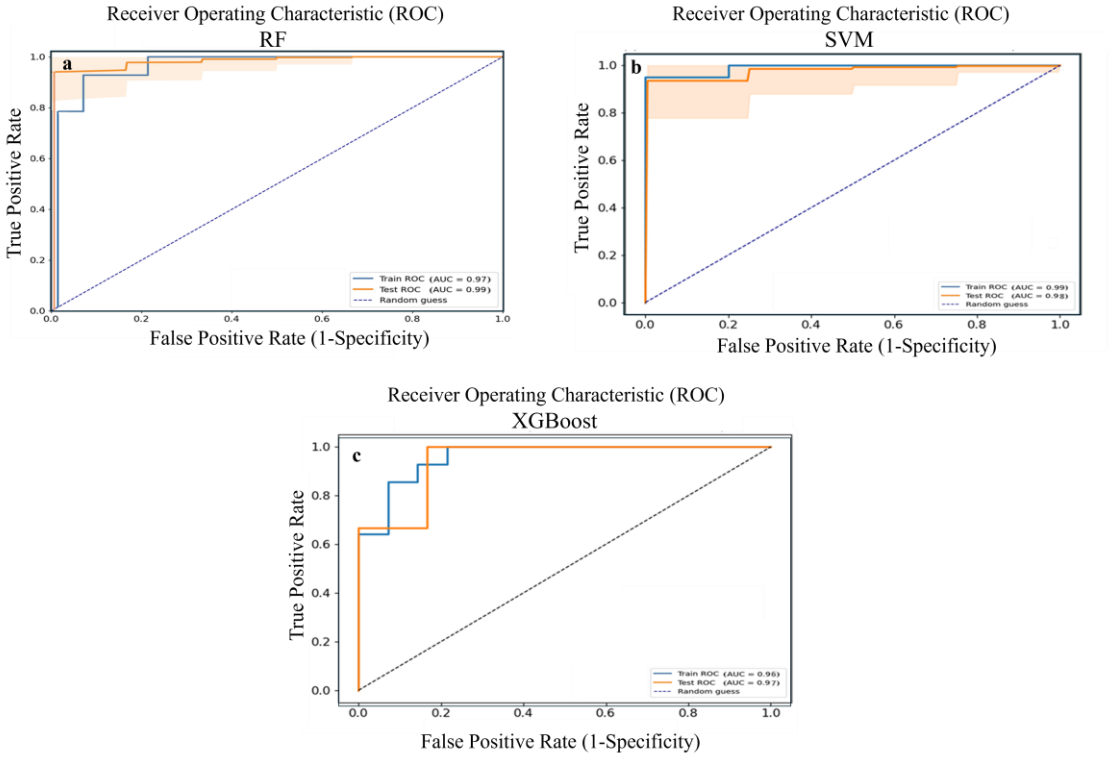

Figure 4-15 ROC curves for training (blue) and testing (orange) performance of RF, SVM, and XGBoost.

4.6. Results and discussion

4.6.1. Mineral Prospectivity Mapping (MPM)

The initial step in MPM involves preparing the input datasets, including both features and targeting criteria. Multi-source datasets were integrated using ESRI ArcGIS version 10.8.2. The model was trained and evaluated using Python 3 (ipykernel), which offers a wide range of machine learning algorithm libraries. Each evidence raster layer was generated with a cell size of 250 meters, a resolution determined by the spatial distribution of known gold occurrences and their associated geological features, i.e. host rocks, contacts, and intrusions, with geophysical and geochemical signatures. This cell size was selected to ensure that no more than one occurrence is represented in any single grid cell, thereby enhancing the spatial accuracy of the analysis (Carranza 2009). The mineral systems approach outlined by McCuaig et al. (2010) was employed to establish a set of evidence layers for mineral prospectivity mapping (McCuaig et al. 2010). Mami Khalifani et al. (2025a) implemented the mineral systems approach as a conceptual framework to translate the key geological processes controlling epithermal gold mineralization into spatially mappable criteria for predictive modeling. The approach identified three essential components (source, pathway, and trap), which are used to construct 24 evidence layers derived from geological, geochemical, and geophysical datasets; Figs. 4-9 to 4-15). In Mami Khalifani et al. (2025b), source regions were characterized by felsic and mafic intrusive and volcanic rocks, considered the primary contributors of heat and metal-rich fluids. Structural elements, such as major (regional) and minor (local) faults, magnetic lineaments, and lithological contacts were used to delineate fluid migration pathways. Trap

zones were identified through multi-element (Au, As, Sb, Pb, and Zn) geochemical anomalies with their correlation confirmed using principal component analysis (PCA) of till geochemical data (Mami Khalifani et al. 2024; Mami Khalifani et al. 2025a, b).

4.6.2. Evaluation of Predictor Variables

ROC curves were employed as a key statistical tool to evaluate the predictive performance of the mineral prospectivity models. The Area Under the Curve (AUC) values derived from the ROC curves quantified the models' ability to distinguish between mineralized and non-mineralized areas. Before conducting predictive modeling, AUC values were calculated for the predictor variables to evaluate their effectiveness in representing epithermal gold mineralization in the study area. As illustrated in Figure 18, the predictor variables exhibit different spatial relationships with the mineralized zones. Predictor screening via ROC/AUC (Fig. 4-18) indicates that magnetic intensity and edges (RTP = 0.98; TDR = 0.94; FVD = 0.91), structure (contacts = 0.97; major faults = 0.96; minor faults = 0.90), and till geochemistry (Mo = 0.95; Cu = 0.92; Sb = 0.89; Au = 0.89; As = 0.84) are the strongest discriminants of mineralization, consistent with an intrusion-linked, structurally focused epithermal system along the Rocky Brook–Millstream corridor. Lithologic masks (intrusive/host ≈0.90–0.91) further support receptive units (Fig. 4-18). By contrast, radiometric variables (K = 0.55; AS = 0.63; eU/eTh ≈0.65–0.76) show weak to moderate separability, likely due to regolith cover and scale mismatch. Accordingly, the RTP map displays the strongest spatial concordance with known mineralization, whereas potassium (K) shows the weakest. Overall, airborne radiometric predictors display limited spatial correspondence with epithermal gold in this setting (Fig. 4-18). These AUC patterns clarify

why the RF, SVM, and XGBoost classifiers weight magnetics, structure, and multi-element geochemistry most heavily and underpin the spatial logic of the prospectivity maps.

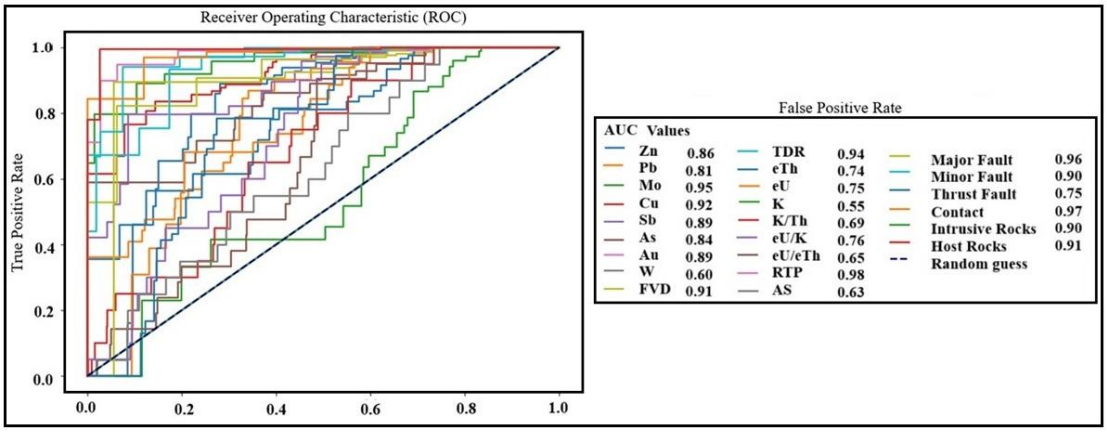

Figure 4-16. ROC curves illustrating the performance of predictor variables used in MPM and their respective calculated AUC values.

4.6.3. Machine Learning Models and Hyperparameter Optimization

To assess model uncertainty, ten bootstrapped subsets of positive and negative samples were generated, each used to train a separate predictive model. Bias and variance were evaluated using fivefold cross-validation. Mineral prospectivity maps were then produced using Random Forest (RF), Support Vector Machine (SVM), and XGBoost algorithms (Fig 4-19). For the RF classifier, hyperparameter optimization was performed using a randomized search strategy. To ensure robust model evaluation and reduce overfitting, a stratified 10-fold cross-validation approach was adopted, maintaining class distribution within each fold. The model underwent 500 randomized iterations, each using nine folds for training and one-fold for validation within a ten-fold cross-validation setup. The F1 score was selected as the primary performance metric, providing a balanced evaluation of precision and recall. A fixed random state of 42 (a commonly used seed value) was set to

ensure the reproducibility of the cross-validation and randomized search results. This strategy enabled comprehensive exploration of the hyperparameter space and reliable estimation of model generalization across data subsets. The specific range of parameters explored is presented in Table 4-2.

Table 4-2. Hyperparameters for the Random Forest algorithm utilized in the randomized search strategy.

Hyperparameter	Set
n_estimators (Number of trees in the forest)	10 to 200 (in increments of 10)
max_depth (Maximum depth of each tree)	None (unlimited depth) and integers from 2 to 7
min_samples_split (Minimum number of samples required to split an internal node)	2, 5, 10
min_samples_leaf (Minimum number of samples required to be at a leaf node)	1, 2, 4
max_features (Number of features to consider when looking for the best split)	'auto', 'sqrt', 'log2'
Bootstrap	True, False
Criterion (Function to measure the quality of a split)	'gini', 'entropy'

In the implemented Support Vector Machine model, the SVC class from scikit-learn was utilized, with hyperparameter optimization conducted via Grid Search CV. The grid search explored combinations of kernel functions, specifically 'linear', 'poly' (polynomial), and 'rbf' (radial basis function), to determine the most effective decision boundary for the

classification task. The hyperparameter tuning of the SVM model was performed using a grid search strategy to optimize model performance. The hyperparameters adjusted during this process are the regularization parameter (C), the kernel coefficient (gamma), and the choice of kernel function. Specifically, the values tested for C were [0.1, 1, 10], which control the trade-off between achieving a low training error and a low testing error. A smaller C value allows for a wider margin, potentially leading to better generalization, whereas a larger C value aims for a lower training error, possibly at the risk of overfitting. The gamma parameter was set to ['scale', 'auto'], defining how far the influence of a single training example reaches with low values meaning 'far' and high values meaning 'close'. Gamma is crucial for non-linear kernels like RBF and polynomial. The kernel options determine the type of decision boundary used by the SVM. It is noteworthy that while the polynomial kernel was included in the parameter grid, associated specific parameters such as degree and coefɵ, were not specified. These parameters control the flexibility and complexity of the polynomial decision boundary. Including these parameters in the grid search could potentially enhance model performance by allowing for a more thorough exploration of the polynomial kernel's capabilities. Incorporating these additional parameters in future tuning processes may lead to improved model accuracy and generalization.

The Extreme Gradient Boosting (XGBoost) model is configured with specific hyperparameters to optimize its performance and generalization capabilities. These hyperparameters play crucial roles in controlling the model's complexity, preventing overfitting, and enhancing predictive accuracy. Key hyperparameters include n estimators set to 100, determining the number of trees in the ensemble. The learning rate is configured

at 0.1 and controls the contribution of each tree to the final model and aids in preventing overfitting by shrinking the weights on each step. The max_depth parameter is fixed at 6 and limits the depth of each tree to prevent the model from becoming overly complex. To further regularize the model, min_child_weight which specifies the minimum sum of instance weight needed in a child node, thus controlling the model's complexity is set to 1. Subsampling techniques are applied through subsample and colsample_bytree, both set to 0.8, to introduce randomness and prevent overfitting by sampling a fraction of the training data and features, respectively. The gamma parameter is set to 0, which indicates no minimum loss reduction required to make a further partition on a leaf node and allows the algorithm to explore more splits. Lastly, regularization terms reg_alpha and reg_lambda are utilized to penalize large coefficients, with reg_alpha applying L1 regularization and reg_lambda applying L2 regularization, both contributing to reducing model complexity and enhancing generalization. These hyperparameters are critical in balancing the bias-variance trade-off, ensuring that the model captures underlying patterns without overfitting to the training data. Proper tuning of these parameters is essential for optimizing model performance.

4.6.4. Mineral Prospectivity Mapping outputs

Following the training and optimization of the machine learning models, spatial mineral prospectivity mappings were generated in ArcGIS 10.8.2 using a uniform grid cell size of 250 meters. Each cell was assigned a normalized prospectivity index ranging from low to high values (e.g., 0.01–0.98), representing the model-estimated likelihood of gold mineralization. These maps produced using RF, SVM, and XGBoost algorithms translate

the spatial patterns of predictor variables into continuous probability surfaces, allowing for the identification of favorable exploration targets. The Random Forest-based MPM (refer to Fig. 4-19a) demonstrates a highly fragmented pattern of prospectivity across the study area. Several discrete high-probability zones (≥0.98) correspond well with known gold occurrences, especially in the central and eastern parts of the map; however, the model also predicts several isolated high-value cells across the study area which may suggest sensitivity to localized anomalies or a tendency toward overfitting.

The SVM-based MPM (Fig. 4-19 b) displays a more cohesive and compact high-prospective region. The model predicts a large continuous area of elevated probability values (up to 0.97), primarily concentrated in the central part of the study area. This smoother prediction surface highlights the SVM's strength in defining a well-bounded target zone but may oversimplify complex geological relationships and miss smaller-scale mineralized features. Nonetheless, the high-probability zone captures a significant number of known gold occurrences, indicating good alignment between prediction and reality. The XGBoost-derived MPM (Fig. 4-19c) provides a balanced spatial distribution of prospectivity values with moderate granularity. The model identifies multiple high-prospective clusters (maximum value 0.96), which correspond closely to known gold occurrences. In contrast to the RF and SVM outputs, the XGBoost map delineates both primary and secondary favorable zones with gradational boundaries, suggesting an effective trade-off between precision and generalization. The prediction patterns indicate the model's capacity to capture complex nonlinear interactions among the predictor variables while controlling overfitting. Together, these maps offer complementary insights into potential gold-bearing regions. While the RF model excels in capturing finer-scale

variability, the SVM provides a conservative and focused delineation of mineralization zones. The XGBoost model strikes a balance, offering both interpretability and predictive robustness. These MPMs are essential decision-support tools in prioritizing exploration targets based on different algorithmic interpretations of the mineral system framework.

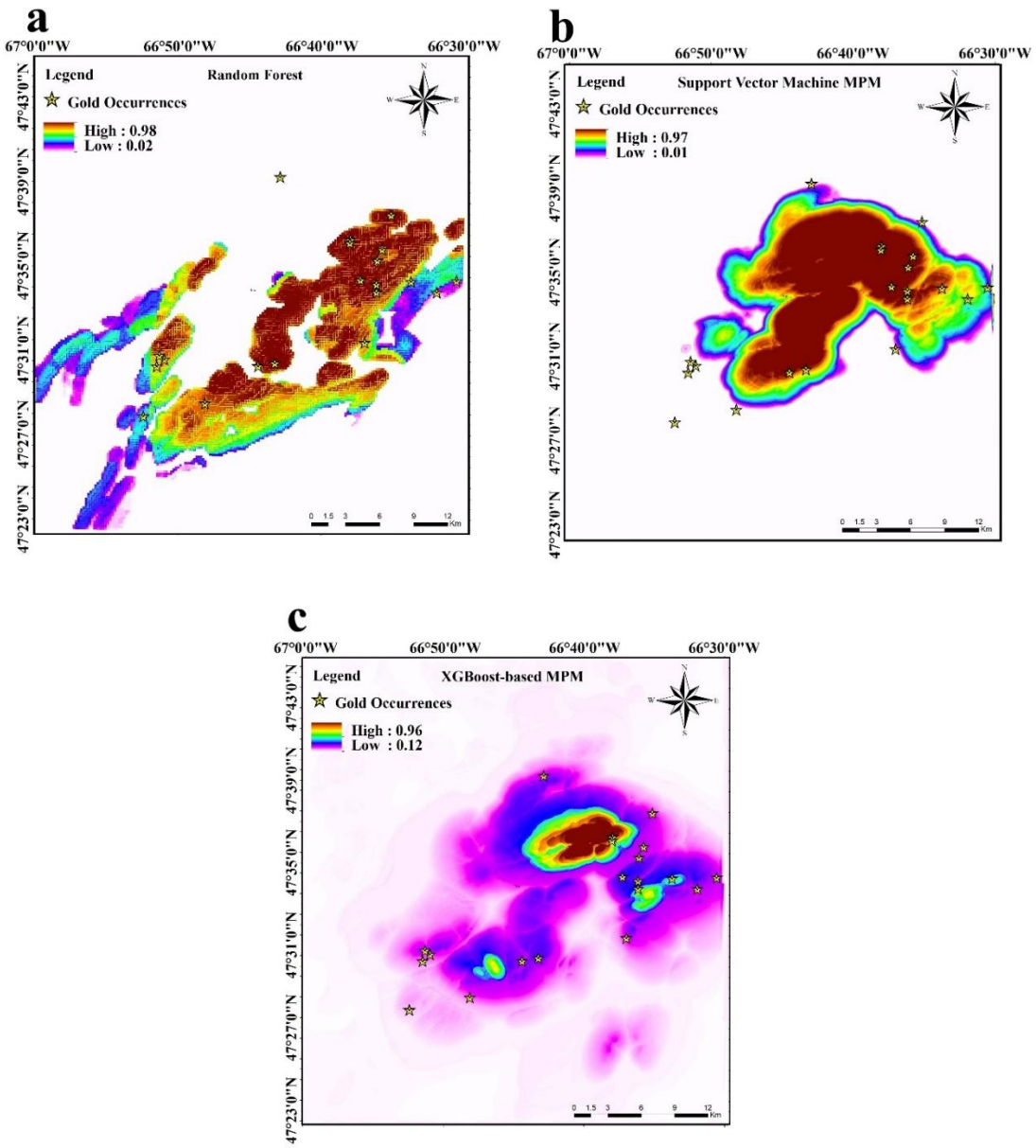

Figure 4-17. Mineral prospectivity maps for the study area generated using (a) Random Forest (RF), (b) Support Vector Machine (SVM), and (c) XGBoost.

4.7. Discussion

4.7.1. Receiver Operating Characteristic (ROC) curve

Based on the ROC curves and AUC values presented in the study by Mami Khalifani et al. (2025a), all three machine learning models, RF, SVM, and XGBoost demonstrate excellent predictive performance (refer to Fig. 4-20). The Random Forest model achieved the highest AUC value of 0.93, indicating strong discrimination between mineralized and non-mineralized areas, with a steep ROC curve suggesting high sensitivity and low false positive rates. The SVM model followed closely with an AUC of 0.92, reflecting similarly robust performance and effective class separation. XGBoost also performed well, with an AUC of 0.91, indicating reliable prediction capabilities and early identification of most known occurrences. Collectively, these results confirm that RF, SVM, and XGBoost are all suitable and effective algorithms for data-driven mineral prospectivity modeling, with consistently high accuracy across various methods.

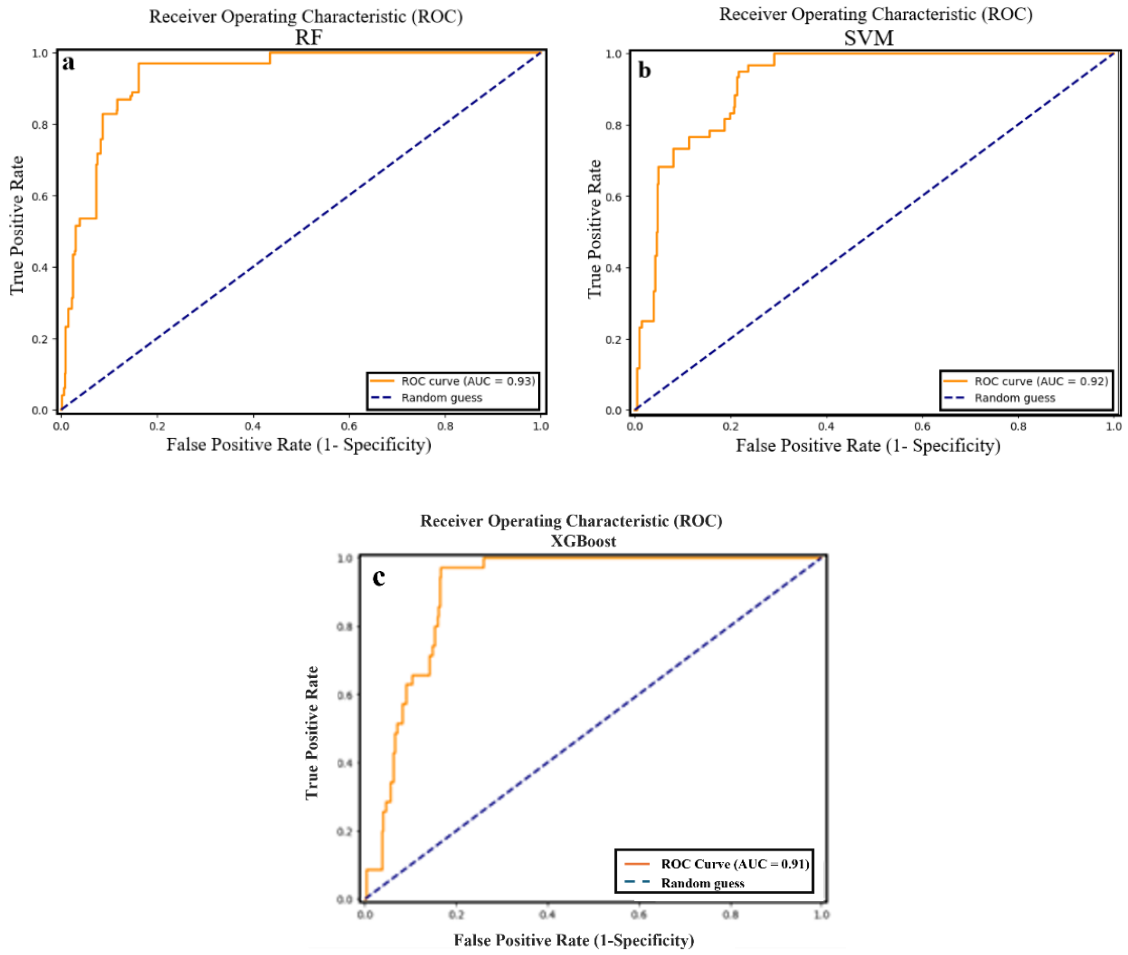

Figure 4-18. ROC validation curves of mineral prospectivity models generated by (a) Random Forest (RF), (b) Support Vector Machine (SVM), and (c) XGBoost methods.

4.7.2. Prediction-Area (P-A) Plot

Prediction–Area (P–A) analysis was performed using the spatial distribution of known drill cores and gold occurrences to evaluate the predictive performance and spatial efficiency of the RF, SVM, and XGBoost models (refer to Fig 4-21). This analysis identifies the minimum proportion of the study area required to capture the maximum number of known gold occurrences, offering a robust, spatially explicit performance metric for mineral prospectivity models (Yousefi and Carranza 2015). The comparative analysis of the P-A

plots for these methods provides critical insight into their relative performance in MPM. These plots, which depict the trade-off between the percentage of known mineral occurrences predicted and the proportion of the study area delineated as favorable, serve as a robust, data-driven means of model evaluation (Yousefi and Carranza 2015). The RF model demonstrates a well-balanced performance, capturing approximately 80% of known mineral occurrences within 25–30% of the study area (Fig 4-21a). This moderate intersection points on the P–A plot suggests that RF is capable of efficiently identifying prospective zones while maintaining spatial economy. The relatively steady slope of the curve further indicates consistent predictive capability across varying thresholds. These results emphasize the strengths of the Random Forest method in managing complex, multi-source geoscientific datasets, demonstrating robustness against overfitting, and effectively handling both categorical and continuous variables. In contrast, the SVM model exhibits comparatively lower efficiency. The P-A plot for SVM indicates that 75–80% of known mineral occurrences are predicted, but only by delineating a substantially larger portion of the study area, approximately 35–40% (Fig 4-21b). This broader spatial coverage reflects a more diffuse targeting capacity, which is less optimal for exploration efficiency. The flatter curve and delayed intersection point further suggest a lower predictive precision. Among the three models, XGBoost yields the most favorable results, capturing roughly 90% of known mineral occurrences within only 15–20% of the study area (Fig. 4-21c). The early intersection and steep gradient of its P-A curve reflect high predictive power concentrated in a compact spatial extent. This indicates that XGBoost is particularly effective in minimizing false positives while maximizing the recovery of mineralized zones, thereby offering the most efficient targeting strategy. Gradient boosting algorithms

such as XGBoost outperform conventional models in MPM due to their iterative refinement, robustness to noise, and ability to model complex nonlinear relationships (Zhang Q et al. 2022).

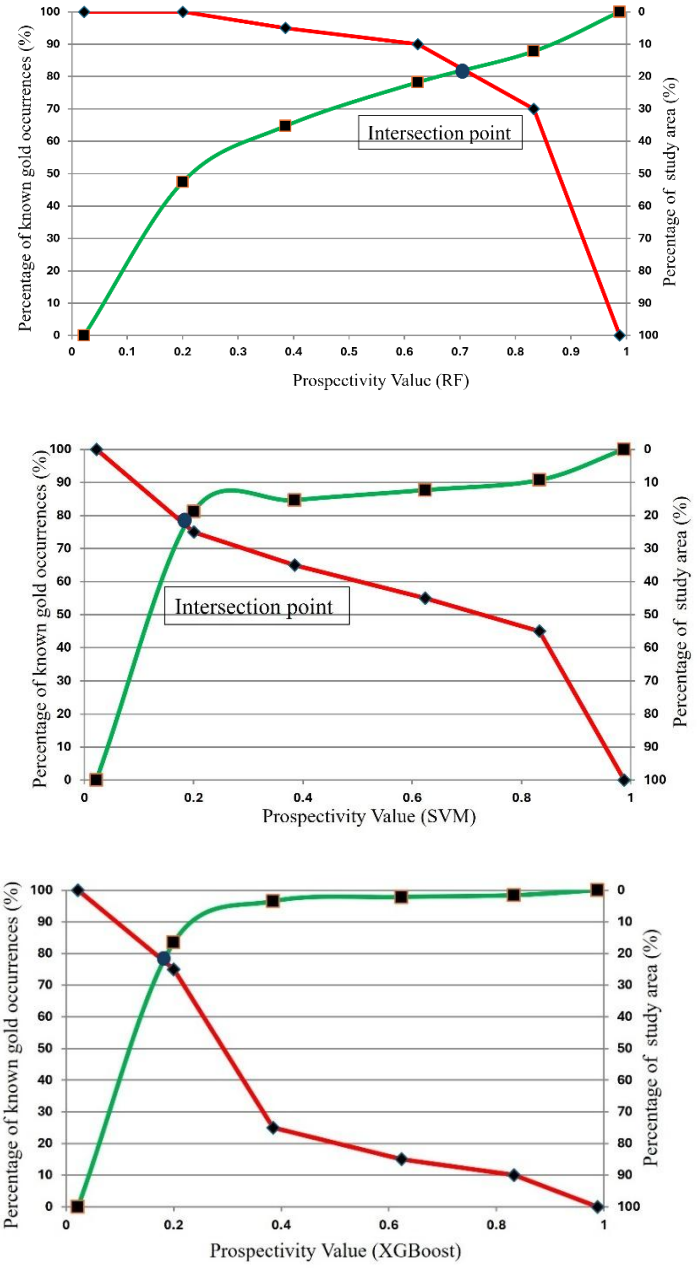

Figure 4-19. Prediction–area (P–A) plot analysis of the three models used in this study: (a) Random Forest (RF), (b) Support Vector Machine (SVM), and (c) Extreme Gradient Boosting (XGBoost). The green line indicates the cumulative percentage of known gold occurrences captured above each prospectivity threshold, while the red line represents the corresponding percentage of the study area.

4.7.3. Ensemble and Confidence Mapping

The Majority Vote map integrates the outputs of three supervised machine learning models RF, SVM, and XGBoost; through an ensemble learning strategy to generate a more robust and reliable mineral prospectivity map for epithermal gold mineralization in northern New Brunswick. This ensemble approach reduces model-specific biases and highlights zones consistently classified as favorable across all models. The map assigns each grid cell a final prospectivity class based on the most frequently predicted class, enhancing prediction stability and spatial coherence. In the map (Fig. 4-22a), the dark blue and purple zones indicate areas classified as highly prospective by the majority of models, overlapping with numerous known gold occurrences and drill core sites. The spatial agreement of high-prospectivity zones with mineralized drill holes and surface gold occurrences underscores the utility of majority voting in reinforcing confidence in exploration targeting outcomes.

The Confidence Index (CI) map quantifies the level of agreement among the individual model predictions (RF, SVM, XGBoost) for each grid cell, providing a spatial measure of epistemic uncertainty across the mineral prospectivity domain. The CI is calculated as the ratio of the mean to the standard deviation of the predicted prospectivity scores across the ensemble models. High CI values (represented by deep blue) correspond to locations where model predictions are both high and consistent, implying a strong consensus among the models. Conversely, low CI areas (yellow to magenta) reflect greater variability and thus lower predictive confidence (Fig. 4-22b). The distribution of known gold occurrences and mineralized drill core within the high-confidence zones suggests that these areas are not only prospective but also predicted with a higher degree of certainty. This approach enhances the interpretability of the ensemble model by enabling prioritization of zones with

both high prospectivity and low uncertainty, facilitating more targeted and cost-effective exploration strategies.

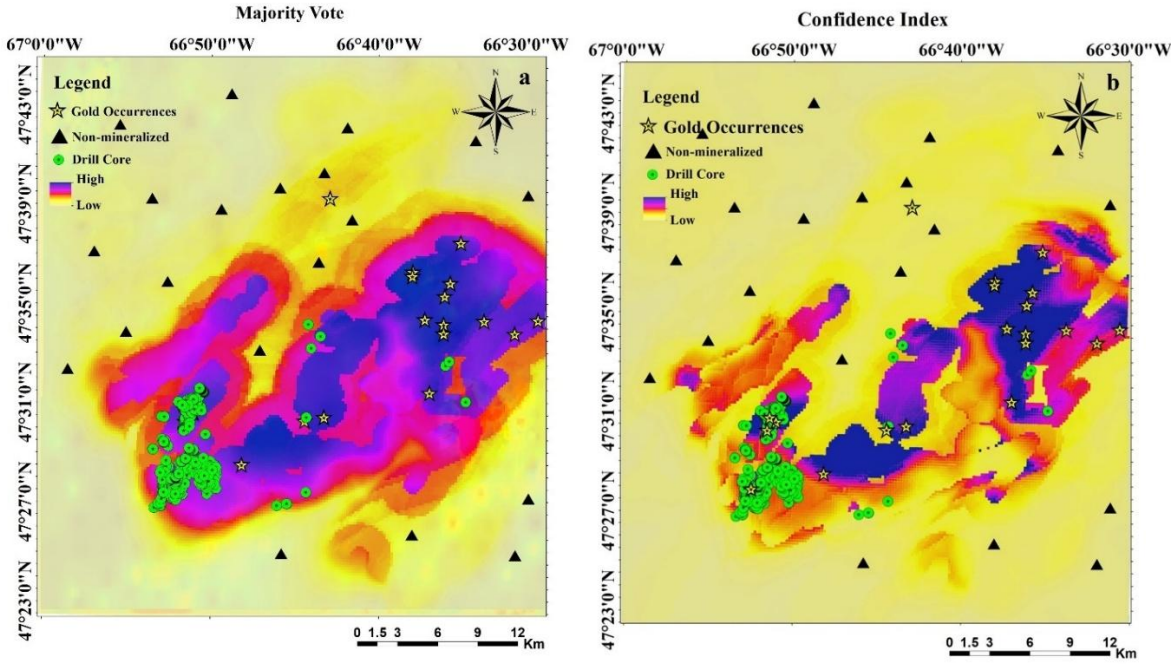

Figure 4-20. Assessment of results of this study (a) Majority voting model derived from the outputs of the prospectivity models; and (b) Confidence index model developed based on the same predictive models.

4.7.4. Comparative Analysis of RF, SVM, and XGBoost

The applied machine learning algorithms each displayed distinct capabilities and constraints in predicting epithermal gold prospectivity, reflecting their differing capacities to model the complex controls defined by the mineral systems approach. The Random Forest (RF) model, with the highest AUC (0.93), effectively integrated heterogeneous geological, geochemical, and geophysical predictor variables, capturing complex, nonlinear relationships among structural corridors, lithological contacts, and multi-element

geochemical anomalies. This capability made RF well-suited to representing the spatial heterogeneity of mineralization zone. However, its tendency to generate spatially scattered high-prospectivity pixels indicates heightened sensitivity to localized anomalies, which, while potentially identifying subtle targets, may also overestimate prospective zones and increase follow-up exploration costs. The Support Vector Machine (SVM) produced more spatially cohesive high-prospectivity zones (AUC=0.92) aligned with known mineralization trends, which is advantageous when exploration prioritizes compact, continuous targets for systematic field evaluation. Nonetheless, the smoother classification surfaces of SVM may obscure smaller-scale, structurally controlled features such as narrow fault splays or localized alteration halos that are often critical in epithermal systems.

The Extreme Gradient Boosting (XGBoost) model (AUC=0.91) achieved an optimal balance between spatial precision and generalization, capturing ~90% of known occurrences within only 15–20% of the study area. Its gradient boosting framework effectively modelled the multi-scale interactions among geological structures, geophysical gradients, and geochemical anomalies, yielding efficient spatial targeting. The main limitation of XGBoost lies in its reliance on careful hyperparameter tuning to avoid model over-complexity and potential overfitting, especially in geologically diverse terrains. These differences illustrate that no single algorithm universally excels across all geological scenarios. In this study, RF was most effective for detecting fine-scale variability, SVM for producing conservative and interpretable prospectivity zones, and XGBoost for maximizing spatial efficiency while maintaining geological plausibility. Their integration through majority voting and uncertainty quantification leveraged complementary strengths, reduced model-specific biases, and generated high-priority targets consistent

with established mineral system controls, improving the reliability and exploration value of the results.

4.7.5. Interpretation of Epithermal Gold Mineralization Controls

The spatial distribution of high-prospectivity zones generated by the machine learning models demonstrates a strong correlation with key geological structures and lithologies within the Tobique–Chaleur Zone. Notably, high-potential areas frequently coincide with the presence of regional and thrust faults, lithological contacts between volcanic and sedimentary sequences, and zones of structural intersection. These associations are consistent with the fundamental principles of the mineral systems approach and support the interpretation that geological structure played a critical role in focusing gold mineralization. The thrust and regional faults in the study area, many of which represent deep-crustal structures formed during the complex accretionary history of the Appalachian orogen, likely acted as long-lived conduits for hydrothermal fluid flow. These structures were reactivated multiple times during orogenesis, enhancing their permeability and capacity to transport mineralizing fluids. Their spatial alignment with geochemical anomalies and known occurrences of gold supports the view that major thrusts and regional faults served as first-order controls on fluid migration and deposition, whereas minor local faults are important second order features that also can focus fluid flow. Furthermore, the lithological boundaries, particularly contacts between mafic volcanic rocks and fine-grained sedimentary units, appear to represent important chemical and mechanical traps for gold-bearing fluids. The contrast in competency between these units likely caused strain localization and brecciation, enhancing porosity and permeability. These conditions favor

fluid mixing, chemical reaction, and ultimately, gold precipitation. The model outputs highlight such contacts as high-ranking predictors, further validating their role in the mineralization process. The intersection zones between regional faults and stratigraphic boundaries exhibit notably elevated prospectivity, suggesting that these areas functioned as structural traps where fluid flow was focused and retained. These intersections would have enhanced dilation and fluid pressure gradients, further promoting metal deposition. Geophysically, regions characterized by anomalous magnetic gradients and radiometric responses (e.g., low Th/K and high U/Th ratios) are closely associated with prospective zones. These signatures are commonly indicative of hydrothermal alteration halos or buried intrusions, both of which are genetically linked to mineralizing systems. Their spatial agreement with predicted gold zones provides additional support for the model's geological validity. Taken together, the results suggest that gold mineralization in the study area is primarily controlled by the interplay of deep-seated major regional and thrust faults, lithological heterogeneity, and structurally complex zones of deformation. These elements created a favorable environment for fluid circulation, reactive wall rocks, and physical-chemical conditions conducive to gold deposition.

In addition to the geological and structural controls, the geochemical characteristics of the study area further support the epithermal gold mineralization model. The geochemical data exhibit significant enrichment in pathfinder elements, such as As, Sb, and Pb that are commonly associated with epithermal systems. These elements display strong spatial correlation with the high-prospectivity zones delineated by the model, suggesting a genetic link between observed surface geochemistry and subsurface mineralizing processes. The application of multifractal analysis helped to identify geochemically anomalous zones with

sharper boundaries, enhancing the interpretability of geochemical halos and improving the input quality for data-driven models. The integration of these geochemical anomaly maps into the machine learning workflows allowed for the detection of subtle but meaningful patterns associated with mineralization. The RF, SVM, and XGBoost models consistently assigned high importance to variables representing geochemical signatures, especially arsenic and antimony concentrations, highlighting their role as reliable indicators of epithermal processes in this region. These findings align with the mineral systems model, where geochemical footprints are expected to be spatially associated with fluid pathways and depositional traps.

From a mineral prospectivity mapping standpoint, the ensemble-based approach successfully captured the multi-scale, multi-source nature of the mineral system. The resulting prospectivity map shows a robust agreement between predicted zones and known gold occurrences, suggesting the validity of the modeling strategy. The overlap between model predictions, field observations, and geophysical anomalies (e.g., magnetic lineaments and radiometric ratios) provides confidence that the approach is capable of detecting mineralized zones beyond the limits of current exploration data. Furthermore, the predicted high-potential areas coincide with zones that exhibit multiple favorable conditions, including structural intersections, lithological contrasts, and elevated geochemical anomalies hallmarks of mineral system fertility. These integrated signatures not only validate the model's performance, but also offer new targets for exploration that remain under-investigated. Together, the results underscore the effectiveness of combining geological, geochemical, and geophysical datasets in a data-driven MPM framework to

reveal the complex controls on epithermal gold mineralization in the Tobique–Chaleur Zone.

4.7.6. Implications and Future Directions

The high-priority zones identified through the ensemble and confidence-based prospectivity approach represent key targets for follow-up exploration. These areas should undergo systematic field validation, including geological mapping, detailed geochemical sampling, and exploratory drilling especially in zones that demonstrate both high model confidence and spatial coincidence with known structural features. Validating these zones in the field will not only test the predictive power of the models but also refine future exploration strategies by confirming or adjusting the interpreted mineralizing controls. To further improve the predictive accuracy and geological realism of mineral prospectivity mapping, future work should focus on incorporating temporal and three-dimensional data. Transitioning from 2D to 3D frameworks using borehole information and geochronological constraints could offer deeper insight into the vertical continuity of mineralization and improve the resolution of subsurface features. Additionally, enhancing the definition of non-mineralized zones by applying exclusion buffers and expert geological reasoning may reduce classification errors and uncertainty within the model outputs.

The machine learning framework developed in this study particularly the use of ensemble modeling and uncertainty quantification can be readily adapted to other mineral deposit types (e.g., VMS, porphyry) and applied in different geological settings across Atlantic Canada and beyond. Broader adoption of such approaches will aid in predictive exploration, especially in underexplored or data-sparse regions. Future studies could also

benefit from implementing more sophisticated ensemble techniques, such as stacking or weighted averaging, as well as incorporating deep learning architectures (e.g., convolutional neural networks or autoencoders). These advanced methods have the potential to capture complex, nonlinear spatial relationships that may remain underrepresented in conventional models.

4.8. Conclusion

This study successfully applied a mineral systems framework to develop robust evidence layers that reflect the key geological processes (source, pathway, and trap) controlling epithermal gold mineralization in northern New Brunswick. A total of 24 evidence layers, including lithological units, structural features (regional/local/thrust faults, contacts), geophysical derivatives (RTP, TDR, AS, FVD), radiometric ratios (K/eTh, eU/eTh), and geochemical anomalies (e.g., Au, As, Sb, Pb, Zn) were generated and integrated. These layers were selected based on their demonstrated spatial correlation with known gold mineralization and their relationship to fluid flow, metal transport, and ore deposition. The predictor variables captured the geological complexity of the region, providing the foundation for data-driven modeling. Among them, geophysical layers such as RTP and magnetic lineaments exhibited the strongest association with gold mineralization, whereas some radiometric variables (e.g., K%) showed lower predictive capacity. The integration of these targeting criteria enabled machine learning algorithms to delineate prospective zones with high spatial accuracy and geological relevance, validating the effectiveness of the mineral systems approach in MPM. The spatial coherence between high-prospectivity areas and mapped evidence layers underscores the critical importance of selecting and

processing geoscientific data that directly reflects ore-forming processes. This study highlights how machine learning, ensemble modeling, and targeted geological data can effectively produce reliable gold prospectivity maps in Northern New Brunswick.

1) This study demonstrates that machine learning models—Random Forest (RF), Support Vector Machine (SVM), and XGBoost are powerful tools for data-driven mineral prospectivity mapping (MPM), especially in complex geological settings such as the Tobique-Chaleur Zone of Northern New Brunswick. All three models yielded high predictive performance, with RF achieving the highest AUC (0.93), followed by SVM (0.92) and XGBoost (0.91).

2) Each algorithm exhibited distinct spatial prediction behaviors: RF effectively captured localized anomalies but showed scattered predictions; SVM provided a smooth and conservative delineation of high-prospectivity zones; and XGBoost achieved a balanced prediction with strong localization and low false positive rates, making it the most efficient model based on prediction–area (P–A) plot analysis.

3) The ensemble strategy using majority voting successfully enhanced model robustness by reducing individual biases and highlighting consistently prospective zones. The confidence index map further quantified model agreement, guiding exploration toward areas with both high prospectivity and low uncertainty.

4) The spatial correspondence of predicted high-prospectivity zones with known gold occurrences, geological structures (e.g., faults and intrusions), and geophysical/geochemical anomalies supports the validity of the applied mineral systems approach and confirms the reliability of the integrated dataset and modeling strategy.

5) While the ensemble and individual machine learning models successfully identified many high-prospectivity zones, a few known gold occurrences were not captured among the top predictions. This may reflect subtle or obscured geophysical and geochemical signatures, or structural and lithological contexts underrepresented in the training data. These limitations underscore the need for refining evidence layers, integrating subsurface or alteration data, and improving model sensitivity through more representative or expert-informed training strategies.

4.9. Recommendations

1. High-priority zones identified through the ensemble and confidence-based approach should be subject to field validation, including geological mapping, geochemical sampling, and drilling, particularly in areas with high confidence indices and spatial overlap with known structural features.

2. Although this study did not incorporate structural complexity metrics, such as Contact Occurrence Density and Orientation Entropy (Holden et al., 2012), these parameters offer valuable insight into deformation intensity and structural variability. Their integration into future models may enhance the delineation of fluid pathways and improve the predictive performance of mineral prospectivity mapping.

3. Future work should consider integrating temporal data or transitioning from 2D to 3D MPM frameworks using borehole and geochronological data to better resolve subsurface continuity of mineralization.

4. The machine learning framework employed herein can be extended to other mineral deposit types (e.g., VMS, porphyry) and geological terranes, enabling broader applications in predictive exploration across Atlantic Canada and globally.

5. Further refinement in defining non-mineralized areas using geological knowledge and exclusion buffers can reduce model uncertainty and enhance classification accuracy.

6. Ensemble techniques beyond majority voting such as stacking or weighted averaging and the implementation of deep learning models (e.g., CNNs or autoencoders) could further enhance the capacity to capture nonlinear spatial relationships in future mineral prospectivity studies.

Author Contributions: Methodology, Software, Formal analysis, Data curation, Writing – original draft, Review and editing, Visualization, Funding.

Farzaneh Mami Khalifani: Methodology, Software, Formal analysis, Data curation, Writing – original draft, Review and Editing, Visualization.,

David R Lentz: Resources, Supervision, Review and Editing, plus Funding.

James A Walker: Resources, Review, and Editing, plus Funding.

Acknowledgements

This study contributes to the PhD research of the first author. The authors extend their gratitude to Prof. Babaie, Editor-in-Chief, for overseeing the manuscript. They also acknowledge the financial support provided by the New Brunswick Department of Natural Resources and Energy Development, and the scholarship awarded to FMK by the University of New Brunswick. All authors have reviewed and approved the submitted version of the manuscript.

Declaration of Competing Interest

The authors declare no competing interests.

Data availability

No, all relevant research data are contained within the submitted manuscript file.

Funding

This research was funded by the University of New Brunswick, the New Brunswick Department of Natural Resources ands Energy Development, and New Brunswick Innovation Foundation.

References

Abdelrady, M., Moneim, M.A., Alarifi, S.S., Abdelrady, A., Othman, A., Mohammed, M.A. and Mohamed, A., 2023. Geophysical investigations for the identification of subsurface features influencing mineralization zones. Journal of King Saud University-Science, 35(7), p.102809.

Abedi M, Torabi SA, Norouzi GH, et al (2012) PROMETHEE II: A knowledge-driven method for copper exploration. Comput Geosci 46:255-263.

Behnia, P., Harris, J., Liu, H., Jørgensen, T.R., Naghizadeh, M. and Roots, E.A., 2023. Random forest classification for volcanogenic massive sulfide mineralization in the Rouyn-Noranda Area, Quebec. Ore Geology Reviews, 161, p.105612.

Bonham-carter GF, Agterberg FP (1999) Arc-WofE: a GIS tool for statistical integration of mineral exploration datasets. Bulletin of the International Statistical Institute 52, pp.497-500.

Bonham-Carter, G.F. and Agterberg, F.P., 1990. Application of a microcomputer-based geographic information system to mineral-potential mapping. In Microcomputer applications in Geology 2 (pp. 49-74). Pergamon.

Bonham-Carter GF, Agterberg FP, Wright DF (1990) Integration of geological datasets for gold exploration in Nova Scotia. Introductory readings in geographic information systems 10, pp.15-23.

Breiman L (2001) Random forests. Machine learning: 5-32.

Carranza EJM (2009) Objective selection of suitable unit cell size in data-driven modeling of mineral prospectivity. Comput Geosci 35(10), pp.2032-2046.

Carranza EJM, Hale M, Faassen C (2008) Selection of coherent deposit-type locations and their application in data-driven mineral prospectivity mapping. Ore Geol Rev 33:33(3–4), pp.536-558.

Carranza EJM, Laborte AG (2015) Random forest predictive modeling of mineral prospectivity with small number of prospects and data with missing values in Abra (Philippines). Comput Geosci 74:60-70.

Carranza EJM, Sadeghi M, Billay A (2015) Predictive mapping of prospectivity for orogenic gold, Giyani greenstone belt (South Africa). Ore Geol Rev 71, pp.703-718.

Chen T, Guestrin C (2016) Xgboost: A scalable tree boosting system. In: In Proceedings of the 22nd acm sigkdd international conference on knowledge discovery and data mining. (pp. 785-794).

Cheng H, Zhenge Y, Wu S, Lin Y, Gao F, Lin D, Wei J, Wang S, Shu D, Wei S, Chen L (2023) GIS-based mineral prospectivity mapping using machine learning

methods: a case study from Zhuonuo ore district, Tibet. Ore Geology Reviews 161: 105627.

Corbett, G.J. and Leach, T.M., 1998. Southwest Pacific Rim gold-copper systems. (No Title).Cox DP, Singer DA (1988) Distribution of gold in porphyry copper deposits.

Cox DP, Singer DA (1988) Distribution of gold in porphyry copper deposits.No. 88-46). US Geological Survey.Daviran M, Maghsoudi A, Ghezelbash R, Pradhan B (2021) A new strategy for spatial predictive mapping of mineral prospectivity: Automated hyperparameter tuning of random forest approach. Comput Geosci 148: 104688.

Einaudi, F., Godard, M., Pezard, P., Cochemé, J.J., Coulon, C., Brewer, T. and Harvey, P., 2003. Magmatic cycles and formation of the upper oceanic crust at spreading centers: Geochemical study of a continuous extrusive section in the Oman ophiolite. Geochemistry, Geophysics, Geosystems, 4(6).

Esmaeiloghli, S., Tabatabaei, S.H. and Carranza, E.J.M., 2021. Spatio-geologically informed fuzzy classification: an innovative method for recognition of mineralization-related patterns by integration of elemental, 3D spatial, and geological information. Natural Resources Research, 30(2), pp.989-1010.

Fyffe, L.R. and Fricker, A., 1987. Tectonostratigraphic terrane analysis of New Brunswick. Atlantic Geology, 23(3), pp.113-122.

Ghezelbash, R., Daviran, M. and Maghsoudi, A., 2025a. Combination of Machine Learning and Fractal approaches for AI-MPM: Identifying Low-Risk

Exploration Targets associated with Porphyry-Cu Deposits in the Kerman Belt, Iran. Remote Sens Appl 38:101596.

Ghezelbash, R., Daviran, M., Maghsoudi, A. and Hajihosseinlou, M., 2025b. Density based spatial clustering of applications with noise and fuzzy C-means algorithms for unsupervised mineral prospectivity mapping. Earth Science Informatics, 18(2), p.217.

Goldfarb, R.J., Baker, T., Dubé, B., Groves, D.I., Hart, C.J. and Gosselin, P., 2005. Distribution, character, and genesis of gold deposits in metamorphic terrane. Society of Economic Geologists 100th Anniverary volume : 45p.

Geological Survey of Canada (GSC) (1987). Aeromagnetic data 300m Campbelltown. Retrieved from https://geophysical-data.canada.ca/Portal/Results?minLong=69.19&maxLong=63.42&minLat=44.19&maxLat=49.59.

Geological Survey of Canada (GSC) (1976). Airborne radiometric data 1000m national-scale maps. Retrieved from https://geophysical-data.canada.ca/Portal/Results?minLong=-69.19&maxLong=63.42&minLat=44.19&maxLat=49.59

GSC Geological Survey of Canada (GSC) Geological Survey of Canada (GSC) (1986). Aeromagnetic data 1000m Campbelltown. Retrieved from https://geophysical-data.canada.ca/Portal/Results?minLong=-90067.868&maxLong=66.7775&minLat=45.4768&maxLat=46.4425.

Harris, J.R., Grunsky, E., Behnia, P. and Corrigan, D., 2015. Data-and knowledge-driven mineral prospectivity maps for Canada's North. Ore Geology Reviews, 71, pp.788-803.

Josso, P., Hall, A., Williams, C., Le Bas, T., Lusty, P. and Murton, B., 2023. Application of random-forest machine learning algorithm for mineral predictive mapping of Fe-Mn crusts in the World Ocean. Ore Geology Reviews, 162, p.105671.

Karbalaeiramezanali, A., Parsa, M., Lentz, D.R. and Thorne, K.G., 2025. Prospectivity Modeling of Devonian Intrusion-Related W–Mo–Sb–Au Deposits in the Pokiok Plutonic Suite, West-Central New Brunswick, Canada, Using a Monte Carlo-Based Framework. Natural Resources Research, 34(2), pp.669-702.

Khammar F, Nykänen V, Beier C, Niiranen T (2024) Translating mineral systems criteria into a prospectivity model for IOCG deposits in the Kolari region, Finland. Ore Geol Rev p.106326.

Lauzon, D. and Gloaguen, E., 2024. Quantifying uncertainty and improving prospectivity mapping in mineral belts using transfer learning and Random Forest: A case study of copper mineralization in the Superior Craton Province, Quebec, Canada. Ore Geology Reviews, 166, p.105918.

Liu, Y., Zhou, K. and Xia, Q., 2018. A MaxEnt model for mineral prospectivity mapping. Natural Resources Research, 27(3), pp.299-313.

Lou, Y. and Liu, Y., 2023. Mineral prospectivity mapping of tungsten polymetallic deposits using machine learning algorithms and comparison of their performance

in the Gannan region, China. Earth and Space Science, 10(10), p.e2022EA002596.

Mami Khalifani F, Bahroudi A, Aliyari F, et al (2019) Generation of an efficient structural evidence layer for mineral exploration targeting. Journal of African Earth Sciences 160, 103609.

Mami Khalifani F, Parsa M, Lentz D, Walker J (2021) Magnetic and radiometric signatures of gold mineralization in northern New Brunswick: constraints from numerical and spatial techniques. GAC-MAC Conference.

Mami Khalifani F, Parsa M, Lentz D, Walker J (2022) Portable XRF-aided pattern recognition for characterization of gold mineralization in Northern New Brunswick. In: Exploration, Mining and Petroleum New Brunswick (EMP 2022) conference.

Mami Khalifani F, Lentz D, Parsa M, Walker J (2023a). Recognizing gold mineralization pathfinders with portable XRF and micro-X-ray fluorescence spectrometry in the Williams Brook epithermal system, NB: Analysis of Indicator Elements and Minerals. In: Atlantic Geoscience Society.

Mami Khalifani, F., Imamalipour, A. and Barak, S., (2023b). The A-pplication of Various Mineral Prospectivity Modeling in the Exploration of Orogenic Gold Deposit in Saqez-Sardasht Region, Northwest Iran. Lithology and Mineral Resources, (4).

Mami Khalifani F, Lentz D, Walker J (2024) Gold Prospectivity Mapping and Exploration Targeting in Northern New Brunswick, Canada: Combined

Application of Random Forest (RF) and Fuzzy Inference System (FIS). In: American Geophysical Union (AGU), Washington. DC.

Mami khalifani F, Lentz D, Walker J (2025a) Machine Learning-Based Framework for Mineral Prospectivity Modeling: Predicting Epithermal Gold Mineralization in Northern New Brunswick, Canada. In: EGU General Assembly 2025, Vienna, Austria.

Mami Khalifani F, Lentz D, Walker J, Khammar F (2025b) Applying Mineral System Criteria to Develop a Predictive Modelling for Epithermal Gold Mineralization in Northern New Brunswick: Using Knowledge-Driven and Data-Driven Methods. Minerals 15(4): 345.

McCuaig TC, Beresford S, Hronsky J (2010) Translating the mineral systems approach into an effective exploration targeting system. Ore Geol Rev 38(3):128-138.

Mccutcheon S R, Anderson H E, Robinson P T (1997) Detection of Mineralization Zones Using Aeromagnetic Data. Applied Sciences. Geol Mag 12(18): 9078.

Mohamed A, Abdelrady M, Alshehri F, Mohammed M, Abdelrady A (2022) Detection of Mineralization Zones Using Aeromagnetic Data. Applied Sciences ,

Mokhtari A, Behnia P, Lafrance B, Naghizadeh M, Simmons J M, Harris J R (2025) Mineral prospectivity mapping of orogenic gold mineralization in the Malartic-Val-d'Or Transect area, Metal Earth project, Canada. Ore Geol Rev: 106498.

NBDNR (2014) NBDNR (2014) New Brunswick Department of Natural Resources. https://www2.gnb.ca/content/gnb/en/departments/erd/open.

Nykänen V, Salmirinne H (2007) Prospectivity analysis of gold using regional geophysical and geochemical data from the Central Lapland Greenstone Belt, Finland. Special Paper of the Geological Survey of Finland 44:251-269.

Nykänen Vesa, Lahti Ilkka, Niiranen Tero, Korhonen Kimmo (2015) Receiver operating characteristics (ROC) as validation tool for prospectivity models — A magmatic Ni–Cu case study from the Central Lapland Greenstone Belt, Northern Finland. Ore Geol Rev 71:853-860.

Porwal A, Carranza EMJ (2015) Introduction to the Special Issue: GIS-based mineral potential modelling and geological data analyses for mineral exploration. Ore Geol Rev 71:477-483.

Sánchez Mora D (2014) Petrogenesis of the low sulfidation gold mineralization in the Williams Brook area, Tobique-Chaleur Zone, New Brunswick. Unpublished MSc thesis, University of New Brunswick, Fredericton, NB Canada.

Sánchez-Mora D, McFarlane CRM, Walker JA, Lentz DR (2021) Geochemistry and U–Pb geochronology of the Williams Brook area, Tobique–Chaleur zone, New Brunswick: stratigraphic and geotectonic setting of gold mineralization. Can J Earth Sci 58(10):1040-1058.

Sibson RH (1990) Deformation Mechanisms, Rheology and Tectonics.Geological Society, London, Special Publication, 54: 15-28.

Sillitoe RH, Hedenquist JW (2005) Linkages between volcanotectonic settings, ore-fluid compositions, and epithermal precious metal deposits. In: pubs.geoscienceworld.org.Silva dos Santos V, Gloaguen E, Hector Abud Louro V, Blouin M (2022) Machine learning methods for quantifying uncertainty in

prospectivity mapping of magmatic-hydrothermal gold deposits: A case study from Juruena mineral province, northern Mato Grosso, Brazil. Minerals (pp. 207-235). Boston, MA: Springer US.

Suthaharan S (2016) Support vector machine. In Machine learning models and algorithms for big data classification: thinking with examples for effective learning. Boston, MA: Springer US: (207-235).

Taylor BE (2007) Epithermal gold deposits. Mineral Deposits of Canada: A synthesis of major deposit-types, district metallogeny, the evolution of geological provinces, and exploration methods. Geological Association of Canada, Mineral Deposits Division, Special Publication 5:113-139.

Thorne KG, Lentz DR, Hoy D, Fyffe LR, Cabri LJ (2008) Characteristics of Mineralization at the Main Zone of the Clarence Stream Gold Deposit, Southwestern New Brunswick, Canada: Evidence for an Intrusion-Related Gold System in the Northern Appalachian Orogen. Exploration and Mining Geology 17(1–2):13-49.

van Staal C R, de Roo J A, Hibbard J P, Cawood P A (1995) Mid-Paleozoic tectonic evolution of the Appalachian Central Mobile Belt in northern New Brunswick, Canada: collision, extensional collapse and dextral transpression. Current Perspectives in the Appalachian-Caledonian Orogen. Geological Association of Canada Special Paper 41:367-389.

Van Staal CR, Whalen JB, Valverde-Vaquero P, Zagorevski A, Rogers N (2009) Pre-Carboniferous, episodic accretion-related, orogenesis along the Laurentian

margin of the northern Appalachians. Geological Society, London, Special Publications: 271-316.

Vapnik V (2013) The nature of statistical learning theory. Springer Science & Business Media.

Wang J, Zuo R, Xiong Y (2020) Mapping mineral prospectivity via semi-supervised random forest. Natural Resources Research 29:189-202.

White NC, Hedenquist JW (1995) Epithermal gold deposits: styles, characteristics and exploration. SEG Newsletter23:1-13.

Wilson RA (2017) The Middle Paleozoic Rocks of Northern and Western New Brunswick, Canada.New Brunswick Department of Energy and Resource Development; Geological Surveys Branch, Memoir, 4: 319.Wilson RA, Kamo SL (2012) The Salinic Orogeny in northern New Brunswick: geochronological constraints and implications for Silurian stratigraphic nomenclature. Can J Earth Sci 49: 222–238

Wilson RA, Parkill MA, Carroll JI (2005) Field Trip B8: New Brunswick Appalachian Transect: Bedrock and Quaternary Geology of the Mount Carleton—Restigouche River Area.

Wu E, Kruse S (2022) Williams Brook Property Lineament Assessment.

Yin J, Li N (2022) Ensemble learning models with a Bayesian optimization algorithm for mineral prospectivity mapping. Ore Geol Rev 145: 104916.

Yousefi M, Carranza E J M (2015) Prediction–area (P–A) plot and C–A fractal analysis to classify and evaluate evidential maps for mineral prospectivity modeling. Comput Geosci 79, pp.69-81.

Yousefi M, Carranza EJM (2015) Fuzzification of continuous-value spatial evidence for mineral prospectivity mapping. Comput Geosci 74: 97-109.

Yousefi M, Lindsay M, Kreuzer O (2024) Mitigating uncertainties in mineral exploration targeting: Majority voting and confidence index approaches in the context of an exploration information system (EIS). Ore Geol Rev 165: 105930.

Yu Z, Li B, Wang X (2024) Mineral prospectivity mapping susceptibility evaluation based on interpretable ensemble learning. Ore Geol Rev 106248

Zhang N, Zhou K, Du X (2017) Application of fuzzy logic and fuzzy AHP to mineral prospectivity mapping of porphyry and hydrothermal vein copper deposits in the Dananhu-Tousuquan island arc, Xinjiang, NW China. Journal of African Earth Sciences 128:84-96.

Zhang Q, Chen J, Xu H, Jia Y, Chen X, Jia Z, Liu H (2022) Three-dimensional mineral prospectivity mapping by XGBoost modeling: A case study of the Lannigou gold deposit, China. Natural Resources Research 31(3):1135-1156.

Zheng C, Yuan F, Luo X, Li X, Liu P, Wen M, Chen Z, Albanese S (2023) Mineral prospectivity mapping based on Support vector machine and Random Forest algorithm–A case study from Ashele copper–zinc deposit, Xinjiang, NW China. Ore Geol Rev 159: 105567.

Zuo R (2020) Geodata Science-Based Mineral Prospectivity Mapping: A Review. Natural Resources Research 29:3415–3424

Zuo R, Carranza EJM (2011) Support vector machine: A tool for mapping mineral prospectivity. Comput 37: Geosci 1967-1975.

5. Conclusion and recommendations for future

5.1. Conclusion

The study area for this PhD research project area is situated in northern New Brunswick, a geologically diverse and structurally complex region within the northern Appalachian orogen. The area has long attracted mineral exploration interest due to its intricate lithological framework, deep crustal fault systems, and historical occurrences of gold and base metals. Despite this potential, much of the region remains underexplored due to data limitations, rugged terrain, and the complexity introduced by multiple phases of deformation, magmatism, and hydrothermal activity. These factors collectively make northern New Brunswick an ideal natural laboratory for developing and testing advanced mineral prospectivity mapping (MPM) methodologies.

The geological backbone of the study area is the Tobique–Chaleur Zone, within the Chaleur Bay Synclinorium, which consists of Upper Silurian to Lower Devonian bimodal volcanic and sedimentary successions. The Tobique-Chaleurs zone is transected by the regionally significant trans-crustal Rocky Brook–Millstream Fault system, which played a major role in fluid migration, mineralization, and structural reactivation. The region hosts bimodal volcanic rocks (rhyolites and basalt with minor volumes of intermediate composition), pyroclastic flows, volcaniclastic sedimentary rocks, and felsic and mafic intrusions, all of which are favorable for epithermal gold mineral systems.

The tectonic fabric of the area is heavily influenced by regional-scale faulting and polyphase deformation. The interplay between deformation and magmatism has led to a mosaic of structural traps, dilatant zones, and brecciated lithologies that provide ideal

settings for the formation of epithermal-style mineralization. The structural overprinting also introduces significant complexity, making predictive modeling particularly useful in unraveling the mineralization architecture. Four primary case study locations were selected based on their contrasting geological settings and known mineralization signatures.

The Williams Brook occurrence is hosted in felsic volcanic units of the Wapske Formation, and is characterized by quartz-carbonate veins containing both disseminated and vein-hosted gold. Alteration zones enriched in sericite, limonite, and chlorite are spatially associated with elevated concentrations of Au, As, Sb, Pb, and Fe.

The McIntyre Brook occurrence features brecciated felsic dykes and multi-phase quartz veining, reflecting a structurally controlled magmatic-hydrothermal system. This site is ideal for studying brittle deformation features and associated gold deposition.

The Mulligan Gulch occurrence, despite being less explored, is characterized by strong magnetic anomalies and coincident geochemical pathfinder element anomalies (Au, As, Sb, Cu,Mo, Pb, and Zn), indicating significant potential for concealed mineralization similar to that at Williams Brook.

The Simpsons Field occurrence is situated within the Silurian Petit Rocher Group, this zone comprises altered sedimentary rocks and quartz-siderite veins spatially related to mafic intrusions (dykes) and major faults.

Chapter 2 laid the foundation for integrating field-portable analytical tools with advanced geochemical data analysis techniques. This chapter focused on the use of portable X-ray fluorescence (pXRF) and micro-XRF (μXRF) instruments to analyze lithogeochemical compositions and alteration mineralogy in mineralized and altered zones at multiple case study locations. These tools enabled rapid, non-destructive, in-situ analysis of elemental

concentrations, significantly reducing turnaround time compared to traditional laboratory assays. Using Compositional Data Analysis (CoDA), the study overcame the closure problem commonly associated with geochemical data and improved the interpretability of element associations. Hierarchical clustering further helped classify geochemical signatures associated with gold-bearing environments. Notably, this chapter identified strong associations between gold (Au) and key pathfinder elements such as arsenic (As), antimony (Sb), lead (Pb), and iron (Fe) which are commonly linked to hydrothermal processes.

An important innovation was the multiscale integration of geochemical data: macro-scale (outcrop and trenching-level) pXRF analyses were combined with micro-scale (thin section) analyses , i.e. μXRF. This approach improved anomaly resolution and enabled the identification of fine-grained alteration halos and geochemical zoning patterns, such as subtle variations in mineral textures and veining. These findings significantly contributed to refining exploration models and enhancing early-stage decision-making in the field.

Chapter 3 advanced the study by translating geological knowledge into a hybrid mineral prospectivity mapping (MPM) framework, combining both conceptual understanding and statistical validation. The knowledge-driven component used fuzzy logic and geometric averaging to incorporate expert-derived criteria such as proximity to faults, presence of specific lithologies, alteration types, and known structural controls. To complement this, a data-driven component was developed using logistic regression on structured spatial datasets (e.g., geochemistry, lithology, structural features). This empirical modeling quantified relationships among known mineral occurrences and geospatial predictors, producing probabilistic prospectivity maps. One of the key methodological enhancements

discussed in this chapter was the application of multifractal concentration–area analysis, which enabled better reclassification of spatial data layers by distinguishing background from anomalous geochemical signatures. This allowed for the refinement of prospectivity zones and improved signal-to-noise ratio in target detection. By comparing outputs from both modeling approaches, the study demonstrated that hybrid methods offer superior predictive performance, interpretability, and reliability. This is particularly useful in complex and underexplored terrains, where conceptual geological models alone may lack spatial precision, and purely statistical models may lack geological context.

Chapter 4 focuses on more advanced supervised machine learning techniques for predictive mineral mapping. Three widely used classification algorithms including RF, SVM, and XGBoost were trained on spatially continuous predictor datasets derived from geophysics, geochemistry, geology, and structural data. The training process involved bootstrap sampling and stratified 10-fold cross-validation, ensuring robust model performance evaluation. Validation metrics such as Receiver Operating Characteristic–Area Under Curve (ROC–AUC) and Prediction–Area curves confirmed the reliability of each model. Notably, XGBoost consistently outperformed the other models, achieving AUC values above 0.91, indicating strong predictive ability and model generalization. A major contribution of this chapter was the development of a confidence index map, which quantified model agreement and spatial uncertainty. This tool allowed researchers and exploration teams to differentiate between zones of high model consensus considered high-priority targets—and areas where predictions diverged. This innovation introduced a transparent framework for risk assessment, making machine learning outcomes more interpretable and actionable for exploration planning. Furthermore, the use of ensemble

modeling (majority voting) increased the stability of prospectivity predictions by integrating multiple classifiers. This approach mitigated the impact of outliers and single-model biases, offering a more balanced and robust prediction system.

5.2. Recommendation

5.2.1. Field Validation and Ground-Truthing

a. Prospecting, detailed geological mapping, and follow-up geochemical and geophysical surveys should be conducted first in areas consistently identified as high-prospectivity by multiple models, particularly where confidence index maps show strong agreement. Where these methods confirm anomalies, trenching and targeted drilling can then be prioritized to validate the predictive reliability of the hybrid and machine learning frameworks.

b. Collect continuous high-resolution geochemical and alteration profiles from drill cores Portable core scanning using pXRF and hyperspectral tools can enrich the geochemical database and refine alteration models developed in this thesis.

c. Perform petrographic and fluid inclusion studies

This will provide microscale mineralogical and thermal insights into the timing, composition, and evolution of hydrothermal fluids responsible for mineralization, enhancing the interpretation of geochemical anomalies.

5.2.2. Geochronology and Paragenesis

a. Apply radiogenic isotope dating

Establishing precise mineralization ages in relation to host rocks and intrusions (especially in Williams Brook and McIntyre Brook) will constrain genetic models and improve exploration targeting.

b. Construct paragenetic sequences at each case study location

Documenting the sequence of veining, alteration, and sulfide deposition will enable better understanding of mineralizing episodes and structural reactivation events.

5.2.3. Data Integration and Methodological Enhancements

a. Transition from 2D raster-based MPM to 3D prospectivity modeling

Incorporate drillhole data, inversion models (e.g., from magnetic, IP, or EM surveys), and geological cross-sections to create 3D volumes of mineral potential. Tools such as Leapfrog, Seequent Central, and GeoModeller may be used for volumetric modeling.

b. Expand the geophysical dataset

Use additional airborne or ground surveys (e.g., gravity, induced polarization, magnetotellurics) to detect subsurface conductive and resistive anomalies. These can serve as complementary predictors in future machine learning models.

c. Explore advanced AI techniques

Deep learning architectures such as Convolutional Neural Networks (CNNs) or Graph Neural Networks (GNNs) can improve the automatic extraction of spatial patterns, especially for detecting non-linear relationships in structurally complex settings.

d. Integrate remote sensing for regional mapping

Use hyperspectral imaging to map alteration minerals (e.g., kaolinite, alunite, chlorite) in areas with limited access. These data can feed directly into future MPM workflows.

5.2.4. Broader Applications and Scalability

a. Apply the developed MPM framework to other deposit types

While this thesis focused on epithermal gold systems, the modular and adaptable workflow (e.g., CoDA, hybrid modeling, ensemble ML) can be applied to orogenic gold, VMS, and porphyry systems by adjusting the predictor variables and criteria.

b. Test the methodology in other regions

Apply the workflow in geologically analogous settings within the northern Appalachians, particularly in areas adjacent to NE-trending fault systems such as the Rocky Brook–Millstream Fault (RBMF), to test its generalizability and to evaluate structural and lithological controls under comparable tectonic conditions.

c. Collaborate with geological surveys and industry

Open-access data sharing and model development with government geological surveys, such as NB DNR or Geological Survey of Canada, can promote reproducibility and real-world uptake.

5.2.5. Sustainability, Environmental, Social, and Governance (ESG), and Responsible Exploration

Use predictive targeting to reduce exploration footprint

By focusing only on the highest-confidence zones, industry can minimize environmental disturbance, reduce exploration drilling volume, and improve cost-efficiency—supporting low-impact exploration goals.

Curriculum Vitae

Candidate's Full Name: Farzaneh Mami Khalifani

EDUCATION

PhD Candidate in Mineral exploration, University of New Brunswick, Fredericton, Canada (2020-present)

Thesis: " Predictive Modelling of Gold Mineral Systems in Northern New Brunswick: Insights from the Analysis of Geophysical, Geological, Geochemical, and Remote Sensing Data".

M.Sc. in Mining Engineering, University of Tehran (2014-2016)

Thesis: "Geo-exploration and Mineral Potential Mapping of orogenic gold deposit within Geological, Geophysical, Geochemical, and Remote sensing data using Arc GIS".

B.Sc. in Mining Engineering, Urmia University of Technology (2009-2013)

Thesis: "Prediction of Water Infiltration Rate for Kuhin railway tunnel using FLAC".

PUBLICATIONS

1. Mami Khalifani, F., Lentz, D.R., Walker, J.A. and Khammar, F., 2025. Applying Mineral System Criteria to Develop a Predictive Modelling for Epithermal Gold Mineralization in Northern New Brunswick: Using Knowledge-Driven and Data-Driven Methods. *Minerals*, *15*(4), p.345.

2. Mami Khalifani, F., Lentz, D.R. and Walker, J.A., 2025. Machine learning-based mineral prospectivity mapping of epithermal gold mineralization in Northern new brunswick: a comparative study of random forest, support vector machine, and XGboost classifiers. Earth Science Informatics, 18(4), p.553.

3. Mami khalifani, F., Lentz, D.R. and Walker, J.A., 2025. Advancing Gold Mineralization Detection in Northern New Brunswick Through Portable X-ray and Micro-X-ray Fluorescence Spectrometry with Multivariate Compositional Data Analysis (CoDA) and Clustering for Pathfinder Elements and Alteration Analysis. *Geochemistry: Exploration, Environment, Analysis*, pp.geochem2024-058.

4. Mami Khalifani, F., Imamalipour, A., Barak, S., Abedi, M. Jozanikohan, G., Bahroudi, A., 2023, The application of Various Mineral Prospectivity Modeling in the Exploration of Orogenic Gold Deposit in Saqez-Sardasht Region, Northern Iran", Lithology and Mineral Resources, 10.1134/S002449022370013.

5. Mami Khalifani, F., Barak, S., Abedi, M., Yousefi, S., 2023, Gold prospectivity mapping through generation and integration of geophysical, geochemical, remote sensing and geological evidence layers in Saqez area, NW Iran. International Journal of Mining and Geo-Engineering, International Journal of Mining andGeo-Engineering,10.22059/IJMGE.2023.358626.595062.

6. Mami Khalifani, F., Bahroudi, A., Aliyari, F., Abedi, M., Mohammad Pour, M., 2019, "Generation of an efficient structural evidence layer for mineral exploration targeting: a case study for gold mineralization in Iran", Journal of African Earth Science. DOI: 10.1016/j.jafrearsci.2019.103609.

7. Mami Khalifani, F., Bahroudi, A., Abedi, M., 2019. An integrated Fuzzy AHP- VIKOR for Mineral Potential Mapping: The Saqez gold deposit", Earth Observation and Geomatics Engineering, 10.22059/eoge.2019.263180.1027.

8. Barak, S., Imamalipour, A., Abedi, M., Mami Khalifani, F., 2021. Comprehensive modeling of mineral potential mapping by integration of multiset geosciences data" Chemie der Erde – Geochemistry, DOI: 10.1016/j.chemer.2021.125824.

9. Imamalipour, A., Barak, S., Mami Khalifani, F., 2020. Quantifying mass changes during hydrothermal alteration in listwaenite-type mercury mineralization, Tavreh area, northwestern Iran", Geochemistry: Exploration, Environment, Analysis Journal, 10.1144/geochem2020-004.

10. Mohammadpour, M., Bahroudi, A., Abedi, M., Rahimipour, G., Jozanikohan, G., Mami Khalifani, F., 2019. "Geochemical distribution mapping by combining number-size multifractal model and multiple indicator kriging", Journal of Geochemical Exploration, S0375-6742(18)30357-1.

SELECTIVE PRESENTATIONS

1. Mami Khalifani, F., Lentz, D.R., Walker, J., 2025, Integrating Monte Carlo Simulation with Machine Learning for Gold Mineralization Prediction" Goldschmidt, Prague

2. Mami Khalifani, F., Lentz, D.R., Walker, J., 2025, A Machine Learning-Based Framework for Mineral Prospectivity Modeling: Predicting Epithermal Gold Mineralization in Northern New Brunswick, Canada" European Geosciences Union (EGU), Vienna, Austria

3. Mami Khalifani, F., Lentz, D.R., Walker, J., 2025, "Enhancing Mineral Prospectivity Mapping for Gold mineralization in Northern New Brunswick using Machine Learning Approach" PDAC, Toronto.

4. Mami Khalifani, F., Lentz, D.R., Walker, J., 2025, “Detecting High-Potential Epithermal Gold Mineralization Through Geological, Till Geochemical, and Geophysical Signatures: A Case Study from Northern New Brunswick” AME Roundup Vancouver.

5. Mami Khalifani, F., Lentz, D.R., Walker, J., 2024, “Gold Prospectivity Mapping and Exploration Targeting in Northern New Brunswick, Canada: Combined Application of Random Forest (RF) and Fuzzy Inference System (FIS)” American Geophysical Union (AGU), Washington. DC.

6. Mami Khalifani, F., Lentz, D. R., Walker, J., 2024, “Predictive Modelling of Gold Mineralized Systems in Northern New Brunswick: Insights from the Analysis of Multiple Geoscience Datasets”, Technical Report.

7. Mami Khalifani, F., Lentz, D. R., Walker, J., 2024, “Mineral Prospectivity Mapping Using Data-Driven Method for Gold Exploration in Northern New Brunswick”

8. Mami Khalifani, F., Lentz, D. R., Parsa, M., Walker, J., 2024 “Integrated analysis geophysical, geochemical, and geological data to define gold exploration targets in the Simpson Field area, northern New Brunswick” Mineral Exploration, Prospectors & Developers Association of Canada (PDAC), Toronto.

9. Mami Khalifani, F., Lentz, D.R., Parsa, M., Walker, J., 2024 “ Integration geology and 3D inversion of aeromagnetic data for deep mineral exploration of McIntyre Brook and Moose Brook gold mineralization in northern New Brunswick” Atlantic Geoscience Society (AGS), Moncton.

10. Mami Khalifani, F., Lentz, D.R., Parsa, M., Walker, J., 2024 “Identifying Prospective Gold Mineralization Zones in the Williams Brook Property of Northern New

Brunswick: Analysis of Airborne Magnetic, Radiometric, and DEM Data" AME Roundup, Vancouver.

11. Mami Khalifani, F., Lentz, D.R., Parsa, M., Walker, J., 2024 "Mineralogy and Lithology from Magnetic Properties Analysis of the Northern New Brunswick's rocks: applications to geological modeling" Exploration, Mining and Petroleum New Brunswick (EMP), Fredericton.

12. Mami Khalifani, F., Butler, K., Parsa, M., 2023," Investigation of Airborne Geomagnetic Data via 3D Modeling: A Novel Approach for Deep Mineral Exploration, Prospectors & Developers Association of Canada (PDAC), Toronto.

13. Mami Khalifani, F., Parsa, M., Lentz, D., Walker, J., 2023," Recognizing gold mineralization pathfinders with portable XRF and micro-X-ray fluorescence spectrometry in the Williams Brook epithermal system, NB: Analysis of Indicator Elements and Minerals", Atlantic Geoscience Society (AGS).

14. Mami Khalifani, F., Lentz, D., Walker, J., Parsa, M., 2022," Predictive Modelling of Gold Mineral System in Northern New Brunswick: Insights from the Analysis of Multiple Geo-science Data", Technical report.

15. Mami Khalifani, F., Parsa, M., Lentz, D., Walker, J., 2022," Mineral Prospectivity Models of Williams Brooks gold property, NB: integration and analysis of multiple geoscientific datasets", Exploration, Mining and Petroleum New Brunswick.

16. Mami Khalifani, F., Parsa, M., Lentz, D., Walker, J., 2022," Portable XRF-aided pattern recognition for characterization of gold mineralization in Northern New Brunswick," Exploration, Mining, and Petroleum New Brunswick.

17. Mami Khalifani, F., Parsa, M., Lentz, D., Walker, J., 2022," Magnetic and radiometric signatures of gold mineralization in northern New Brunswick: constraints from numerical and spatial techniques" GAC-MAC, Halifax 2022.

18. Mami Khalifani, F., Parsa, M., Lentz, D., Walker, J., 2022," A targeting tool for gold mineralization in the Williams Brook epithermal system: insights from compositional geochemical balances", Atlantic Geoscience Society (AGS).

19. Mami Khalifani, F., Lentz, D., Walker, J., 2021," Structural Analysis of Gold Mineralization in Northern New Brunswick: preliminary analysis in aid of Mineral Potential Mapping," Exploration, Mining, and Petroleum New Brunswick.